

NACA RM L50H07

7207



RESEARCH MEMORANDUM

LONGITUDINAL STABILITY AND CONTROL CHARACTERISTICS AT
HIGH-SUBSONIC SPEEDS OF TWO MODELS OF A TRANSONIC
RESEARCH AIRPLANE WITH WINGS AND HORIZONTAL

TAILS OF ASPECT RATIOS 4.2 AND 2

By Arvo A. Luoma and John B. Wright

Langley Aeronautical Laboratory
Langley Air Force Base, Va.

NATIONAL ADVISORY COMMITTEE
FOR AERONAUTICS

WASHINGTON
September 29, 1950



NATIONAL ADVISORY COMMITTEE FOR AERONAUTICS

RESEARCH MEMORANDUM

LONGITUDINAL STABILITY AND CONTROL CHARACTERISTICS AT
HIGH-SUBSONIC SPEEDS OF TWO MODELS OF A TRANSONIC
RESEARCH AIRPLANE WITH WINGS AND HORIZONTAL
TAILS OF ASPECT RATIOS 4.2 AND 2

By Arvo A. Luoma and John B. Wright

SUMMARY

An investigation was made in the Langley 8-foot high-speed tunnel of two transonic research airplane models for Mach numbers up to approximately 0.95. The test Reynolds number at the highest speed was 1.6×10^6 for one model and 2.3×10^6 for the other model. The models were $\frac{1}{16}$ -scale and were supported in the tunnel on a sting. The wing and horizontal tail of one model were both of aspect ratio 4.2; the wing and horizontal tail of the other model were both of aspect ratio 2. The same fuselage and vertical tail were used on both models. The sweep of the 50-percent-chord line of the wings was 0° ; the sweep of the 75-percent-chord line of the horizontal tails was 0° . Both wings had NACA 65-110 airfoil sections and both horizontal tails had NACA 65-008 airfoil sections. Lift, drag, and pitching moment were determined by means of a strain-gage balance within the fuselage. Tare measurements were made to eliminate the interference effect of the sting.

A reduction in aspect ratio increased the force-break Mach number and reduced the magnitude of adverse compressibility effects on lift, drag, and pitching moment. Undesirable stability and control characteristics at high speeds were generally improved or delayed to higher Mach numbers by a reduction in aspect ratio. However, the expected improvement in elevator-effectiveness characteristics at high speeds as a result of a decrease in aspect ratio of the horizontal tail was modified probably by interference effects associated with the fuselage and vertical tail and perhaps by scale effects. The component parameters affecting the over-all stability and control characteristics varied in a generally nonlinear manner at supercritical speeds with abrupt changes occurring in relatively small Mach number ranges.

INTRODUCTION

The available experimental data on the aerodynamic characteristics of complete airplane configurations at high-subsonic speeds have been augmented by the results of tests in the Langley 8-foot high-speed tunnel of two airplane models with unswept wings and unswept horizontal tails of aspect ratios 4.2 and 2. The main part of these tests was concerned with the model which had a wing and horizontal tail both of aspect ratio 4.2. This model was a scaled version of a transonic research airplane powered by a turbojet engine and designed to fly at a level-flight Mach number of 0.85. Previous results of the wind-tunnel tests of this model already have been published in references 1 to 5. A wing and horizontal tail, both of aspect ratio 2, also were tested with the same fuselage and vertical tail used with the configuration of aspect ratio 4.2. Preliminary lift and drag results for the configuration of aspect ratio 2 have been presented in reference 1.

The present paper contains additional analysis of the data of references 1 to 5 and also presents new test data on these models. The results of reference 6 showed that a reduction in the aspect ratio of a wing delayed to higher Mach numbers the Mach number range in which serious compressibility effects occurred. To show the effect of aspect ratio on the characteristics at high-subsonic speeds of models with unswept wings and horizontal tails, some of the results of investigations of a complete model with a wing of aspect ratio 6 (reference 7), of a wing of aspect ratio 9 mounted on a fuselage (reference 8), and of a horizontal tail of aspect ratio 4 (reference 9) are included in the present paper.

SYMBOLS

The term "complete model" as used herein refers to the combination of wing, fuselage, vertical tail, and horizontal tail. The aerodynamic coefficients and other symbols used in this paper are defined as follows:

A	aspect ratio of wing (b^2/S)
A_t	aspect ratio of horizontal tail (b_t^2/S_t)
a	speed of sound in undisturbed stream
b	span of wing
b_t	span of horizontal tail
C_D	drag coefficient (D/qS)

- C_L lift coefficient (L/qS)
- C_m pitching-moment coefficient about lateral axis which passes through center of gravity ($M_{cg}/qc'S$)
- $(\Delta C_D)_t$ incremental drag coefficient of horizontal tail (drag of configuration consisting of fuselage, vertical tail, and horizontal tail (elevators undeflected) at a given angle of attack minus drag of configuration consisting of fuselage and vertical tail at same angle of attack and divided by qS)
 $((C_D)_{wc} - (C_D)_{twc})$
- $(\Delta C_L)_t$ incremental lift coefficient of horizontal tail (lift of configuration consisting of fuselage, vertical tail, and horizontal tail (elevators undeflected) at a given angle of attack minus lift of configuration consisting of fuselage and vertical tail at same angle of attack and divided by qS)
 $((C_L)_{wc} - (C_L)_{twc})$
- $(\Delta C_m)_b$ incremental pitching-moment coefficient of air brakes about lateral axis which passes through center of gravity (M_{cg} of configuration consisting of wing, fuselage, vertical tail, horizontal tail (elevators undeflected), and air brakes at a given angle of attack minus M_{cg} of configuration consisting of wing, fuselage, vertical tail, and horizontal tail (elevators undeflected) at same angle of attack and divided by $qc'S$)
 $((C_m)_{cb} - (C_m)_c)$
- $(\Delta C_m)_b'$ incremental pitching-moment coefficient of air brakes about lateral axis which passes through center of gravity (M_{cg} of configuration consisting of wing, fuselage, vertical tail, and air brakes minus M_{cg} of configuration consisting of wing, fuselage, and vertical tail and divided by $qc'S$)
 $((C_m)_{tcb} - (C_m)_{tc})$
- c section chord of wing, measured parallel to plane of symmetry of model
- c' mean aerodynamic chord of wing $\left(\frac{2c_r}{3} \frac{1 + \lambda + \lambda^2}{1 + \lambda}\right)$
- c_g nominal tip chord of wing, obtained by extending leading and trailing edges of wing to plane parallel to plane of symmetry of model and passing through wing tip
- c_r root chord of wing, obtained by extending leading and trailing edges of wing to plane of symmetry of model

c_t	section chord of horizontal tail, measured parallel to plane of symmetry of model
c_t'	mean aerodynamic chord of horizontal tail $\left(\frac{2}{3}c_{tr} \frac{1 + \lambda_t + \lambda_t^2}{1 + \lambda_t}\right)$
c_{tg}	nominal tip chord of horizontal tail, obtained by extending leading and trailing edges of horizontal tail to plane parallel to plane of symmetry of model and passing through tip of horizontal tail
c_{tr}	root chord of horizontal tail, obtained by extending leading and trailing edges of horizontal tail to plane of symmetry of model
D	drag
g	acceleration due to gravity
i_t	incidence of horizontal tail, measured by angle between plane of horizontal tail (stabilizer) and fuselage reference axis
L	lift
l	tail length, distance from center of gravity of airplane to the 25-percent point of the mean aerodynamic chord of the horizontal tail and measured parallel to direction of undisturbed stream
M	Mach number (V/a)
M_{cg}	pitching moment about lateral axis which passes through center of gravity (figs. 4 and 5)
q	dynamic pressure in undisturbed stream $\left(\frac{1}{2}\rho V^2\right)$
q_t	dynamic pressure at tail location
R	Reynolds number $(\rho V c' / \mu)$
S	area of wing $\left(\left(\frac{b}{2}\right)(c_r + c_g)\right)$
S_t	area of horizontal tail, including area of elevator $\left(\left(\frac{b_t}{2}\right)(c_{tr} + c_{tg})\right)$

V	velocity in undisturbed stream
α	angle of attack of airplane model, measured by angle between fuselage reference axis and direction of undisturbed stream
α_t	angle of attack of horizontal tail, measured by angle between plane of horizontal tail (stabilizer) and direction of flow at the tail ($\alpha + i_t - \epsilon$)
α_t'	free-stream angle of attack of horizontal tail, measured by angle between plane of horizontal tail (stabilizer) and direction of undisturbed stream ($\alpha + i_t$)
δ_e	elevator deflection, measured in plane perpendicular to elevator hinge axis
ϵ	effective downwash angle in region of horizontal tail as determined from tests of configuration consisting of complete model and configuration consisting of complete model less horizontal tail
η	horizontal tail height, distance from center of gravity of airplane to the 25-percent point of the mean aerodynamic chord of the horizontal tail and measured perpendicular to direction of undisturbed stream
λ	taper ratio of wing (c_g/c_r)
λ_t	taper ratio of horizontal tail (c_{tg}/c_{tr})
μ	coefficient of viscosity in undisturbed stream, pounds per foot-second
ρ	mass density in undisturbed stream, slugs per cubic foot

Subscripts:

$C_m=0$	value at zero pitching moment about lateral axis which passes through center of gravity
$C_L=0$	value at zero lift
$\alpha=0$	value at zero angle of attack of airplane
c	value for configuration consisting of complete model which is defined to be configuration consisting of wing, fuselage, vertical tail, and horizontal tail

- tc value for configuration consisting of complete model less horizontal tail (that is, configuration consisting of wing, fuselage, and vertical tail)
- wc value for configuration consisting of complete model less wing (that is, configuration consisting of fuselage, vertical tail, and horizontal tail)
- twc value for configuration consisting of complete model less wing and less horizontal tail (that is, configuration consisting of fuselage and vertical tail)
- cb value for configuration consisting of complete model plus air brakes (that is, configuration consisting of wing, fuselage, vertical tail, horizontal tail, and air brakes)
- tcb value for configuration consisting of complete model less horizontal tail plus air brakes (that is, configuration consisting of wing, fuselage, vertical tail, and air brakes)

APPARATUS AND METHODS

Tunnel, Model Support, and Balance System

The tests were made in the Langley 8-foot high-speed tunnel for Mach numbers up to approximately 0.95. For these tests, the tunnel was of the closed-throat type with the test section of circular cross section. The models were supported in the tunnel on a sting, which was in turn attached to a vertical strut downstream of the model. A photograph of one of the models mounted in the test section is shown as figure 1 and the general layout of the support system is shown in figure 2.

A three-component strain-gage balance was housed within the model fuselage which was hollow. (See figs. 2 and 3.) The internal balance was a part of the sting, and there was clearance between the fuselage and the sting except at the forward portion of the fuselage where the fuselage was attached to the sting.

Models

Two airplane models, which were constructed of duralumin, were tested. The wing and horizontal tail of one model airplane were both of aspect ratio 4.2; the wing and horizontal tail of the other were both of aspect ratio 2. The same fuselage and vertical tail were used with

both configurations. Drawings of the two models are shown in figures 4 and 5, and photographs are shown as figure 6. Table I gives the various geometrical dimensions of the two configurations. The wing section, wing area, wing taper ratio, wing dihedral, location of the 25-percent point of the mean aerodynamic chord of the wing along the fuselage, and the sweep (0°) of the 50-percent-chord line of the wing were the same for the two models. The horizontal-tail section, horizontal-tail area, horizontal-tail taper ratio, horizontal-tail dihedral, and the sweep (0°) of the 75-percent-chord line (hinge line) of the horizontal tail were also the same for the two models. Aspect ratio, therefore, was the principal variable.

In the tests of the airplane model of aspect ratio 4.2, the fuselage included a canopy. In the tests of the airplane model of aspect ratio 2, the fuselage did not include a canopy since, from canopy on-and-off tests, it was found that the canopy had no significant effect on the measurements. Some tests were made of side-opening air brakes mounted on the airplane model of aspect ratio 4.2 (fig. 7).

Test Procedure

Normal force, axial force, and pitching moment were measured with a strain-gage balance at various Mach numbers up to a maximum Mach number of approximately 0.95. The normal force and axial force were resolved into the rectangular components lift and drag by trigonometric methods. Various horizontal-tail incidences and elevator deflections were tested.

The angle of attack of the model was varied by changing a coupling in the sting (fig. 2) prior to a run. The run consisted of going through the Mach number range at the set angle of attack. Flexibility of the strain-gage balance and sting under aerodynamic loads caused a change in the angle of attack during the run, and this change in angle of attack was measured with an optical cathetometer at each test condition. The aerodynamic data obtained were plotted against the corrected angle of attack, and data at a constant angle of attack were obtained from these plots. The angle of attack is estimated to be accurate to $\pm 0.1^\circ$.

Corrections

Tests were made to determine the aerodynamic interference of the sting upon the model and for these tests an auxiliary three-component balance was used to support the models in place of the regular sting support. The auxiliary internal balance was supported in turn by swept-back arms of 6-percent-thickness ratio which extended through the model fuselage and back to the vertical strut downstream of the model. Two

arrangements of the tare system were required for the determination of the sting interference (fig. 8). In the tare "A" arrangement, an external dummy sting of the same size and shape as that used in the normal runs was present but not connected to the fuselage. In the tare "B" arrangement, the dummy sting was removed. By subtracting the results of the tare B tests from those of the tare A tests, the interference effect of the sting on the measured aerodynamic forces could be obtained. Subtraction of this interference effect from the data obtained in the normal runs gave results corrected for the interference effect of the sting. Tests were made for sufficient configurations (horizontal tail on and off, and various values of horizontal-tail incidence and elevator deflection) and angles of attack to define the sting interference.

The data in this paper, unless otherwise noted, represent the airplane with power off and do not include the effects of jet exhaust or a solid sting. Typical plots used in determining sting interference are shown in figure 9. For the configuration represented in the illustration, the effect of sting interference on pitching-moment coefficient was approximately -0.02 for most angles of attack and Mach numbers. The effect of sting interference on drag coefficient was approximately -0.004 at low speeds and of somewhat greater magnitude at high speeds. The effect of sting interference on lift coefficient was negligible.

Corrections for solid and wake blockage have been computed as in references 1 and 2 and have been applied to the data. The corrections to Mach number and dynamic pressure were negligible at Mach numbers below 0.90. Aerodynamic data were obtained up to a maximum corrected Mach number of approximately 0.96, at which speed choking occurred not at the model but at the support strut downstream of the model. The data were not affected by choke phenomena occurring at the strut since the strut was well back of the model and tunnel-wall pressure measurements indicated no irregularities in the velocity field in the region of the model at speeds near or at the choking Mach number.

The effect of temperature on the reading of the strain gages was determined by static-load tests in a controllable-temperature oven. In the tunnel tests, the temperature of the metal adjacent to the strain gages was measured and corrections were applied to compensate for temperature. These corrections were small.

RESULTS AND DISCUSSION

Test Reynolds numbers are shown in figure 10 based on the mean aerodynamic chord of both the wing and the horizontal tail. The airplane lift coefficient corresponding to level flight at two altitudes for an assumed wing loading of 66.7 pounds per square foot is given in figure 11.

This wing loading was used in the preparation of several of the figures presented in this paper.

Airplane Model of Aspect Ratio 4.2

Test data for the configuration of aspect ratio 4.2 have been given in references 1 to 5. Some of the figures from those references are presented herein, together with new data and data for other configurations for purposes of comparison. The airplane model with a wing and a horizontal tail, both of aspect ratio 4.2, is designated as $A = 4.2$ in the figures.

Stability.- The variation of pitching-moment coefficient with lift coefficient for the configuration consisting of complete model and the configuration consisting of complete model less horizontal tail is shown in figure 12 with horizontal-tail incidence as a parameter, and for the configuration consisting of complete model in figure 13 with elevator deflection as a parameter. Static instability at lift coefficients in the vicinity of zero lift was indicated for a small Mach number range near a Mach number of 0.9 for all incidences and most of the elevator deflections tested. The data indicated that, for some combinations of horizontal-tail incidence and elevator deflection, the pitching-moment coefficient of the model would be zero at three values of airplane lift coefficient (for example, in fig. 12 at a Mach number of 0.905 where two of these lift coefficients are negative). Presented in figure 14 is the parameter $\partial C_m / \partial C_L$ for elevators undeflected at airplane lift coefficients corresponding to level flight at two altitudes (not for trim conditions except in fig. 14(e)); it is seen that instability occurred at low incidences at a Mach number of 0.9 at the sea-level conditions and that an increase in horizontal-tail incidence eliminated this instability. The stability parameter at an incidence of 6.2° indicated a tendency toward instability at a Mach number of approximately 0.93 for the 35,000-foot-altitude conditions. The data on the stability parameter $\partial C_m / \partial C_L$ for level-flight trim conditions with the elevator undeflected and the horizontal tail used for obtaining trim (fig. 14(e)), however, indicated that there was no serious decrease in stability. For these trim conditions, the required horizontal-tail incidences were such as to avoid the unstable incidence ranges at each Mach number.

The variation with Mach number of the stick-fixed neutral-point location is shown in figure 15 at airplane lift coefficients corresponding to level flight at two altitudes. At the higher-altitude condition, the neutral point shifted rearward from 35 percent mean aerodynamic chord at a Mach number of 0.8 to 44 percent mean aerodynamic chord at a Mach number of 0.85. A forward movement then occurred to 30 percent mean aerodynamic chord at a Mach number of 0.93, followed by a rearward trend

at the highest Mach numbers. At the sea-level condition, a rapid rearward shift occurred at speeds above a Mach number of 0.9, the location at a Mach number of 0.95 being 50 percent mean aerodynamic chord.

Control.- The variation of pitching-moment coefficient with horizontal-tail incidence is shown in figures 16(a) and 16(b) and with elevator deflection in figure 16(c) for the configuration consisting of complete model at airplane lift coefficients corresponding to level flight at two altitudes. There was a reduction in horizontal-tail effectiveness $(\partial C_m / \partial i_t)_{\delta_e = 0^\circ}$ (slopes of curves shown in figs. 16(a) and 16(b)) at high Mach numbers but otherwise the horizontal-tail effectiveness appeared to be satisfactory. The elevator effectiveness $(\partial C_m / \partial \delta_e)_{i_t = 2.2^\circ}$ (slopes of curves shown in fig. 16(c)) was zero at a Mach number somewhat higher than 0.875 for a small range of elevator deflections in the vicinity of zero deflection. At higher Mach numbers up to 0.95, the elevator effectiveness became reversed for an elevator-deflection range which increased with Mach number and, in some cases, this elevator-deflection range extended up to the maximum deflection tested. In such cases, elevator deflections greater than those tested would probably show a return to positive effectiveness. The loss and reversal in elevator effectiveness for small deflections at high speeds shown by these tests have been observed in other investigations. References 9 and 10 showed, by means of detailed pressure measurements, that the ability of an elevator or a flap on a conventional unswept surface to produce changes of lift over the whole airfoil was reduced at small deflections as the critical speed was exceeded.

The Reynolds numbers of the present tests (fig. 10) were believed at first to be greater than the critical values of 3×10^5 to 5×10^5 given in wing-flow investigations (reference 11) by an amount sufficient to preclude low Reynolds number effects. As a check on this belief, a few runs were made with a transition strip on the wing at the 25-percent-chord line. These data (fig. 17), for Mach numbers up to 0.9, showed little effect due to the transition strip on the wing except for an increase in drag. Some of the results of the test data proper, such as the reversal in elevator effectiveness at high speeds, gave rise to further question about the importance of scale effects. A subsequent check test was made with a strip of 0.005-inch carborundum particles located at the 20-percent-chord line of the horizontal tail. Figure 18 shows the variation of pitching-moment coefficient with elevator deflection at a model angle of attack of 0° with and without the transition strip on the horizontal tail. The tests with roughness on the horizontal tail did not show the reversal in elevator-effectiveness characteristics noted for the tests with natural transition but still showed a reduction in elevator effectiveness at high Mach numbers. These results are in variance to those of reference 9 for a similar type of horizontal tail (30-percent-chord elevators) of larger scale which showed a reversal in

elevator effectiveness at small deflections at a Mach number of approximately 0.92 with and without the transition strip. The Reynolds number for those tests was over 1.2×10^6 . In the tests of reference 9, however, the horizontal tail was mounted on a reflection plane so that general inconsistencies in results from those tests and the present tests possibly may be attributable to differences in testing techniques. Horizontal-tail effectiveness was not materially changed by the transition strip on the horizontal tail in the tests of reference 9, and there was indication that this was also true in the present tests on the basis of the data of figure 18 and the assumption that the zero-lift angle of attack of the horizontal tail was not affected by a transition strip on the horizontal tail. In summation, it may be said that the elevator-effectiveness data of the present tests with natural transition are subject to scale effects and that these data would be modified at full-scale Reynolds numbers.

The horizontal-tail effectiveness for trim conditions with the elevator undeflected and the horizontal tail used for obtaining trim and the elevator effectiveness for trim conditions with the horizontal-tail incidence set at 2.2° and the elevators used for obtaining trim are shown in figure 19 at airplane lift coefficients corresponding to level flight at two altitudes and were obtained from the data of figure 16 (at $C_m = 0$). A reversal in elevator effectiveness for the trim condition was not evident until a Mach number of approximately 0.94 was reached at the 35,000-foot-altitude conditions. The data of figure 16(c) indicate that a horizontal-tail incidence greater than the 2.2° shown in the figure would probably result in a reversal in elevator effectiveness for trim conditions at Mach numbers lower than 0.94.

The horizontal-tail incidence required for obtaining trim and the elevator deflection required for obtaining trim at airplane lift coefficients corresponding to level flight at two altitudes were obtained from figure 16 at zero pitching-moment coefficient and are shown in figures 20(a) and 20(b), respectively. The horizontal-tail incidence and the elevator deflection required for obtaining trim gradually increased up to a Mach number of approximately 0.80 and then decreased with further increase of Mach number up to approximately 0.86. At Mach numbers above 0.86, there was further increase in both the horizontal-tail incidence and the elevator deflection required for obtaining trim. The horizontal-tail incidence required for obtaining trim decreased above a Mach number of approximately 0.91. Two elevator deflections required for obtaining trim were indicated in some cases at Mach numbers above 0.92 because of the reversal in elevator characteristics. The more positive elevator deflections required for obtaining trim appear to be the more suitable values for obtaining trim, considering the changes shown in figure 16(c). The airplane angle of attack corresponding to the conditions of figure 20(a) is shown figure 20(c). An increase in the angle of attack occurred between Mach numbers of 0.85 and 0.90 and a decrease at higher Mach numbers.

Incremental horizontal-tail characteristics.- The variation of lift coefficient, pitching-moment coefficient, and drag coefficient with Mach number at various model angles of attack for the configuration consisting of the fuselage and vertical tail is shown uncorrected for sting interference in figures 21 and 22. The variation of lift coefficient, pitching-moment coefficient, model angle of attack, and drag coefficient with Mach number at several values of horizontal-tail incidence with elevators undeflected for the configuration consisting of the fuselage, vertical tail, and horizontal tail is shown uncorrected for sting interference in figures 23 and 24; the model angle of attack remained at a value of approximately -0.3° . Tests were made of the configuration consisting of the fuselage, vertical tail, and horizontal tail with the horizontal-tail incidence held at 2.2° and the model angle of attack varied, and the data uncorrected for sting interference are shown in figures 25 and 26.

Incremental horizontal-tail characteristics were obtained by subtraction of lift and drag data uncorrected for sting interference for the configuration consisting of the fuselage and vertical tail from corresponding data at the same model angle of attack for the configuration consisting of the fuselage, vertical tail, and horizontal tail on the assumption that the sting interference on drag and lift was the same for each set of data. The incremental characteristics do not include wing downwash effects but do include any interference effects from the fuselage and vertical tail. Figure 27 shows the incremental lift coefficient and incremental drag coefficient of the horizontal tail obtained by subtraction of the lift and drag data in figures 21 and 22 from those in figures 23 and 24. The results are shown as a function of the free-stream angle of attack of the horizontal tail α_t' which, in figure 27, represented variations of horizontal-tail incidence with the model angle of attack held at approximately -0.3° .

The value of α_t' when $(\Delta C_L)_t = 0$ was taken from figure 27 and is shown in figure 28 as a function of Mach number. If it is assumed that the incremental lift coefficient of the horizontal tail, which was symmetrical, was zero at an angle of attack of the horizontal tail of 0° , then, the values shown in figure 27 indicate the effective direction of the flow in the region of the horizontal tail with only a fuselage, vertical tail, and horizontal tail present. These data show the importance of interference effects on the direction of the flow in the region of a tail. Unless such an initial effective angle of flow were included in the estimation of wing downwash in the design of an airplane, calculated horizontal-tail incidences at low speeds could be in error by approximately 1.5° . The increase in this angle from approximately 1.5° at low Mach numbers to approximately 3.5° at the highest Mach numbers would cause even greater errors in estimating control requirements and airplane trim conditions at high speeds.

The slope of the horizontal-tail incremental lift curve in figure 27 was determined at $(\Delta C_L)_t = 0$ and is shown in figure 28. Since the horizontal-tail incremental lift coefficient was based on wing area, the magnitude of the parameter $\partial(\Delta C_L)_t / \partial \alpha_t'$ was small. The value of the parameter $\partial(\Delta C_L)_t / \partial \alpha_t'$ was 0.015 at low speeds and decreased at high speeds to 0.006 at a Mach number of 0.905.

The lift-curve slope for a horizontal tail of aspect ratio 4.01 as determined in the tests of reference 9 is also shown in figure 28. Since the two horizontal tails differed only by 0.2 in aspect ratio and by 0.1 in design lift coefficient, it would be expected that the magnitude of lift losses would be similar and would begin at approximately the same Mach number. The measured slopes for the model of aspect ratio 4.2 showed good agreement with those for the model of aspect ratio 4.01 for Mach numbers up to 0.75, but, at higher Mach numbers, the loss in lift was much greater and the onset of the loss in lift occurred at lower Mach numbers for the model of aspect ratio 4.2. The variance at high speeds was probably associated with the interference effects of the fuselage and vertical tail used in the present tests, with differences in testing techniques, and with differences in scale between the two models. Interference from the fuselage and vertical tail also may have been a factor in producing the loss in elevator effectiveness previously discussed.

Downwash.- The data for the plot showing the variation of effective downwash angle with lift coefficient (fig. 29) were taken from reference 4. The effective downwash angle was determined at a given horizontal-tail incidence by finding the model angle of attack at which the pitching-moment coefficient of the configuration consisting of complete model was equal to that of the configuration consisting of complete model less horizontal tail. The sum of the model angle of attack thus found and the horizontal-tail incidence gave the effective downwash angle in the region of the tail. The effect of the horizontal-tail drag on pitching moment was neglected. The effective downwash at airplane lift coefficients corresponding to level flight at two altitudes (fig. 30) increased rapidly at Mach numbers above 0.85. The increase caused a change in the control settings required for obtaining trim, as is shown subsequently. The rate of change of effective downwash with lift coefficient (fig. 31), obtained from figure 29 at airplane lift coefficients corresponding to level flight at two altitudes, decreased rapidly at Mach numbers above 0.8, reaching a minimum at a Mach number of approximately 0.9. This decrease indicated a stabilizing effect.

It has been shown previously that an initial effective flow angle in the vicinity of the horizontal tail for the configuration with no wing present was induced by fuselage, vertical-tail, and horizontal-tail interference effects. This initial effective downflow gave an effective downwash, as presented herein, which probably was larger than would be found for the wing alone.

Horizontal-tail load.- The horizontal-tail load required to trim the airplane at various flight conditions was found by using the pitching-moment data of figure 12 for the configuration consisting of complete model less horizontal tail. The incremental lift coefficient of the horizontal tail (based on wing area and the dynamic pressure in the undisturbed stream) was found as follows:

$$(\Delta C_L)_t' = (C_m)_{tc} \frac{c'}{l}$$

where $(\Delta C_L)_t'$ is the estimated value of incremental horizontal-tail lift coefficient required for trimming the airplane. It was assumed that the center of pressure of the lift on the horizontal tail was located at the 25-percent point of the mean aerodynamic chord of the horizontal tail. The resulting incremental horizontal-tail lift coefficient for sea-level conditions is shown in the lower part of figure 32 plotted against Mach number. For level flight ($g = 1$), there was a decrease in incremental horizontal-tail lift coefficient as the Mach number was increased to 0.85. The incremental horizontal-tail lift coefficient increased with further increase in Mach number up to a Mach number of 0.90 and again decreased at still higher speeds. For the accelerated conditions, similar effects occurred with a more-positive incremental horizontal-tail lift coefficient throughout the Mach number range. The maximum unloading and changes in loading with Mach number at high Mach numbers occurred at a normal acceleration of approximately $4g$.

The curves at the top of figure 32 show the relative airplane lift coefficient at any constant value of Mach number plotted against altitude for various values of acceleration factor as a parameter. The relative airplane lift coefficient is defined herein to be the ratio of the lift coefficient at a given Mach number and at any value of g and altitude to the lift coefficient at the same Mach number and at a value of g of 1.0 and at sea-level altitude. The incremental horizontal-tail lift coefficient at any altitude and acceleration condition is found by first determining the relative airplane lift coefficient from the top of figure 32. The relative airplane lift coefficient thus found, if applied to an airplane under sea-level conditions, would develop a sea-level acceleration numerically equal to the relative airplane lift coefficient. This sea-level acceleration then is used with the curves at the bottom of figure 32 to get the incremental horizontal-tail lift coefficient. For example, a $4.2g$ sea-level condition would have the same relative airplane lift coefficient as a $1g$ (level-flight) condition at 35,000 feet or a $2g$ condition at 19,000 feet, and these various altitude- g conditions would be represented by data between the $g = 4$ and $g = 5$ conditions at sea level shown at the bottom of figure 32. From these data, it is seen that the lift coefficient of the horizontal tail remains small for various flight conditions.

The angle of attack of the horizontal tail at airplane lift coefficients corresponding to level flight for trim conditions with the elevator undeflected and the horizontal tail used for obtaining trim is shown in figure 33(a). The change in angle of attack of the horizontal tail with Mach number was similar to that of the incremental horizontal-tail lift coefficient shown in figure 32. The angle of attack of the horizontal tail at airplane lift coefficients corresponding to level flight for trim conditions with the horizontal-tail incidence set at 2.2° and the elevators used for obtaining trim are shown in figure 33(b). The angle of attack of the horizontal tail decreased as the Mach number was increased. When the horizontal tail is used for obtaining trim, the angle of attack of the horizontal tail is limited to smaller over-all changes over the speed range than when the elevators are used for obtaining trim.

Stability factors.- The various parameters affecting stability were considered in an attempt to determine the cause of the instability at low lift coefficients in the vicinity of a Mach number of 0.9. The effect of Mach number on these parameters at a constant medium value (0.3) of airplane lift coefficient and a low value (0.05) of airplane lift coefficient is shown in figure 34.

The approximate constant-speed longitudinal stability equation neglecting horizontal-tail drag is as follows:

$$\left(\frac{\partial C_m}{\partial C_L}\right)_c \approx \left(\frac{\partial C_m}{\partial C_L}\right)_{tc} - \left[\frac{1}{\left(\frac{\partial C_L}{\partial \alpha}\right)_{tc}} - \left(\frac{\partial \epsilon}{\partial C_L}\right)_{tc} \right] \frac{\partial(\Delta C_L)_t}{\partial \alpha t} \frac{q_t}{q} \frac{l}{c'}$$

The parameter $(\partial C_m / \partial C_L)_{tc}$ for the configuration consisting of complete model less horizontal tail increased at speeds somewhat less than a Mach number of approximately 0.9 at a lift coefficient of 0.05 (fig. 34(a)). The increase of the parameter $(\partial C_m / \partial C_L)_{tc}$ at supercritical speeds is associated with a forward movement of the center of pressure on the wing as discussed in reference 4. The details of such center-of-pressure movements at supercritical speeds are shown by the pressure-distribution studies over airfoil surfaces presented in references 9 and 10. The increase in the parameter $(\partial C_m / \partial C_L)_{tc}$ was not changed by a transition strip and can be expected therefore to occur at higher Reynolds numbers. The increase in the parameter $(\partial C_m / \partial C_L)_{tc}$ would tend to increase the stability parameter $(\partial C_m / \partial C_L)_c$; that is, the increase in the parameter $(\partial C_m / \partial C_L)_{tc}$ would tend to have a destabilizing effect on the stability parameter $(\partial C_m / \partial C_L)_c$. At a lift

coefficient of 0.3 and a Mach number of approximately 0.9, the negative value of the parameter $(\partial C_m / \partial C_L)_{t_c}$ would tend to cause a negative value, that is, a stable value, of the stability parameter $(\partial C_m / \partial C_L)_c$.

The lift-curve slope $(\partial C_L / \partial \alpha)_{t_c}$ for the configuration consisting of complete model less horizontal tail was obtained at the two lift coefficients considered (fig. 34(b)). The low magnitude of this parameter at a lift coefficient of 0.05 at a Mach number of 0.9 would tend to have a favorable effect on the stability parameter $(\partial C_m / \partial C_L)_c$. The resultant tendency toward instability shown by the stability parameter $(\partial C_m / \partial C_L)_c$ probably was not caused by changes in lift-curve slope.

The variation with Mach number of the rate of change of downwash angle with respect to lift coefficient $(\partial \epsilon / \partial C_L)_{t_c}$ is shown in figure 34(c). The low magnitude of this parameter at a lift coefficient of 0.05 and a Mach number of 0.9 would tend to have a favorable effect on the stability parameter $(\partial C_m / \partial C_L)_c$.

The horizontal-tail incidence was considered to be held constant at 2.2° for the purposes of figure 34(d). The slope of the horizontal-tail lift curve $\partial(\Delta C_L)_t / \partial \alpha_t$ was determined from figure 27. In figure 34(d), the horizontal-tail lift-curve slope decreased at a lift coefficient of 0.05 at Mach numbers somewhat less than approximately 0.9. This decrease would tend to have a destabilizing effect on the stability parameter $(\partial C_m / \partial C_L)_c$. The slope at the larger lift coefficient decreased by a greater amount at these Mach numbers.

In reference 5, it was found that the dynamic pressure ratio q_t/q did not exceed 2 to 3 percent above or below 1.0 so that changes in the factor q_t/q had only minor influence on stability characteristics. A constant value of the tail-length factor l/c' of 2.39 (at $\alpha = 0^\circ$) was used. The assumption was made that the center of pressure of the lift on the horizontal tail was located at the 25-percent point of the mean aerodynamic chord of the horizontal tail. If the center of pressure on the horizontal tail were ahead of the 25-percent point so that the moment arm between the center-of-gravity position and the horizontal tail were decreased by 5 percent, for example, then the stability parameter $(\partial C_m / \partial C_L)_c$ would be changed in a positive direction by only approximately 0.02 at a Mach number of 0.9 at the low-lift-coefficient condition.

The data of figure 34 indicate that the characteristics of the configuration consisting of complete model less horizontal tail were principally responsible for the static instability at a Mach number of 0.9 at a

lift coefficient of 0.05 shown by the configuration consisting of complete model. A forward movement of the center of pressure on the wing at low lift coefficients in a small range of Mach numbers near 0.9 evidently caused the unstable condition. There may have been a small contributing factor toward instability associated with the decreases in the lift-curve slope of the horizontal tail. The resultant instability would have been greater except for the changes in downwash characteristics which had a favorable effect on the stability.

The stability parameter $(\partial C_m / \partial C_L)_c$ was computed for a few cases from the factors shown in figure 34 and compared with the measured values. Figure 34(e) shows the variation of measured $(\partial C_m / \partial C_L)_c$ at a lift coefficient of 0.05 for the configuration consisting of complete model with a horizontal-tail incidence of 2.2° and an elevator deflection of 0° . The calculated point at a Mach number of 0.905 was considerably out of agreement with the measured value. This discrepancy may be charged in part to lack of sufficient downwash data in the vicinity of zero lift at a Mach number of 0.905 to fair the downwash curve properly (fig. 29). The other estimated values obtained at various Mach numbers agreed reasonably well with the measured values.

Control factors.- The factors causing control changes are considered herein. The horizontal-tail incidence required for obtaining trim (with elevator undeflected) at a given lift coefficient is computed by the following equation:

$$i_t(C_m)_{c=0} \approx - \frac{(C_m)_{tc}}{\left(\frac{\partial C_m}{\partial i_t}\right)_c} + \epsilon - \alpha(C_L)_{tc=0} - \frac{(C_L)_{tc}}{\left(\frac{\partial C_L}{\partial \alpha}\right)_{tc}}$$

It was assumed that the horizontal-tail lift was zero at an angle of attack of the horizontal tail of zero.

The variation with Mach number of the individual parameters at a lift coefficient of 0.3 is shown in figure 35. The pitching-moment coefficient of the configuration consisting of complete model less horizontal tail $(C_m)_{tc}$ at a lift coefficient of 0.3 is shown in figure 35(a). An increase in this moment would tend to increase (algebraically) the horizontal-tail incidence required for obtaining trim. The variation of the parameter $(C_m)_{tc}$ with Mach number would tend to decrease (algebraically) the horizontal-tail incidence required for obtaining trim at speeds up to a Mach number of 0.85, would tend to increase (algebraically) the horizontal-tail incidence required for obtaining trim at higher speeds up to a Mach number of 0.9, and would tend to decrease (algebraically) the horizontal-tail incidence required for obtaining trim at the highest speeds up to a Mach number of 0.95.

The horizontal-tail effectiveness (fig. 35(b)) gradually increased (algebraically) at Mach numbers above 0.8. Such a change would tend to increase (algebraically) the horizontal-tail incidence required for obtaining trim if the pitching-moment coefficient $(C_m)_{t_c}$ were positive in sign and would tend to decrease (algebraically) the horizontal-tail incidence required for obtaining trim if the pitching-moment coefficient $(C_m)_{t_c}$ were negative in sign.

The downwash angle (fig. 35(c)) was essentially constant at speeds up to a Mach number of 0.875. The large increase in downwash angle between Mach numbers of 0.875 and 0.93 would tend to increase (algebraically) the horizontal-tail incidence required for obtaining trim.

The model angle of attack for zero lift (fig. 35(d)) increased between Mach numbers of 0.85 and 0.9; this change would tend to decrease (algebraically) the horizontal-tail incidence required for obtaining trim. At higher speeds up to a Mach number of 0.95 there was a decrease in the model angle of attack for zero lift and this decrease would tend to increase (algebraically) the horizontal-tail incidence required for obtaining trim. The lift-curve slope for the configuration consisting of complete model less horizontal tail (fig. 35(e)) increased for speeds up to a Mach number of 0.8; this change for the lift coefficient being considered would tend to increase (algebraically) the horizontal-tail incidence required for obtaining trim. The slope decreased at higher speeds up to a Mach number of 0.875 and then increased at the highest Mach numbers.

Figure 35(f) shows the horizontal-tail incidence required for obtaining trim at a lift coefficient of 0.3 computed from the preceding equation and using the various parameters shown in figure 35. The magnitude and change in magnitude of the computed horizontal-tail incidence required for obtaining trim agreed quite well with the experimental or measured values at the same lift condition. The qualitative effect of the various factors on the horizontal-tail incidence required for obtaining trim at a lift coefficient of 0.3 is summarized in table II. The direction of the resultant change in the measured horizontal-tail incidence required for obtaining trim $i_t(C_m)_{c=0}$ is given for various Mach number ranges and was obtained from the data of figure 35(f). Also given for the same Mach number ranges is the direction in which the change in any one of the various factors would tend to change the parameter $i_t(C_m)_{c=0}$. The term "same direction" means that the change in a parameter, such as $(\partial C_L / \partial \alpha)_{t_c}$, in a given Mach number range would tend to change $i_t(C_m)_{c=0}$ in the same direction as the actual resultant change in the measured parameter $i_t(C_m)_{c=0}$ in the same given Mach

number range. The terms "no change" and "opposite direction" have a corresponding significance.

It is evident that changes in pitching moment of the configuration consisting of complete model less horizontal tail, changes in downwash, and changes in horizontal-tail effectiveness as a result of compressibility effects were the chief causes for the rapid changes in the horizontal-tail incidence required for obtaining trim at Mach numbers greater than 0.85.

The parameters affecting the elevator deflection required for obtaining trim at a lift coefficient of 0.3 and at a constant value of horizontal-tail incidence of 2.2° were also investigated. The following equation gives the elevator deflection required for obtaining trim:

$$\delta_e (C_m)_{c=0} \approx \frac{-(C_m)_{tc} - \left(\frac{\partial C_m}{\partial i_t}\right)_c \left[-\epsilon + \alpha (C_L)_{tc=0} + \frac{(C_L)_{tc}}{(\partial C_L / \partial \alpha)_{tc}} + i_t\right]}{\left(\frac{\partial C_m}{\partial \delta_e}\right)_c}$$

The same parameters used in getting the horizontal-tail incidence required for obtaining trim (fig. 35) are included with the addition of elevator effectiveness. The elevator effectiveness (fig. 36(a)) greatly increased (algebraically) at speeds above a Mach number of approximately 0.85 with a reversal in effectiveness for certain values of elevator deflection at Mach numbers from 0.9 to 0.95. At high speeds, the magnitude of the elevator-effectiveness parameter at any given Mach number varied appreciably with elevator deflection because of the nonlinearity of the variation of pitching-moment coefficient with deflection.

An increase (algebraically) in elevator effectiveness would require a greater deflection to produce a given pitching moment. The numerator of the right-hand side of the foregoing equation represents the pitching-moment coefficient which must be developed by the elevators to produce trim conditions, and this moment is equal, but of reversed sign, to the moment of the complete model with the horizontal tail at a given incidence and with the elevators undeflected. The algebraic sign of the numerator and that of the elevator effectiveness must be known to determine the direction of elevator travel. The numerator of the equation, which herein is called C_{me} (fig. 36(b)), was calculated from the data of figures 35(b) and 35(f) and a value of horizontal-tail incidence of 2.2° by the equivalent equation

$$C_{me} = \left(\frac{\partial C_m}{\partial i_t}\right)_c \left\{ \left[i_t (C_m)_{c=0} \right]_{\text{computed}} - 2.2 \right\}$$

The elevator deflections required for obtaining trim and computed from the factors in figures 36(a) and 36(b) are presented in figure 36(c). A wide band of the computed elevator deflections required for obtaining trim is shown since maximum and minimum values of elevator effectiveness over the deflection range were used. When the more negative elevator effectiveness was used, the computed values of the elevator deflection required for obtaining trim were generally close to the measured values for most of the Mach number range. The large differences between computed and measured values at Mach numbers from 0.9 to 0.93 probably resulted because the computations did not take into account the non-linearity of elevator effectiveness with deflection.

The factors producing changes in the elevator deflection required for obtaining trim are summarized in table III. The individual parameters are shown in columns indicating whether the change in a parameter in a given Mach number range would tend to cause a change in the elevator deflection required for obtaining trim in the same direction as the actual resultant change in the measured parameter $\delta_e(C_m)_{c=0}$, a change in the opposite direction, or no change when the value of the parameter did not change. The change in $\delta_e(C_m)_{c=0}$ which tends to result from a change in either $(\partial C_m / \partial \delta_e)_c$ or $(\partial C_m / \partial i_t)_c$ has an algebraic sign which is also dependent on the algebraic sign of $\delta_e(C_m)_{c=0}$. In table III the sign of the measured $\delta_e(C_m)_{c=0}$ was used for these cases.

At high Mach numbers, the changes in the elevator deflection required for obtaining trim at a constant value of horizontal-tail incidence of 2.2° are shown to have been caused by changes in pitching moment of the complete model less horizontal tail, changes in downwash angle, changes in horizontal-tail effectiveness, and to some extent by changes in elevator effectiveness and lift-curve slope. The more negative or larger values of elevator effectiveness (fig. 36(a)) were used for table III because of the generally close agreement between the computed deflections required for obtaining trim and the measured deflections required for obtaining trim. The maximum loss in effectiveness in this case did not occur until a Mach number of 0.95 was reached, and for these conditions little balancing moment was required from the elevators.

It is seen that the various parameters were affected by compressibility effects and that these parameters combined differently over small speed ranges to produce changes in the elevator deflection required for obtaining trim or the horizontal-tail incidence required for obtaining trim. The need for having information on the detailed characteristics of these parameters at all Mach numbers, as well as on the interference effects, is evident when the design of a transonic airplane is contemplated or prediction of flight characteristics is made.

Air brakes.- The effect of fuselage air brakes opening from the sides of the configuration consisting of complete model (fig. 5) was shown in reference 3 to have caused a drag-coefficient increment of about 0.03 to 0.04. The effect on terminal Mach number (figs. 37 and 38) was shown to have been small and incapable of reducing the Mach number at high altitudes to values below that at which difficulties in control and stability have been indicated. A wing loading of 58 pounds per square foot was used in the preparations of figures 37 and 38.

A small change in trim was produced by the brakes (fig. 39). Small pull-out moments were evident throughout the speed range except at a Mach number of approximately 0.9 and at lift coefficients greater than 0.2 at which conditions little change was noted. A similar brake on a midwing model (reference 7) produced larger trim shifts with varying pull-out and diving tendencies throughout the speed range. The pull-out tendency at the highest Mach number, however, was less than that of the brakes considered herein.

Additional tests have been made with the brakes on the configuration consisting of complete model less horizontal tail, the results of which are shown in figure 40. The effect of the brakes on the pitching-moment coefficient of the configuration consisting of complete model and on that of the configuration consisting of complete model less horizontal tail are shown in figure 41. Also shown is the difference between these data which gives the effect of the brakes on the pitching-moment coefficient of the horizontal tail. It appears that the brakes caused slight changes in the flow over the tail except in a few instances; the brakes in the tests of reference 7 caused generally similar flow changes of somewhat greater magnitude over the tail.

Airplane Model of Aspect Ratio 2

The airplane model having a wing and horizontal tail both of aspect ratio 2 is designated as $A = 2$ in the figures. The pitching-moment results are referred to a center-of-gravity position located at 10 percent of the mean aerodynamic chord and 0.31 inch below the fuselage center line. The vertical location of the center of gravity and the wing loading for this configuration were assumed to be the same as those for the airplane model of aspect ratio 4.2. The longitudinal location was chosen so that the static-longitudinal-stability parameter $\partial C_m / \partial C_L$ at a Mach number of 0.6 had the same value as that for the model airplane of aspect ratio 4.2 at a Mach number of 0.6.

The variation of lift, pitching-moment, and drag coefficient with Mach number at various angles of attack is shown in figures 42 to 48. Analysis of these data is contained in the following sections.

Stability.- The variation of pitching-moment coefficient with lift coefficient for the configuration consisting of complete model with the horizontal tail at two incidences and for the configuration consisting of complete model less horizontal tail is shown in figure 49. The variation of pitching-moment coefficient with lift coefficient for the configuration consisting of complete model at three elevator deflections at a constant value of horizontal-tail incidence of -2.1° is shown in figure 50. The stability at an incidence of -2.1° and at some of the deflections became neutral at approximately zero lift for Mach numbers from 0.85 to 0.875, and there were local decreases in stability at higher Mach numbers in the lift-coefficient range from 0.1 to 0.3 (fig. 50). There was indication that the horizontal tail may have been the principal cause of some of the reductions in stability since changes in stability for the two horizontal-tail incidences tested were not similar in several cases (fig. 49). In general, the tendencies toward instability were scattered and occurred over small lift-coefficient ranges so that their existence may have little serious effect on the flight of the airplane. The static-stability parameter $\partial C_m / \partial C_L$ for elevators undeflected at airplane lift coefficients corresponding to level flight at two altitudes is shown in figure 51 (not for trimmed conditions except in fig. 51(c)). A tendency toward instability is indicated at sea-level conditions at a horizontal-tail incidence of -2.1° at Mach numbers from 0.85 to 0.87 (fig. 51(b)). With the elevator undeflected and the horizontal tail used for obtaining trim (fig. 51(c)), the stability characteristics appeared to be satisfactory for Mach numbers up to 0.95. It is to be noted that, since only two horizontal-tail incidences were tested, a linear variation in parameters was assumed between the two points for purposes of interpolation.

Control.- The variation of pitching-moment coefficient with horizontal-tail incidence and elevator deflection at lift coefficients corresponding to level flight at two altitudes is shown in figure 52. The elevator effectiveness $\partial C_m / \partial \delta_e$ (slopes of curves in figs. 52(c) and 52(d)) at Mach numbers greater than 0.875 became zero and possibly reversed for some of the elevator deflections in the range from 0° to 6° . The loss in elevator effectiveness occurred over an elevator-deflection range which increased with Mach number. It is probable that elevator effectiveness could be obtained at the higher Mach numbers by use of larger elevator deflections than those tested. Possible reasons for the loss of elevator effectiveness at supercritical speeds were discussed previously for the airplane of aspect ratio 4.2. Zero elevator effectiveness occurred at Mach numbers as low as those for the horizontal tail of aspect ratio 4.2. The Mach number at which elevator-effectiveness losses would be expected to begin should be approximately 0.03 higher for a horizontal tail of aspect ratio 2 than for one of aspect ratio 4.2, as based on the results of reference 12. Full-span flaps were investigated in the tests of reference 12 on surfaces which had aspect ratios of 1.75 and 3.0, and there were no indications of zero or negative effectiveness,

although large reductions in effectiveness occurred at supercritical speeds. From interpolation of those data, the elevator effectiveness of a horizontal tail of aspect ratio 2 at a Mach number of 0.93 would be expected to be approximately 50 percent of the low-speed value. It would appear therefore that the reduction to zero and the reversal in elevator effectiveness as found in the present tests for the model of aspect ratio 2 at relatively low Mach numbers were associated with interference effects from the fuselage and vertical tail and perhaps with scale effects.

The horizontal-tail effectiveness for trim conditions with the elevator undeflected and the horizontal tail used for obtaining trim and the elevator effectiveness for trim conditions with the horizontal-tail incidence set at -2.1° and the elevators used for obtaining trim at lift coefficients corresponding to level flight at two altitudes were obtained from the data of figure 52 (at $C_m = 0$) and are shown in figure 53. Because of the low aspect ratio, the horizontal-tail effectiveness was small but the decrease in effectiveness at high speeds was much less than for the configuration of aspect ratio 4.2. The sea-level elevator effectiveness at a Mach number of 0.85 had decreased by about 50 percent from its low-speed value. Trim conditions at speeds greater than those shown in figure 53 were not obtained, but the data of figure 52 indicate further losses in elevator effectiveness at the higher speeds. If a larger value of horizontal-tail incidence were used, nearer a trim value at higher speeds, the beginning of the loss in elevator effectiveness could be delayed to higher Mach numbers (figs. 52(c) and 52(d)).

The horizontal-tail incidences required for obtaining trim and the elevator deflection required for obtaining trim at airplane lift coefficients corresponding to level flight at two altitudes were obtained from figure 52 at zero pitching-moment coefficient and are shown in figures 54(a) and 54(b), respectively. An increase in the horizontal-tail incidence required for obtaining trim resulted with increase in speed except for a small decrease in the Mach number range of approximately 0.82 to 0.88. The elevator deflection required for obtaining trim increased with Mach number. The angle of attack corresponding to the conditions of figure 54(a) is shown in figure 54(c). A large variation with Mach number occurred up to a Mach number of 0.9. A small increase in angle of attack corresponding to the loss in wing lift occurred in the Mach number range from 0.9 to 0.93.

Incremental horizontal-tail characteristics.- The lift and drag coefficients of the configuration consisting of complete model less wing less horizontal tail shown in figures 21 and 22 were subtracted from the corresponding data for the configuration consisting of complete model less wing (fig. 47), and these results provide information on incremental horizontal-tail characteristics at two incidences at a model angle of

attack of -0.2° . The incremental horizontal-tail lift and drag coefficients are shown in figure 55 plotted against the free-stream angle of attack of the horizontal tail α_t' . The free-stream angle of attack of the horizontal tail at which the horizontal-tail lift was zero is plotted in figure 56 and was approximately the same as that for the horizontal tail of aspect ratio 4.2 (fig. 28) since the same fuselage and vertical tail were used with both models. The slope of the horizontal-tail lift curve remained approximately constant throughout the Mach number range (fig. 56).

Downwash.- The variation of effective downwash angle with lift coefficient as found from tests with the horizontal tail on and off is shown in figure 57. Abrupt changes in the slope of the downwash curves occurred at low lift coefficients at Mach numbers of 0.875 and above. The lower slopes which occurred between lift coefficients of 0.1 and 0.2 would tend to have a favorable effect on stability, although no general increase in stability was found for the complete model. There was a decrease in downwash angle at lift coefficients corresponding to level flight at two altitudes (fig. 58) up to a Mach number of approximately 0.83, followed by an increase to the highest test speed. This increase in downwash was a factor in producing the increase in the horizontal-tail incidence required for obtaining trim at the highest Mach numbers shown in figure 54.

Horizontal-tail load.- The incremental horizontal-tail lift coefficient required for obtaining trim at various values of g is shown in figure 59. Negative loads existed for all accelerations and Mach number conditions. For level-flight conditions ($g = 1$) the down loads were essentially unaffected for speeds up to a Mach number of 0.6; at higher speeds, there was an increase in the down loads for Mach numbers up to approximately 0.9. Increasing the value of g increased the Mach number at which the down loads began to increase. A rapid decrease in down load followed by a rapid increase occurred in the Mach number range from approximately 0.9 up to 0.95. The changes were much less severe than for the model of larger aspect ratio (fig. 32).

The angle of attack of the horizontal tail for trim conditions with the elevator undeflected and the horizontal tail used for obtaining trim is shown in figure 60(a). The changes in angle of attack of the horizontal tail when the horizontal tail was used for obtaining trim were similar to the changes in horizontal-tail lift coefficient. When the horizontal-tail incidence was held constant and the elevators were used for obtaining trim (fig. 60(b)), large decreases in angle of attack of the horizontal tail occurred with increases in Mach number.

Stability factors.- The factors affecting the stability are shown in figure 61 at lift coefficients of 0.05, 0.15, and 0.3. The measured values of the static longitudinal-stability parameter are shown in

figure 61(e), together with several points computed from the various factors. A horizontal-tail incidence of -2.1° was used for this example.

There was an indication of instability at a Mach number of 0.85 at a lift coefficient of 0.05, but, at the larger values of lift, no instability was present (fig. 61(e)). One cause for the decrease in stability may be attributed to the increase in the stability factor $(\partial C_m / \partial C_L)_{tc}$ for the complete model less horizontal tail at a lift coefficient of 0.05 (fig. 61(a)) which probably was caused by a forward shift in the center of pressure. The changes in the lift-curve slope of the horizontal tail (fig. 61(d)) would also tend to have a destabilizing effect on the stability parameter $(\partial C_m / \partial C_L)_c$. The downwash factor (fig. 61(c)) at a Mach number of 0.85 would tend to have favorable effect on the stability parameter $(\partial C_m / \partial C_L)_c$. The calculated values of the stability parameter $(\partial C_m / \partial C_L)_c$ using these factors did not agree too well with the experimental values. The main reason for the discrepancies is probably due to the inaccuracies involved in the determination of slopes from nonlinear variations in the parameters.

Figure 61 shows that the various component factors which combine to determine the resultant stability parameter $(\partial C_m / \partial C_L)_c$ changed appreciably with Mach number in relatively small Mach number ranges. In many cases, these changes were quite irregular.

Tailless configuration.- When the aspect ratio of a wing is reduced, the magnitude of the change in downwash approaches that of the change in wing angle of attack (that is, $\frac{\partial \epsilon}{\partial \alpha} \rightarrow 1$). This effect causes the horizontal tail to lose its stabilizing effect at a wing aspect ratio somewhat less than 2.0. The possibility of having a tailless airplane with a wing of aspect ratio 2 was therefore considered as regards stability characteristics.

The center-of-gravity position for the complete model less horizontal tail was located 5.6 percent of the mean aerodynamic chord ahead of the leading edge of the mean aerodynamic chord (or at 6 percent of the root chord) to give stable characteristics. The drag component was ignored in this calculation. In figure 62 is shown the static longitudinal stability at lift coefficients corresponding to level flight at two altitudes for the configuration consisting of complete model less horizontal tail with the center of gravity at 10 percent of the mean aerodynamic chord (as used for the tests with the complete model) and ahead of the mean aerodynamic chord a distance 5.6 percent of the mean aerodynamic chord. No great improvement in $(\partial C_m / \partial C_L)_{tc}$ characteristics for the tailless configuration were noted as compared to those for the complete model (fig. 51(c)). However, from information

presented in reference 13, it appears possible that a position of the wing on the fuselage different from the low-wing position tested may show smaller changes in stability and general improvement in other aerodynamic characteristics.

An indication of the effect of small inboard wing tabs on longitudinal control characteristics was obtained from the data of reference 9. In that investigation, a horizontal tail of aspect ratio 4.01 with an inverted NACA 65-108 section was tested with trim tabs at deflections of -10° , 0° , and 10° . The pitching-moment data from this reference were recomputed about an axis 5.6 percent of the mean aerodynamic chord ahead of the leading edge of the mean aerodynamic chord. The data for the inverted NACA 65-108 section were then changed so that the data were applicable to the upright position (camber-up condition). These data for the camber-up condition were combined with the fuselage and vertical-tail data given in figure 21 to obtain the variation with normal-force coefficient of the pitching-moment coefficient of a tailless airplane with a wing of aspect ratio 4.01 (fig. 63). These results indicate that large tab deflections would be required to produce sufficient changes in trim. The tab had a chord 10 percent of the wing chord and a span 50 percent of the wing semispan, and the results are for a wing of aspect ratio 4.01. Tabs of larger area on a wing of aspect ratio 2 would be expected to produce larger trim changes because of the larger loads produced by the tabs and a greater moment arm between the center of gravity and the center of pressure of the load due to the tabs.

Comparisons

Comparison plots have been made of some of the parameters previously presented for the individual configurations. Data from references 7 and 8 also are included. These combined data provide information for aspect ratios from 9 to 2.

Lift and drag.— For each configuration, the angle of attack at a lift coefficient of 0.1 and 0.4 at a Mach number of 0.4 was found. This angle of attack was then held constant, and the resulting variation in lift coefficient with Mach number is shown in figure 64. The effect of decreasing aspect ratio was to increase the force-break Mach number and reduce the lift losses.

The angle of attack for zero lift (fig. 65) showed small change with Mach number until the critical speed was reached. The configuration with wing of aspect ratio 9 and the configuration with wing of aspect ratio 6 experienced large increases in angle of attack for zero lift at speeds above a Mach number of 0.8. The angle of attack for the configuration with wing of aspect ratio 4.2 increased by only 0.7° at speeds

above a Mach number of about 0.86, and the configuration with wing of aspect ratio 2 had a slightly larger change in the angle of attack for zero lift but at speeds above a Mach number of 0.9.

Figure 66 indicates that a decrease in aspect ratio from 4.2 to 2 reduced the drag coefficient at high Mach numbers. The drag of the wing of aspect ratio 9 included calculated induced drag but did not include fuselage and tail effects and therefore was below the general drag level of the other models compared herein. The drag coefficient of the configuration with wing of aspect ratio 6 at trim lift for a wing loading of 40 pounds per square foot was approximately the same as for the configuration with wing of aspect ratio 4.2 above the force-break Mach number. This small difference in drag coefficient for configurations having wings of different aspect ratio may be attributed to improvement in characteristics resulting from the midwing position on the configuration of aspect ratio 6.

Figure 67 indicates more clearly the effect of aspect ratio on the force-break Mach number and on theoretical critical Mach number. The theory of reference 14 has been used to determine approximately the increase in critical Mach number with decrease in aspect ratio for the NACA 65-110 airfoil section (fig. 67) using a two-dimensional maximum critical Mach number of 0.765, which occurs at a lift coefficient somewhat different from zero. Experimental lift-break Mach numbers for the configurations of aspect ratio 2, 4.2, and 6 (reference 7) with wings of NACA 65-110 section are also shown. The lift force-break Mach number for the configuration of aspect ratio 9 with wing of NACA 65-210 section was approximately 0.78. The lift force-break Mach number for a configuration of aspect ratio 9 with a wing of NACA 65-110 section was estimated to be 0.015 higher than the value of 0.78, and this higher value is plotted in figure 67. The lift force-break values were chosen at lift coefficients corresponding approximately to level flight. It may be noted that the difference between the critical and lift force-break Mach numbers increased with an increase in the critical speed (or with a decrease in aspect ratio) and that differences of as much as 0.1 existed at the lower aspect ratios.

Included in figure 67 are the critical Mach numbers for the wings incorporating the NACA 0012 airfoil section predicted by the methods of reference 14 and the experimental lift force-break Mach numbers for the wings incorporating the NACA 0012 section from the data of reference 6. The models tested were untapered surfaces with no fuselage present. The difference between critical Mach number and lift force-break Mach number for the wings of NACA 0012 section for the higher aspect ratios was approximately double that found for the airplane models reported herein. The difference at the low aspect ratios was about the same as that for the complete configurations. Fuselage effects probably reduced the root lift force-break Mach numbers for

wings of large aspect ratio to values below those for the wing-alone case. At lower aspect ratios, the tip relief not only provided higher critical speeds for the surface but also probably reduced the magnitude of the fuselage interference so that the lift force-break and critical Mach number differences were more nearly the same as for the wing-alone conditions.

The difference between the predicted critical Mach number and the lift force-break Mach number at a given aspect ratio can be expressed by the following empirical equation:

$$M_{fb} - M_{cr} = K \frac{M_{cr}}{A} \approx \frac{M_{cr}}{4A}$$

where M_{fb} is the lift force-break Mach number, M_{cr} is the critical Mach number, and K is approximately constant. It was found that, for the model aircraft configurations with tapered wings of NACA 65-110 airfoil section, a value of K of 0.23 gave good agreement with the difference between calculated critical and measured lift force-break Mach numbers. A value of K of 0.28 used with the calculated critical Mach number of the untapered wings of NACA 0012 airfoil section gave good agreement with the measured values. A value of K of 0.25 used with both sets of calculated critical Mach numbers gave estimated force-break Mach numbers different from the measured value by no more than 0.01. It should be remembered that the differences discussed are between the calculated maximum critical Mach number and the lift force-break Mach number at lift coefficients of approximately 0.05 to 0.10.

Drag-coefficient force-break Mach numbers also are shown in figure 67 for the model airplane configurations and the wings of reference 6. Decreasing the aspect ratio increased the drag force-break Mach number, but the drag force-break Mach number was lower than the lift force-break Mach number. In the case of the model airplane configurations, the drag force breaks occurred at Mach numbers which were only from 0 to 0.03 higher than the predicted critical values. In the case of the NACA 0012 wings, the drag force-break Mach numbers were from 0.02 to 0.07 higher than the critical values and much closer to the lift-break Mach numbers than in the case of the model airplane configurations. The differences noted between the wing-alone and model airplane configurations probably were due chiefly to fuselage interference effects and differences in wing section and wing taper. The difference between the critical and the drag force-break Mach number is difficult to estimate by a generalized formula because of sensitivity of drag to small interference effects.

The lift-drag ratio (fig. 68) was reduced considerably at low speeds by a decrease in aspect ratio. At high Mach numbers and low lift

coefficients, however, the lift-drag ratio of the configuration of aspect ratio 2 was greater than that of the configurations of aspect ratio 4.2 and 6.

Stability.- The static-longitudinal-stability parameter $\partial C_m / \partial C_L$ at lift coefficients corresponding to level flight at two altitudes for trim conditions is shown in figure 69. The center-of-gravity position for the configuration of aspect ratio 2 was chosen to give the same stability as that of the configuration of aspect ratio 4.2 at low speeds. Decreasing the aspect ratio reduced the magnitude of the changes in static stability occurring at high Mach number and delayed the onset of the changes to higher Mach numbers. The configuration of aspect ratio 6 experienced static instability at lift coefficients corresponding to level flight at sea level in the Mach number range from 0.86 to 0.89. The configurations of aspect ratios 4.2 and 2 showed no instability for the trim conditions (fig. 69), although instability or a tendency toward instability was evident for some of the untrimmed conditions (figs. 14 and 51). The Mach number range in which serious instability may occur is indicated in figure 67. The range occurred at Mach numbers from 0.03 to 0.07 larger than the lift force-break Mach numbers and increased with a decrease in aspect ratio. The configuration of aspect ratio 2 showed a tendency toward instability at a Mach number of approximately 0.85 (fig. 51(b) and fig. 61(e) at an airplane lift coefficient of 0.05) which was less than the lift force-break Mach number.

Control.- Figure 70 shows the effectiveness of the horizontal tail and elevator for the various configurations at airplane lift coefficients corresponding to level flight at two altitudes for trim conditions. At low Mach numbers, the configuration of aspect ratio 2 had much lower horizontal-tail and elevator effectiveness than the configurations of aspect ratio 4.2 and 6 (horizontal-tail aspect ratios of 4.2 and 5, respectively) because of the low lift-curve slope of the horizontal tail of aspect ratio 2. At Mach numbers above approximately 0.8, there was a large reduction in horizontal-tail effectiveness for the configurations of aspect ratios 4.2 and 6 (horizontal-tail aspect ratios of 4.2 and 5, respectively). For the configuration of aspect ratio 2, there was relatively small change in horizontal-tail effectiveness up to the highest test Mach number. The elevator effectiveness of the configurations of aspect ratio 4.2 and 6 (horizontal-tail aspect ratios of 4.2 and 5, respectively) varied abruptly at the high speeds. The elevator effectiveness of the configuration of aspect ratio 2 gradually decreased with Mach number so that the value at a Mach number of 0.85 was about 50 percent of that at low speeds. It has been brought out previously that zero or reversed elevator effectiveness can be expected at higher Mach numbers for configurations of both aspect ratio 2 and 4.2. It appears that reducing the horizontal-tail aspect ratio, at least for the configurations tested, did not improve high-speed elevator effectiveness and that scale effects and interference effects from the fuselage and vertical tail may have nullified the expected improvement.

Figure 71 presents the horizontal-tail incidence and the elevator deflection required for obtaining trim at airplane lift coefficients corresponding to level flight at two altitudes. A gradual increase in the horizontal-tail incidence and the elevator deflection required for obtaining trim occurred for all configurations up to a Mach number which was between the drag and lift force-break Mach numbers. At higher Mach numbers, abrupt changes of the horizontal-tail incidence and the elevator deflection required for obtaining trim were necessary. The magnitude of the changes in the horizontal-tail incidence required for obtaining trim appeared to be approximately the same for all three aspect ratios, probably because the lower lift-curve slope of the horizontal tails of smaller aspect ratio required larger horizontal-tail incidence changes to obtain trim, even though adverse compressibility effects were reduced by the lower aspect ratio. The changes in the elevator deflection required for obtaining trim at supercritical Mach numbers appeared to be increased for the lower aspect ratios for the same reason. It appears that abrupt changes in control positions will be necessary at Mach numbers near the lift force-break Mach number.

The airplane angle of attack at airplane lift coefficients corresponding to level flight at two altitudes for trim conditions is shown in figure 72. This figure shows that much larger angles of attack were required for the configuration of aspect ratio 2.0 than for the configuration of aspect ratio 4.2, even though the former configuration had a wing incidence which was 0.5° greater. The level-flight lift coefficient of the configuration of aspect ratio 6 was less than that of the configuration of aspect ratio 4.2; the data of figure 72, however, illustrate the effect of aspect ratio on the compressibility changes. The angle of attack decreased up to the lift force-break Mach numbers. At higher speeds, an increase in angle of attack was required, the amount being less for the lower aspect ratios. In the Mach number range in which an increase in angle of attack was required, the horizontal-tail incidence in most cases had to be increased to obtain trim.

CONCLUSIONS

An investigation was made in the Langley 8-foot high-speed tunnel of two transonic research airplane models for Mach numbers up to approximately 0.95. The wing and horizontal tail of one model were both of aspect ratio 4.2; the wing and horizontal tail of the other were both of aspect ratio 2. Both models had unswept wings with NACA 65-110 airfoil sections and unswept horizontal tails with NACA 65-008 airfoil sections. The test Reynolds number at the highest speed was 1.6×10^6 for one model and 2.3×10^6 for the other model. The following conclusions are indicated:

1. A reduction in aspect ratio increased the force-break Mach number and reduced the magnitude of the compressibility effects on lift, drag, and pitching moment. Adverse stability and control characteristics usually appeared after force-break Mach numbers had been reached.

2. Static longitudinal instability was noted for the configuration of aspect ratio 4.2 at low and negative lift coefficients in the Mach number range from 0.87 to 0.92, which was approximately 0.05 above the lift force-break Mach number. The chief cause of the instability was the wing-fuselage characteristics. A small localized instability was noted for the configuration of aspect ratio 2 at a Mach number of 0.85, but no severe supercritical instability was observed for the speeds covered. The component parameters which determined the over-all stability characteristics varied in a generally nonlinear manner at supercritical speeds with abrupt changes occurring in relatively small Mach number ranges.

3. The horizontal-tail effectiveness for the configuration of aspect ratio 4.2 decreased at high speeds but otherwise appeared satisfactory. The horizontal-tail effectiveness for the configuration of aspect ratio 2 was appreciably less than that for the configuration of aspect ratio 4.2; the decrease in effectiveness at high speeds was much smaller and the onset of the decrease occurred at higher Mach numbers for the model of lower aspect ratio.

4. The elevator effectiveness was zero in a small range of elevator deflections for both aspect ratios at a Mach number of 0.875; at higher speeds, there was a reversal in elevator effectiveness for both aspect ratios. The expected improvement in elevator-effectiveness characteristics as a result of the lower aspect ratio was modified probably by interference effects from the fuselage and vertical tail and perhaps by scale effects. Tests on the configuration of aspect ratio 4.2 with artificial roughness on the horizontal tail did not show the reversal in elevator effectiveness observed at high speeds for the model in the smooth condition. The roughness tests still showed the reduction in elevator effectiveness at high Mach numbers.

5. An appreciable effective downflow in the vicinity of the horizontal tail as a result of interference effects between the fuselage, vertical tail, and horizontal tail was observed for the configuration consisting of fuselage, vertical tail, and horizontal tail. This downflow increased with Mach number.

6. Air brakes on the fuselage of the configuration of aspect ratio 4.2 were not sufficiently effective to decrease the terminal Mach number to values below those at which difficulties in stability

and control were indicated. The effect of the brakes was indicated to be due to the direct action of the brakes and not due to the brakes changing the flow over the tail.

Langley Aeronautical Laboratory
National Advisory Committee for Aeronautics
Langley Air Force Base, Va.

REFERENCES

1. Wright, John B., and Loving, Donald L.: High-Speed Wind-Tunnel Tests of a $\frac{1}{16}$ -Scale Model of the D-558 Research Airplane. Lift and Drag Characteristics of the D-558-1 and Various Wing and Tail Configurations. NACA RM L6J09, 1947.
2. Wright, John B.: High-Speed Wind-Tunnel Tests of a $\frac{1}{16}$ -Scale Model of the D-558 Research Airplane. Basic Longitudinal Stability of the D-558-1. NACA RM L7K24, 1948.
3. Wright, John B.: High-Speed Wind-Tunnel Tests of a $\frac{1}{16}$ -Scale Model of the D-558 Research Airplane. D-558-1 Speed Reduction Brake and Symmetrical-Profile Wing Characteristics. NACA RM L8B06, 1948.
4. Wright, John B.: High-Speed Wind-Tunnel Tests of a $\frac{1}{16}$ -Scale Model of the D-558 Research Airplane. Longitudinal Stability and Control of the D-558-1. NACA RM L8C23, 1948.
5. Robinson, Harold L.: High-Speed Wind-Tunnel Tests of a $\frac{1}{16}$ -Scale Model of the D-558 Research Airplane - Dynamic Pressure and Comparison of Point and Effective Downwash at the Tail of the D-558-1. NACA RM L8H05, 1948.
6. Stack, John, and Lindsey, W. F.: Characteristics of Low-Aspect-Ratio Wings at Supercritical Mach Numbers. NACA Rep. 922, 1949.
7. Mattson, Axel T., and Loving, Donald L.: Force, Static Longitudinal Stability, and Control Characteristics of a $\frac{1}{16}$ -Scale Model of the Bell XS-1 Transonic Research Airplane at High Mach Numbers. NACA RM L8A12, 1948.
8. Whitcomb, Richard T.: An Investigation of the Effects of Sweep on the Characteristics of a High-Aspect-Ratio Wing in the Langley 8-Foot High-Speed Tunnel. NACA RM L6J01a, 1947.
9. Bielat, Ralph P.: An Investigation at High Speeds of a Horizontal-Tail Model in the Langley 8-Foot High-Speed Tunnel. NACA RM L6L10b, 1947.

10. Lindsey, W. F.: Effect of Compressibility on the Pressures and Forces Acting on an NACA 65,3-019 Airfoil Having an 0.2 Chord Flap. NACA ACR L5G31a, 1946.
11. Zalovcik, John A., and Sawyer, Richard H.: Longitudinal Stability and Control Characteristics of a Semispan Airplane Model at Transonic Speeds from Tests by the NACA Wing-Flow Method. NACA ACR L6E15, 1946.
12. Sandahl, Carl A.: Free-Flight Investigation of Control Effectiveness of Full-Span, 0.2-Chord Plain Ailerons at High Subsonic, Transonic, and Supersonic Speeds to Determine Some Effects of Wing Sweepback, Taper, Aspect Ratio, and Section Thickness Ratio. NACA RM L7F30, 1947.
13. Mathews, Charles W., and Thompson, Jim Rogers: Comparison of the Transonic Drag Characteristics of Two Wing-Body Combinations Differing Only in the Location of the 45° Sweptback Wing. NACA RM L7I01, 1947.
14. Hess, Robert V., and Gardner, Clifford S.: Study by the Prandtl-Glauert Method of Compressibility Effects and Critical Mach Number for Ellipsoids of Various Aspect Ratios and Thickness Ratios. NACA TN 1792, 1949.

TABLE 1

SPECIFICATIONS OF AIRPLANE MODELS

	<u>Airplane model of aspect ratio 4.2</u>	<u>Airplane model of aspect ratio 2</u>
Wing section	NACA 65-110	NACA 65-110
Wing aspect ratio	4.17	2.00
Wing taper ratio	0.54	0.54
Wing span, in.	18.76	13.00
Wing area, sq ft	0.587	0.587
Wing mean aerodynamic chord, in.	4.656	6.687
Wing incidence angle, deg	2.0	2.5
Wing dihedral, deg	4.0	4.0
Wing sweep angle, 50 percent chord, deg	0	0
Wing root chord, in.	5.88	8.44
Wing tip chord, in.	3.17	4.55
Location of 25 percent M.A.C. from nose-inlet station, in.	11.96	11.96
Center of gravity to 25 percent M.A.C., in.	0	1.0
Tail length, $l_{\alpha=0}$, in.	11.13	11.64
Tail height, $h_{\alpha=0}$, in.	2.84	2.84
Horizontal-tail section	NACA 65-008	NACA 65-008
Horizontal-tail aspect ratio	4.17	2.07
Horizontal-tail taper ratio	0.55	0.56
Horizontal-tail area, sq ft	0.14	0.14
Horizontal-tail span, in.	9.18	6.50
Horizontal-tail mean aerodynamic chord, in.	2.26	3.24
Horizontal-tail dihedral, deg	0	0
Horizontal-tail sweep, 75 percent chord, deg	0	0
Horizontal-tail root chord, in.	2.84	4.04
Horizontal-tail tip chord, in.	1.56	2.25
Elevator area, percent horizontal- tail area	25	25
Elevator chord, percent horizontal- tail chord	25	25

TABLE II
EFFECT OF VARIOUS PARAMETERS ON THE HORIZONTAL-TAIL INCIDENCE REQUIRED FOR OBTAINING TRIM

Mach number range	Direction of resultant change in measured $i_t(C_m)_{c=0}$ (from fig. 35(f))	Direction in which the change in any one of the various parameters would tend to change the parameter $i_t(C_m)_{c=0}$									
		Same direction				No change		Opposite direction			
0.4 - 0.75	Gradual increase	$\left(\frac{\partial C_L}{\partial \alpha}\right)_{tc}$				ϵ	$\alpha(C_L)_{tc=0}$	$(C_m)_{tc}$	$\left(\frac{\partial C_m}{\partial i_t}\right)_c$		
0.75 - 0.8	Gradual increase	$\left(\frac{\partial C_L}{\partial \alpha}\right)_{tc}$	$\left(\frac{\partial C_m}{\partial i_t}\right)_c$			ϵ	$\alpha(C_L)_{tc=0}$	$(C_m)_{tc}$			
0.8 - 0.825	Decrease	$(C_m)_{tc}$	$\left(\frac{\partial C_m}{\partial i_t}\right)_c$	$\left(\frac{\partial C_L}{\partial \alpha}\right)_{tc}$		ϵ	$\alpha(C_L)_{tc=0}$				
0.825 - 0.85	Decrease	$(C_m)_{tc}$	$\left(\frac{\partial C_m}{\partial i_t}\right)_c$	$\alpha(C_L)_{tc=0}$	$\left(\frac{\partial C_L}{\partial \alpha}\right)_{tc}$	ϵ					
0.85 - 0.875	Slight decrease	$\left(\frac{\partial C_m}{\partial i_t}\right)_c$	ϵ	$\alpha(C_L)_{tc=0}$		$\left(\frac{\partial C_L}{\partial \alpha}\right)_{tc}$		$(C_m)_{tc}$			
0.875 - 0.91	Increase	$(C_m)_{tc}$	$\left(\frac{\partial C_m}{\partial i_t}\right)_c$	ϵ	$\left(\frac{\partial C_L}{\partial \alpha}\right)_{tc}$			$\alpha(C_L)_{tc=0}$			
0.92 - 0.93	Decrease	$(C_m)_{tc}$						ϵ	$\alpha(C_L)_{tc=0}$	$\left(\frac{\partial C_L}{\partial \alpha}\right)_{tc}$ $\left(\frac{\partial C_m}{\partial i_t}\right)_c$	
0.93 - 0.95	Decrease	$(C_m)_{tc}$	ϵ	$\left(\frac{\partial C_m}{\partial i_t}\right)_c$				$\alpha(C_L)_{tc=0}$	$\left(\frac{\partial C_L}{\partial \alpha}\right)_{tc}$		



TABLE III
EFFECT OF VARIOUS PARAMETERS ON THE ELEVATOR DEFLECTION REQUIRED FOR OBTAINING TRIM

Mach number range	Direction of resultant change in measured $\delta_e (C_m)_{c=0}$ (from fig. 36(a))	Direction in which the change in any one of the various parameters would tend to change the parameter $\delta_e (C_m)_{c=0}$											
		Same direction*			No change			Opposite direction*					
0.4 - 0.5	Increase		$\left(\frac{\partial C_L}{\partial \alpha}\right)_{tc}$	$\left(\frac{\partial C_m}{\partial \delta_e}\right)_c$		ε	$\alpha(C_L)_{tc=0}$		$(C_m)_{tc}$	$\left(\frac{\partial C_m}{\partial \delta_e}\right)_c$			
0.5 - 0.6	Increase	$\left(\frac{\partial C_m}{\partial \delta_e}\right)_c$	$\left(\frac{\partial C_L}{\partial \alpha}\right)_{tc}$			ε	$\alpha(C_L)_{tc=0}$		$(C_m)_{tc}$	$\left(\frac{\partial C_m}{\partial \delta_e}\right)_c$			
0.6 - 0.8	Increase	$\left(\frac{\partial C_m}{\partial \delta_e}\right)_c$	$\left(\frac{\partial C_L}{\partial \alpha}\right)_{tc}$			ε	$\alpha(C_L)_{tc=0}$		$\left(\frac{\partial C_m}{\partial \delta_e}\right)_c$	$(C_m)_{tc}$			
0.8 - 0.825	Decrease	$\left(\frac{\partial C_L}{\partial \alpha}\right)_{tc}$	$\left(\frac{\partial C_m}{\partial \delta_e}\right)_c$	$(C_m)_{tc}$		ε	$\alpha(C_L)_{tc=0}$	$\left(\frac{\partial C_m}{\partial \delta_e}\right)_c$					
0.825 - 0.85	Decrease	$\left(\frac{\partial C_L}{\partial \alpha}\right)_{tc}$	$\alpha(C_L)_{tc=0}$	$(C_m)_{tc}$		ε	$\left(\frac{\partial C_m}{\partial \delta_e}\right)_c$		$\left(\frac{\partial C_m}{\partial \delta_e}\right)_c$				
0.85 - 0.875	No change*	$\left(\frac{\partial C_m}{\partial \delta_e}\right)_c$	$(C_m)_{tc}$			$\left(\frac{\partial C_L}{\partial \alpha}\right)_{tc}$			$\left(\frac{\partial C_m}{\partial \delta_e}\right)_c$	ε	$\alpha(C_L)_{tc=0}$		
0.875 - 0.88	Increase	$\left(\frac{\partial C_L}{\partial \alpha}\right)_{tc}$	$(C_m)_{tc}$	ε	$\left(\frac{\partial C_m}{\partial \delta_e}\right)_c$				$\alpha(C_L)_{tc=0}$	$\left(\frac{\partial C_m}{\partial \delta_e}\right)_c$			
0.88 - 0.91	Increase	ε	$(C_m)_{tc}$	$\left(\frac{\partial C_m}{\partial \delta_e}\right)_c$	$\left(\frac{\partial C_L}{\partial \alpha}\right)_{tc}$				$\left(\frac{\partial C_m}{\partial \delta_e}\right)_c$	$\alpha(C_L)_{tc=0}$			
0.92 - 0.93	Decrease	$(C_m)_{tc}$	$\left(\frac{\partial C_m}{\partial \delta_e}\right)_c$						ε	$\alpha(C_L)_{tc=0}$	$\left(\frac{\partial C_L}{\partial \alpha}\right)_{tc}$	$\left(\frac{\partial C_m}{\partial \delta_e}\right)_c$	
0.93 - 0.95	Decrease	$(C_m)_{tc}$	ε	$\left(\frac{\partial C_m}{\partial \delta_e}\right)_c$					$\alpha(C_L)_{tc=0}$	$\left(\frac{\partial C_L}{\partial \alpha}\right)_{tc}$	$\left(\frac{\partial C_m}{\partial \delta_e}\right)_c$		

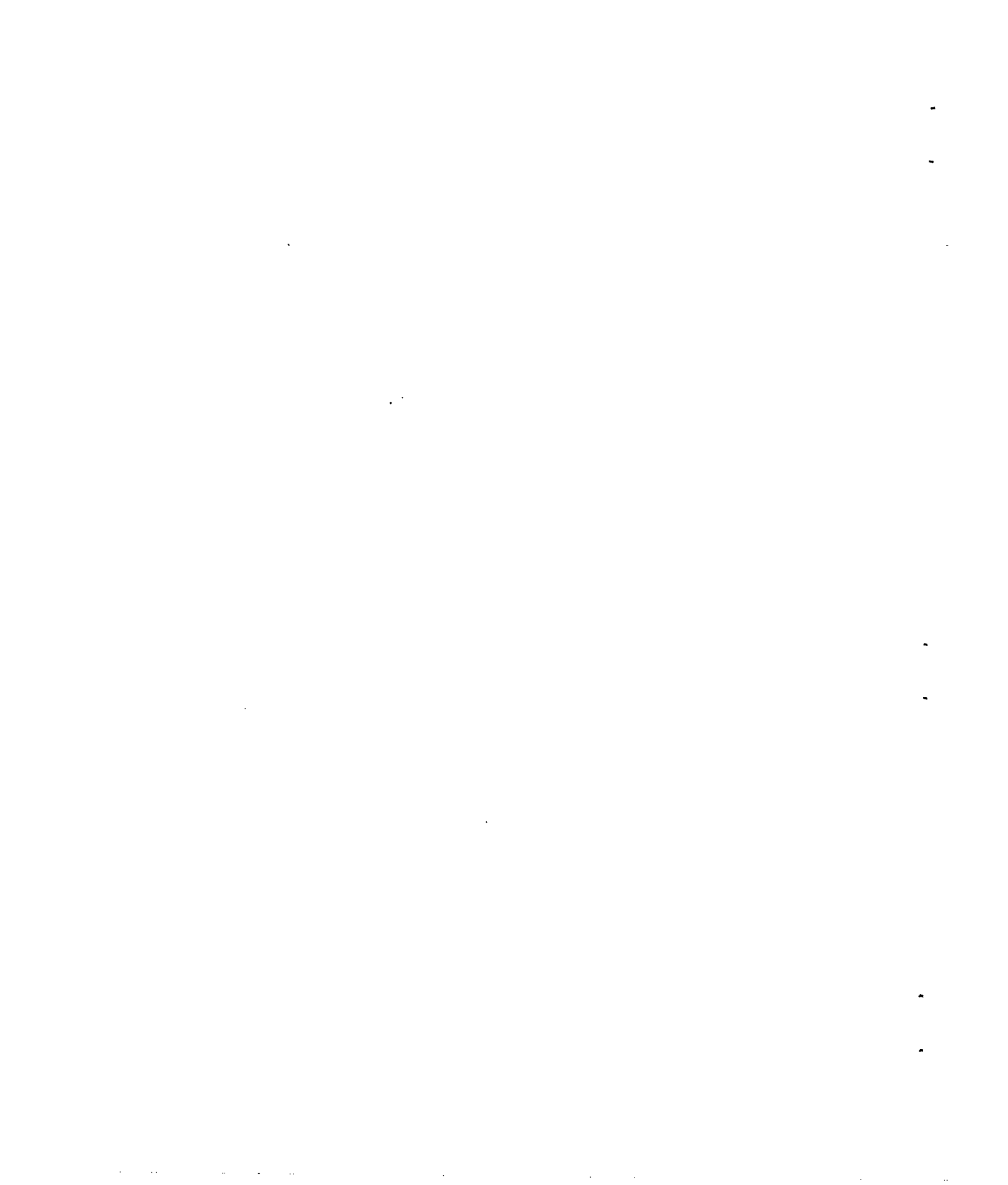
*One Mach number range existed in which there was no resultant change in the elevator deflection required for obtaining trim. In this case, a parameter was listed under "Same direction" if its change would tend to increase the elevator deflection required for obtaining trim, or under "Opposite direction" if its change would tend to decrease the elevator deflection required for obtaining trim.







Figure 1.- Airplane model on sting support in test section of Langley
8-foot high-speed tunnel.



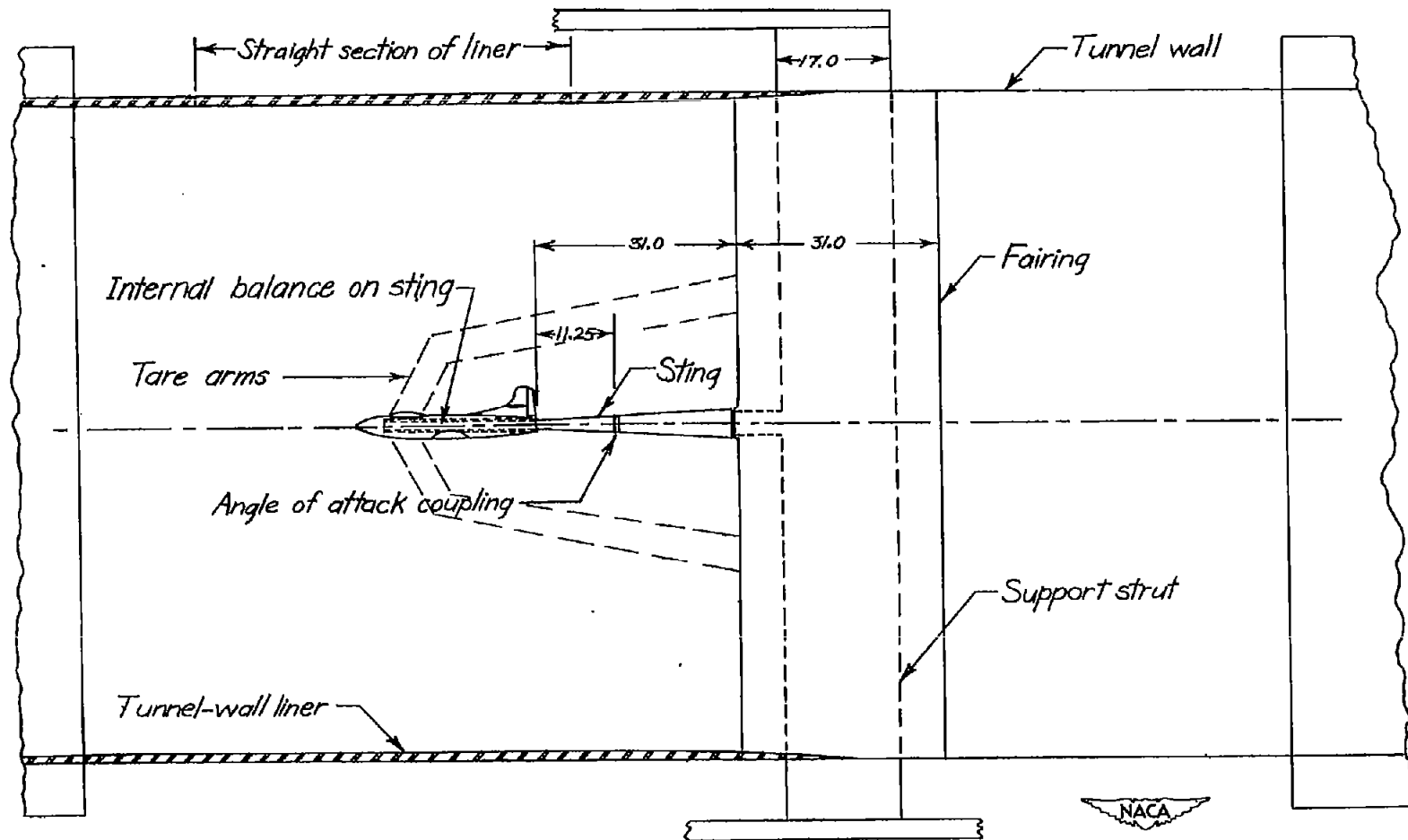


Figure 2.- Location of model on sting support in the Langley 8-foot high-speed tunnel. All dimensions in inches.

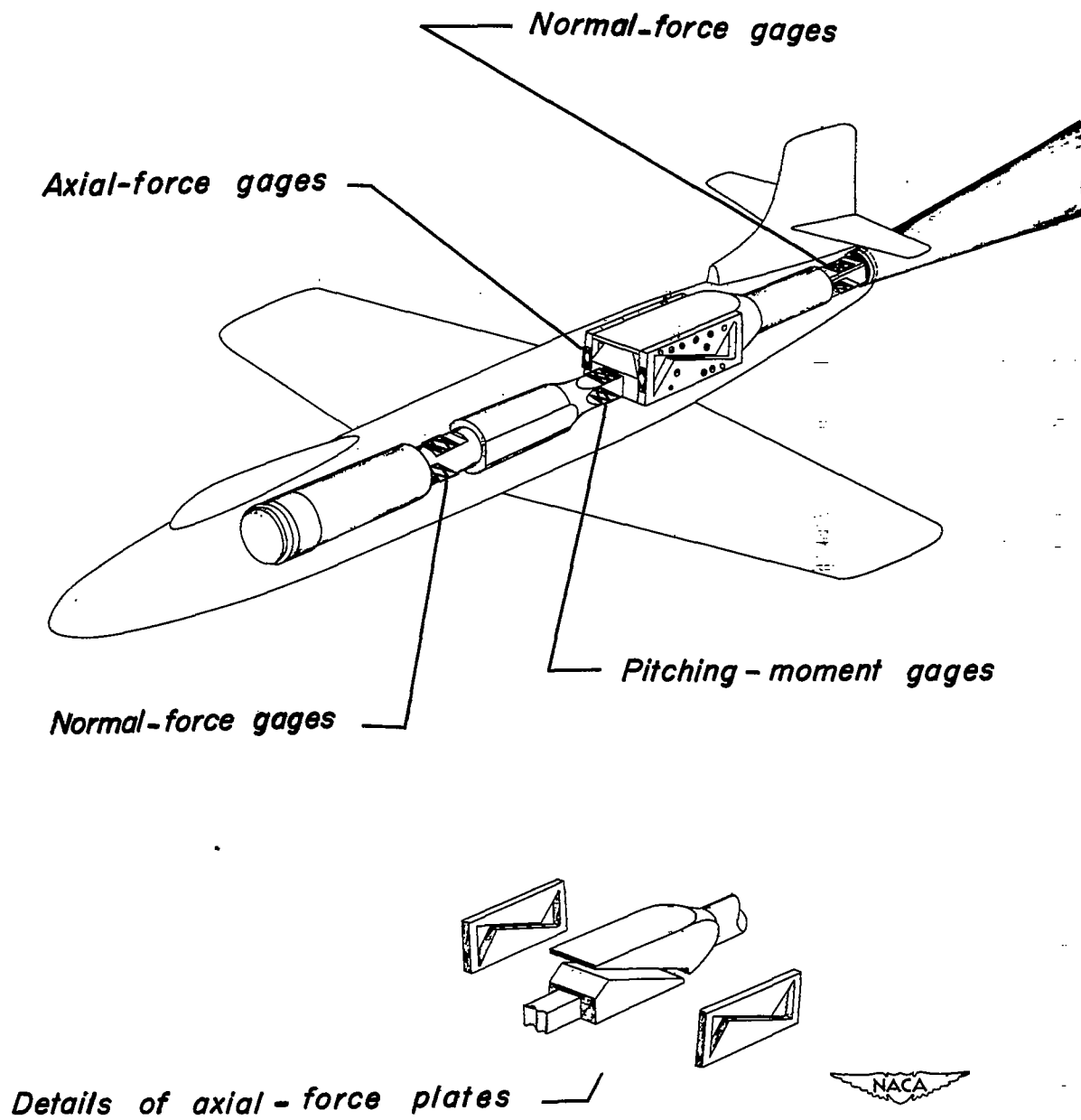


Figure 3.- Internal strain-gage balance.

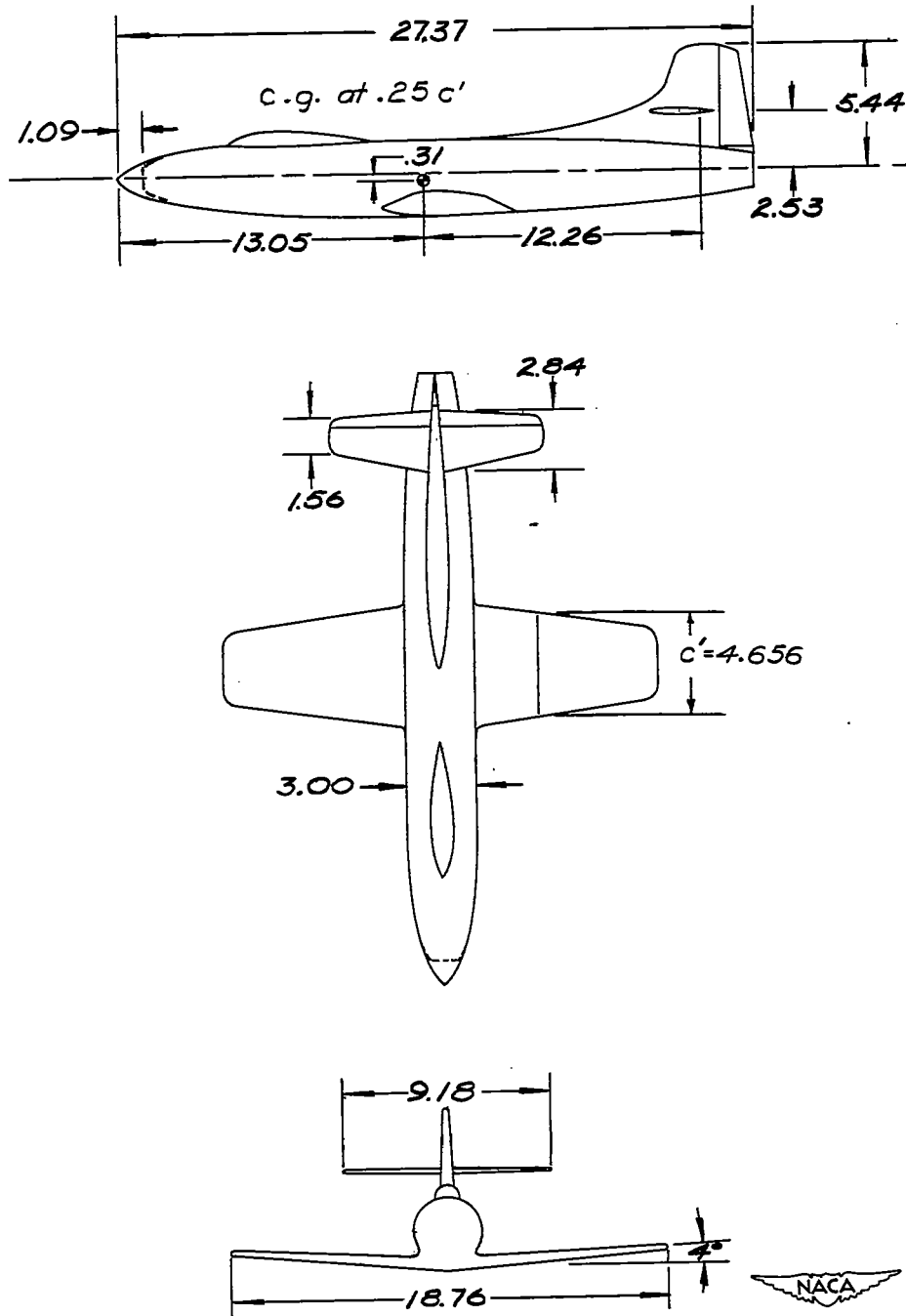


Figure 4.- Dimensions of $\frac{1}{16}$ -scale model with wing and horizontal tail of aspect ratio 4.2. All dimensions in inches.

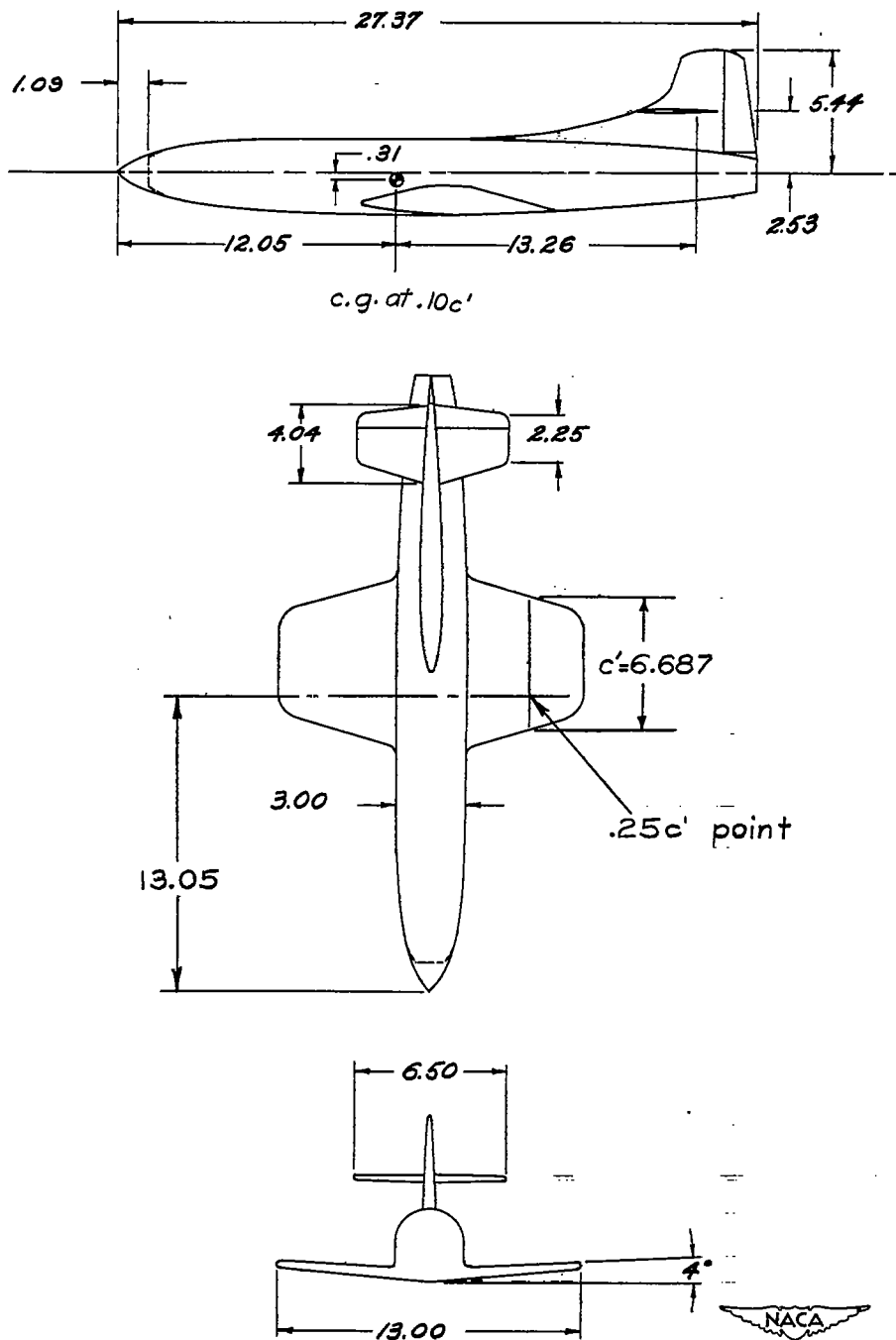
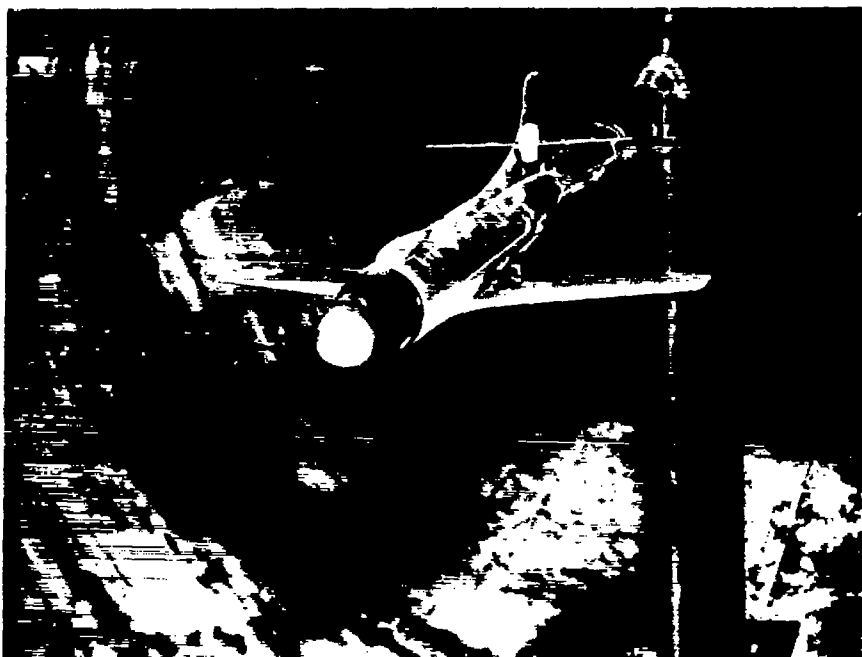
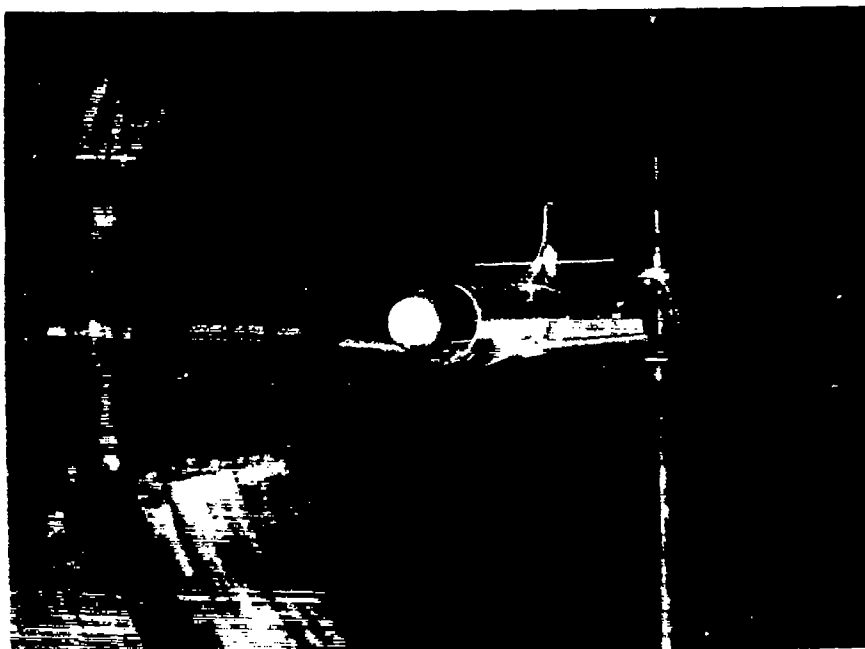


Figure 5.- Dimensions of $\frac{1}{16}$ -scale model with wing and horizontal tail of aspect ratio 2. All dimensions in inches.



(a) Airplane model of aspect ratio 4.2.

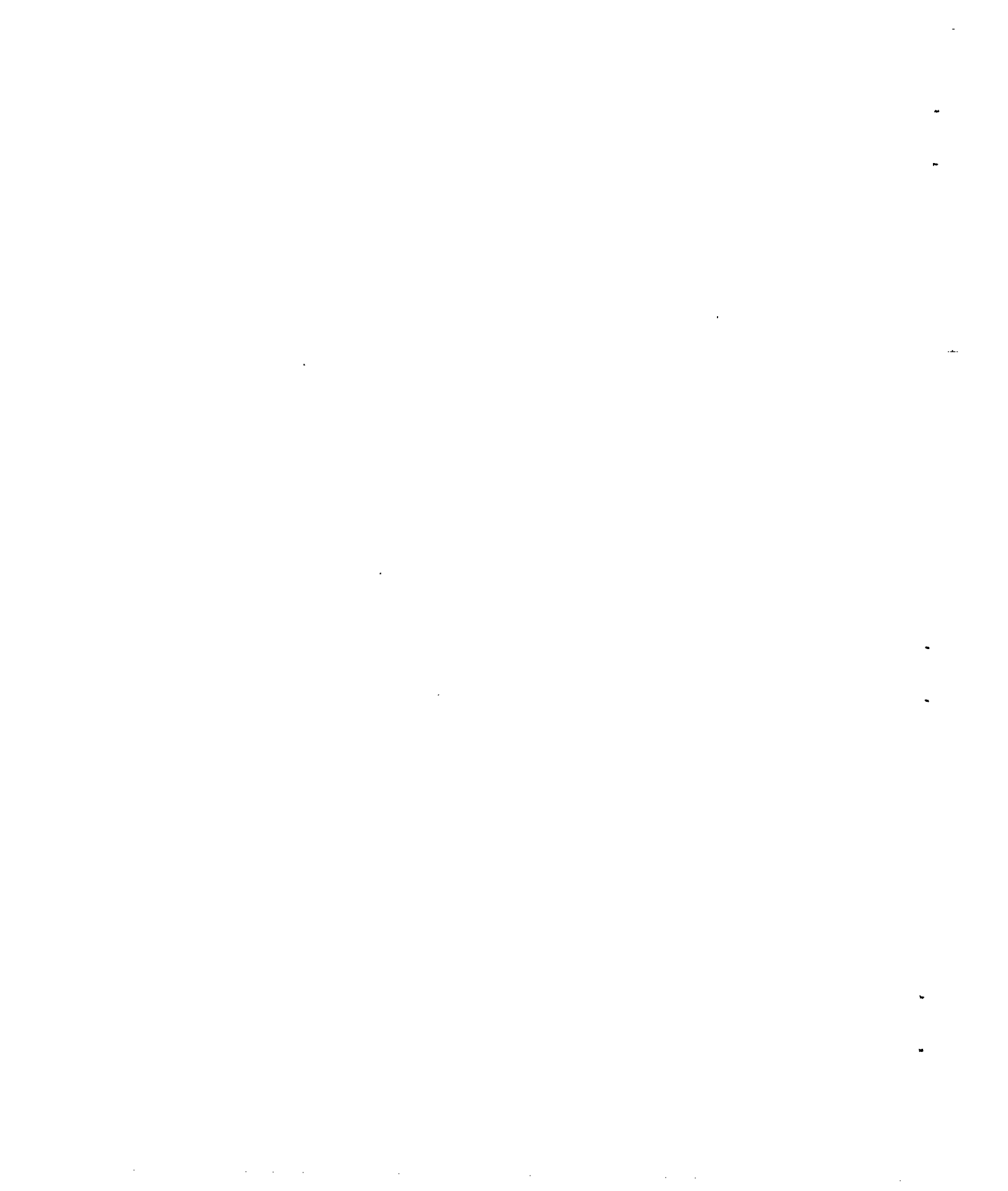
NACA
L-53727



(b) Airplane model of aspect ratio 2.

Figure 6.- Airplane models tested.

NACA
L-53787



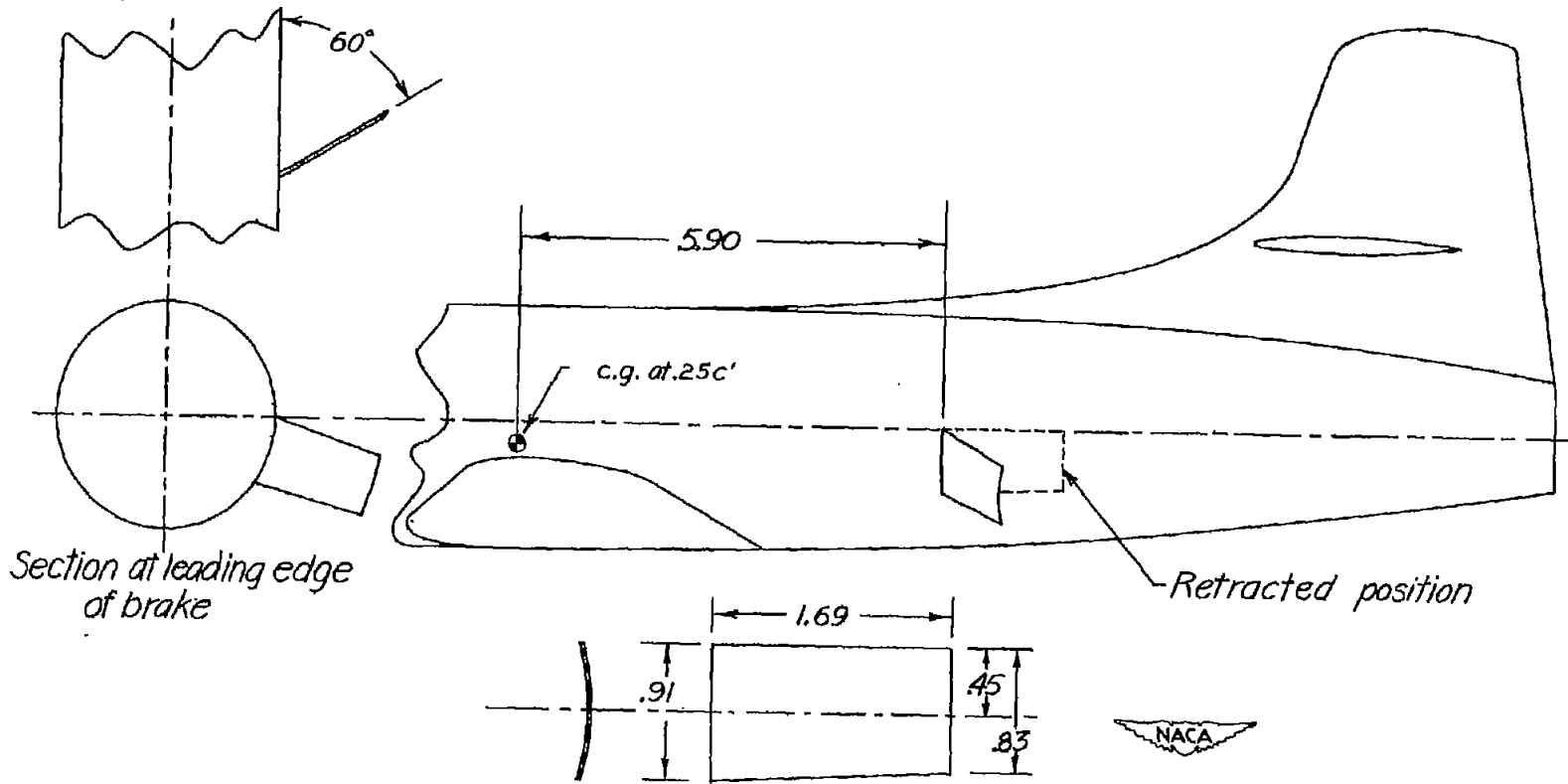
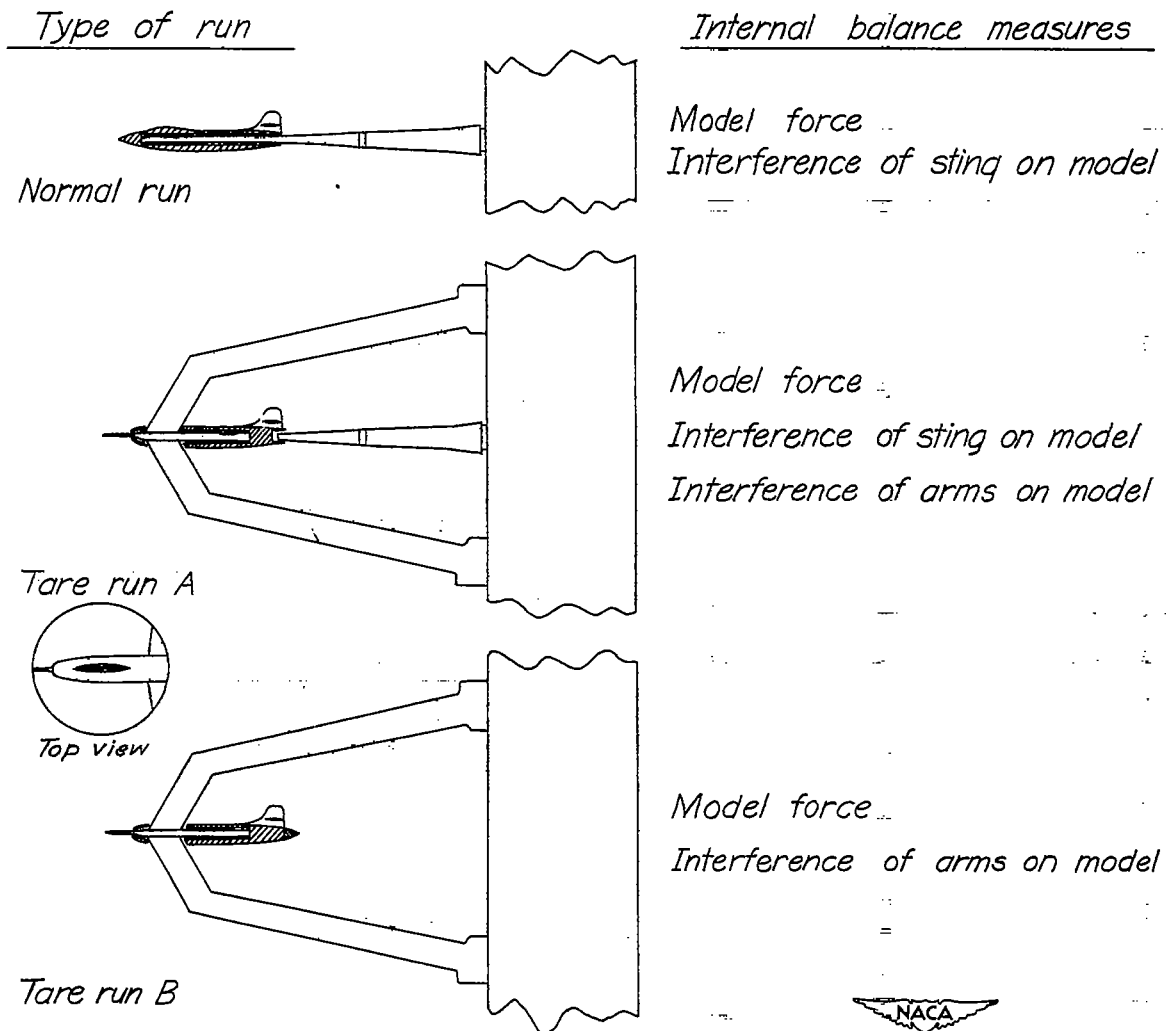


Figure 7.- Dimensions and location of air brakes tested on airplane model of aspect ratio 4.2. All dimensions in inches.



$Tare\ run\ A - Tare\ run\ B = Interference\ of\ sting\ on\ model$

$Normal\ run - (A - B) = Model\ force$

Figure 8.- Procedure for determining aerodynamic interference of sting on model.

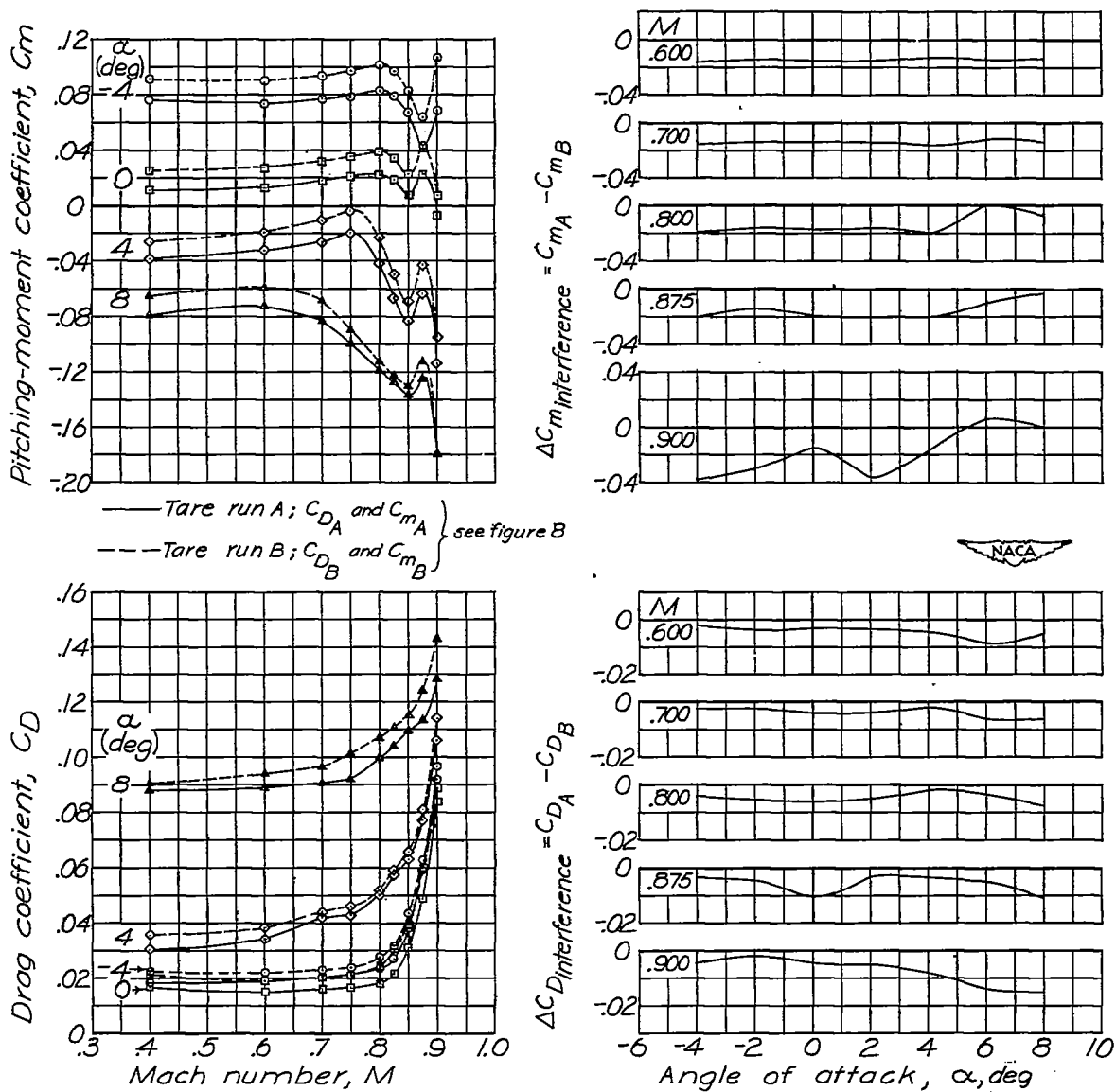


Figure 9.- Typical plots used in determining sting interference on pitching-moment coefficient and drag coefficient. Complete model; $A = 4.2$; $i_t = 2.2^\circ$; $\delta_e = 0^\circ$.

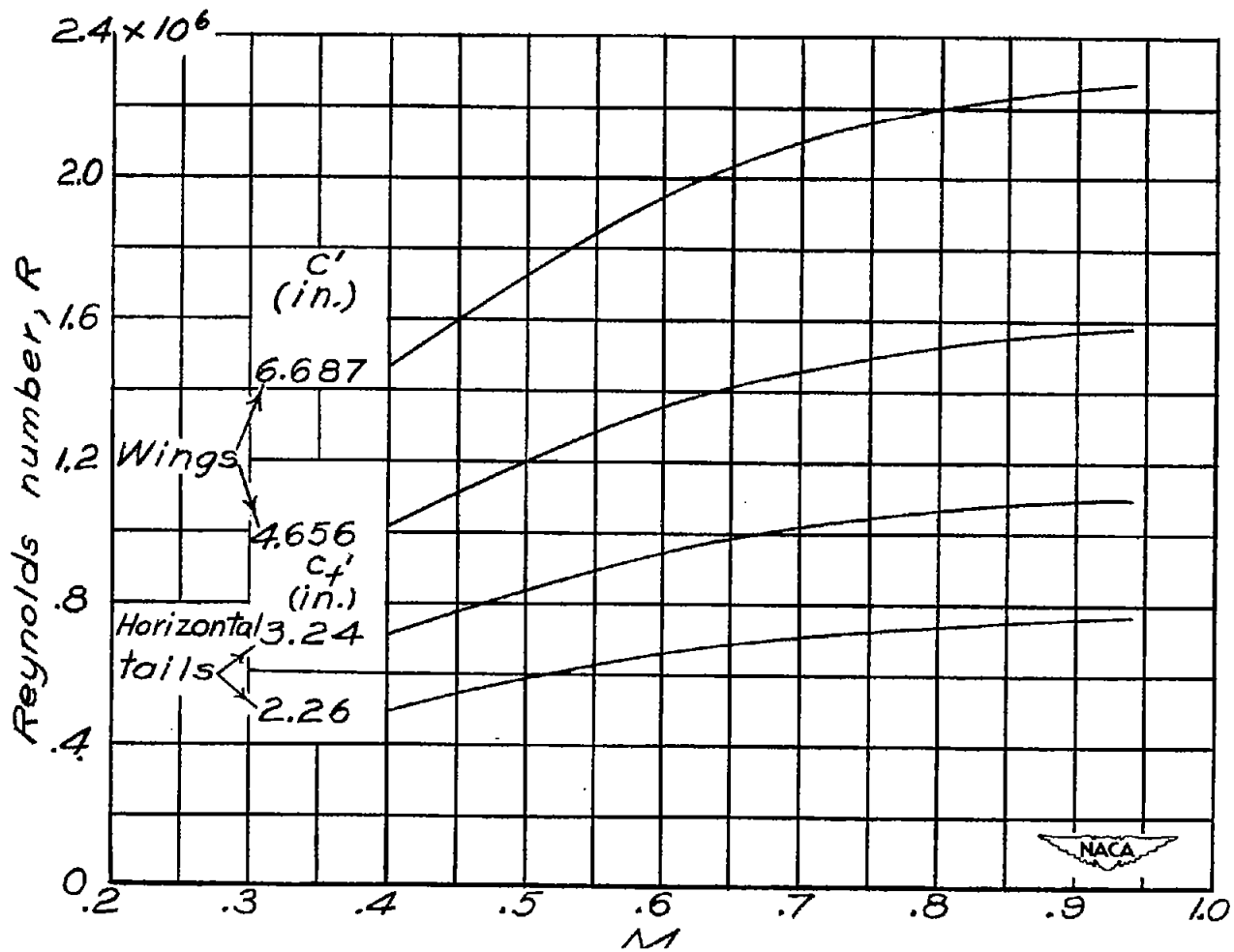


Figure 10.- Variation of test Reynolds number with test Mach number.

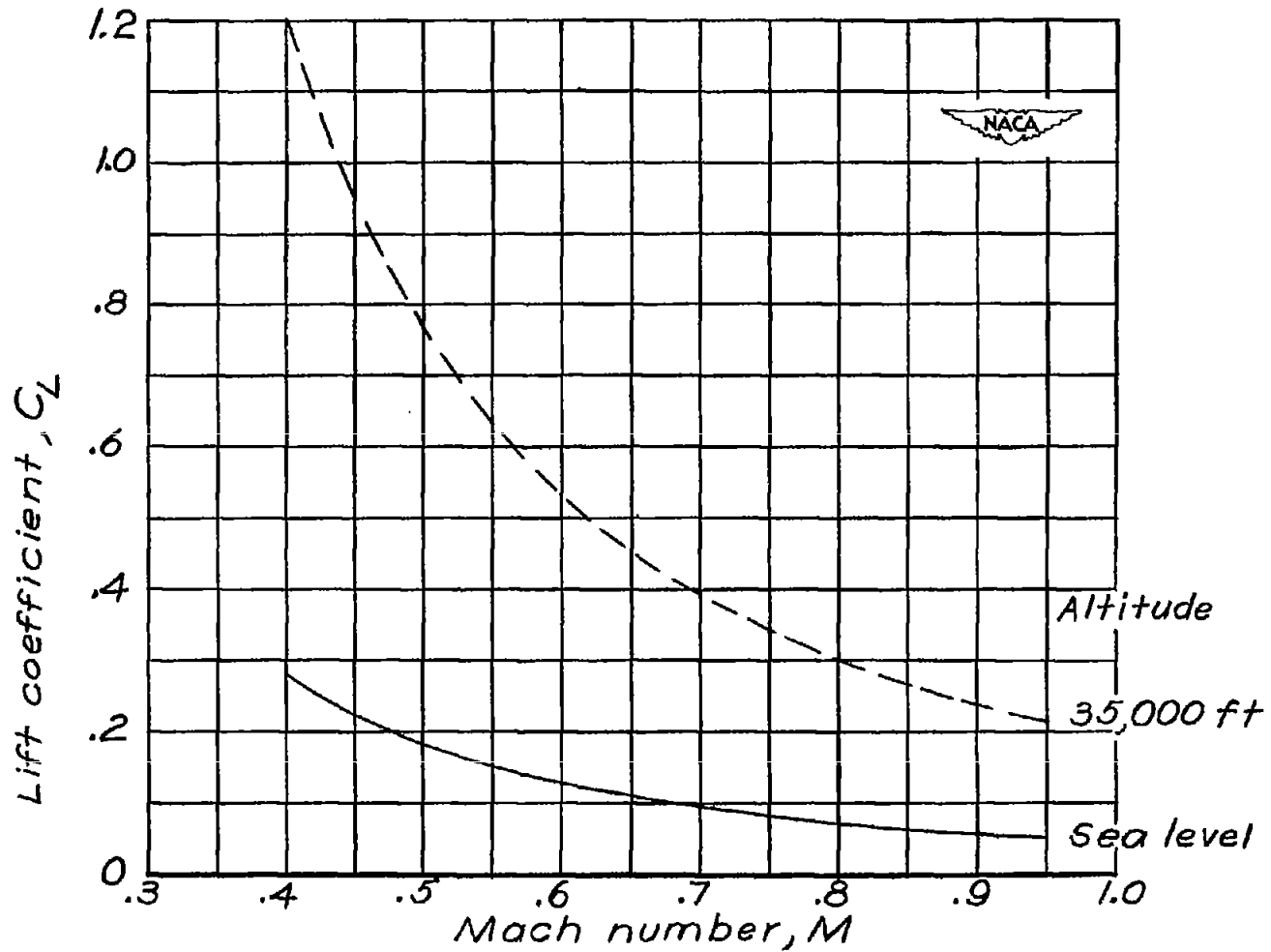


Figure 11.- Variation with Mach number of the airplane lift coefficient corresponding to level flight at two altitudes for a wing loading of 66.7 pounds per square foot.

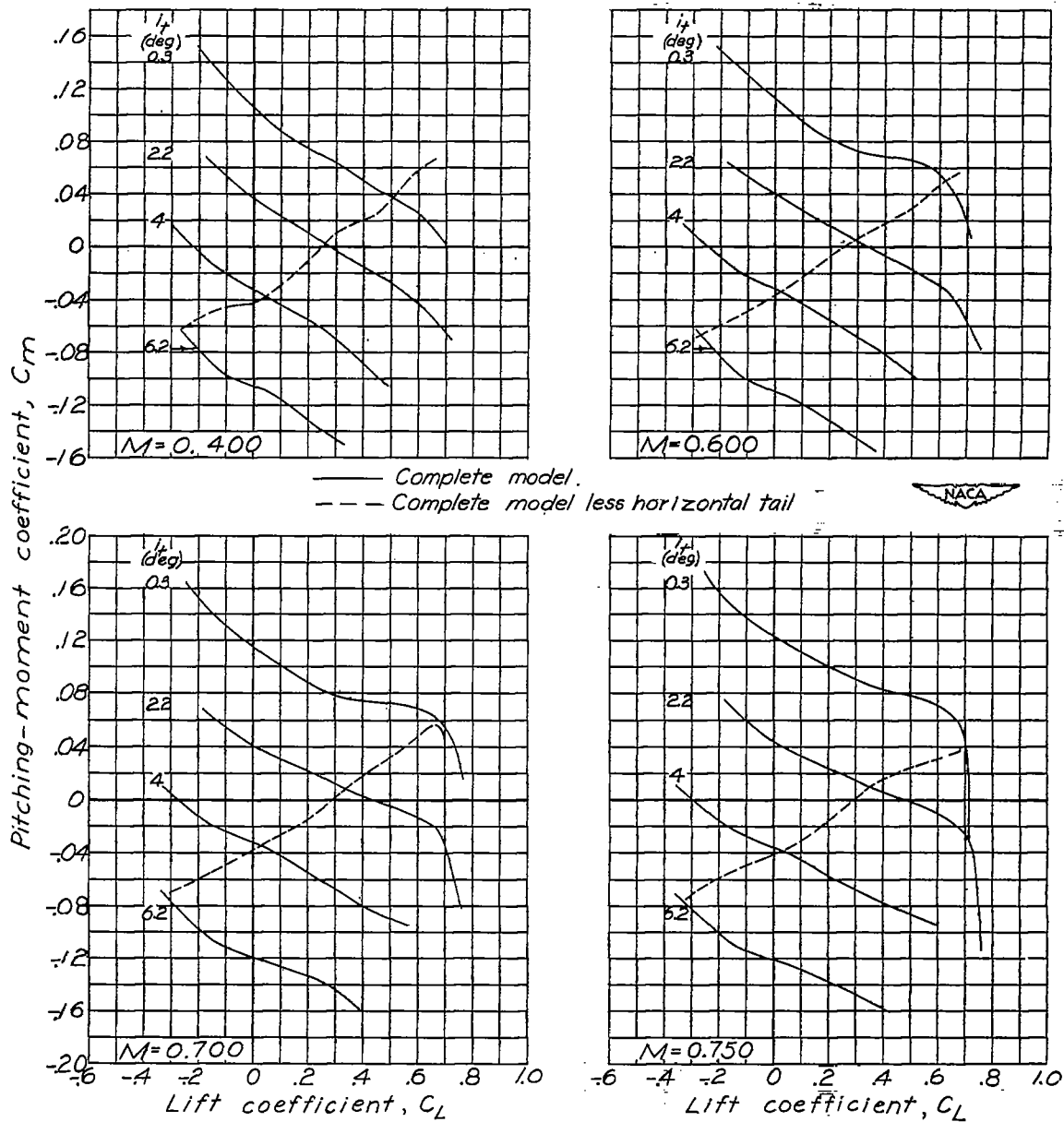


Figure 12.- Variation of pitching-moment coefficient with lift coefficient. Complete model at various horizontal-tail incidences, $\delta_e = 0^\circ$, and complete model less horizontal tail. $A = 4.2$.

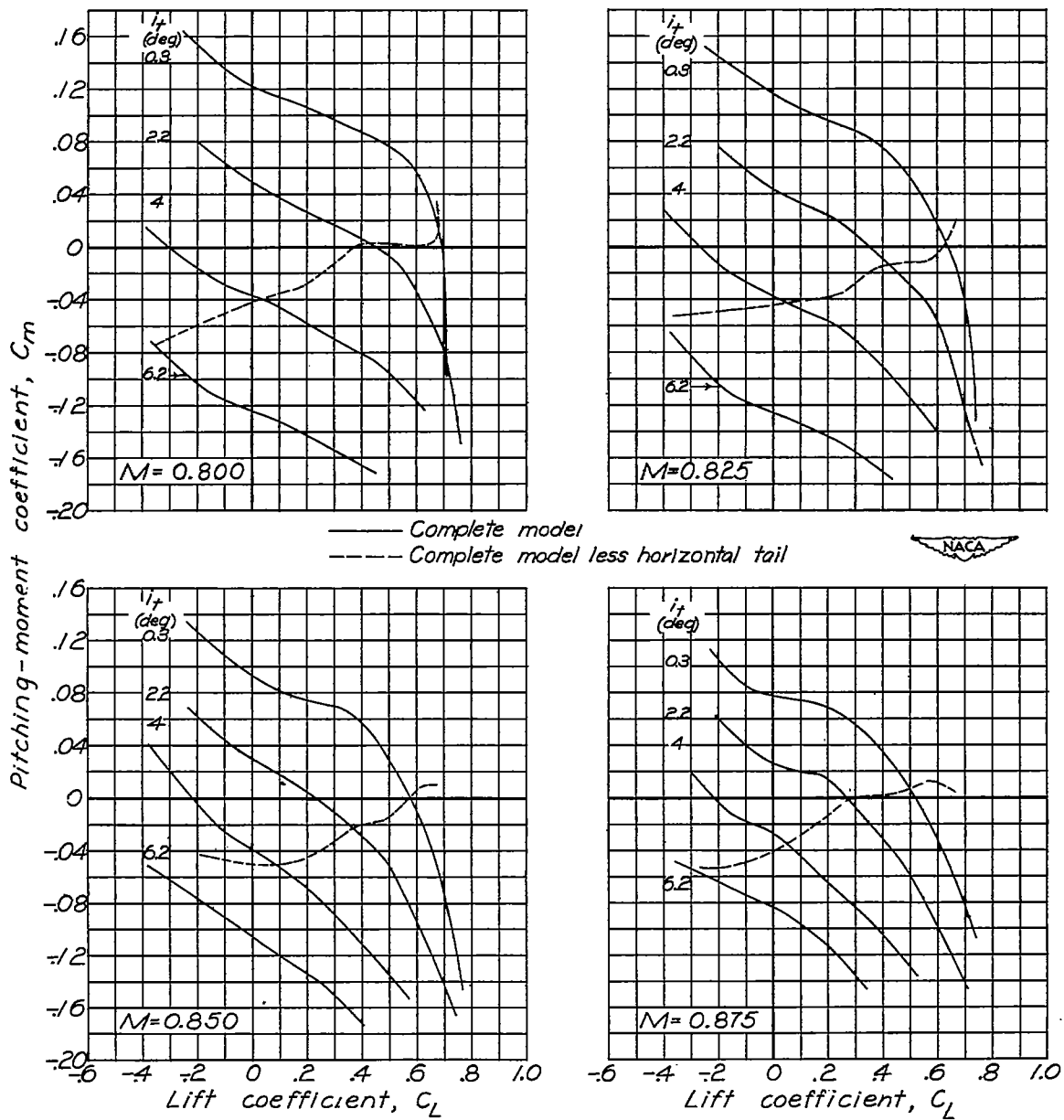


Figure 12.- Continued.

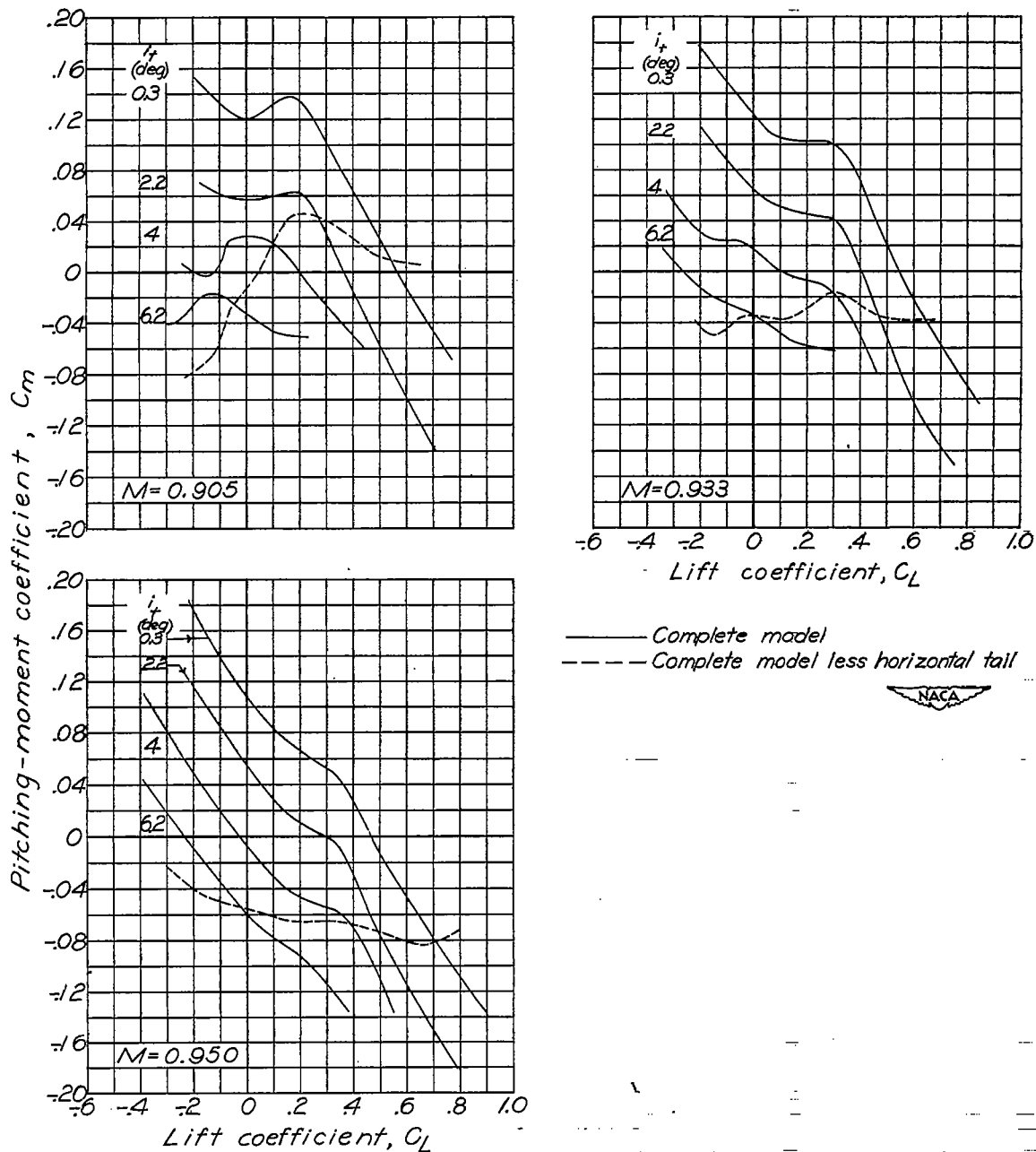


Figure 12.- Concluded.

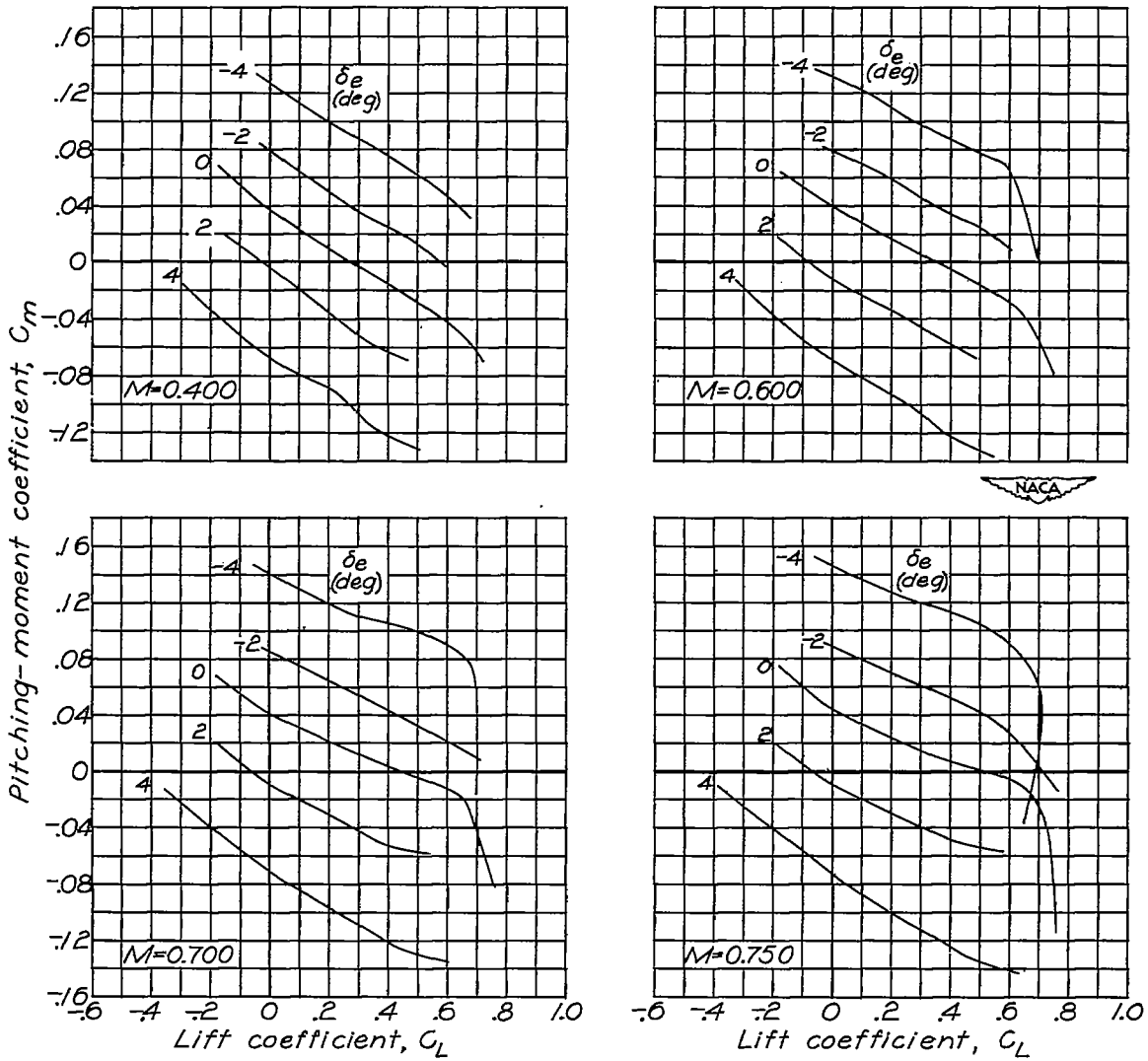


Figure 13.- Variation of pitching-moment coefficient with lift coefficient at various elevator deflections. Complete model; $A = 4.2$; $i_t = 2.2^\circ$.

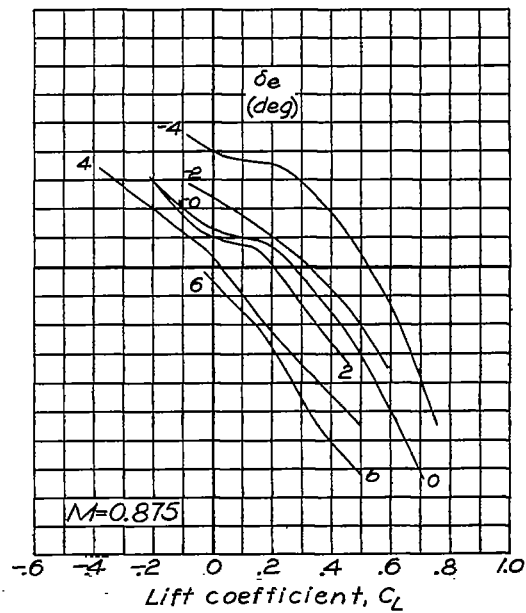
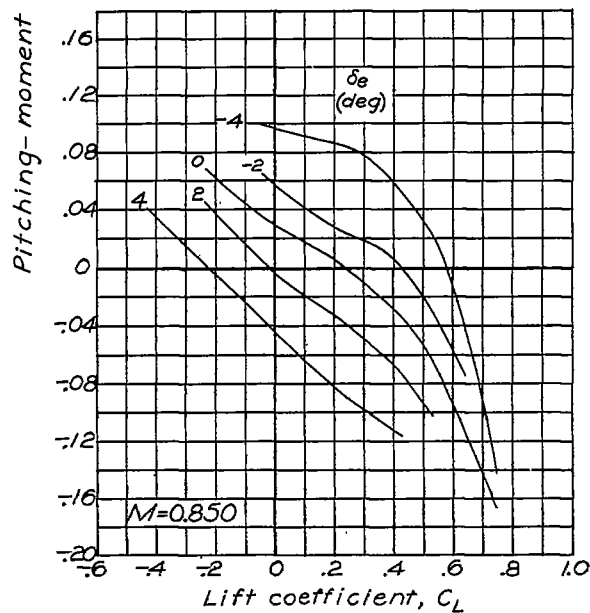
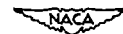
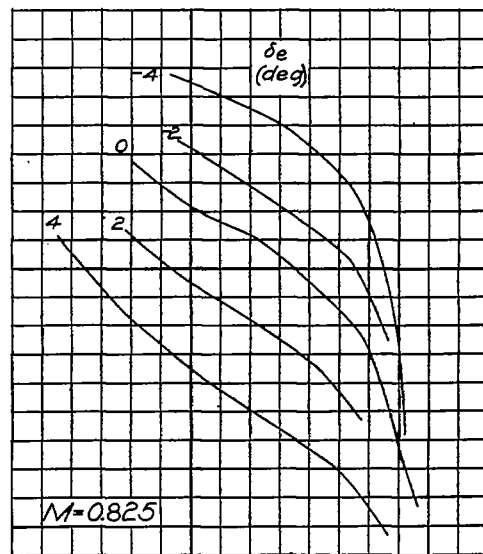
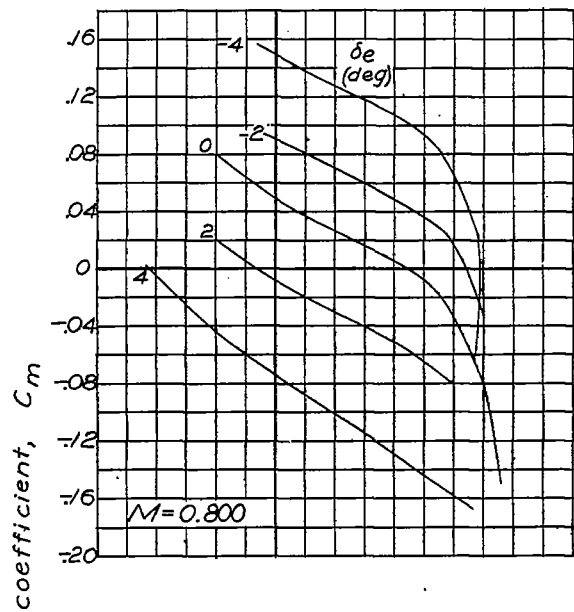


Figure 13.- Continued.

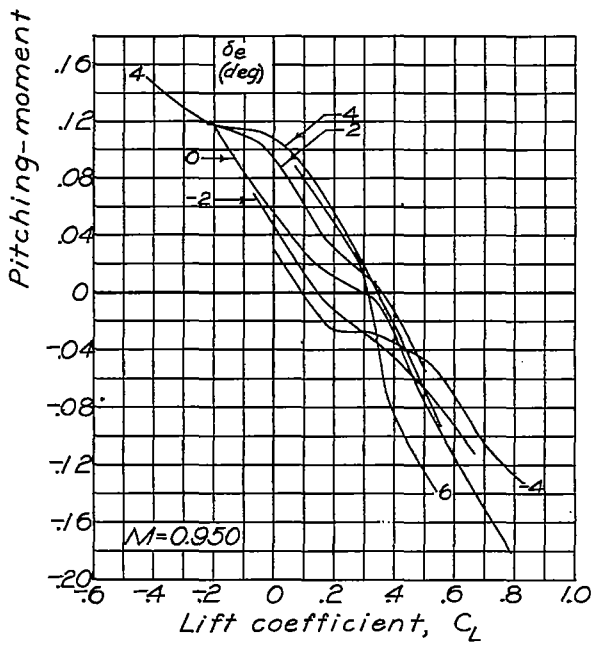
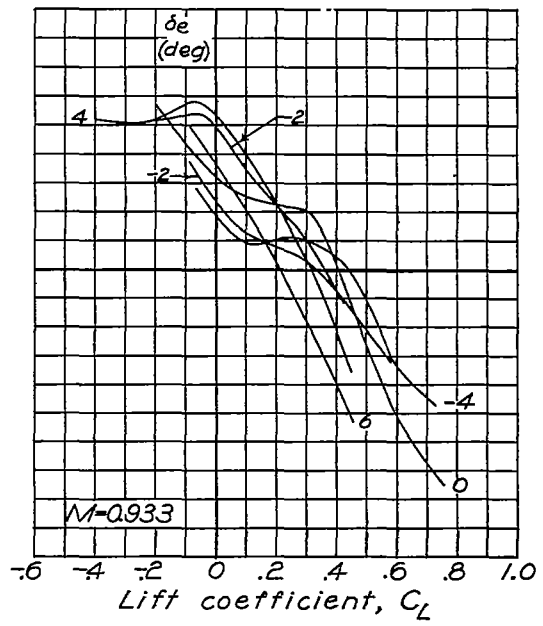
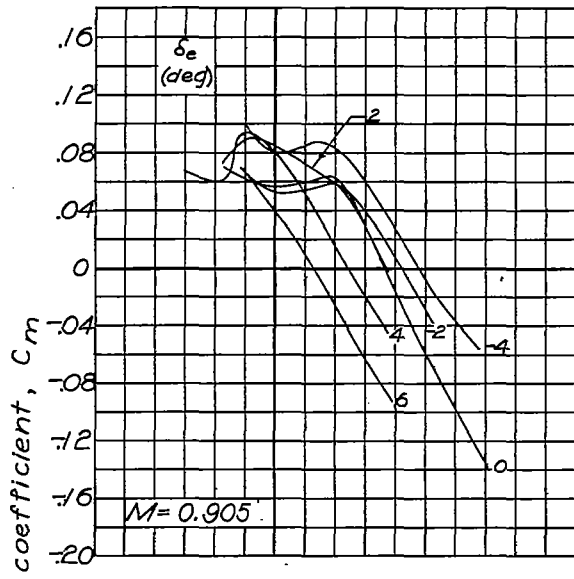


Figure 13.- Concluded.

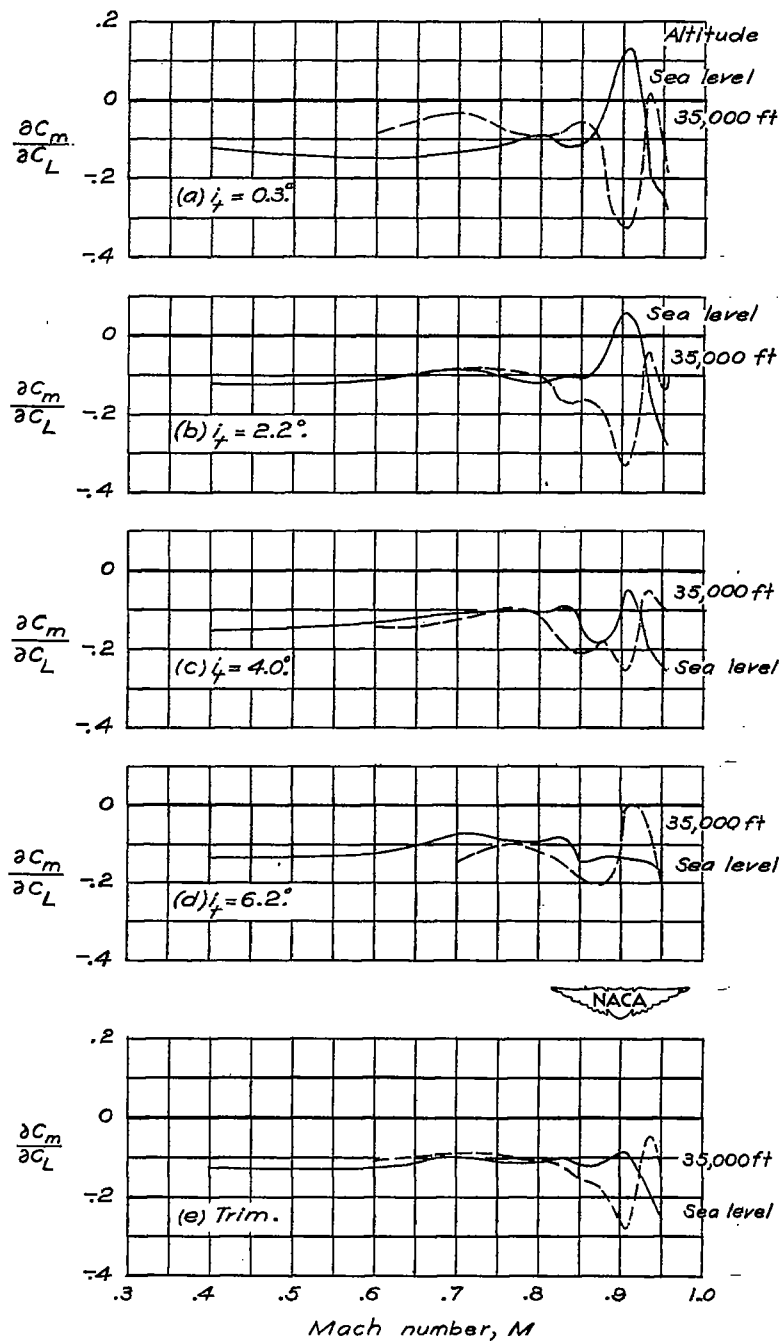


Figure 14.- Variation of the static-longitudinal-stability parameter $\frac{\partial C_m}{\partial C_L}$ with Mach number at airplane lift coefficients corresponding to level flight at two altitudes. Complete model; $A = 4.2$; $\delta_e = 0^\circ$; $\frac{W}{S} = 66.7$ pounds per square foot.

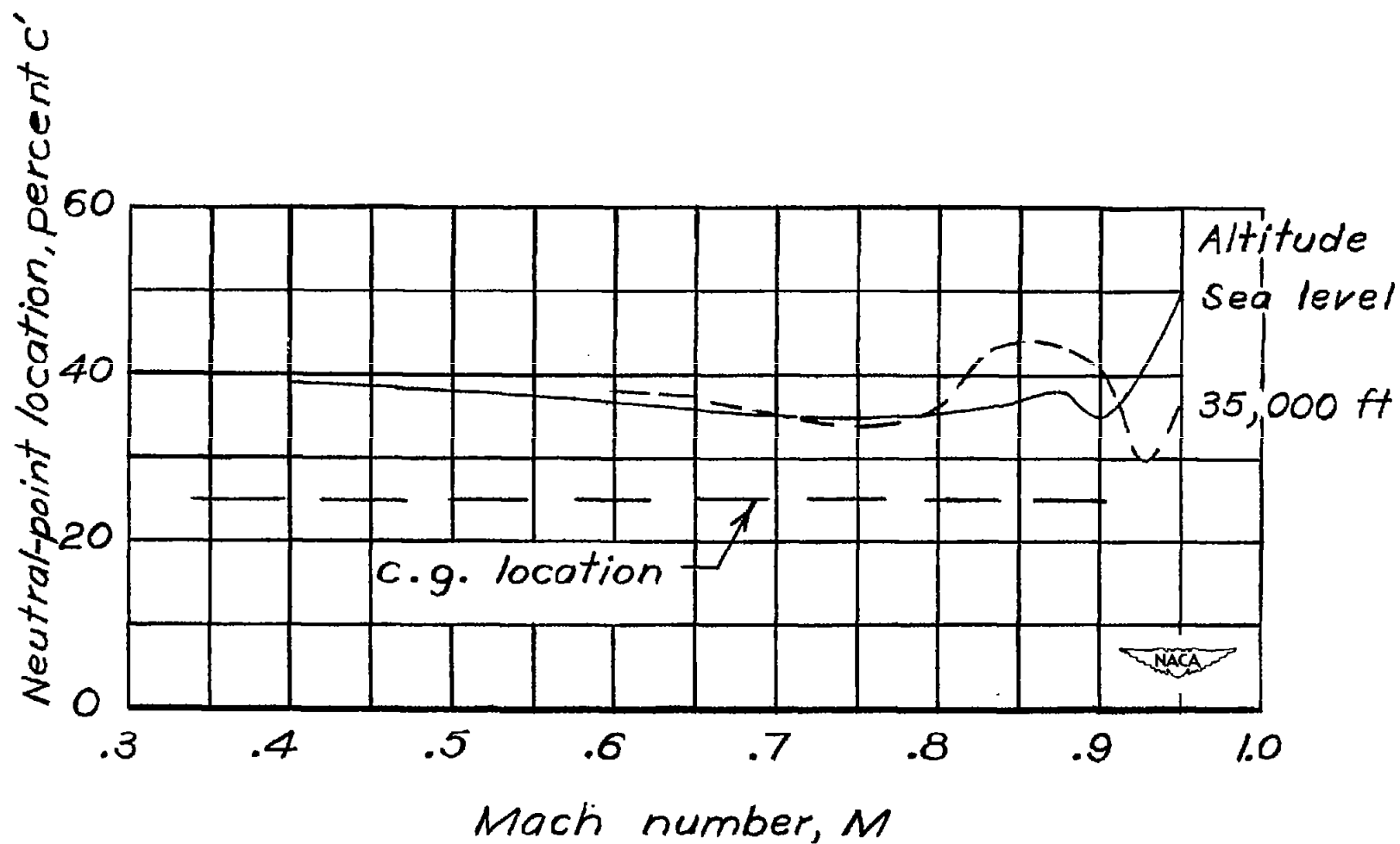
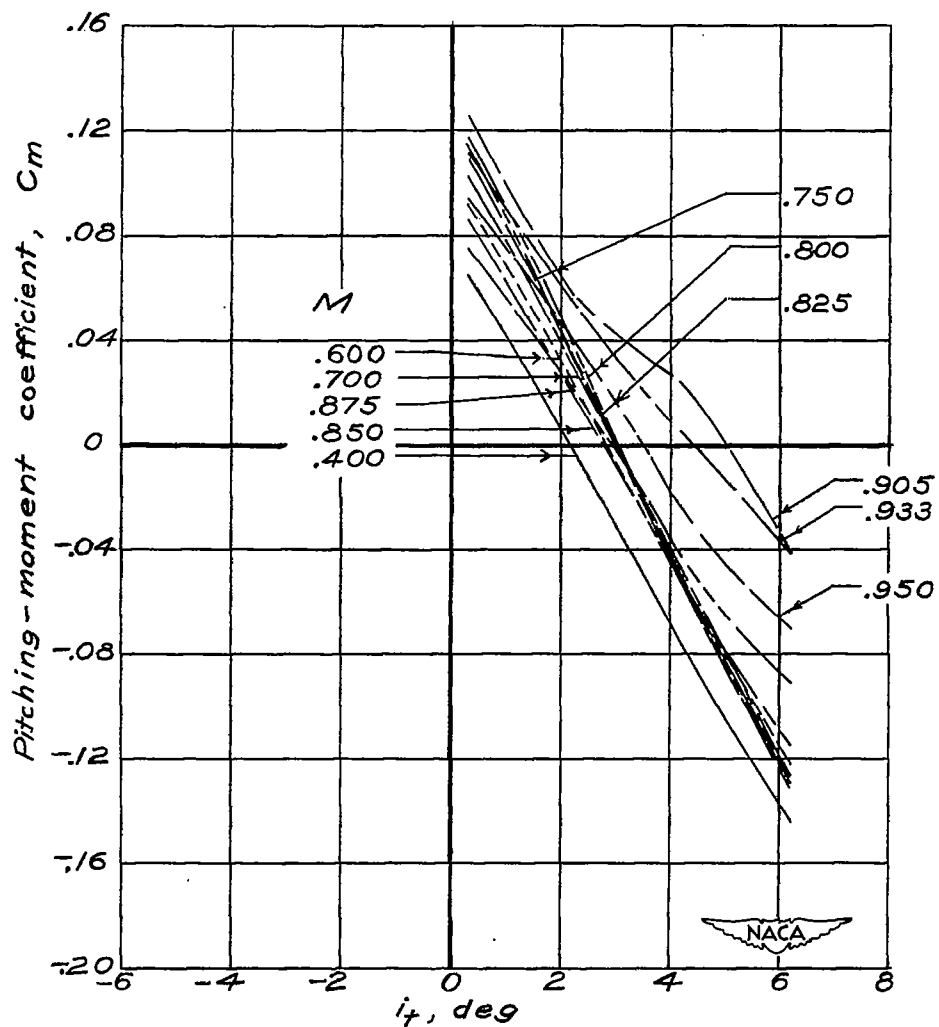
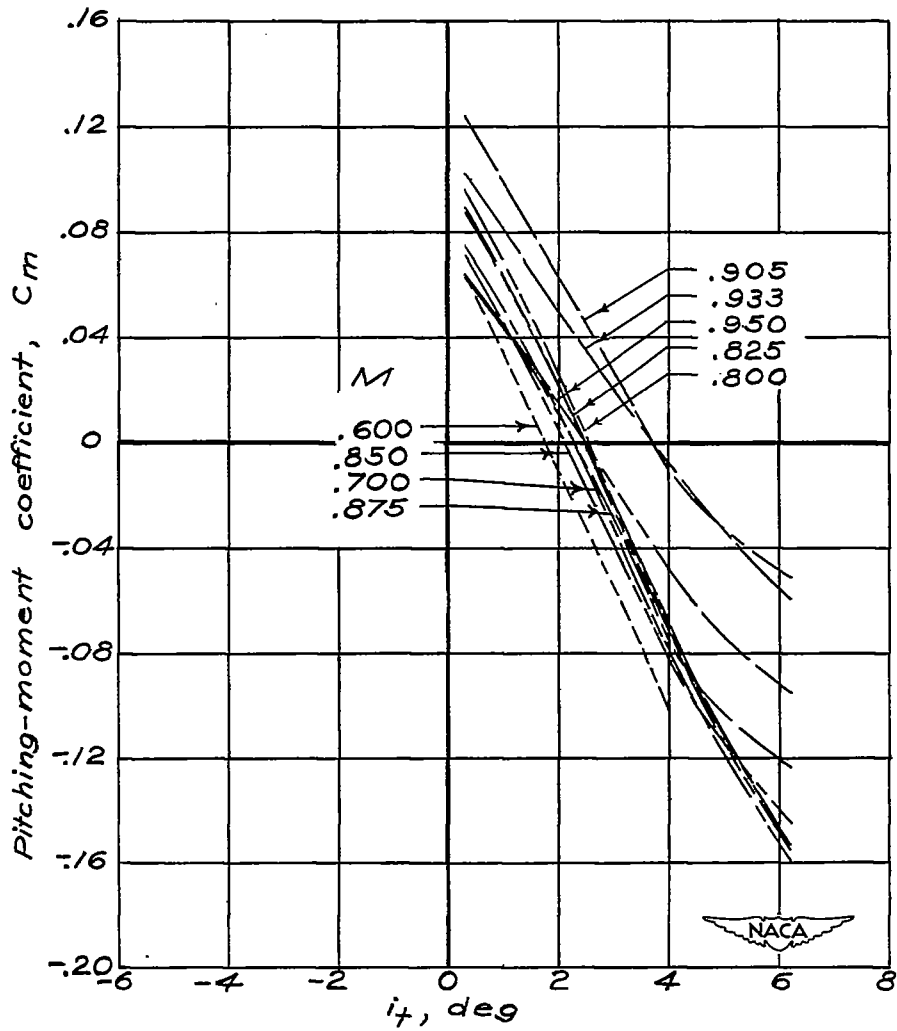


Figure 15.- Variation of neutral-point location with Mach number at airplane lift coefficients corresponding to level flight at two altitudes. Complete model; $A = 4.2$; $\delta_e = 0^\circ$; $\frac{W}{S} = 66.7$ pounds per square foot.



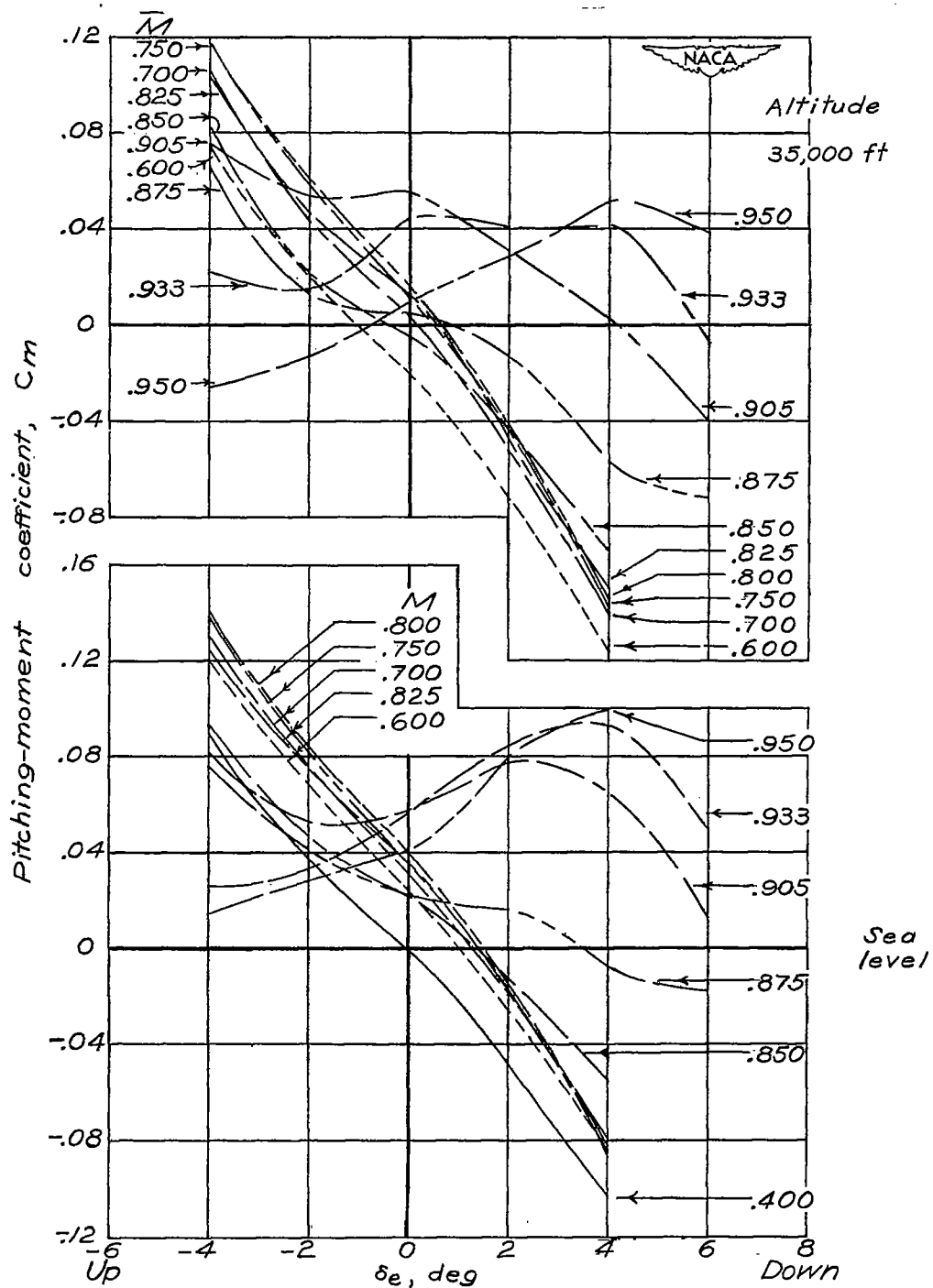
(a) $\delta_e = 0^\circ$; sea level.

Figure 16.- Variation of pitching-moment coefficient with horizontal-tail incidence and with elevator deflection at airplane lift coefficients corresponding to level flight at two altitudes. Complete model; $A = 4.2$; $\frac{W}{S} = 66.7$ pounds per square foot.



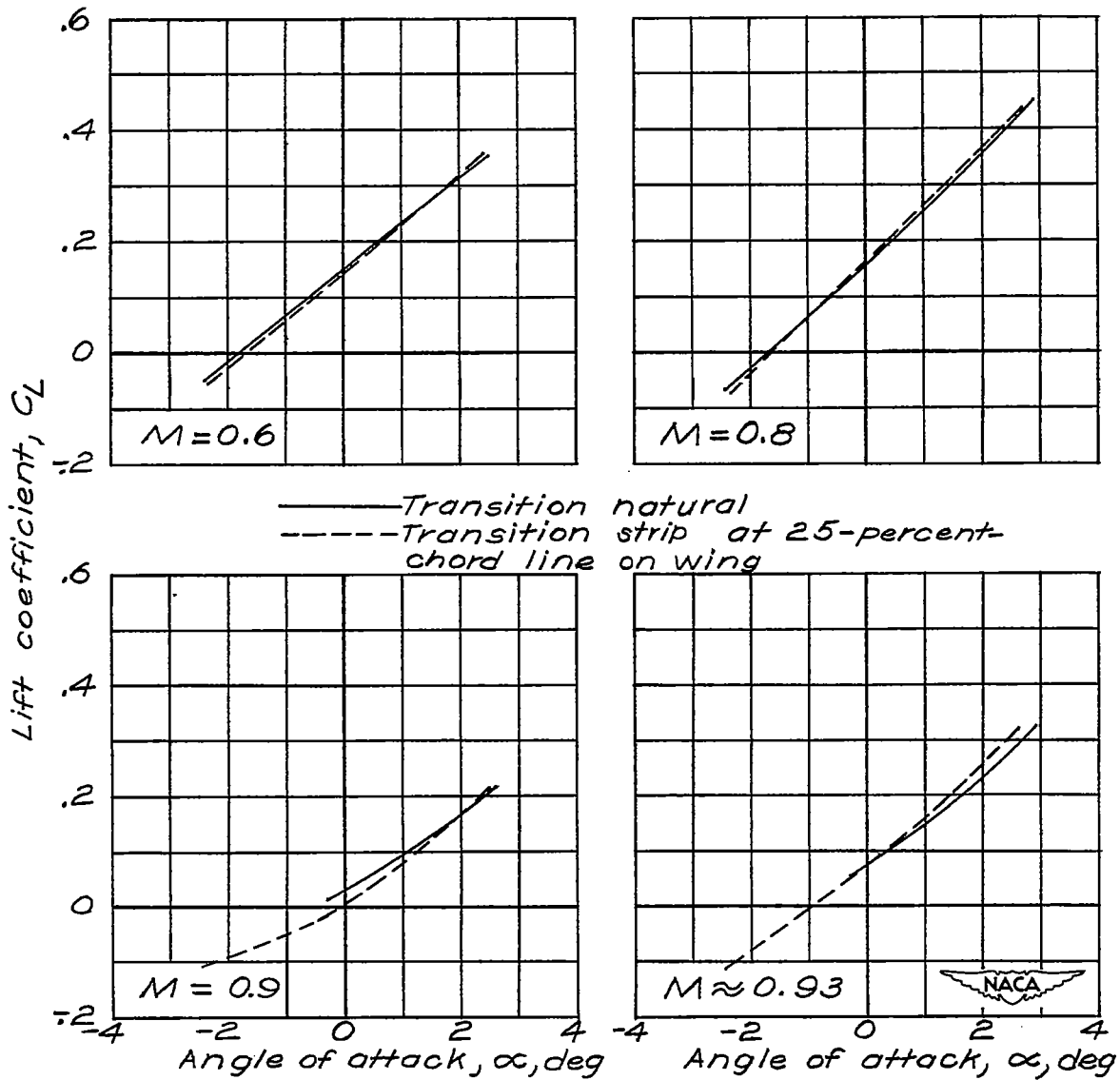
(b) $\delta_e = 0^\circ$; altitude, 35,000 feet.

Figure 16.- Continued.



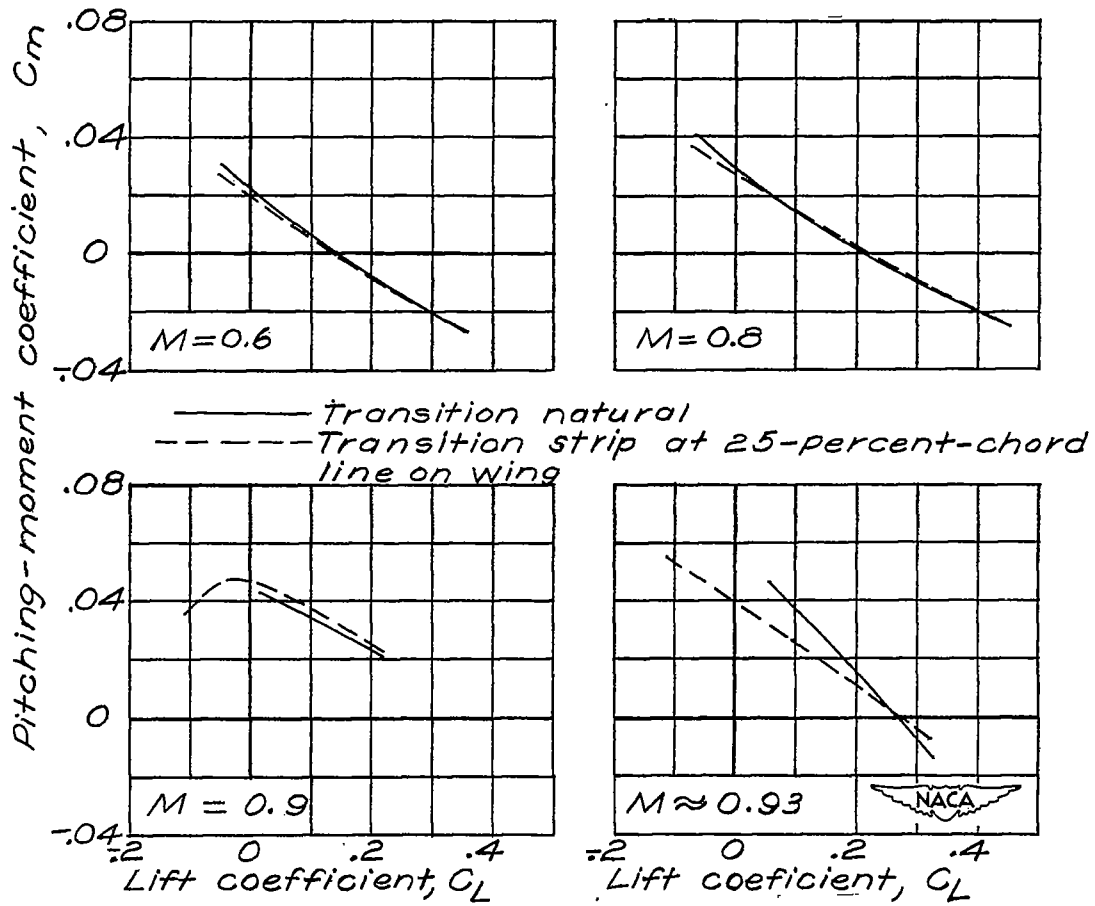
(c) $i_t = 2.2^\circ$; altitudes, sea level and 35,000 feet.

Figure 16.- Concluded.



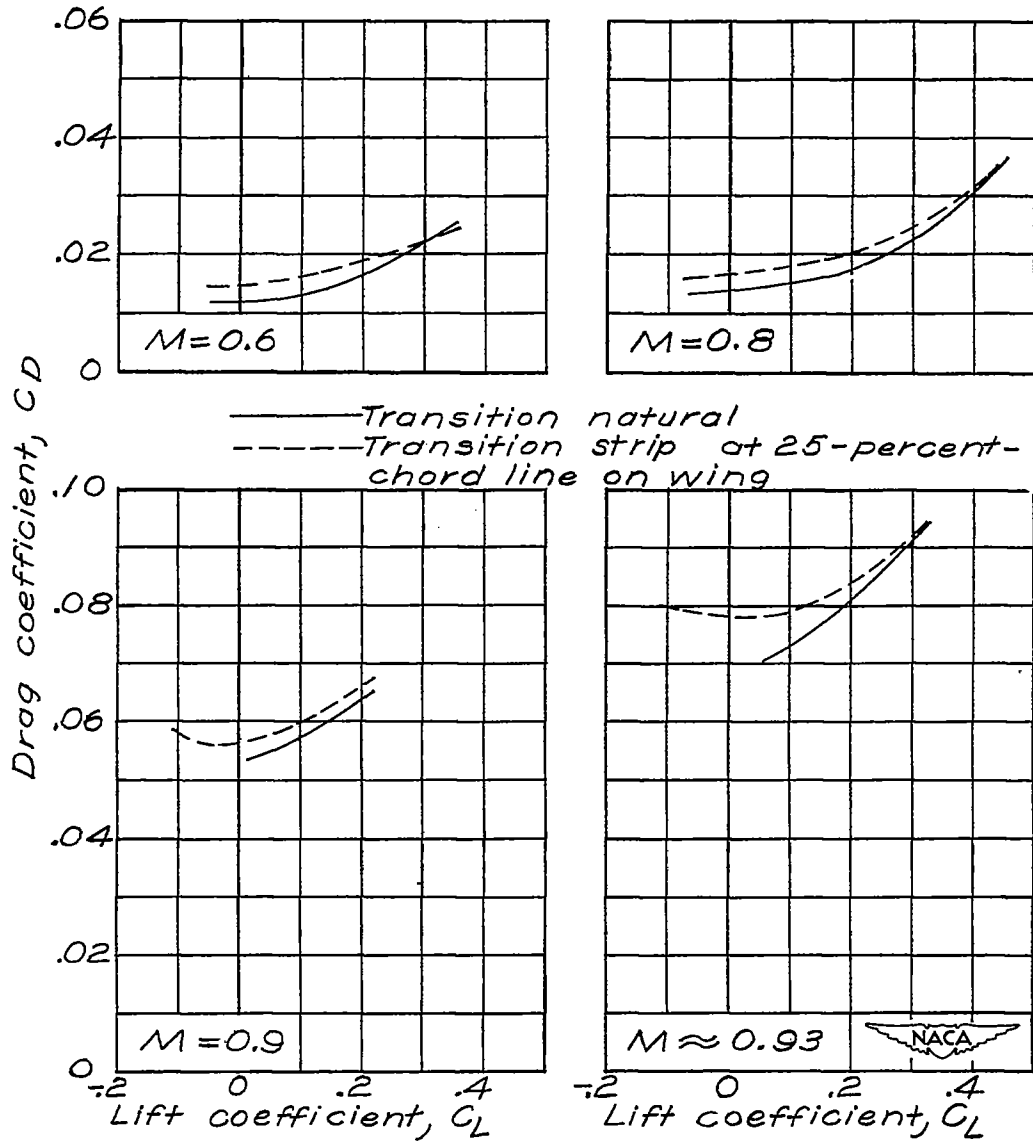
(a) C_L against α .

Figure 17.- Variation of lift coefficient with angle of attack, pitching-moment coefficient with lift coefficient, and drag coefficient with lift coefficient with natural transition and with a transition strip at 25-percent-chord line on wing. Coefficients uncorrected for sting interference. Complete model; $A = 4.2$; $i_t = 2.35^\circ$.



(b) C_m against C_L .

Figure 17.- Continued.



(c) C_D against C_L .

Figure 17.- Concluded.

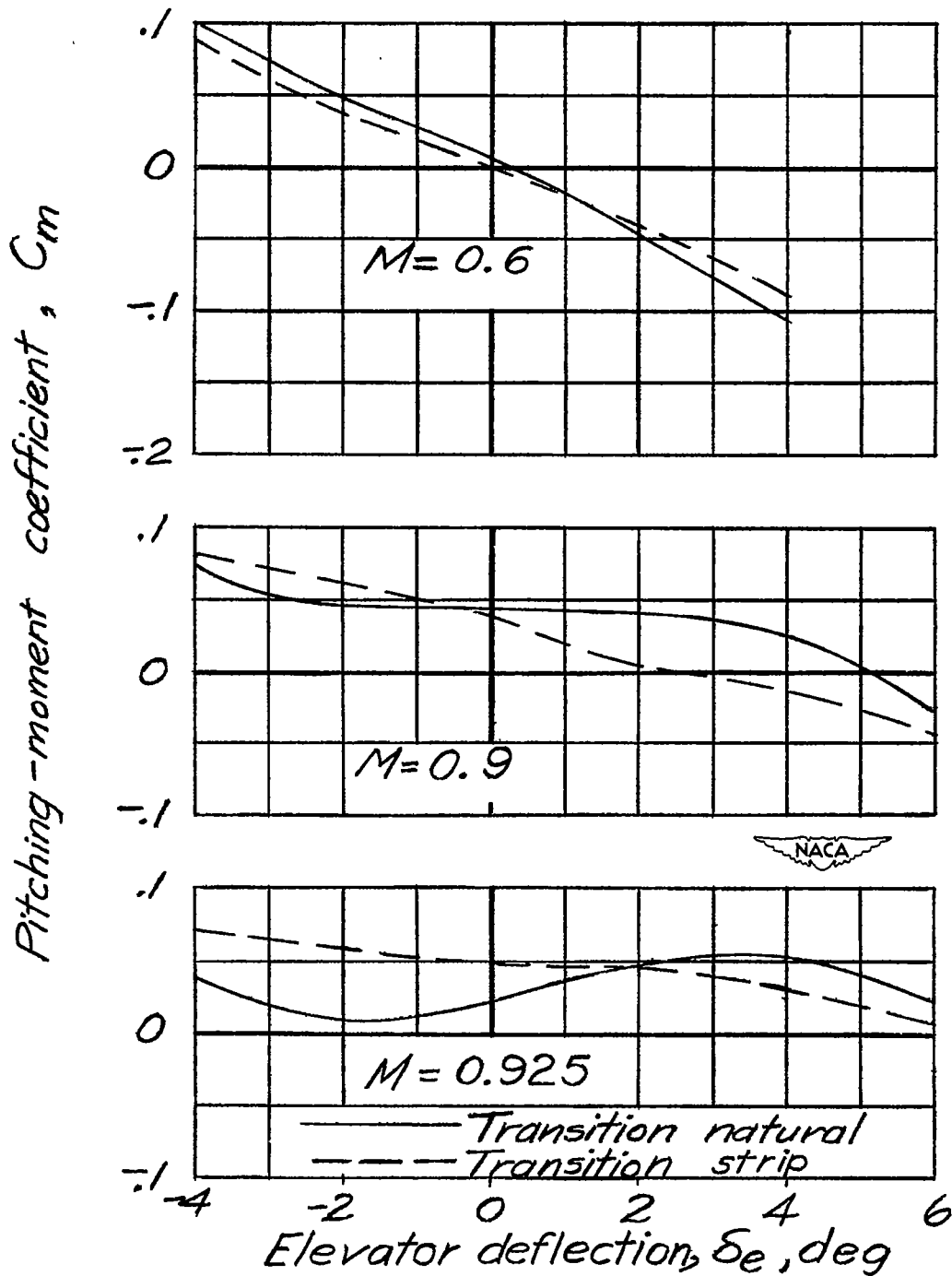


Figure 18.- Variation of pitching-moment coefficient with elevator deflection with natural pitching transition and with a transition strip on horizontal tail. Pitching-moment coefficient uncorrected for sting interference. Complete model; $A = 4.2$; $i_t = 2.2^\circ$; $\alpha = 0^\circ$.

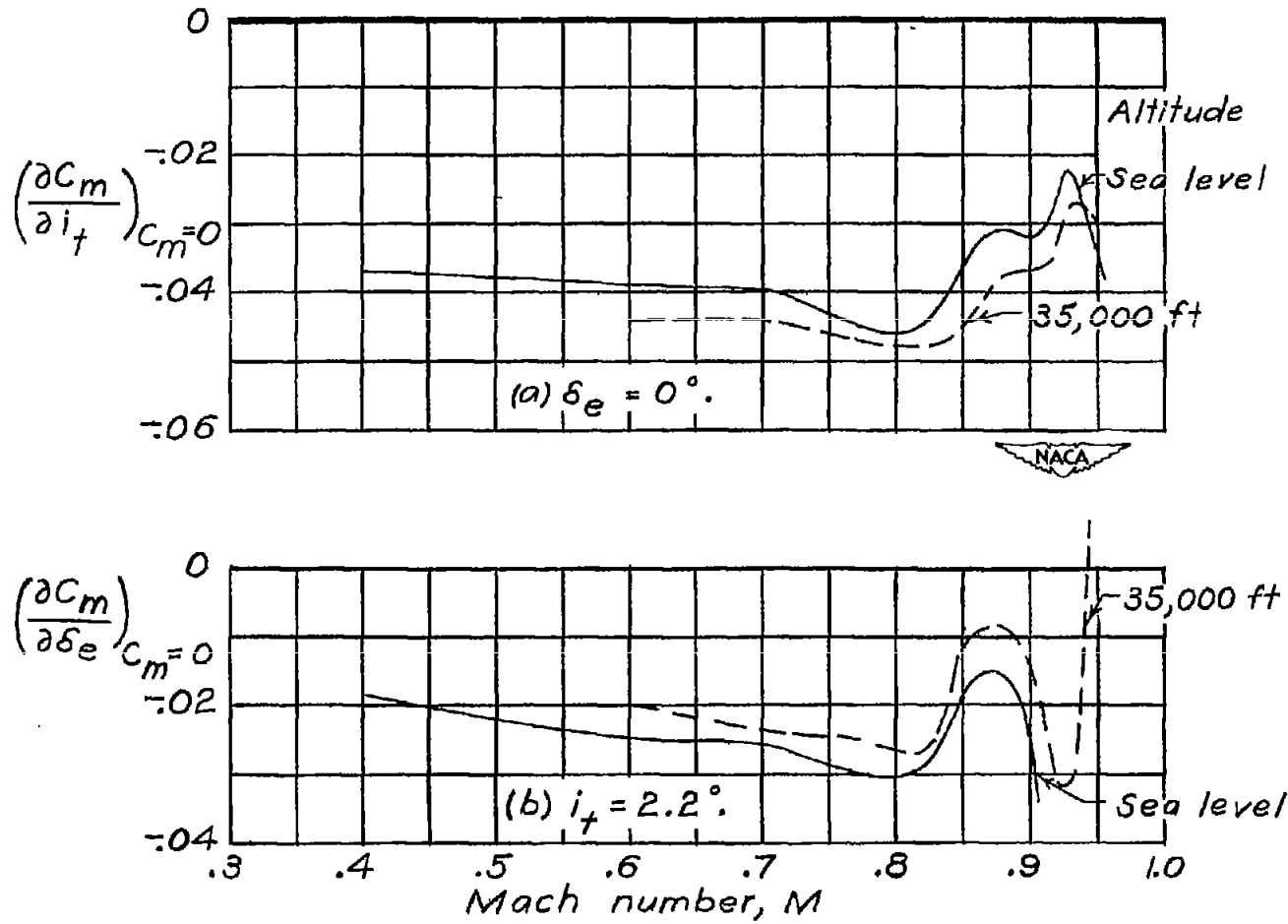


Figure 19.- Variation of horizontal-tail effectiveness $\frac{\partial C_m}{\partial i_t}$ and elevator effectiveness $\frac{\partial C_m}{\partial \delta_e}$ with Mach number for trim conditions at airplane lift coefficients corresponding to level flight at two altitudes. Complete model; $A = .4.2$; $\frac{W}{S} = 66.7$ pounds per square foot.

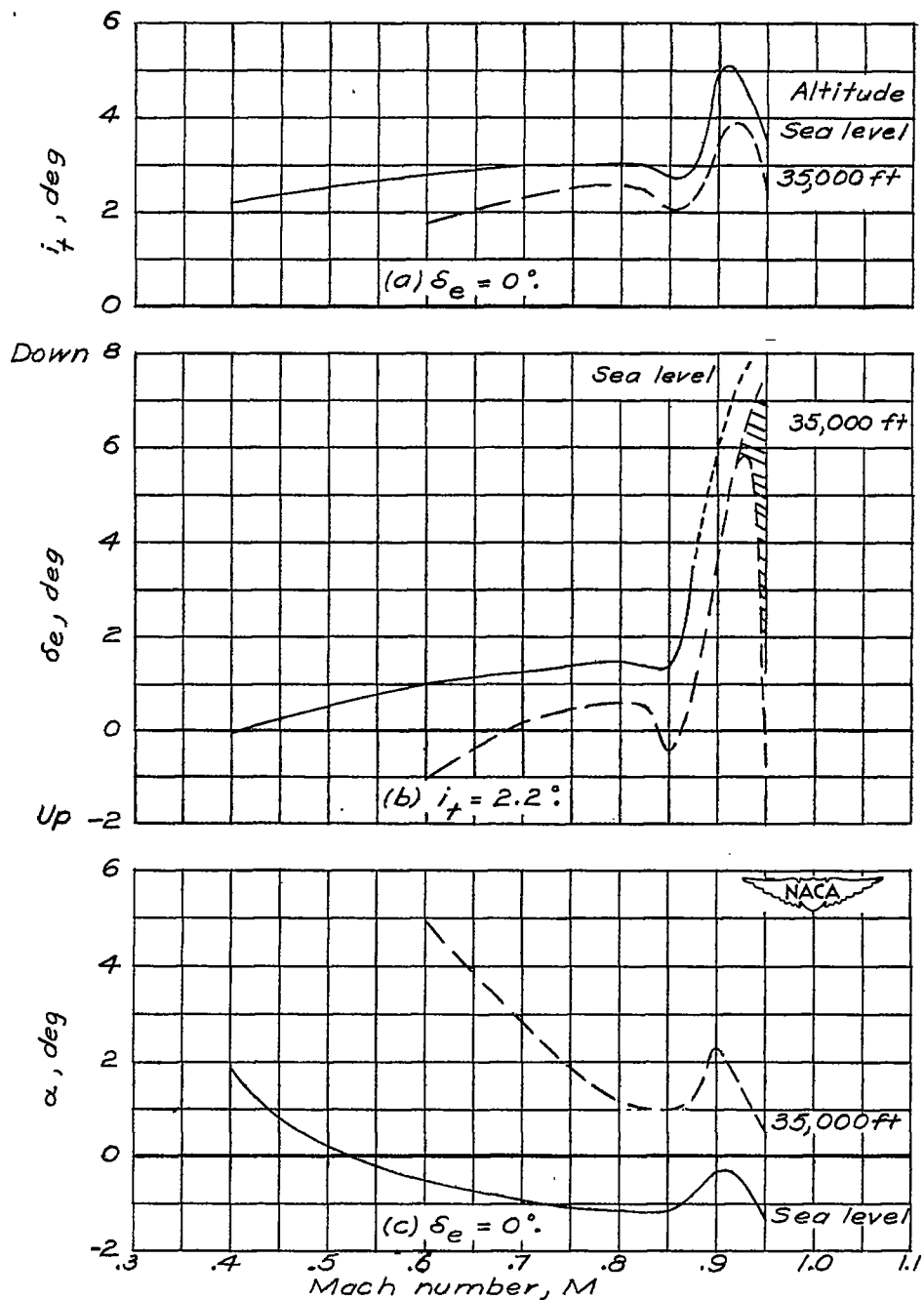


Figure 20.- Variation with Mach number of the horizontal-tail incidence required for obtaining trim, the elevator deflection required for obtaining trim, and the model angle of attack for trim conditions (horizontal tail used for obtaining trim) at airplane lift coefficients corresponding to level flight at two altitudes. Complete model; $A = 4.2$;

$$\frac{W}{S} = 66.7 \text{ pounds per square foot.}$$

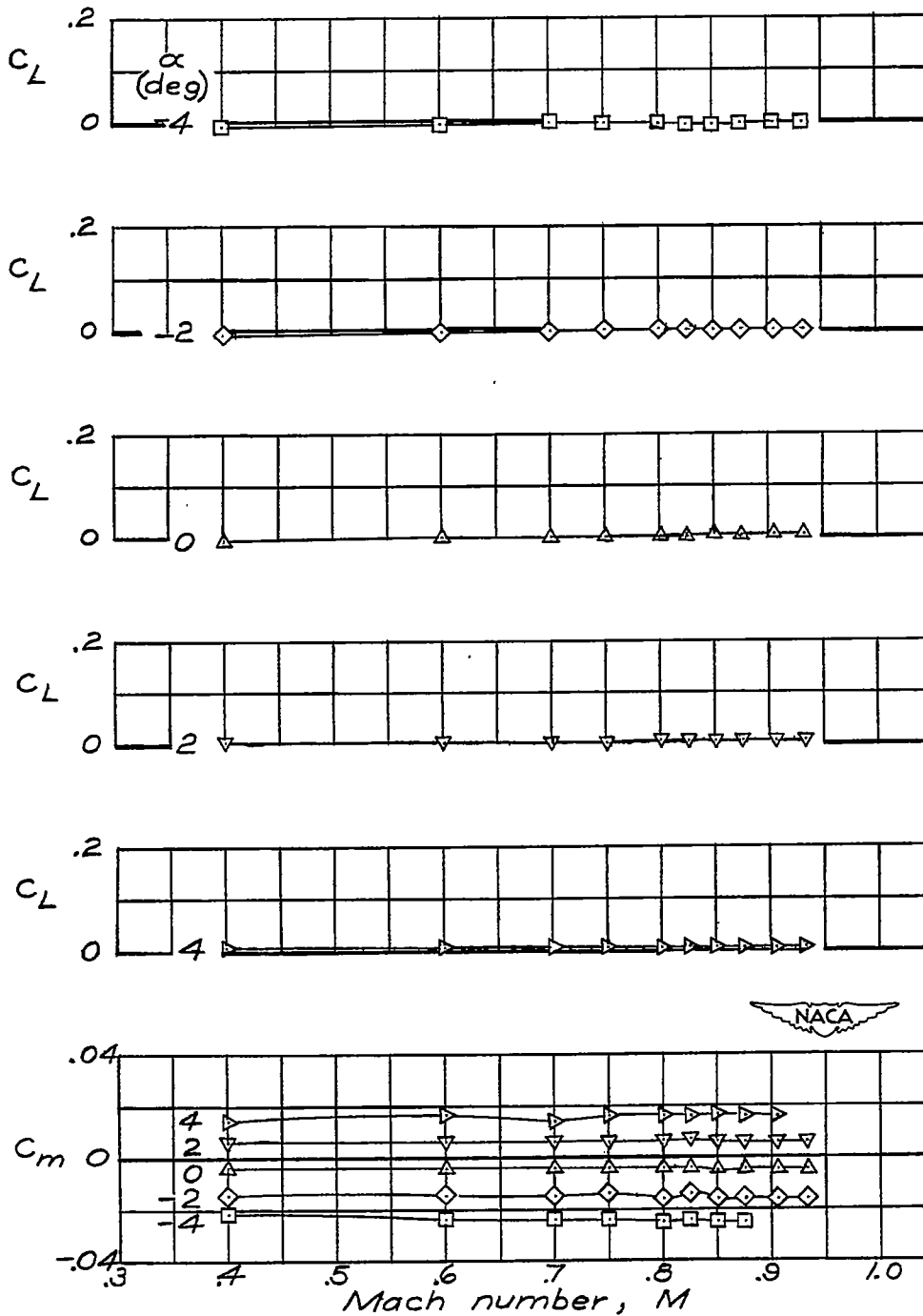


Figure 21.- Variation of lift coefficient and pitching-moment coefficient with Mach number at various model angles of attack. Coefficients uncorrected for sting interference. Complete model less wing and less horizontal tail.

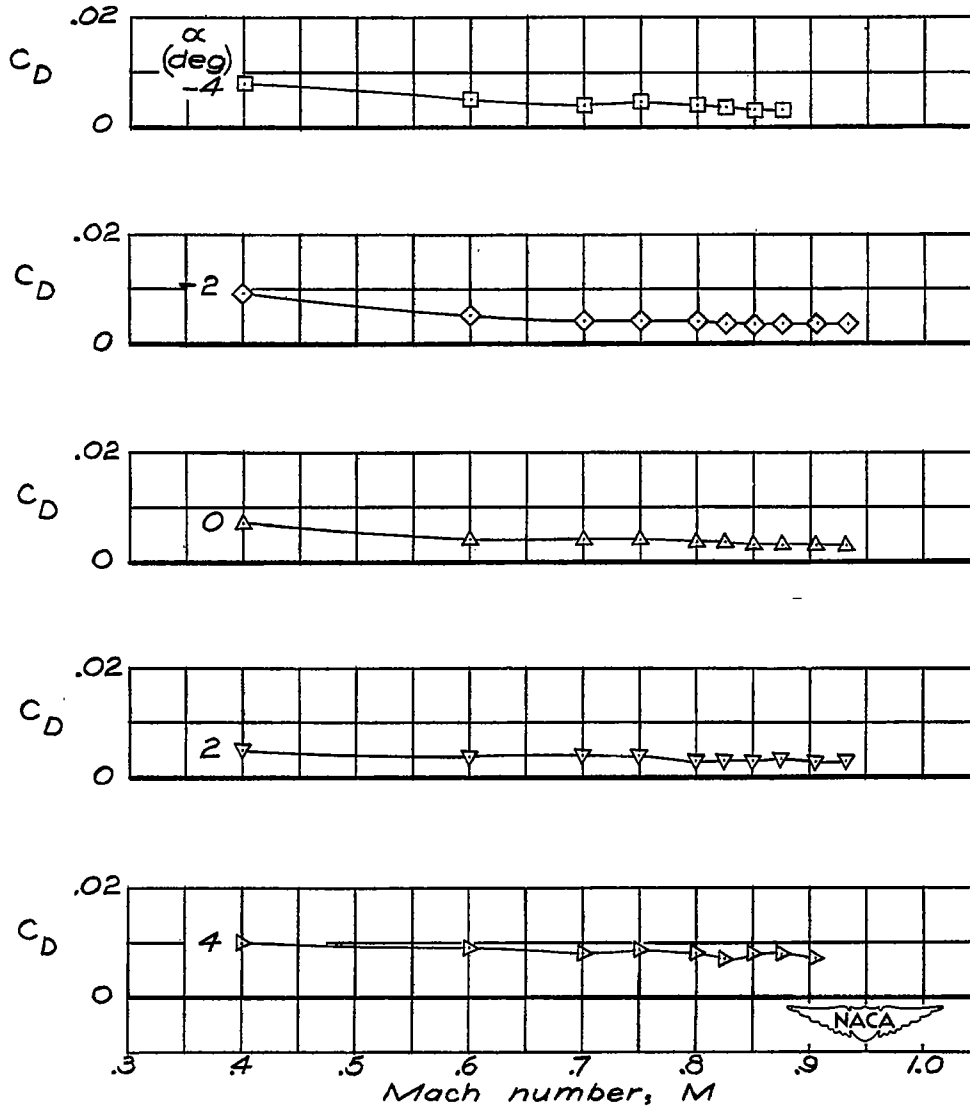


Figure 22.- Variation of drag coefficient with Mach number at various model angles of attack. Drag coefficient uncorrected for sting interference. Complete model less wing and less horizontal tail.

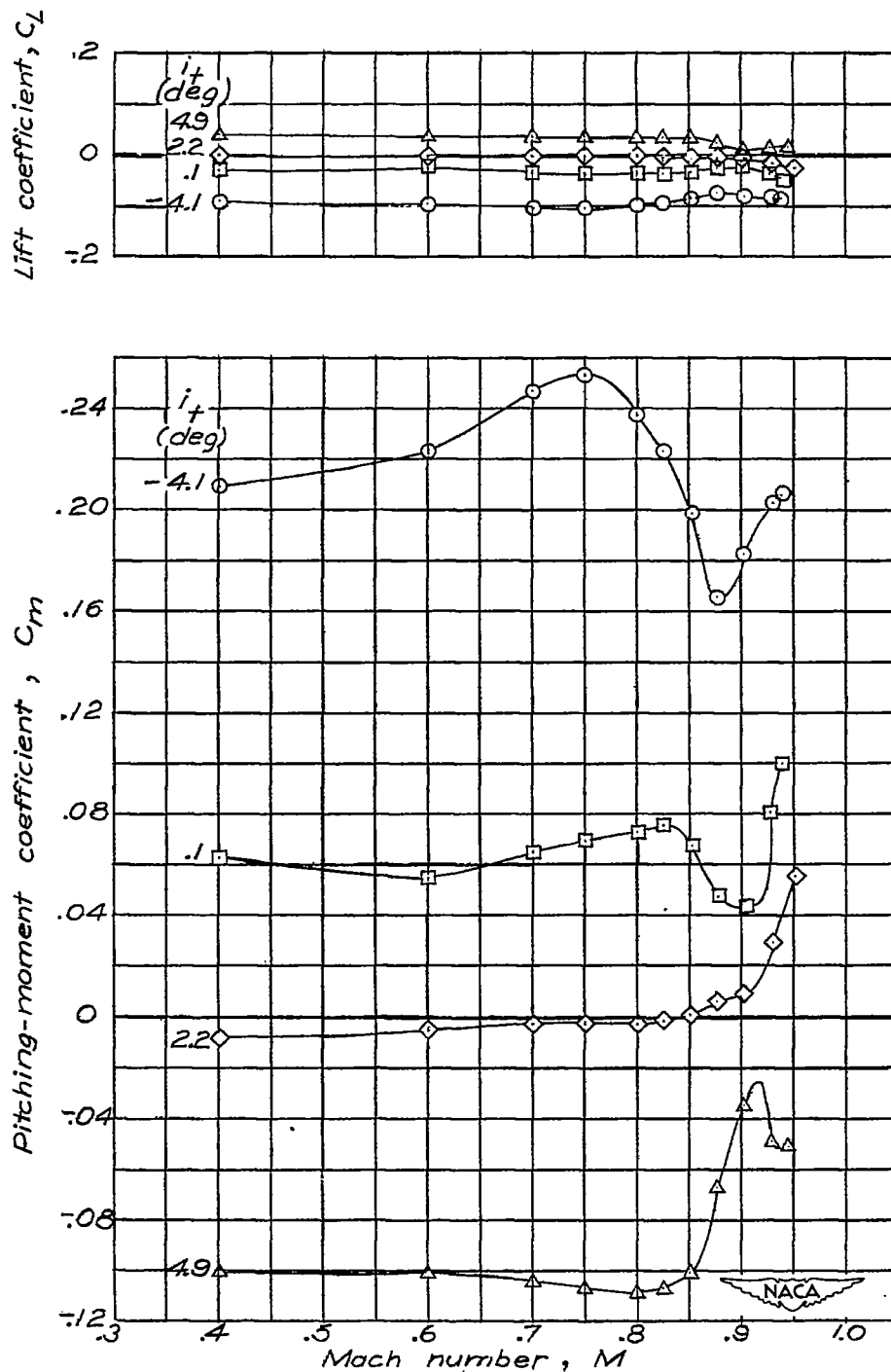


Figure 23.- Variation of lift coefficient and pitching-moment coefficient with Mach number at various horizontal-tail incidences. Coefficients uncorrected for sting interference. Complete model less wing; $A = 4.2$; $\alpha \approx -0.3^\circ$; $\delta_e = 0$.

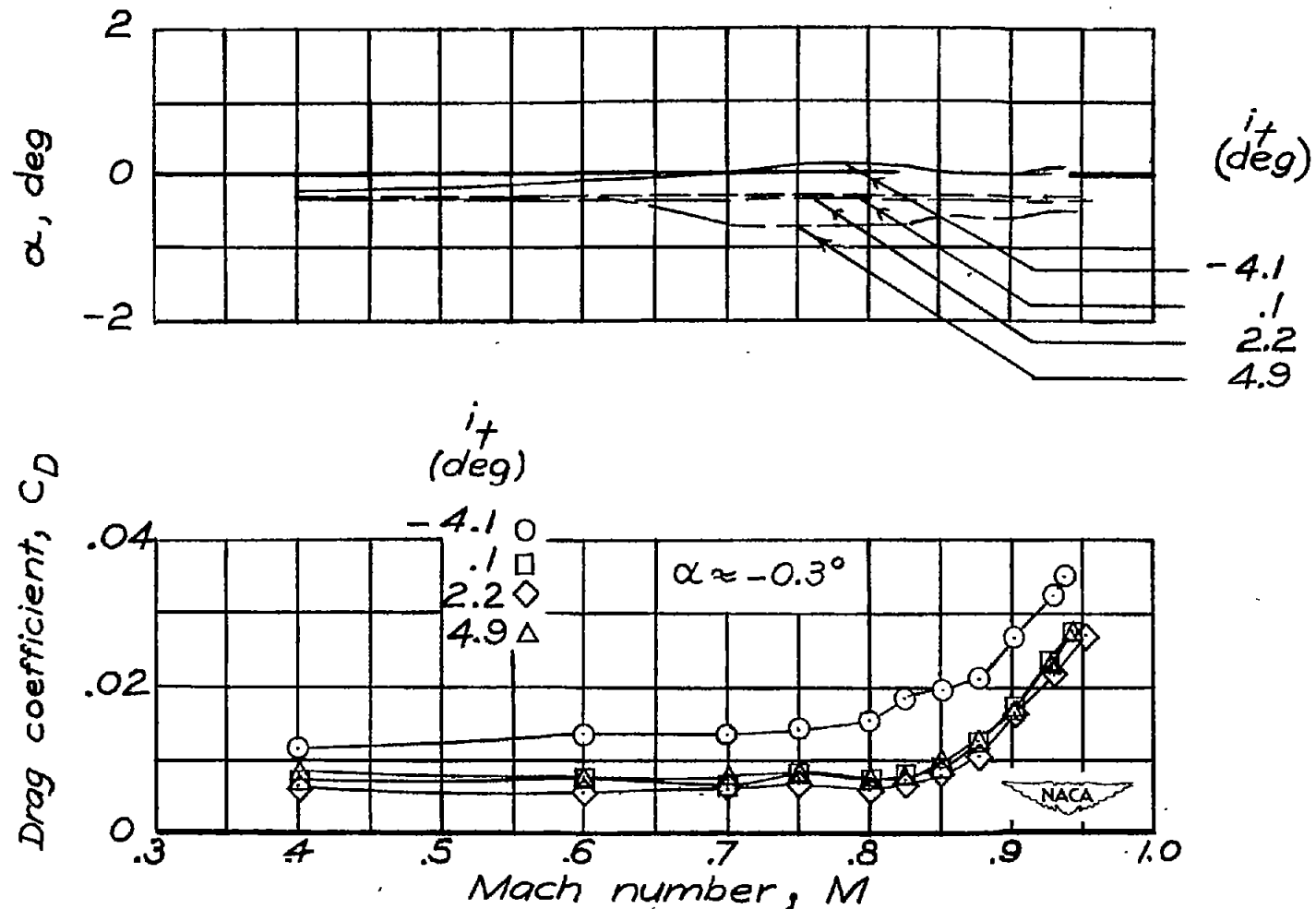


Figure 24.- Variation of model angle of attack and drag coefficient with Mach number at various horizontal-tail incidences. Drag coefficient uncorrected for sting interference. Complete model less wing; $A = 4.2$; $\delta_e = 0^\circ$.

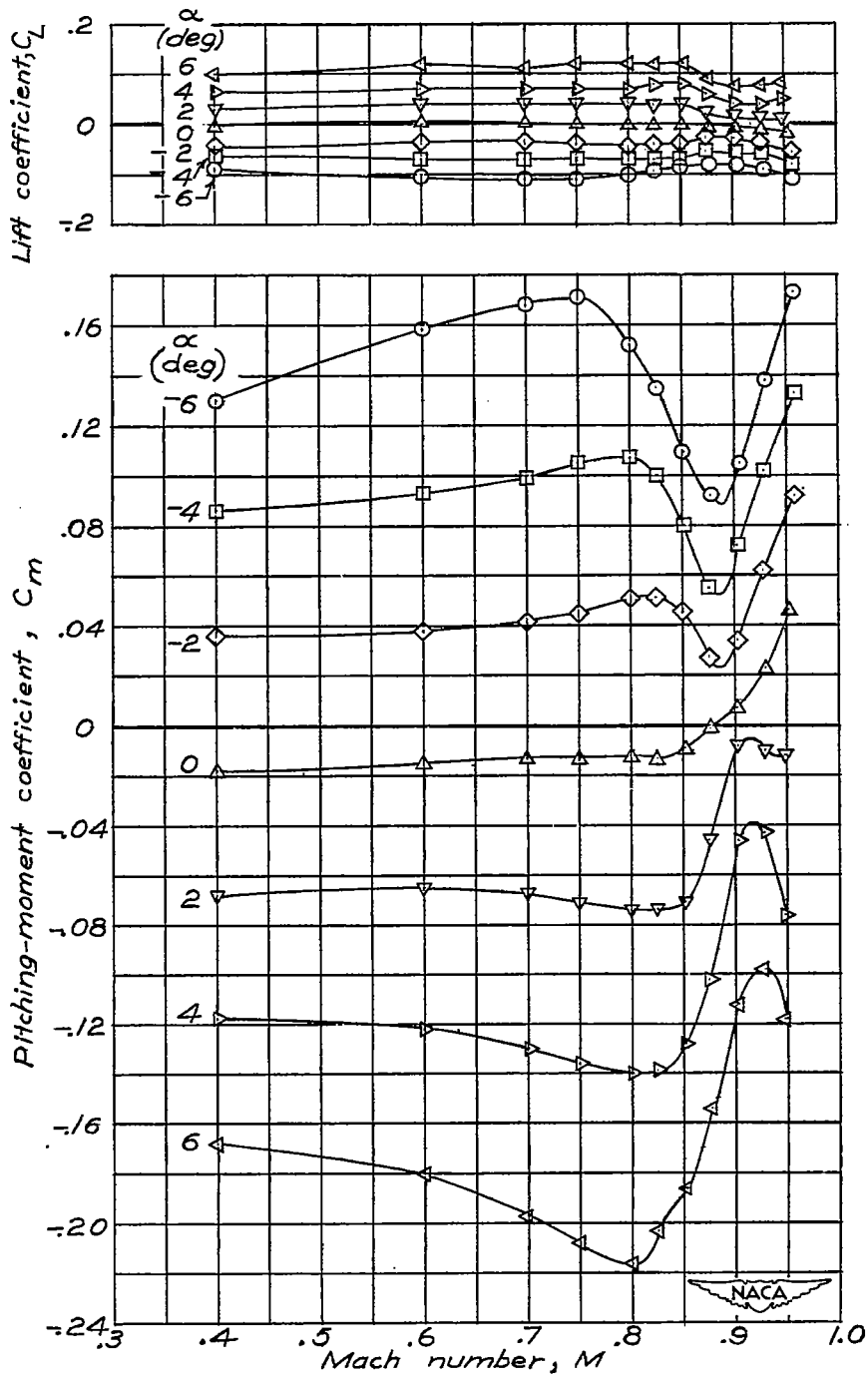


Figure 25.- Variation of lift coefficient and pitching-moment coefficient with Mach number at various model angles of attack. Coefficients uncorrected for sting interference. Complete model less wing; $A = 4.2$; $i_t = 2.2^\circ$; $\delta_e = 0^\circ$.

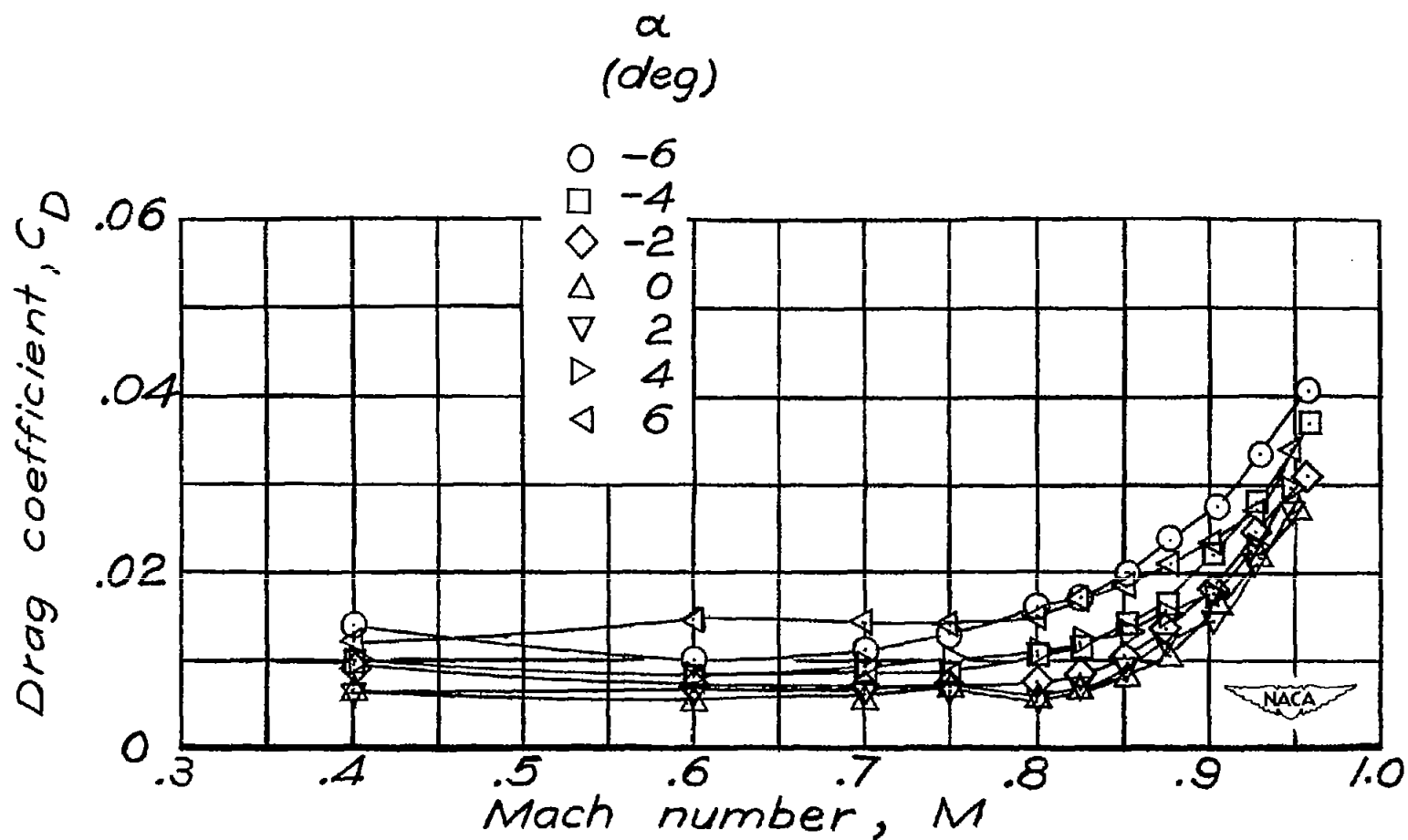


Figure 26.- Variation of drag coefficient with Mach number at various model angles of attack. Drag coefficient uncorrected for sting interference. Complete model less wing; $A = 4.2$; $t_t = 2.2^\circ$; $\delta_e = 0^\circ$.

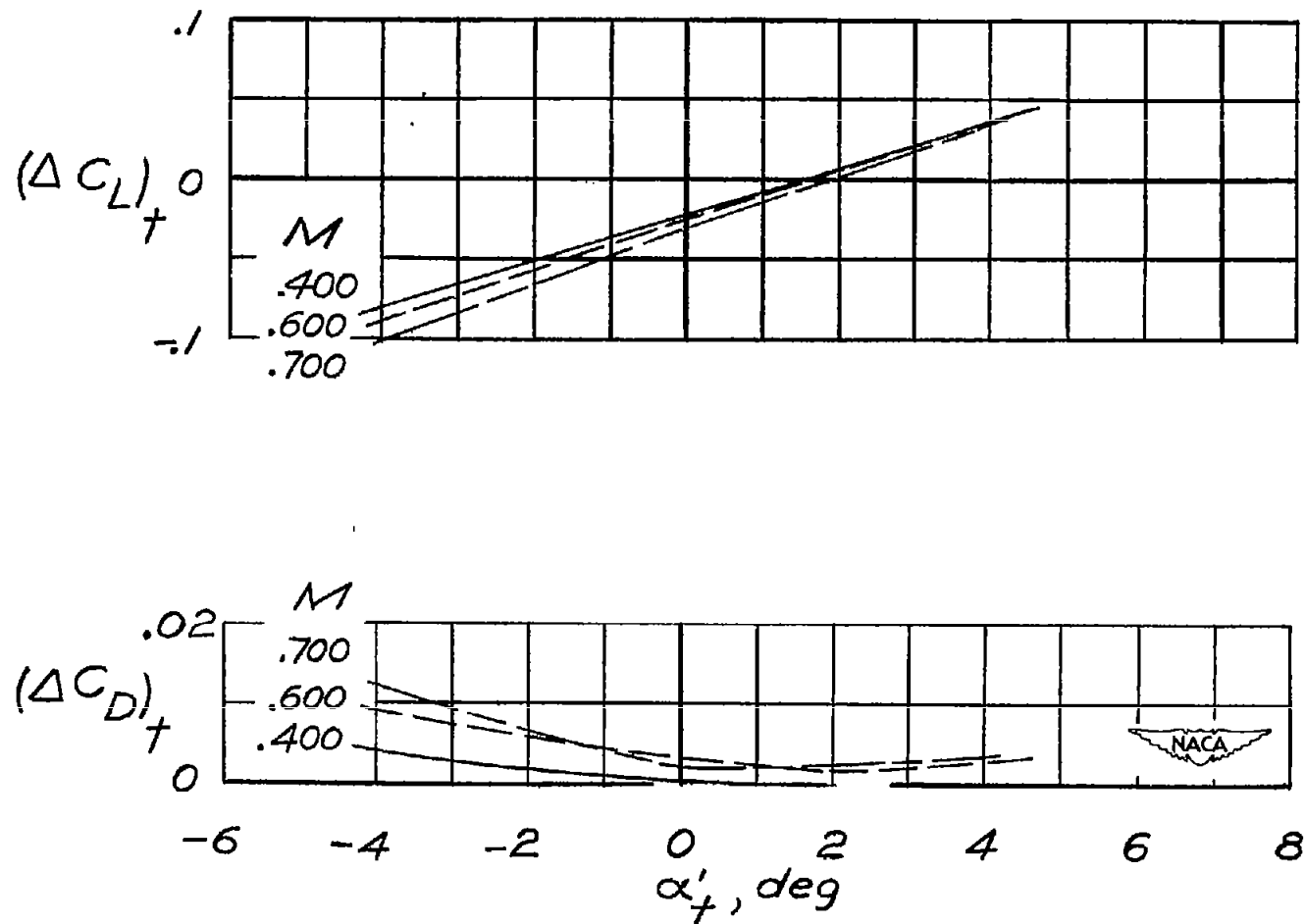


Figure 27.- Variation of incremental lift coefficient and incremental drag coefficient of horizontal tail with free-stream angle of attack of horizontal tail. Complete model less wing; $A = 4.2$; $\alpha \approx -0.3^\circ$; $\delta_e = 0^\circ$.

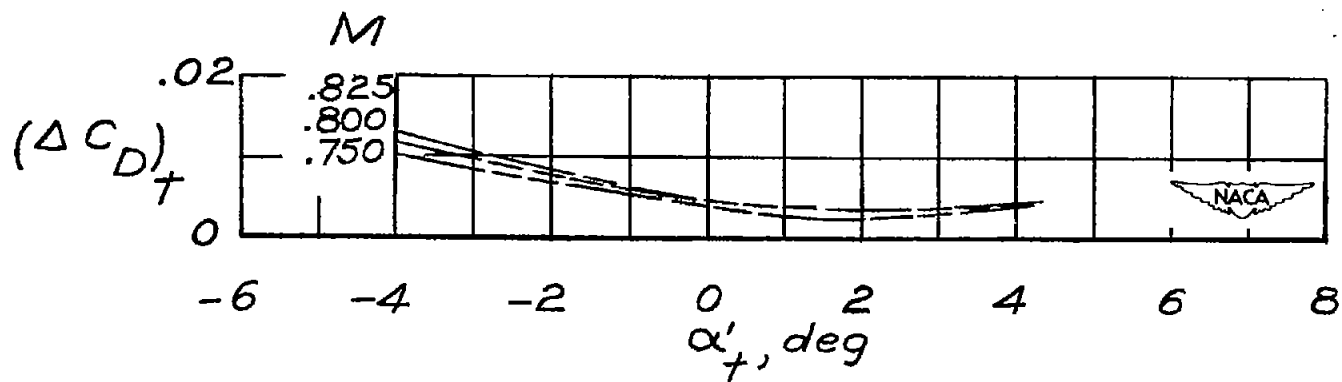
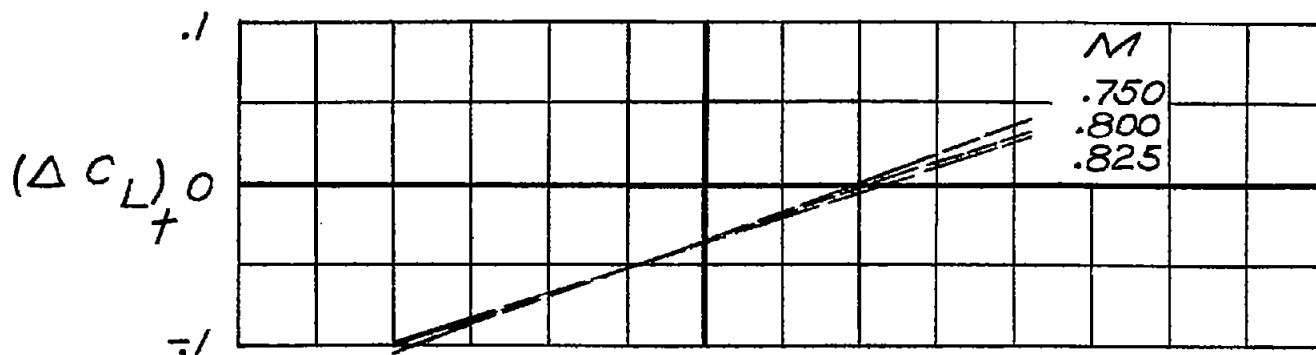


Figure 27.- Continued.

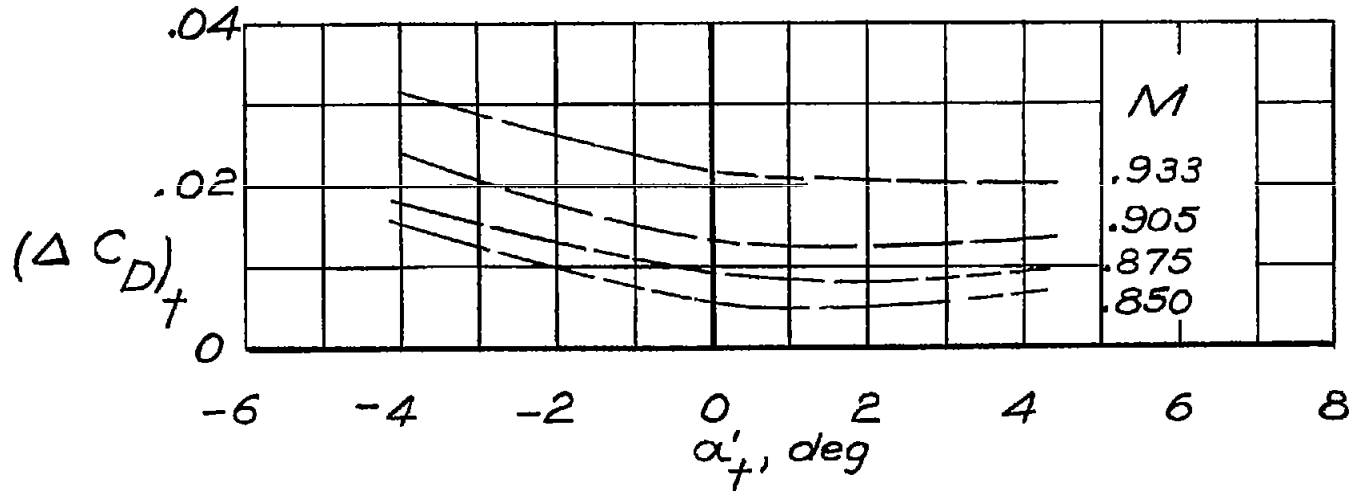
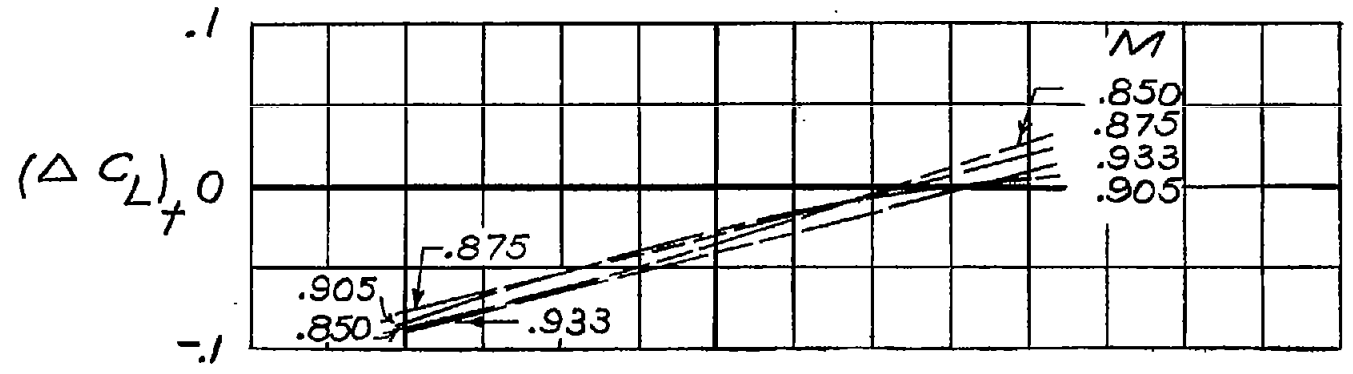


Figure 27.- Concluded.

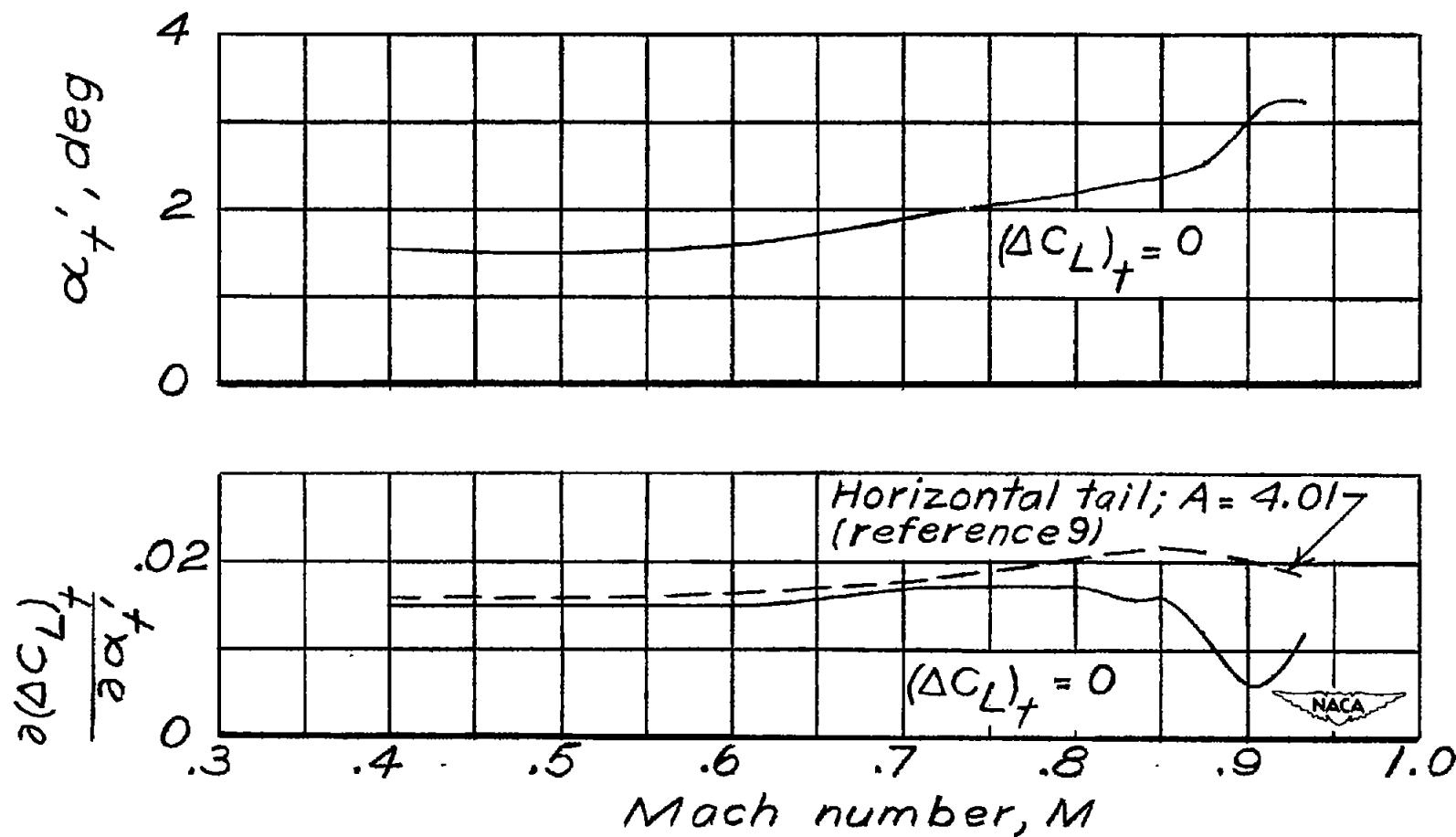


Figure 28.- Variation with Mach number of free-stream angle of attack of horizontal tail at incremental lift coefficient of horizontal tail of zero, and variation with Mach number of incremental lift-curve slope $\frac{d(\Delta C_L)_t}{d\alpha_t'}$. Complete model less wing; $A = 4.2$; $\alpha \approx -0.3^\circ$; $\delta_e = 0^\circ$.

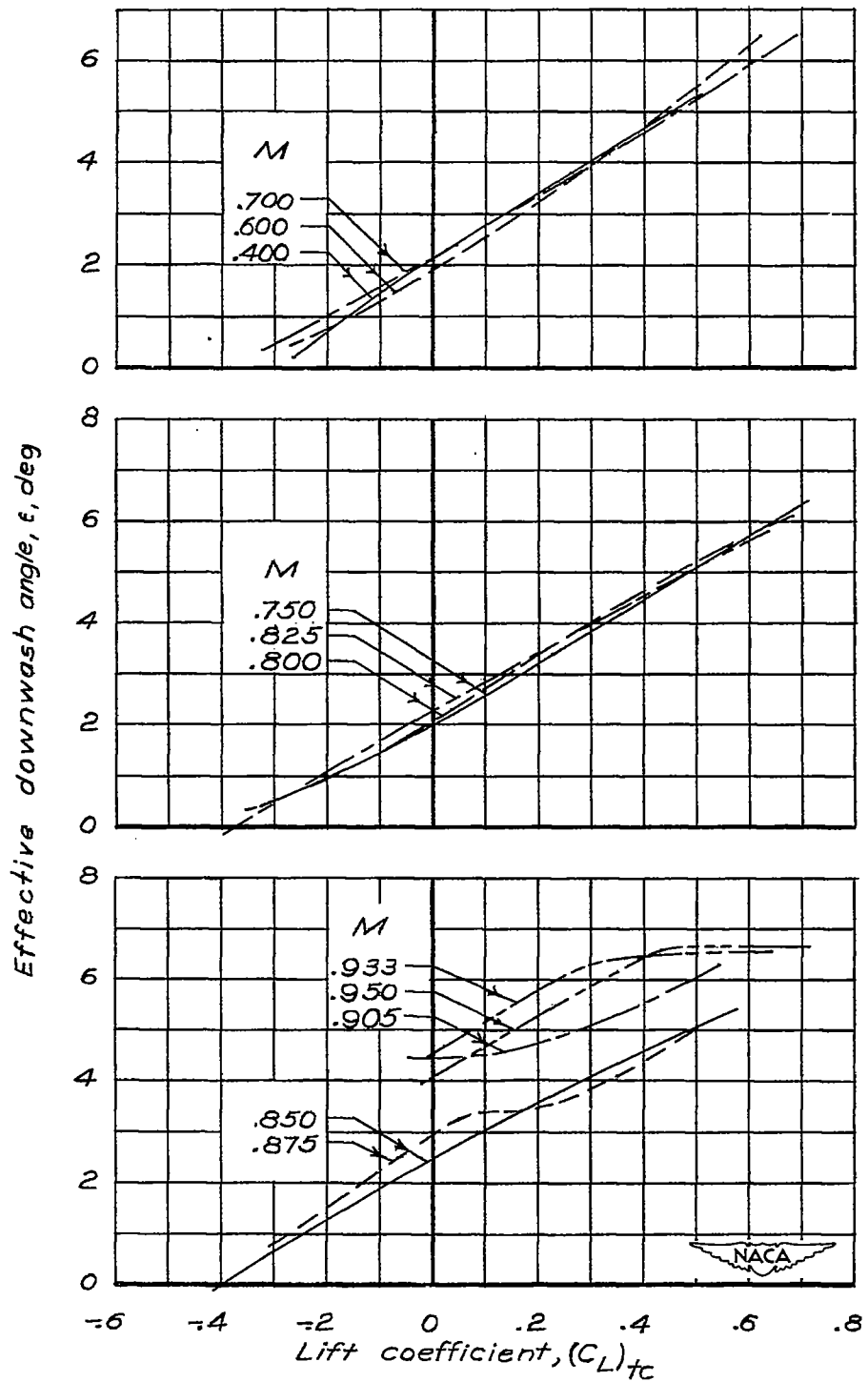


Figure 29.- Variation of effective downwash angle with lift coefficient at various Mach numbers. $A = 4.2$.

Effective downwash angle, ϵ , deg

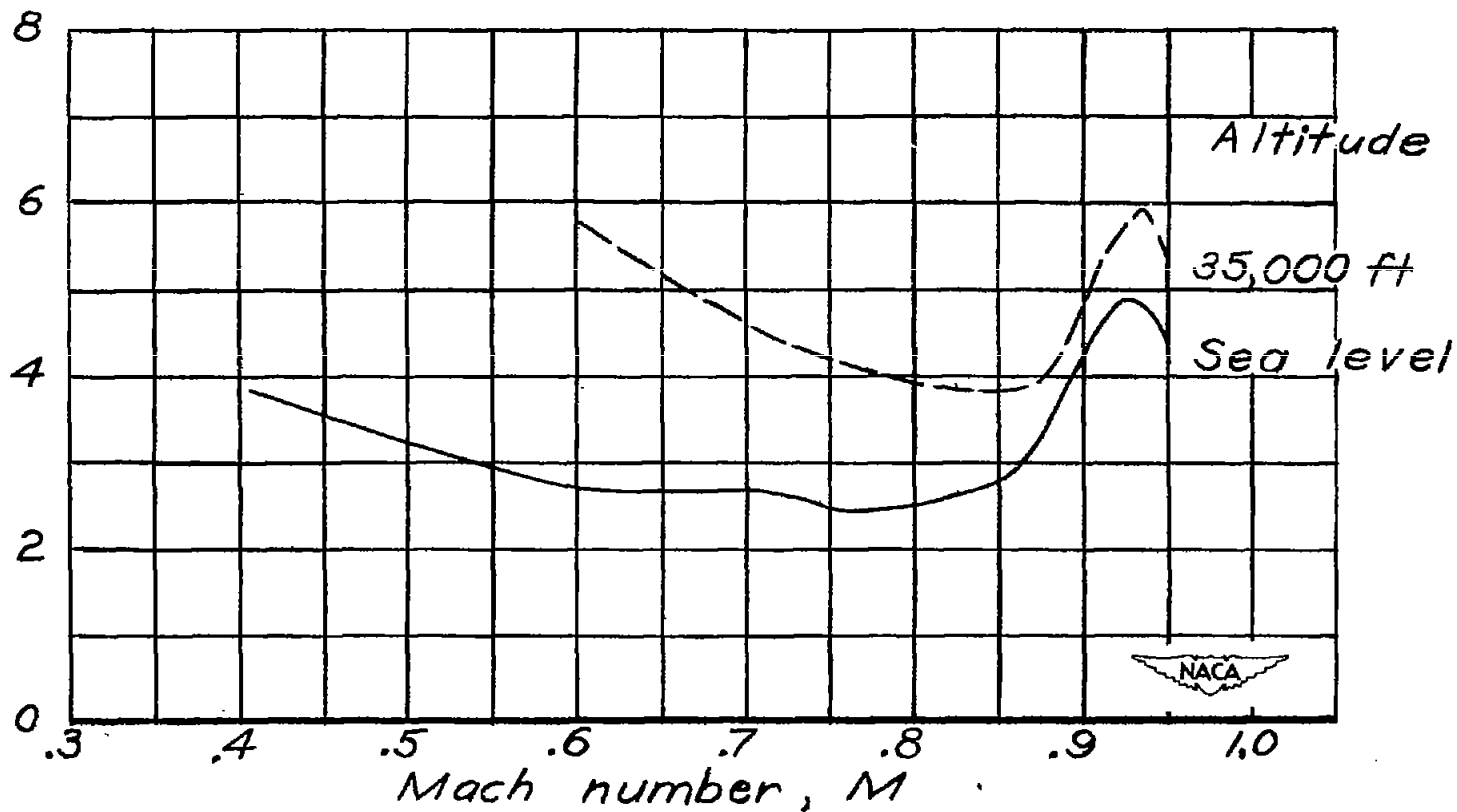


Figure 30.- Variation of effective downwash angle with Mach number at airplane lift coefficients corresponding to level flight at two altitudes for trim conditions with elevators undeflected and horizontal tail used for obtaining trim. $A = 4.2$; $\frac{W}{S} = 66.7$ pounds per square foot.

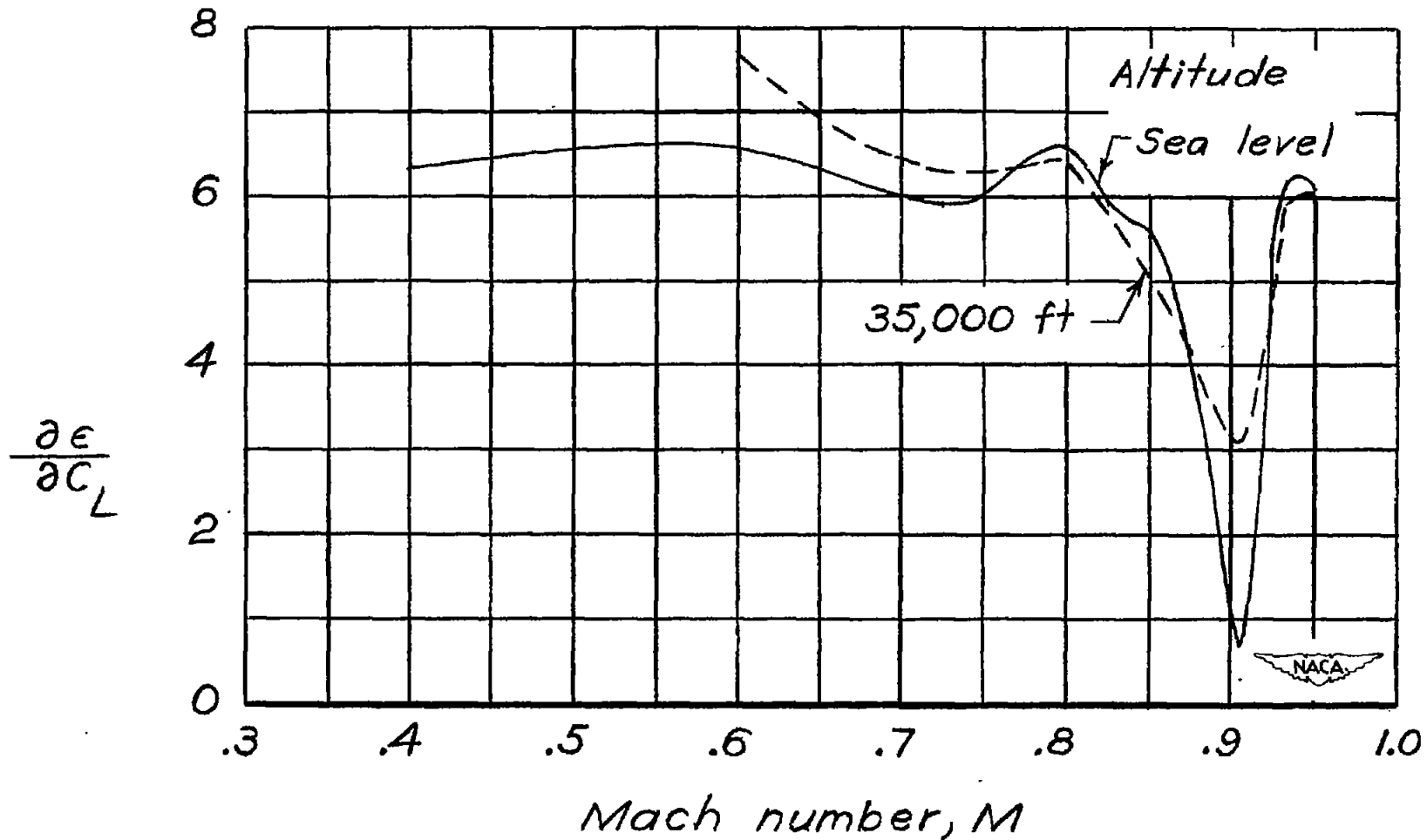


Figure 31.- Variation with Mach number of rate of change of effective downwash angle with respect to lift coefficient at airplane lift coefficients corresponding to level flight at two altitudes for trim conditions with elevators undeflected and horizontal tail used for obtaining trim. $A = 4.2$; $\frac{W}{S} = 66.7$ pounds per square foot.

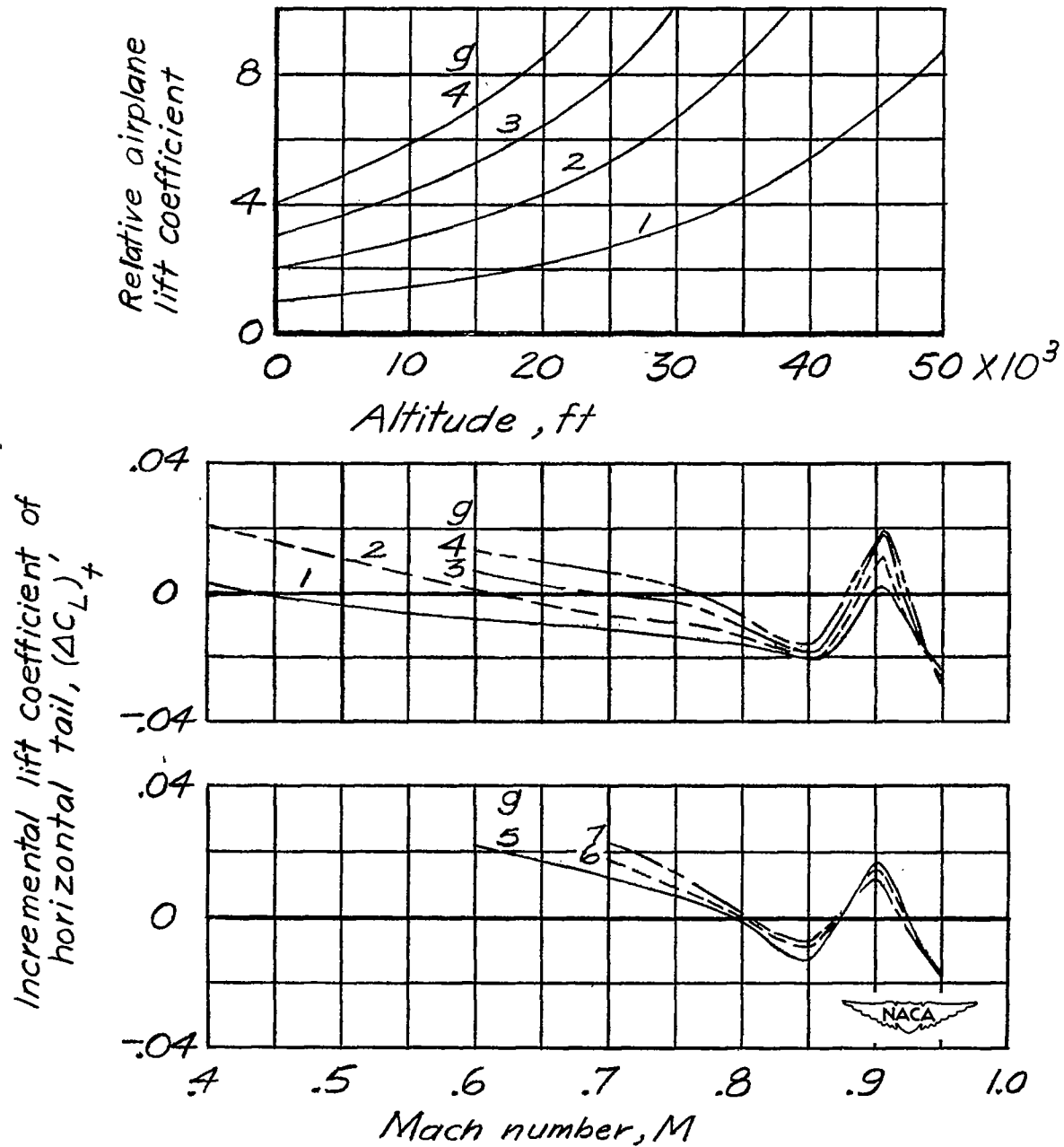


Figure 32.- Variation with Mach number of the incremental lift coefficient of the horizontal tail for trim conditions at various values of g for flight at sea level, and variation with altitude of the relative airplane lift coefficient at various values of g . Complete model;

$A = 4.2$; $\frac{W}{S} = 66.7$ pounds per square foot.

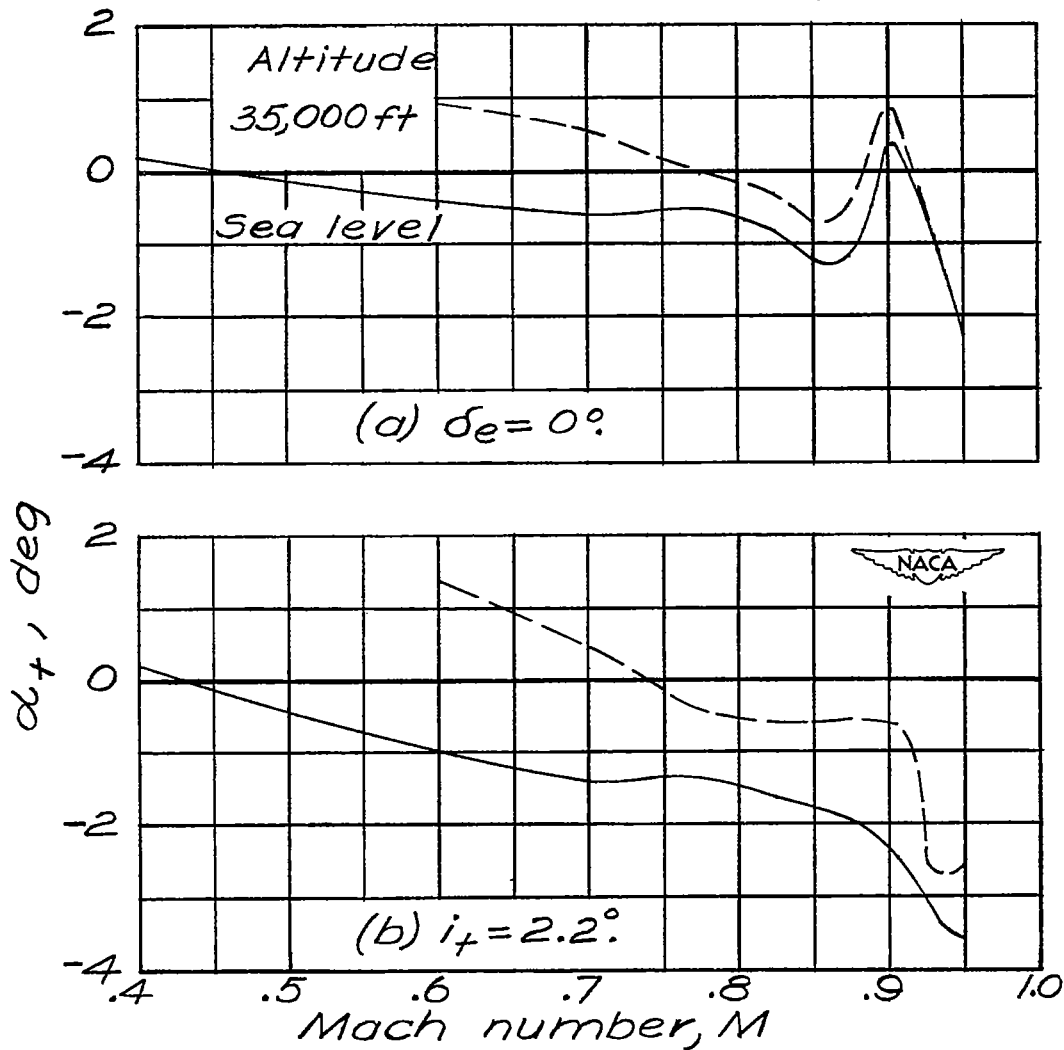


Figure 33.- Variation with Mach number of the angle of attack of the horizontal tail for trim conditions at airplane lift coefficients corresponding to level flight at two altitudes. Complete model; $A = 4.2$; $\frac{W}{S} = 66.7$ pounds per square foot.

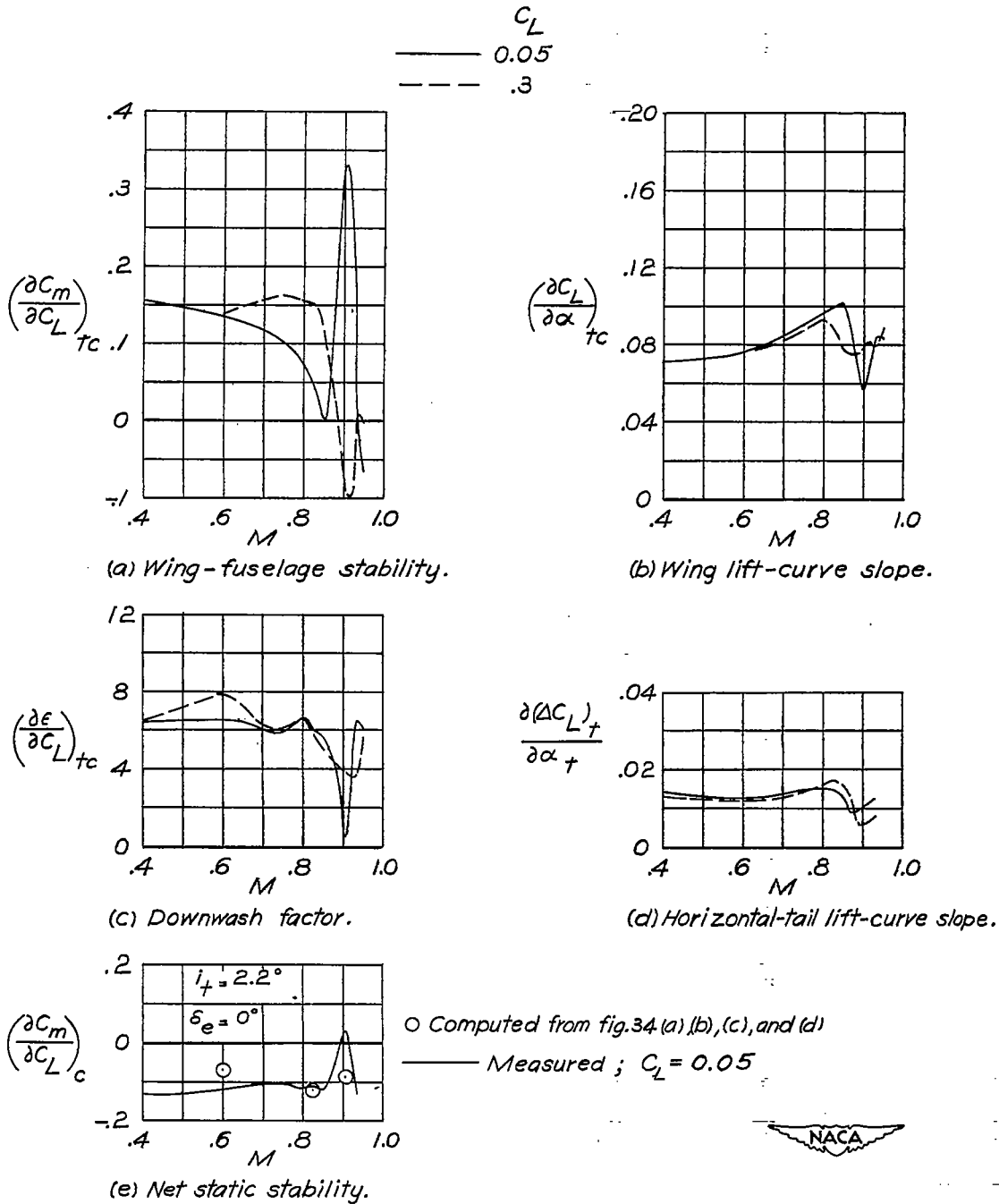
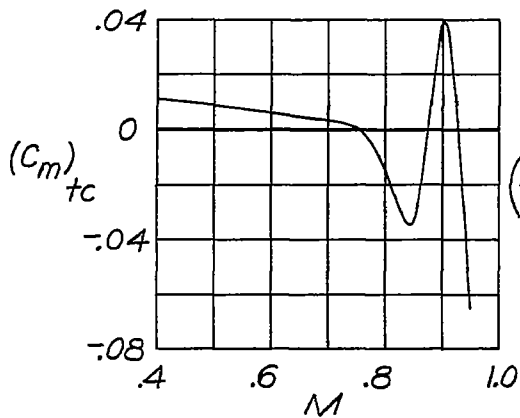
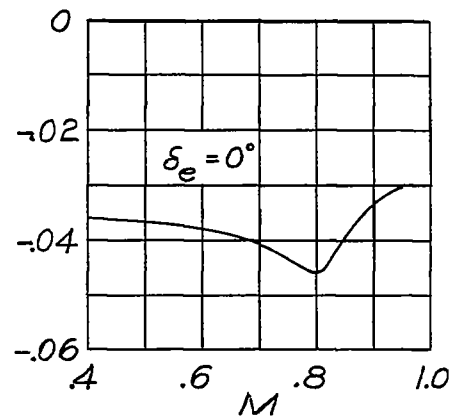


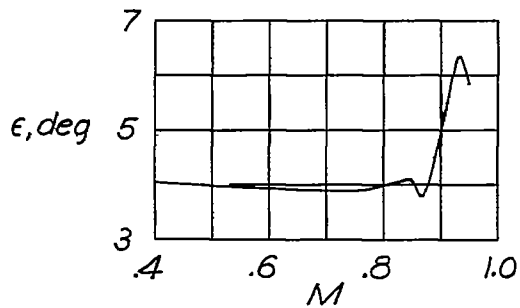
Figure 34.- Variation with Mach number of the static-longitudinal-stability parameter $(\partial C_m / \partial C_L)_C$ and of the various factors affecting longitudinal stability at two values of lift coefficient. $A = 4.2$.



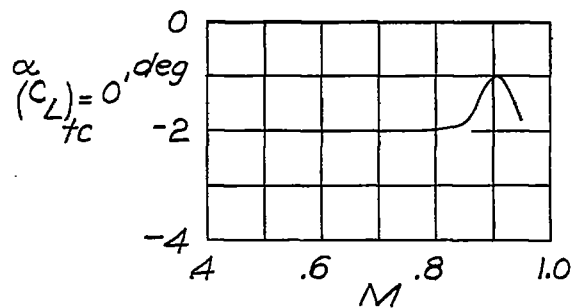
(a) Wing-fuselage moment.



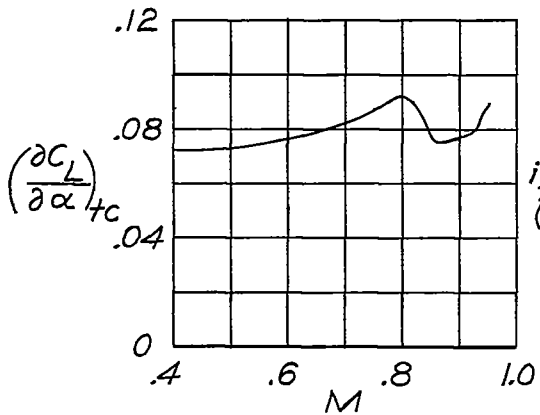
(b) Horizontal-tail effectiveness.



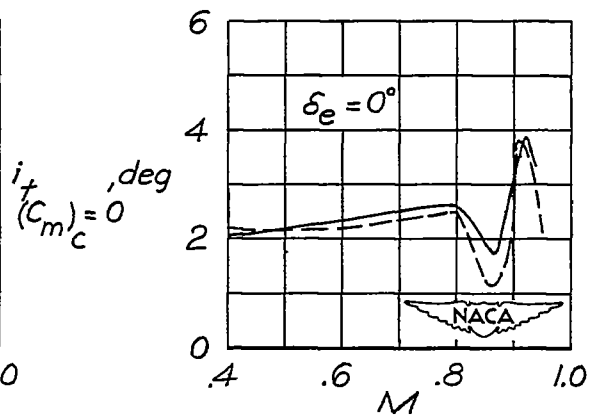
(c) Downwash angle.



(d) Angle of attack for zero lift.



(e) Lift-curve slope.



(f) Horizontal-tail incidence required for obtaining trim.

———— Measured
 - - - - - Computed

Figure 35.- Variation with Mach number of the horizontal-tail incidence required for obtaining trim and of the various factors affecting this parameter at a lift coefficient of 0.3. $A = 4.2$.

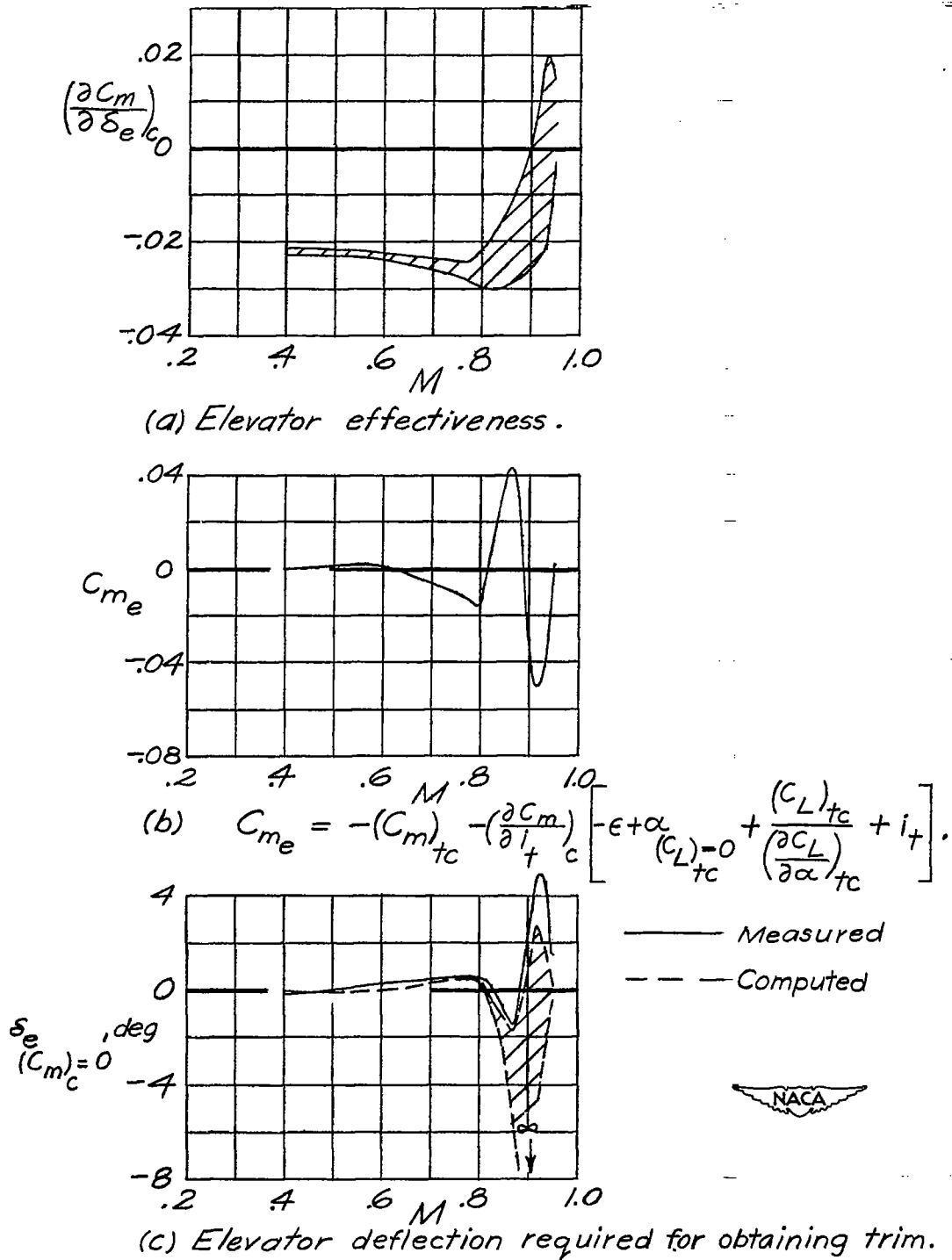


Figure 36.- Variation with Mach number of the elevator deflection required for obtaining trim and of the various factors affecting this parameter at a lift coefficient of 0.3. $A = 4.2$; $i_t = 2.2^\circ$.

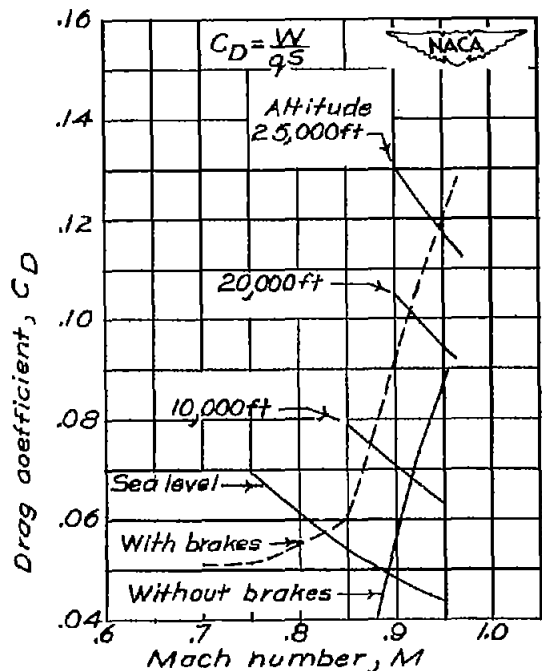


Figure 37.- Variation of drag coefficient with Mach number at an airplane lift coefficient of zero. Complete model and complete model plus air brakes; $A = 4.2$; $i_t = 2.2^\circ$; $\delta_e = 0^\circ$. Also shown is variation of drag coefficient with Mach number when drag is equal to weight of airplane and wing loading is equal to 58 pounds per square foot.

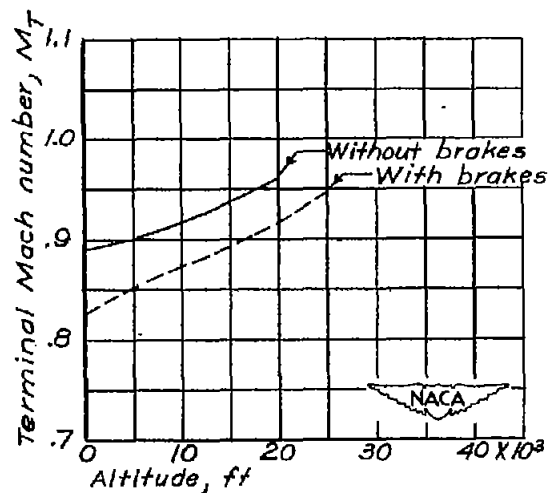


Figure 38.- Variation of terminal Mach number with altitude. Complete model and complete model plus air brakes; $A = 4.2$; $i_t = 2.2^\circ$; $\delta_e = 0^\circ$; $\frac{W}{S} = 58$ pounds per square foot.

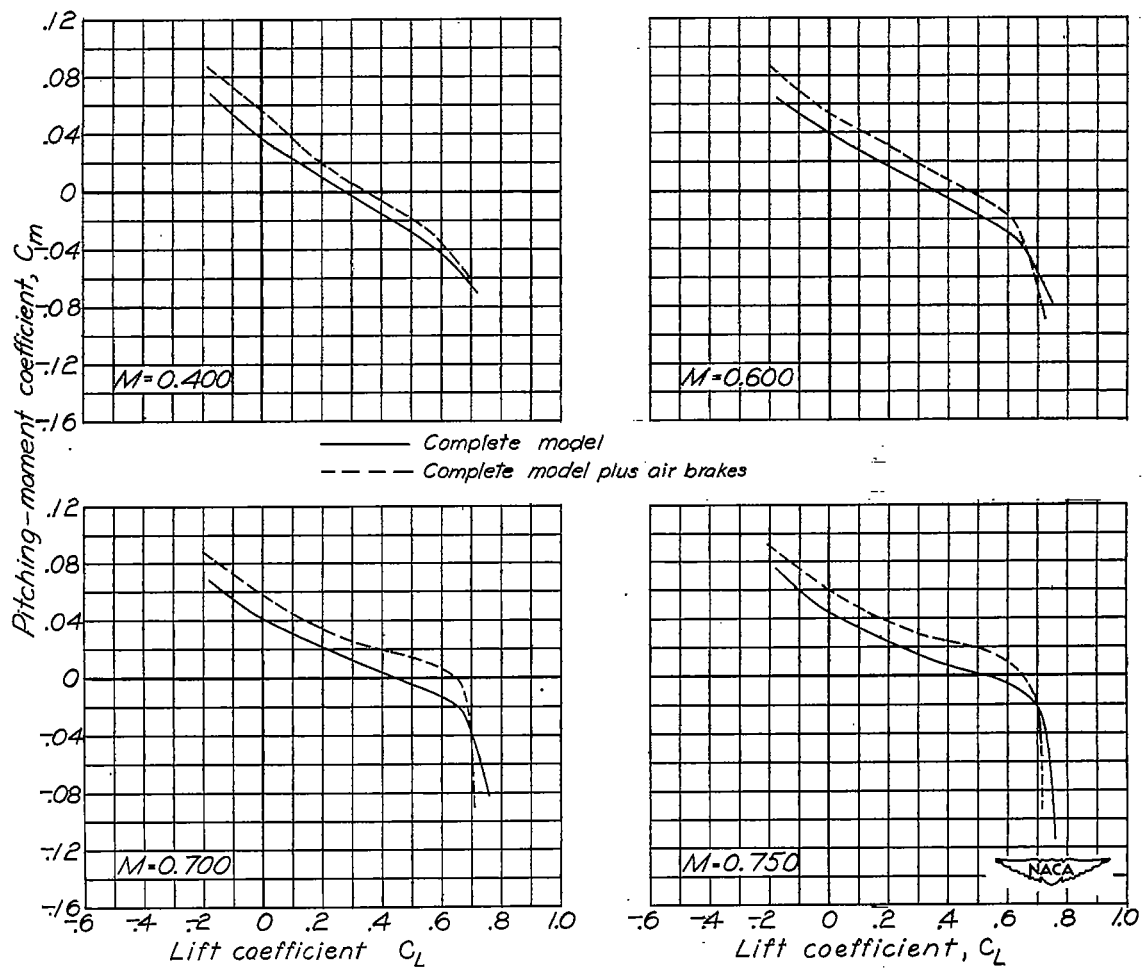


Figure 39.- Variation of pitching-moment coefficient with lift coefficient. Complete model and complete model plus air brakes; $A = 4.2$; $i_t = 2.2^\circ$; $\delta_e = 0^\circ$.

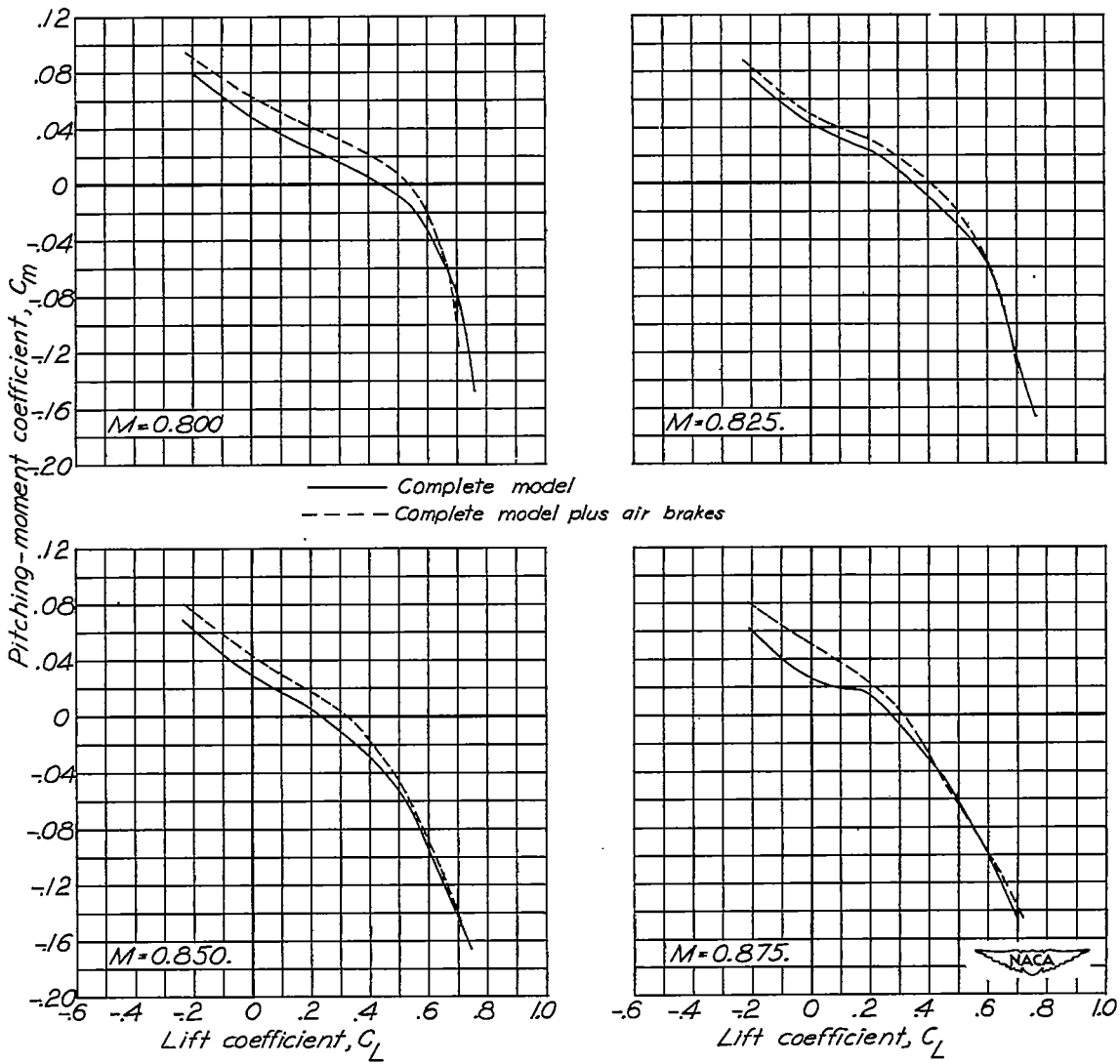


Figure 39.- Continued.

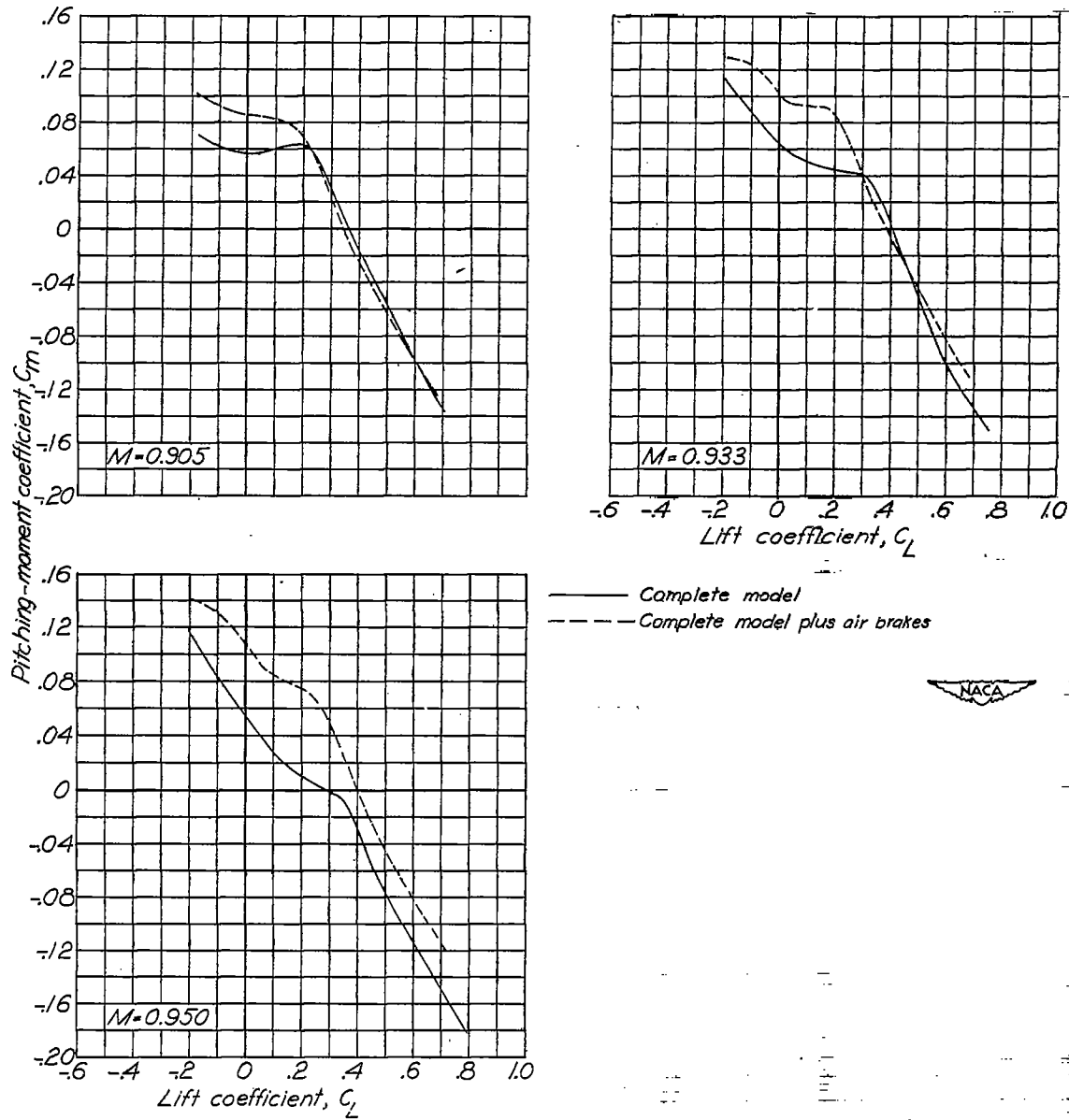


Figure 39.- Concluded.

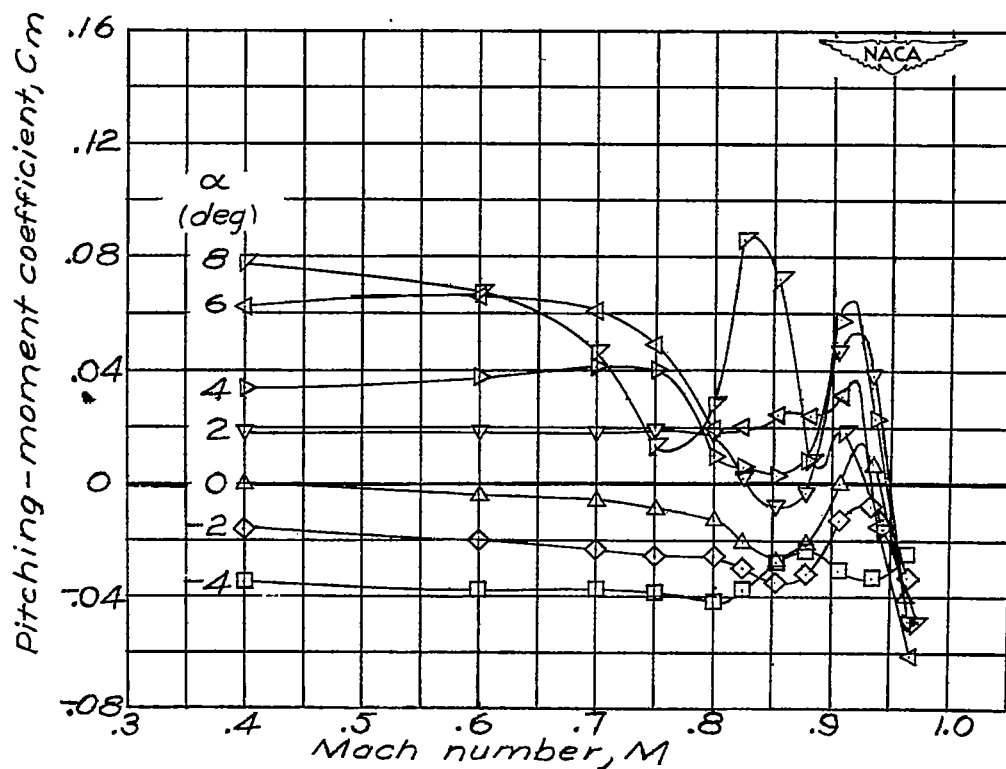
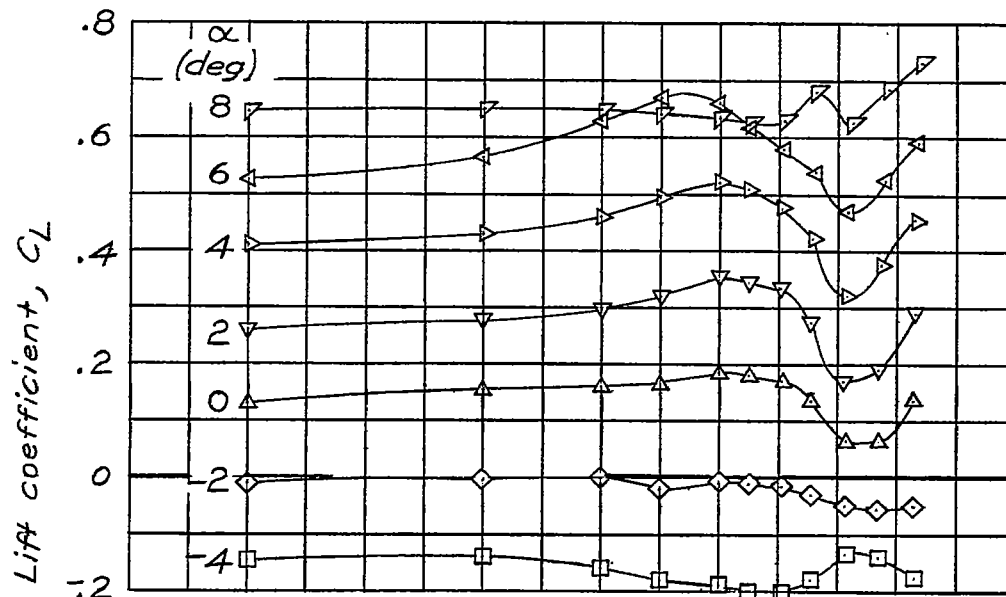


Figure 40.- Variation of lift coefficient and pitching-moment coefficient with Mach number at various model angles of attack. Complete model less horizontal tail plus air brakes; $A = 4.2$.

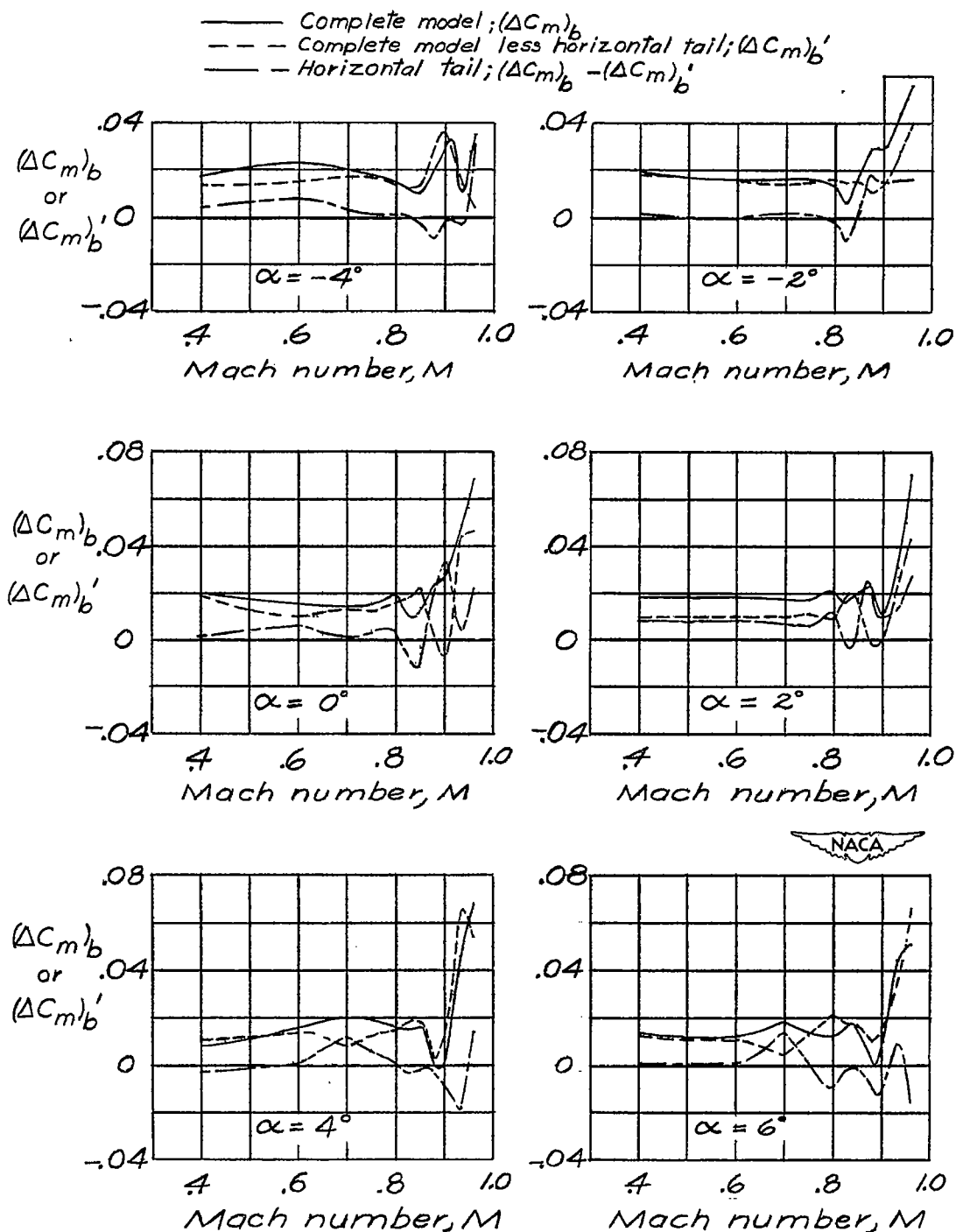


Figure 41.- Effect of air brakes on pitching-moment coefficient of complete model, $i_t = 2.2^\circ$, $\delta_e = 0^\circ$; on pitching-moment coefficient of complete model less horizontal tail; and on incremental pitching-moment coefficient of horizontal tail. $A = 4.2$.

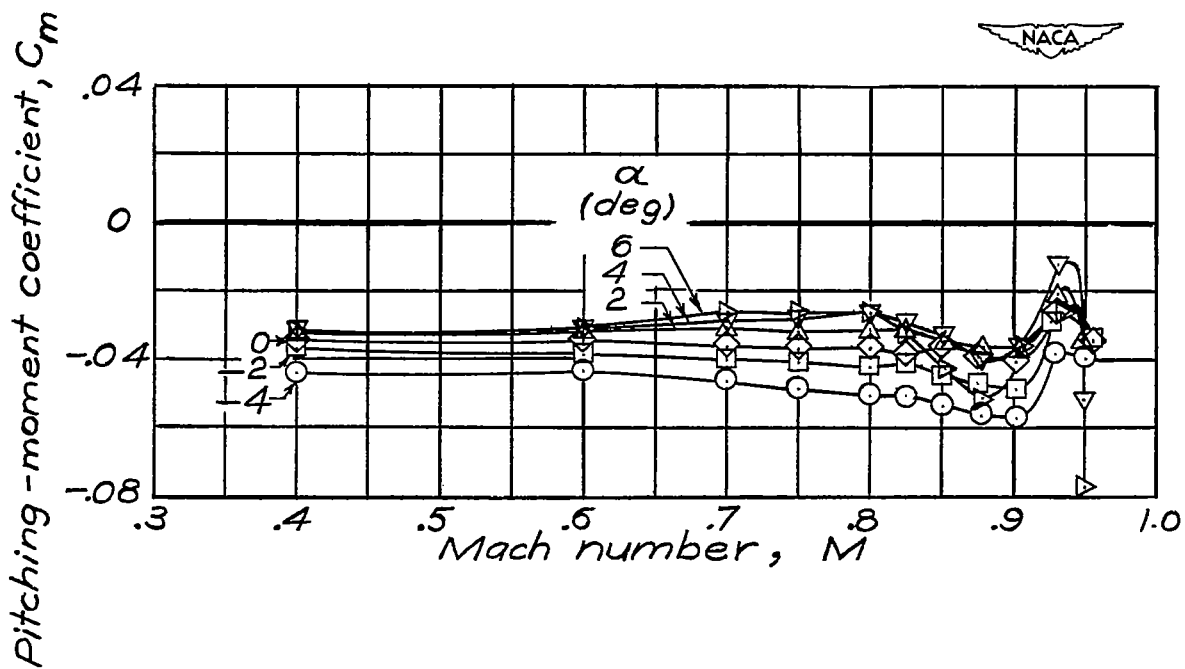
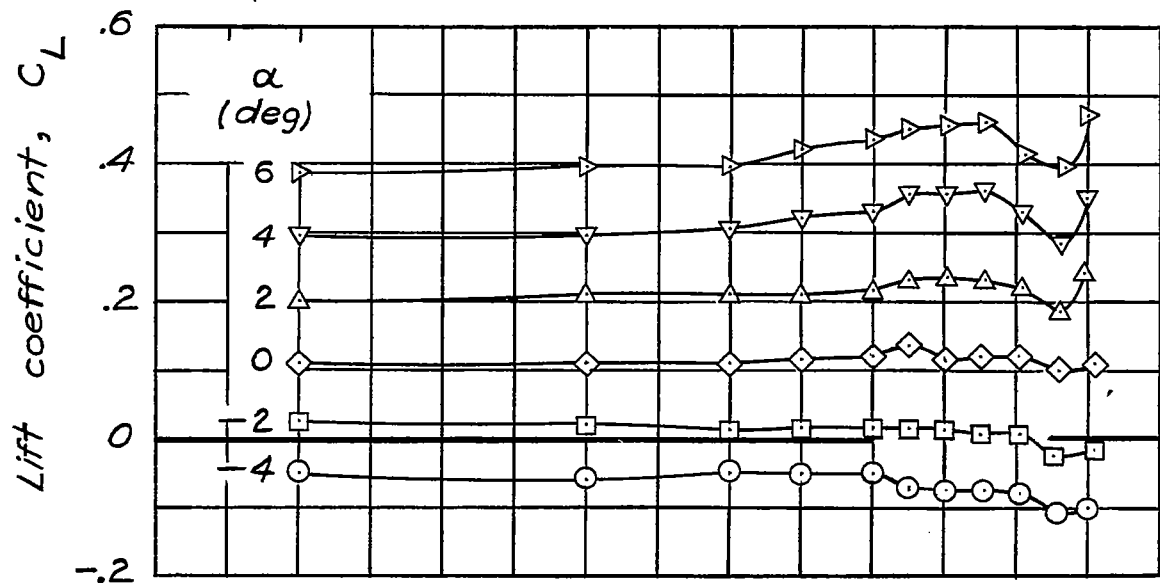


Figure 42.- Variation of lift coefficient and pitching-moment coefficient with Mach number at various model angles of attack. Complete model less horizontal tail; $A = 2$.

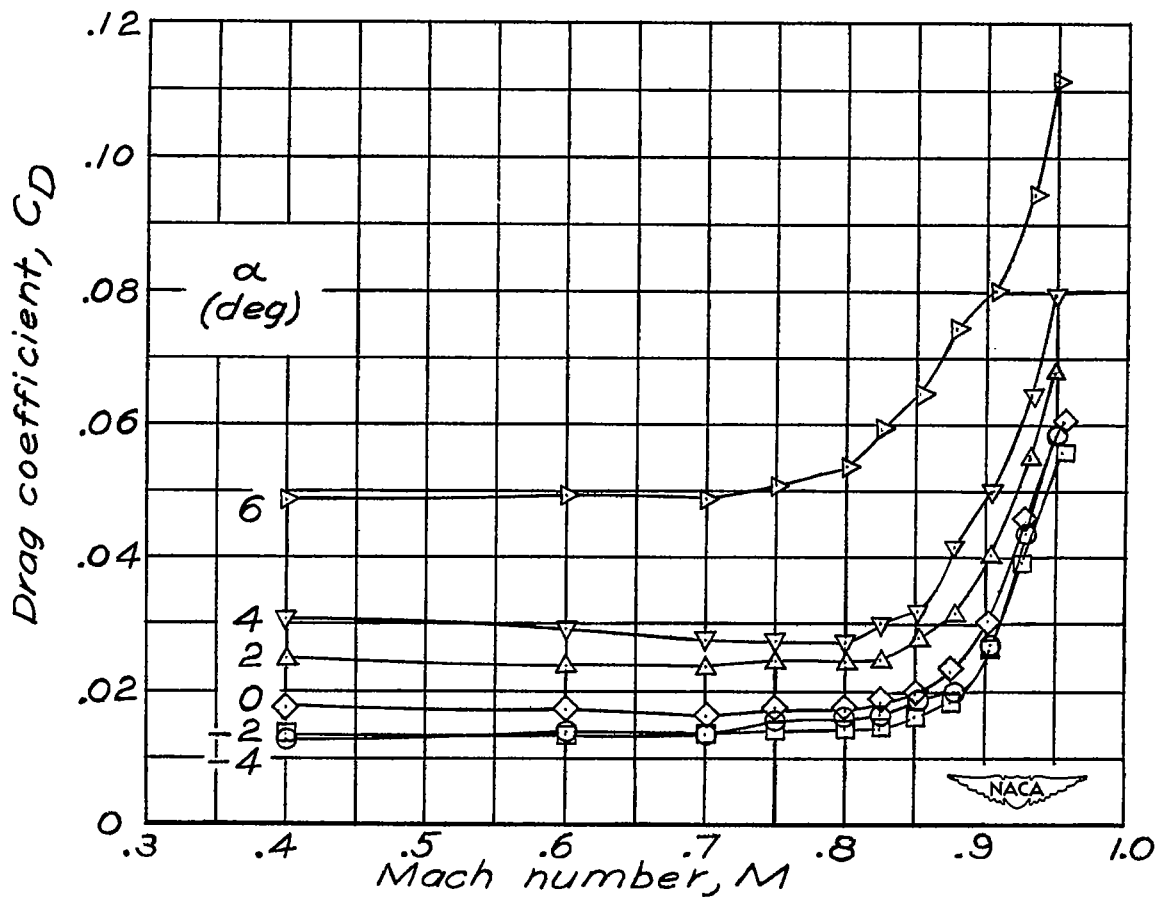
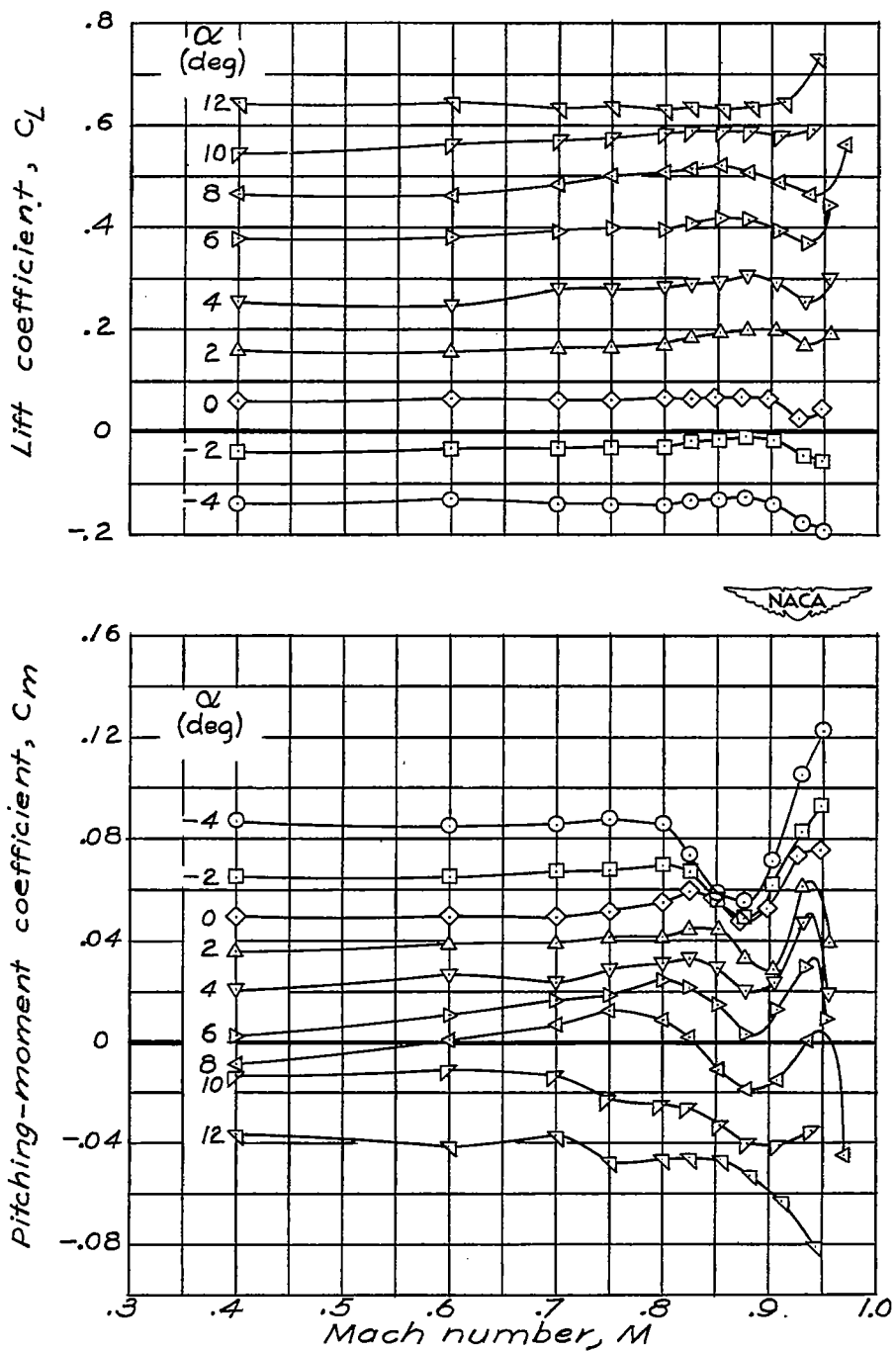
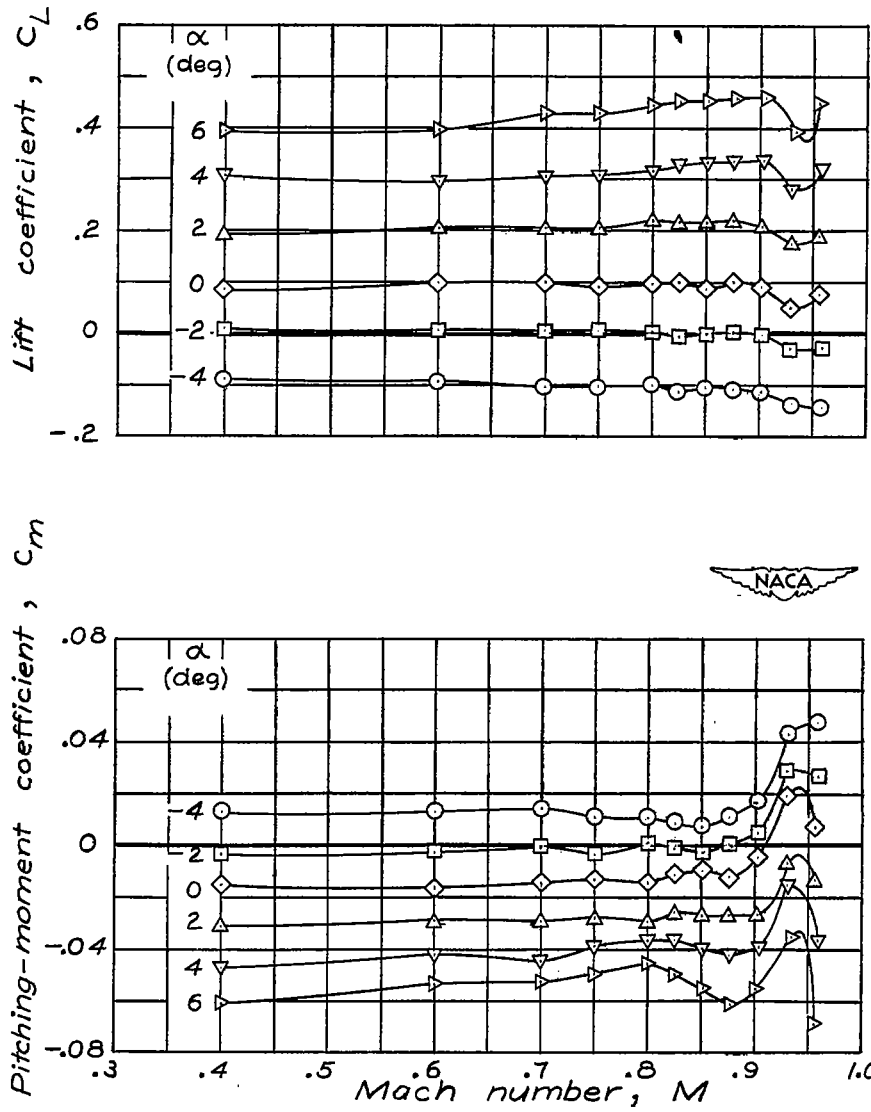


Figure 43.- Variation of drag coefficient with Mach number at various model angles of attack. Complete model less horizontal tail; $A = 2$.



(a) $i_t = -2.1^\circ$.

Figure 44.- Variation of lift coefficient and pitching-moment coefficient with Mach number at various model angles of attack. Complete model; $A = 2$; $\delta_e = 0^\circ$.



(b) $i_t = 2.1^\circ$.

Figure 44.- Concluded.

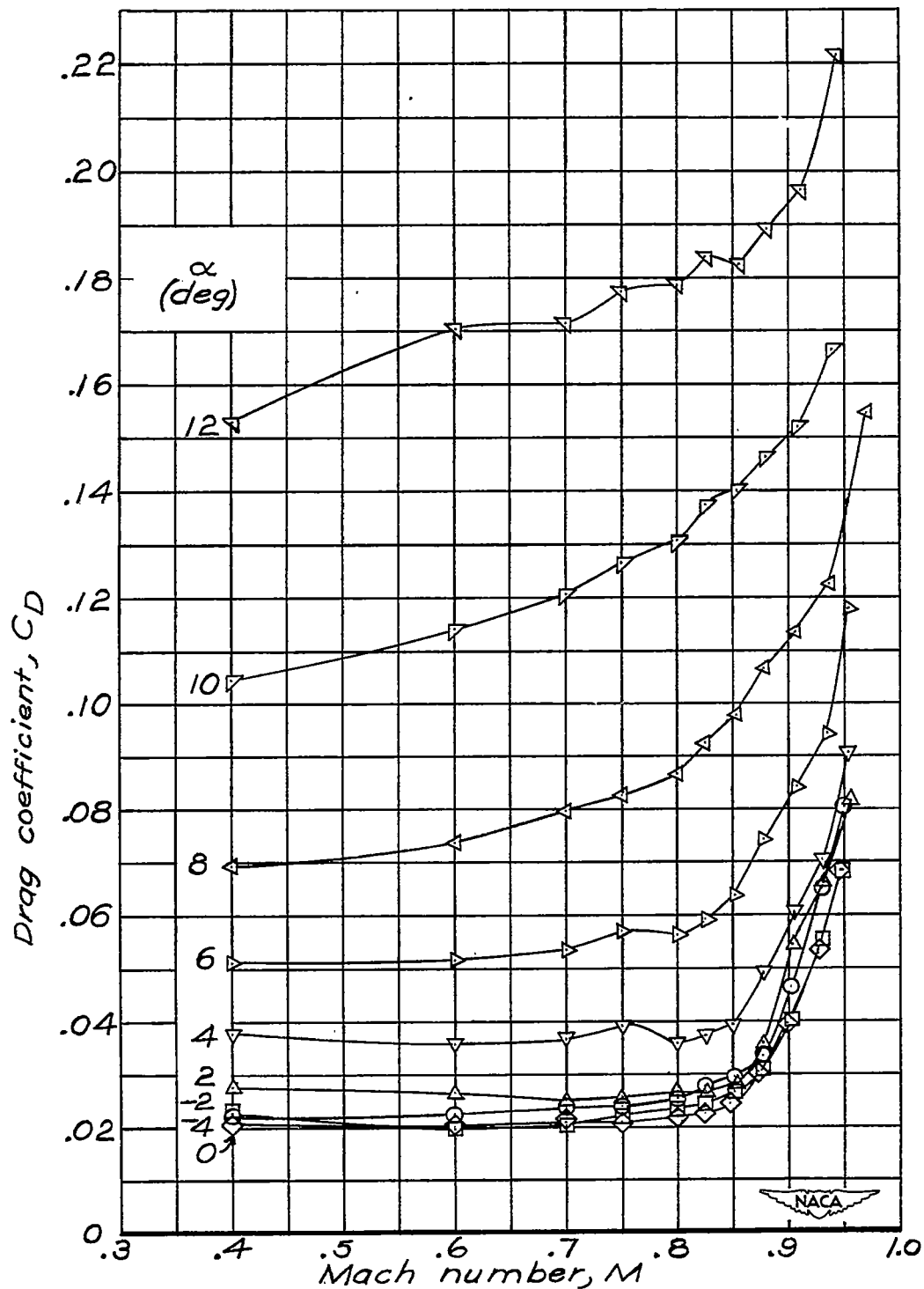


Figure 45.- Variation of drag coefficient with Mach number at various model angles of attack. Complete model; $A = 2$; $i_t = -2.1^\circ$; $\delta_e = 0^\circ$.

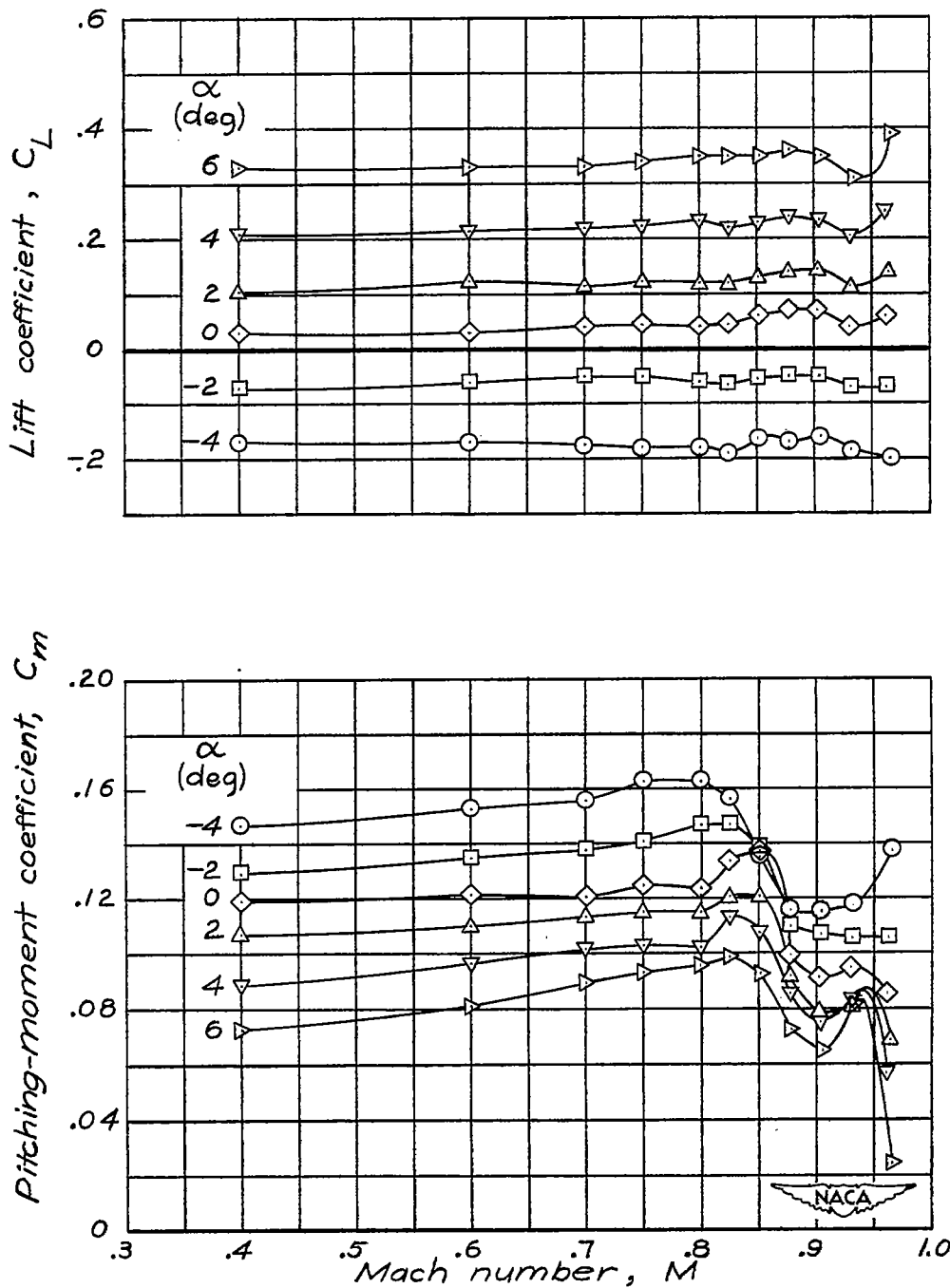
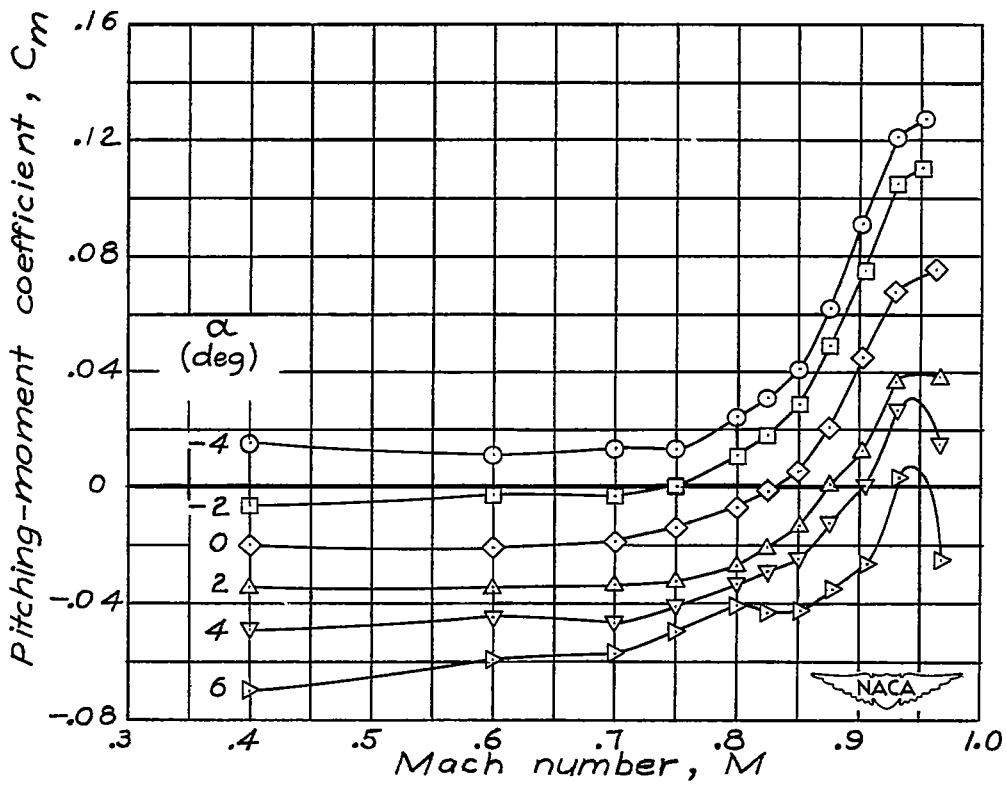
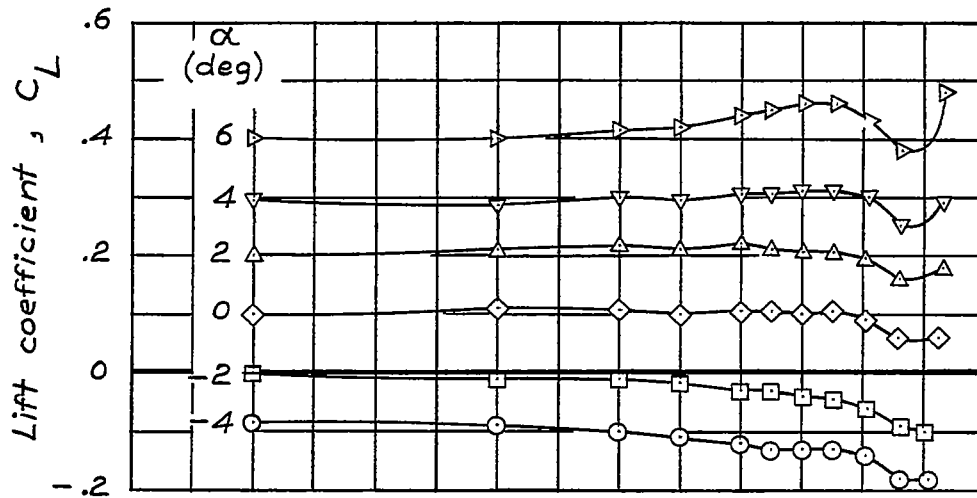
(a) $\delta_e = -6^\circ$.

Figure 46.- Variation of lift coefficient and pitching-moment coefficient with Mach number at various model angles of attack. Complete model; $A = 2$; $i_t = -2.1^\circ$.



(b) $\delta_e = 6^\circ$.

Figure 46.- Concluded.

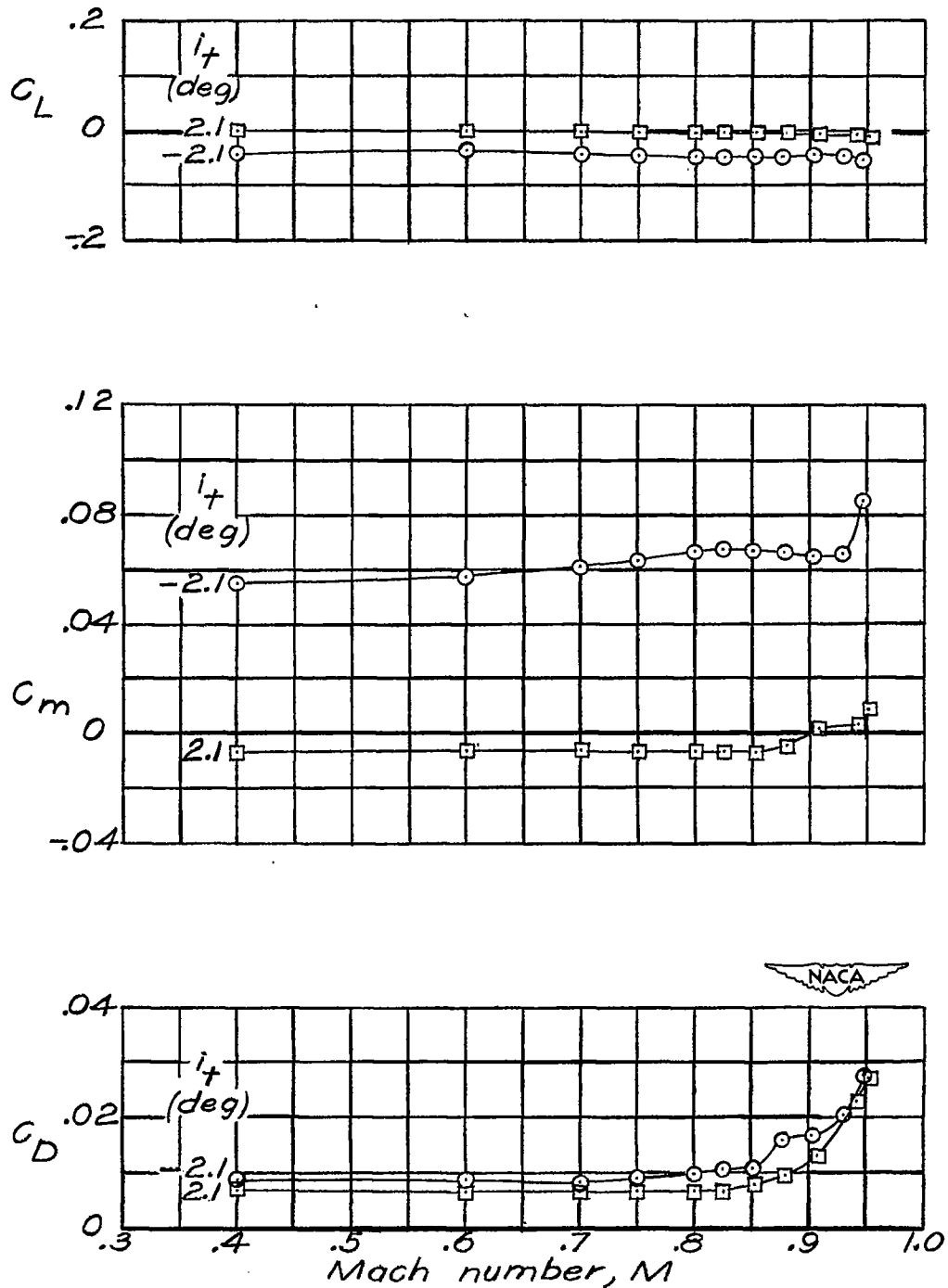


Figure 47.- Variation of lift coefficient, pitching-moment coefficient, and drag coefficient with Mach number at two horizontal-tail incidences. Coefficients uncorrected for sting interference. Complete model less wing; $A = 2$; $\alpha = -0.2^\circ$; $\delta_e = 0^\circ$.

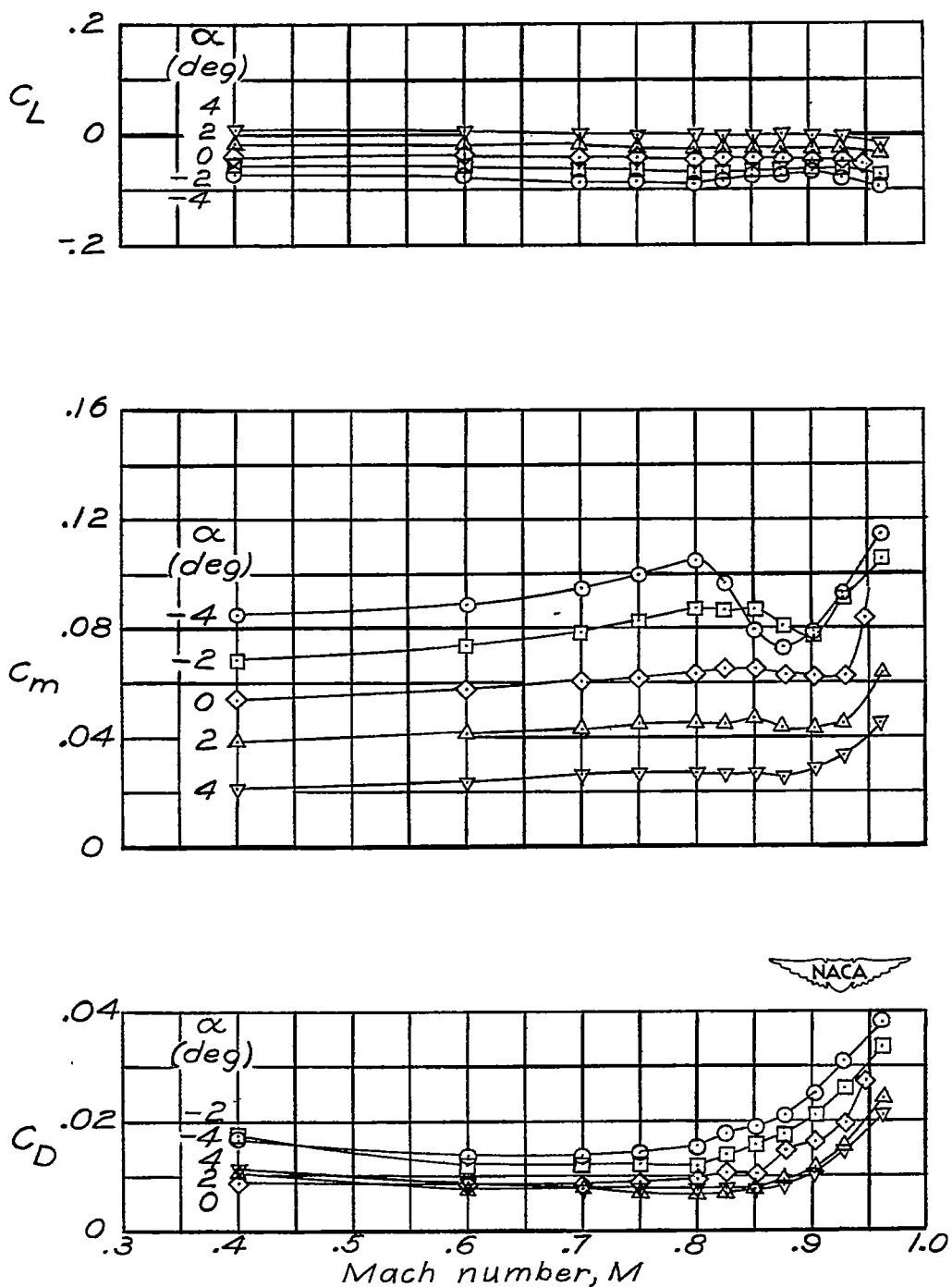


Figure 48.- Variation of lift coefficient, pitching-moment coefficient, and drag coefficient with Mach number at various model angles of attack. Coefficients uncorrected for sting interference. Complete model less wing; $A = 2$; $i_t = -2.1^\circ$; $\delta_e = 0^\circ$.

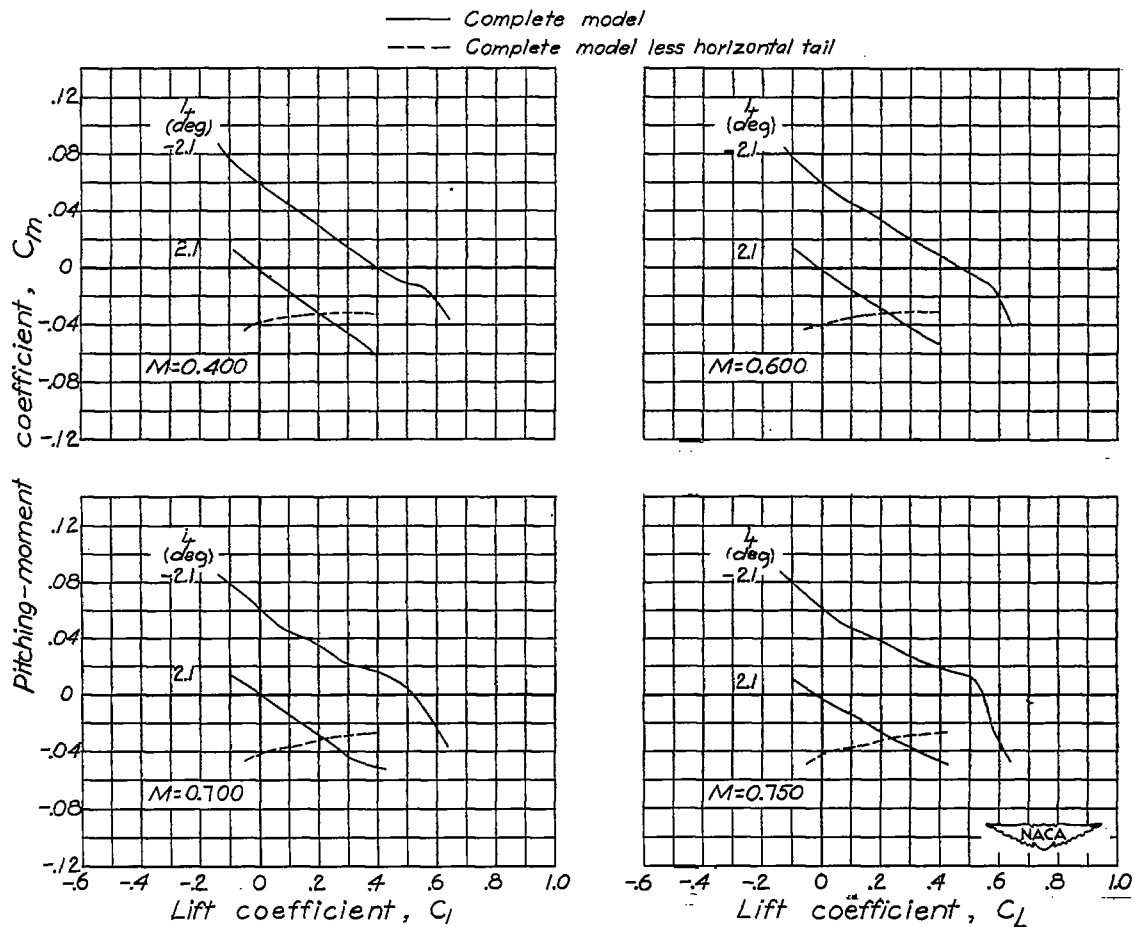


Figure 49.- Variation of pitching-moment coefficient with lift coefficient. Complete model at two horizontal-tail incidences, $\delta_e = 0^\circ$; and complete model less horizontal tail. $A = 2$.

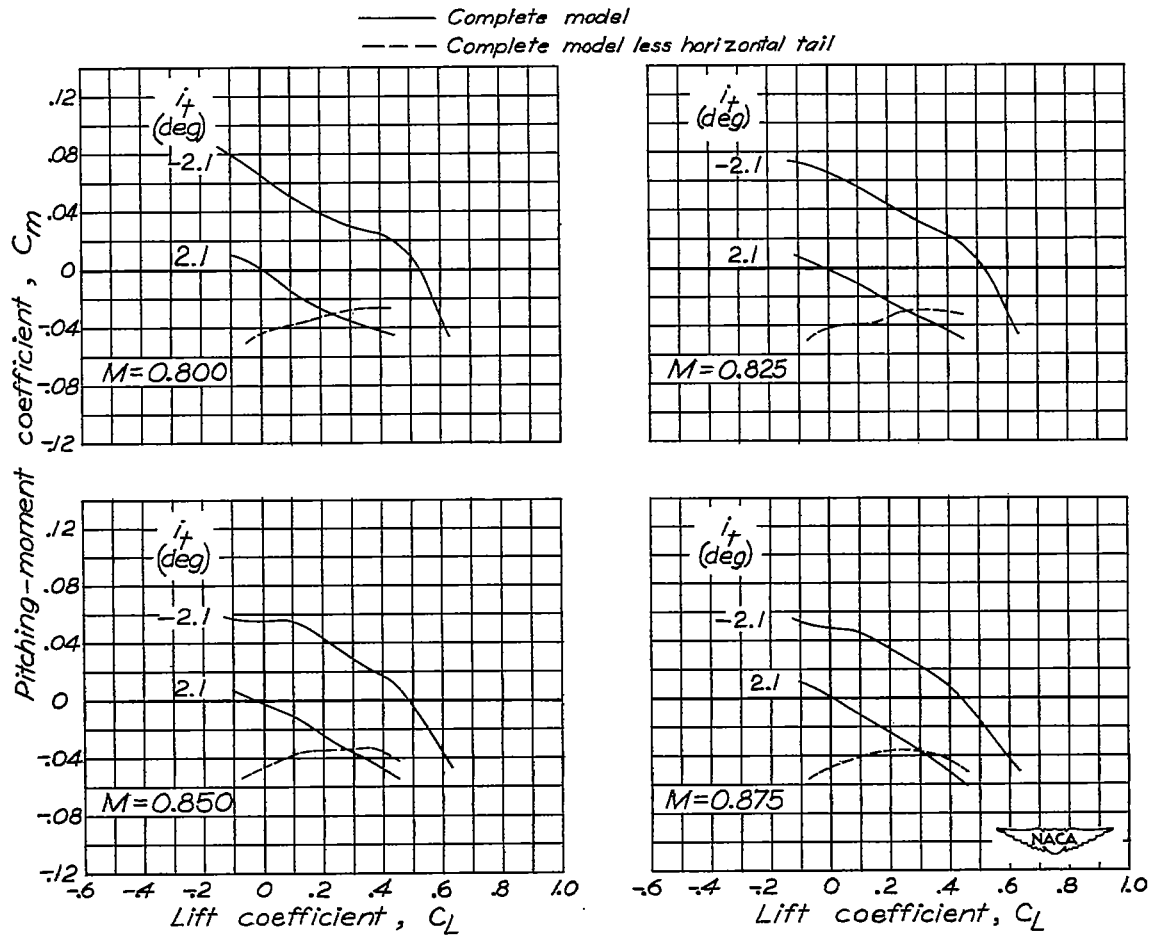


Figure 49.- Continued.

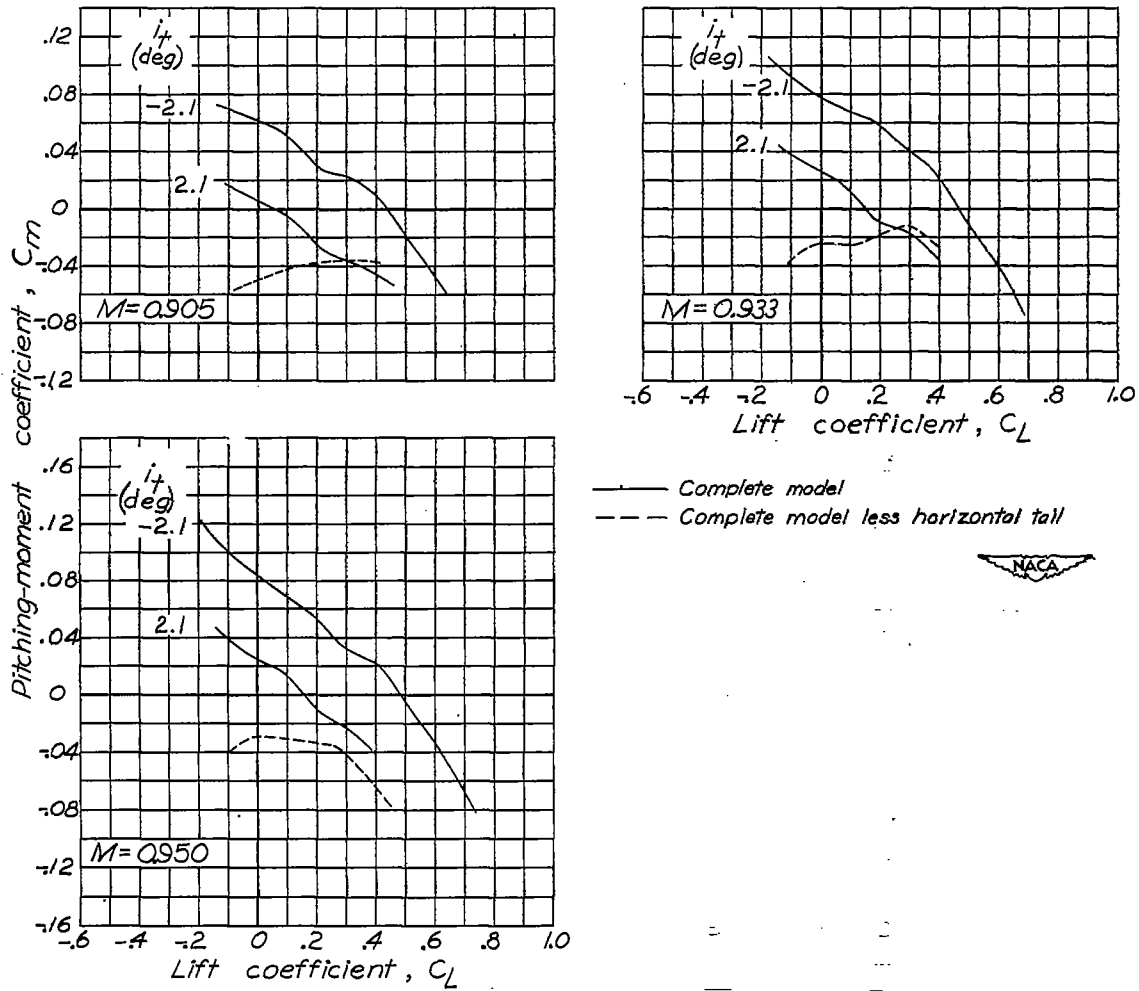


Figure 49.- Concluded.

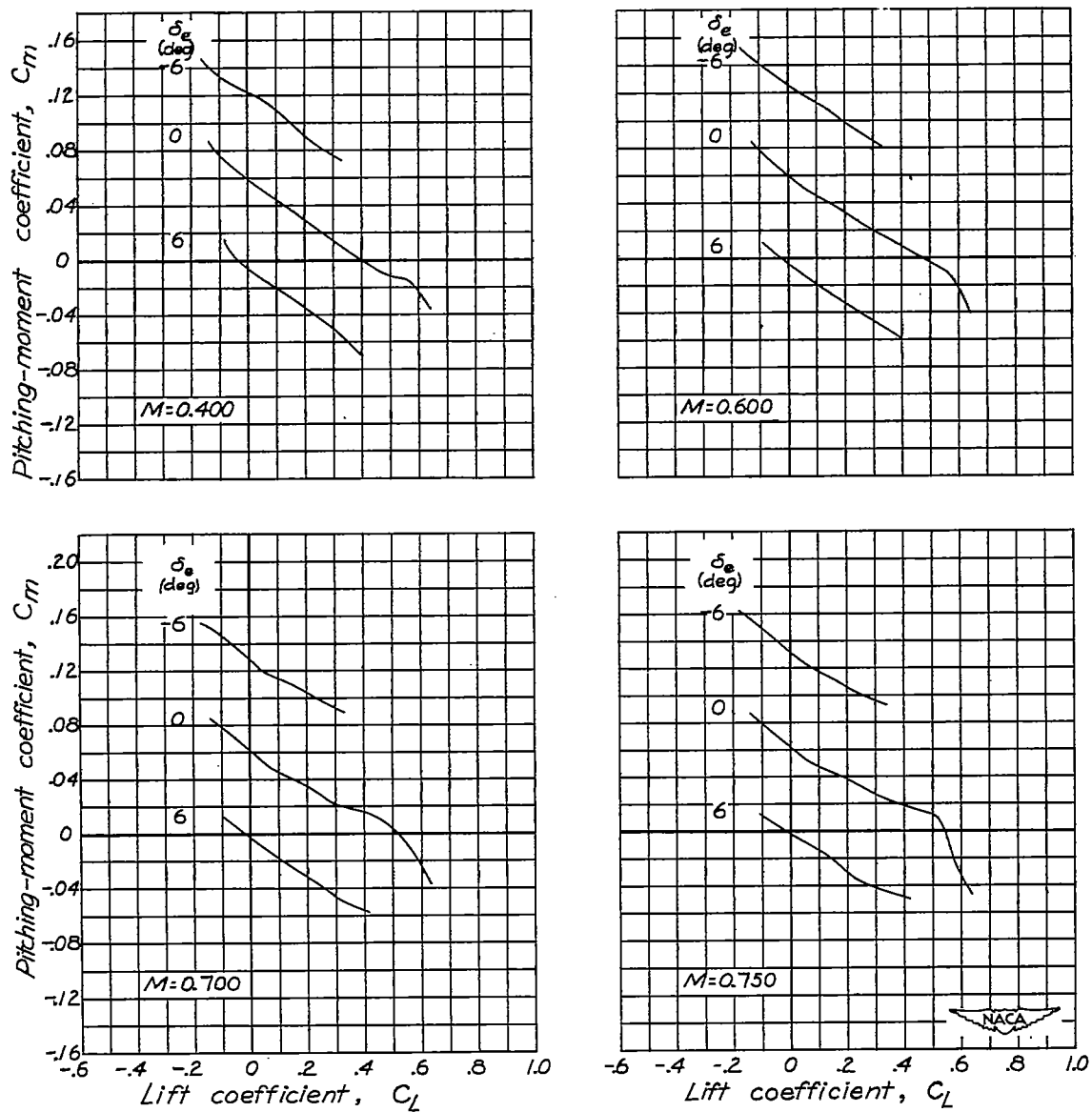


Figure 50.- Variation of pitching-moment coefficient with lift coefficient at various elevator deflections. Complete model; $A = 2$; $i_t = -2.1^\circ$.

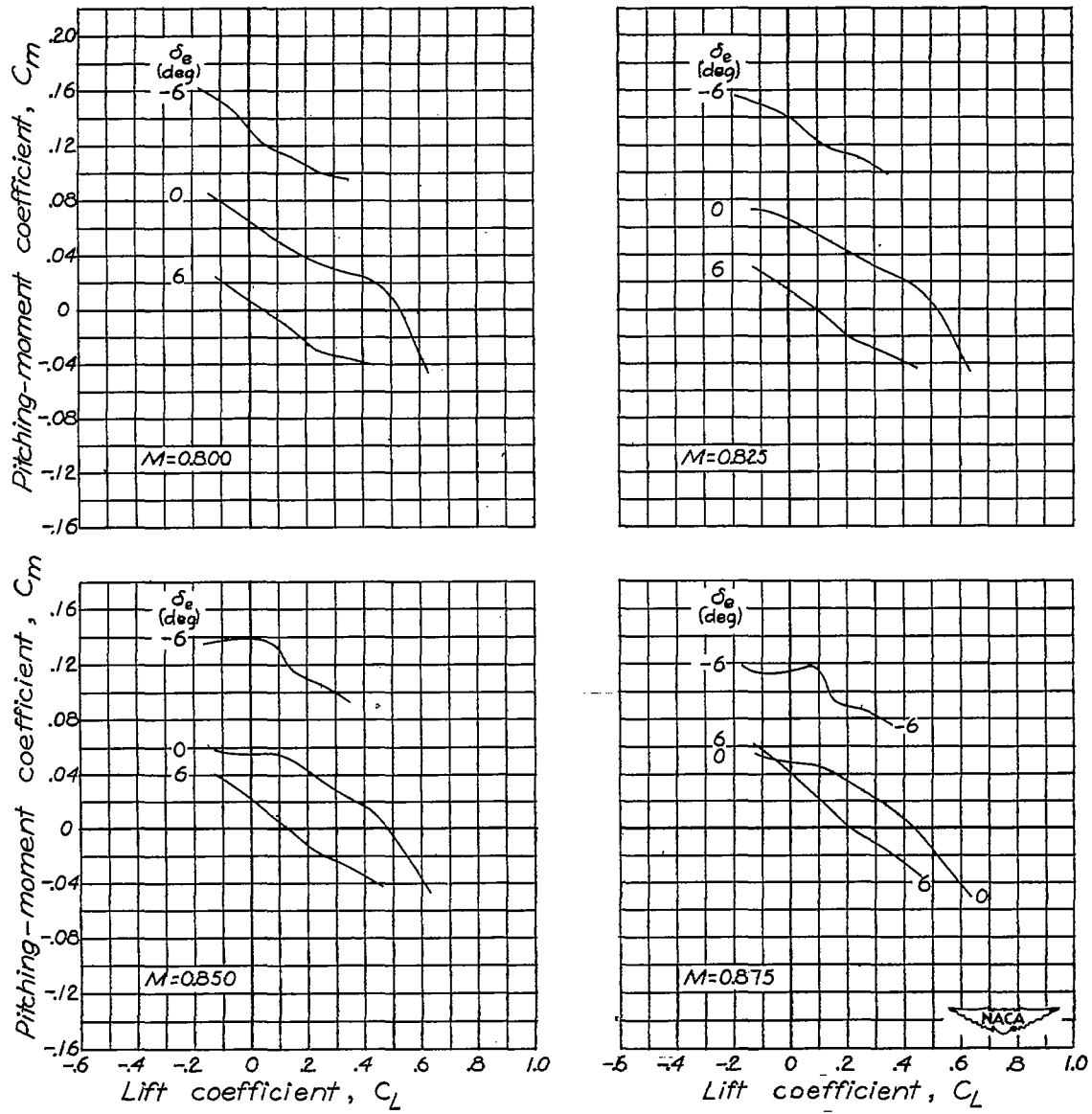


Figure 50.- Continued.

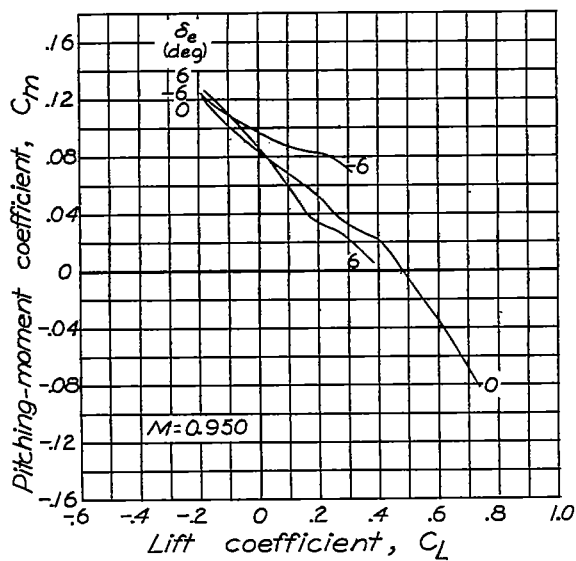
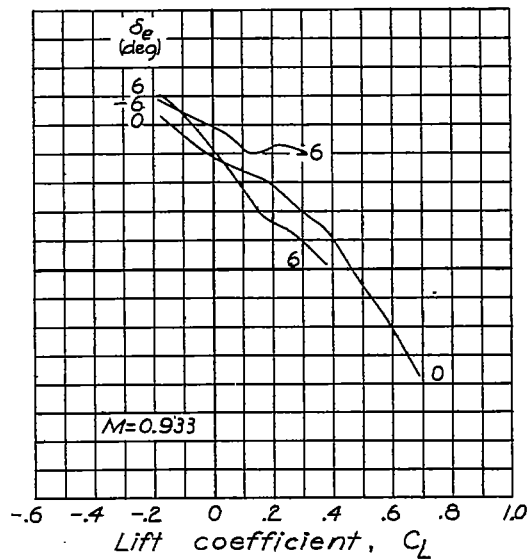
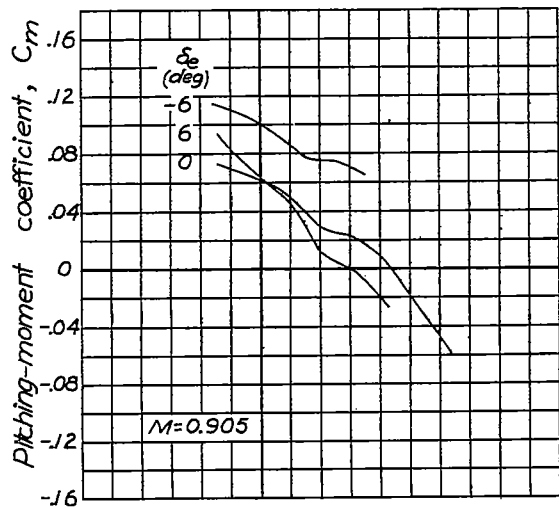


Figure 50.- Concluded.

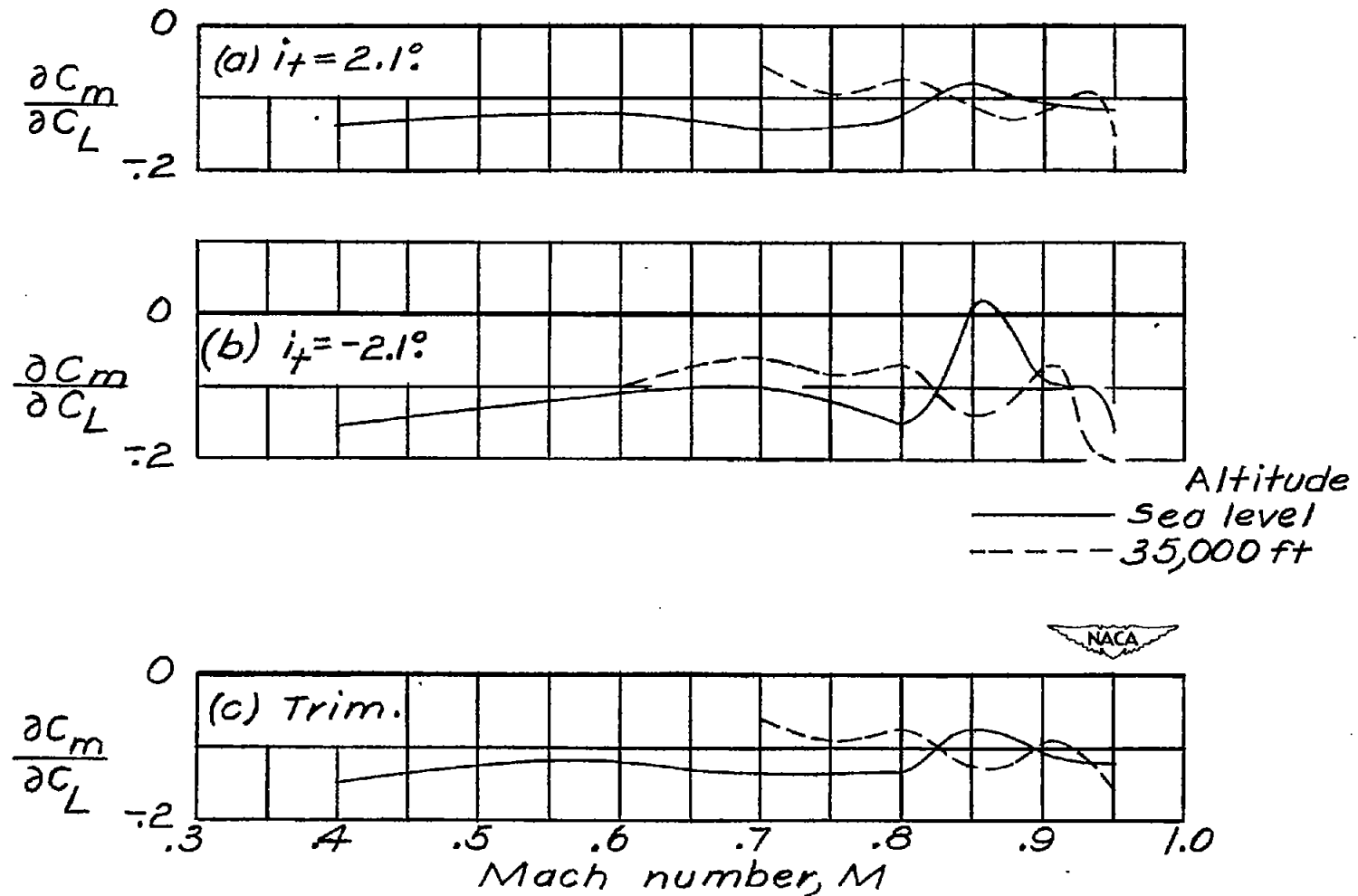
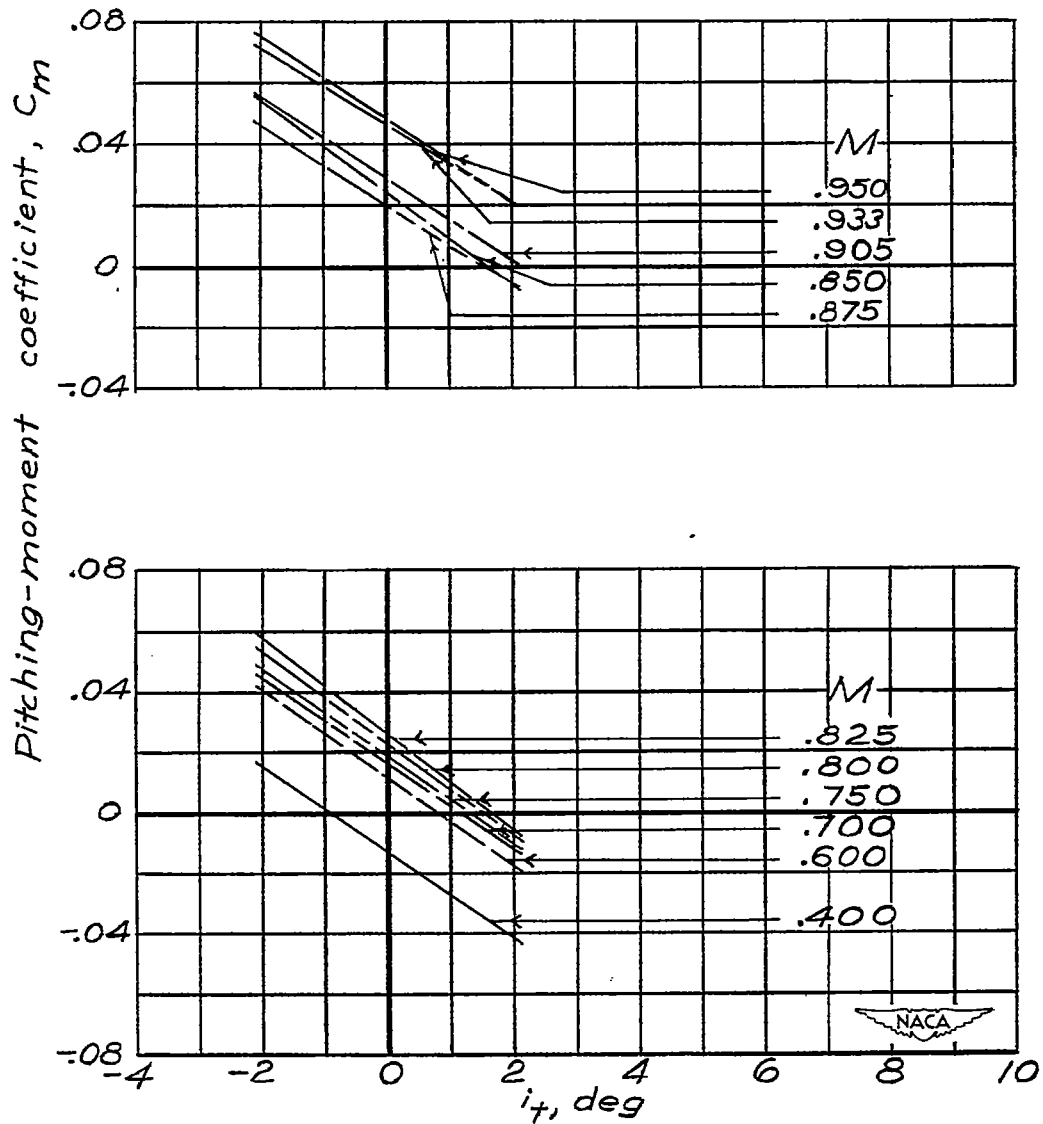
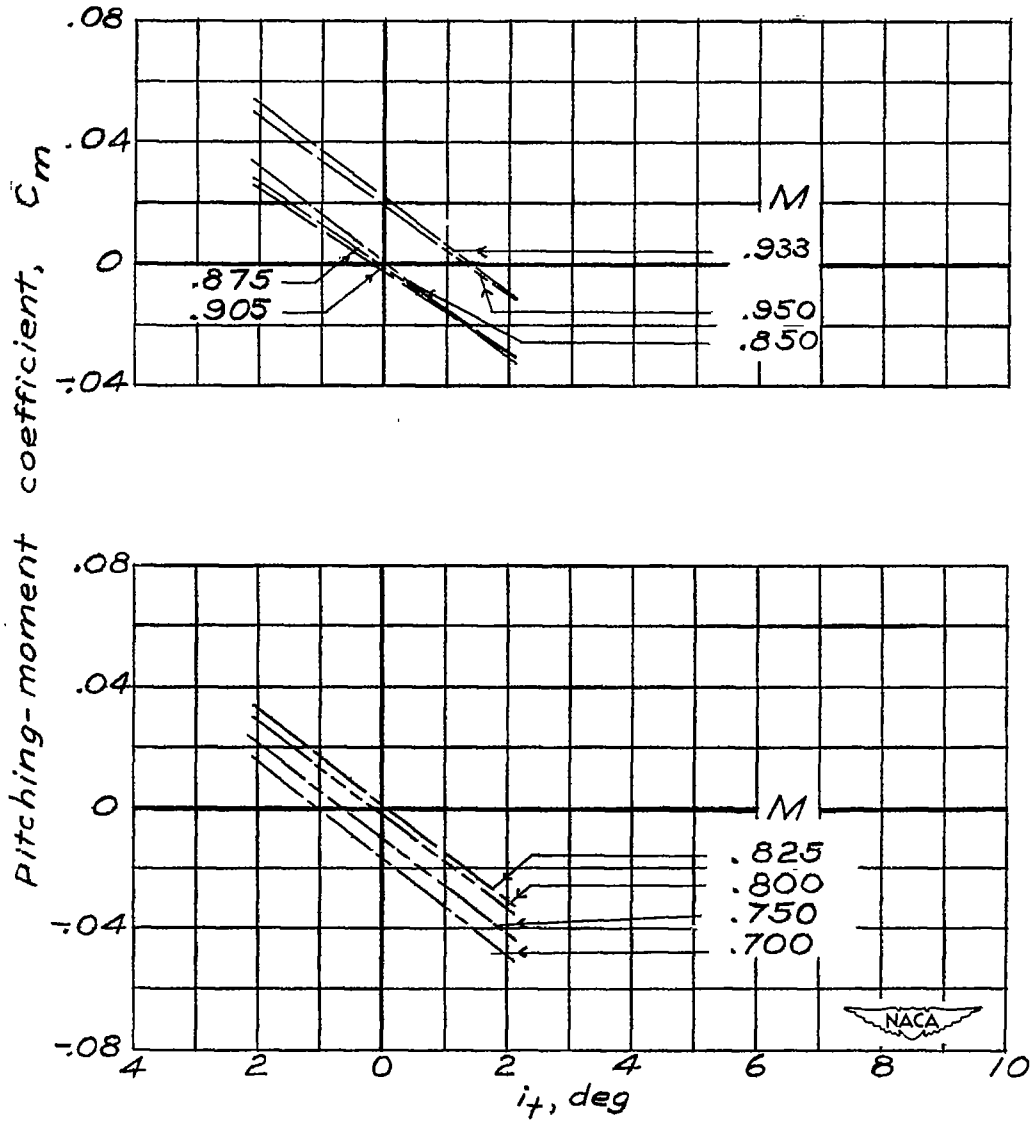


Figure 51.- Variation of the static-longitudinal-stability parameter $\frac{\partial C_m}{\partial C_L}$ with Mach number at airplane lift coefficients corresponding to level flight at two altitudes. Complete model; $A = 2$; $\delta_e = 0^\circ$; $\frac{W}{S} = 66.7$ pounds per square foot.



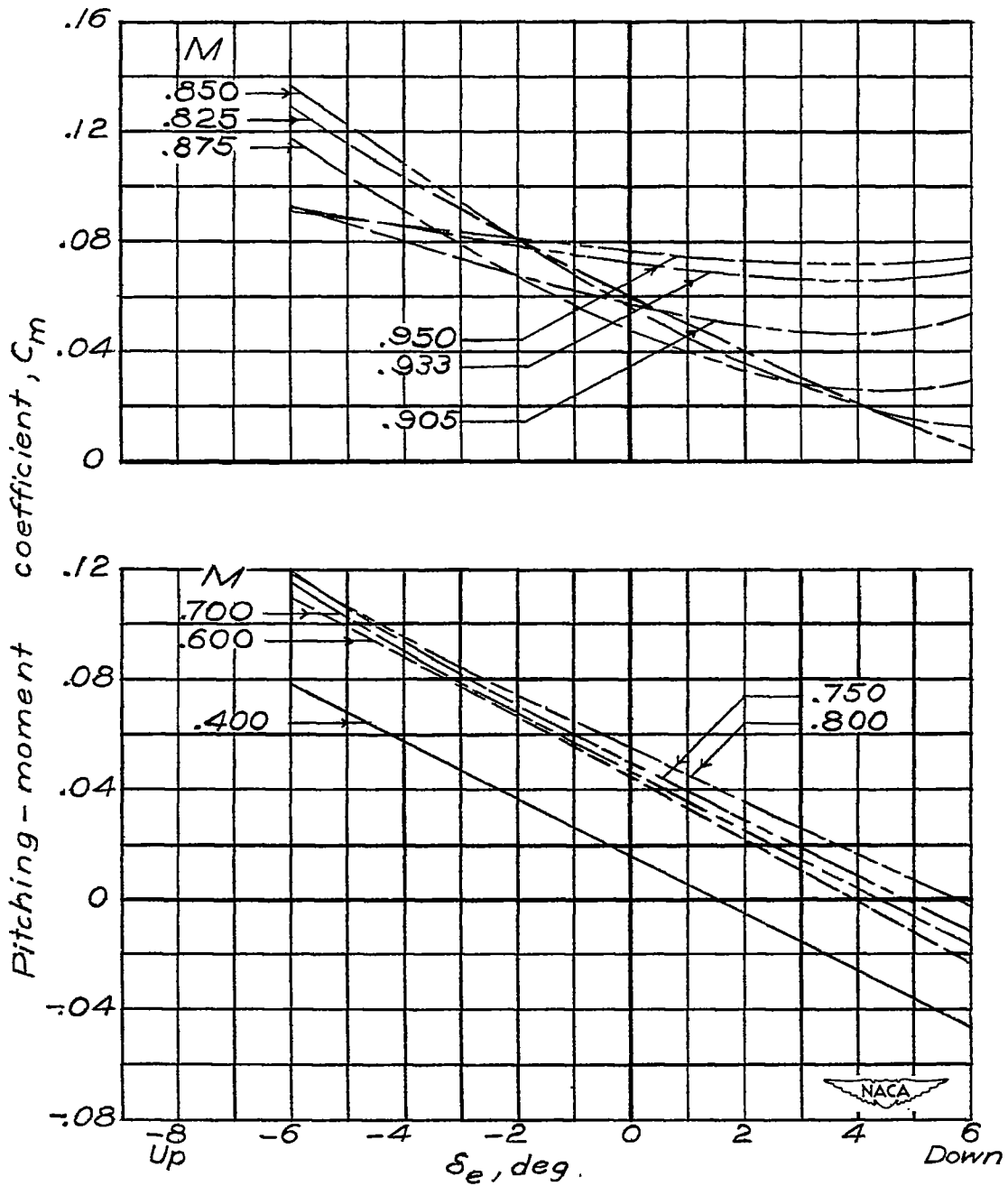
(a) $\delta_e = 0^\circ$; sea level.

Figure 52.- Variation of pitching-moment coefficient with horizontal-tail incidence and with elevator deflection at airplane lift coefficients corresponding to level flight at two altitudes. Complete model; $A = 2$; $\frac{W}{S} = 66.7$ pounds per square foot.



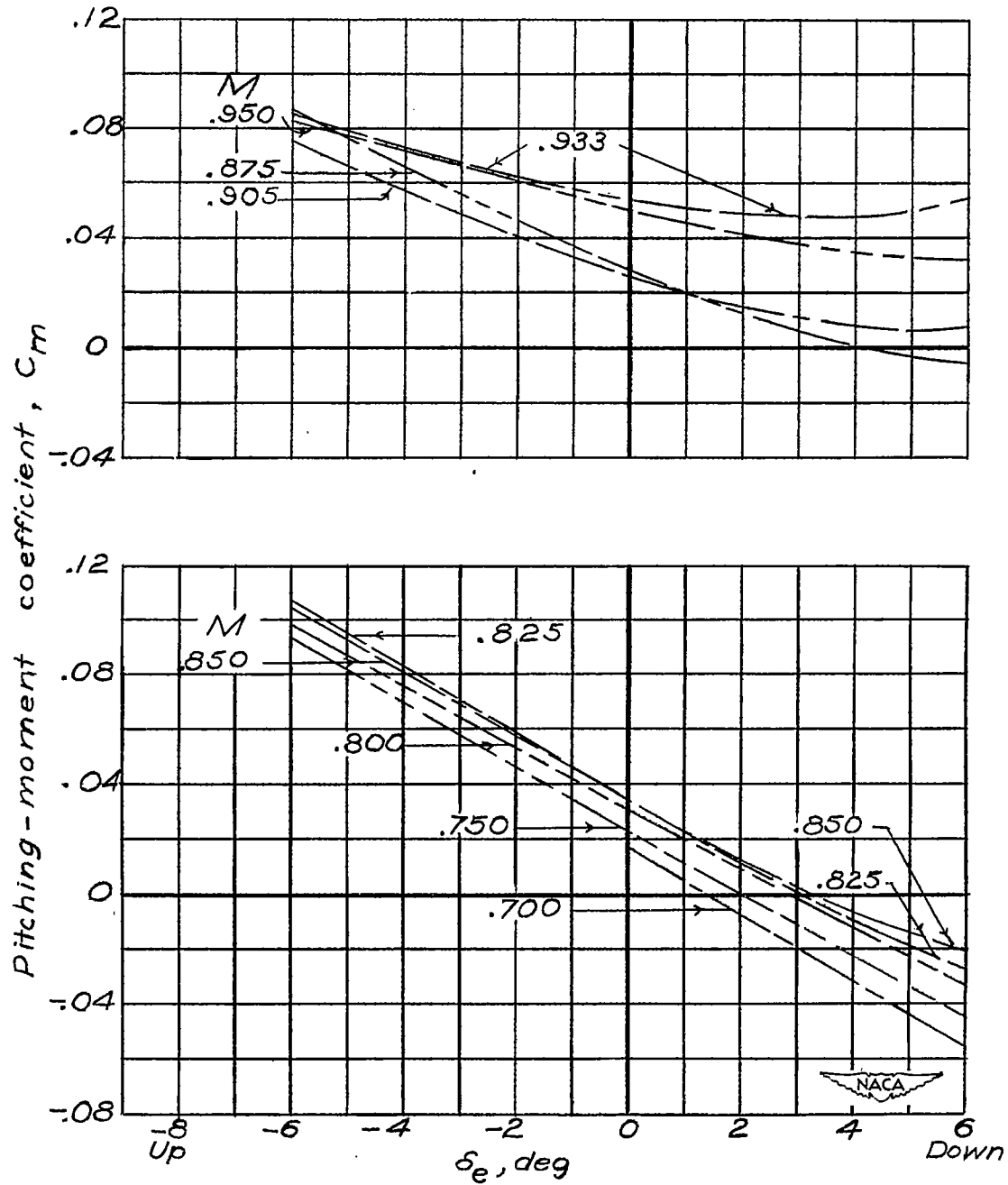
(b) $\delta_e = 0^\circ$; altitude, 35,000 feet.

Figure 52.- Continued.



(c) $i_t = -2.1^\circ$; sea level.

Figure 52.- Continued.



(d) $i_t = -2.1^\circ$; altitude, 35,000 feet.

Figure 52.- Concluded.

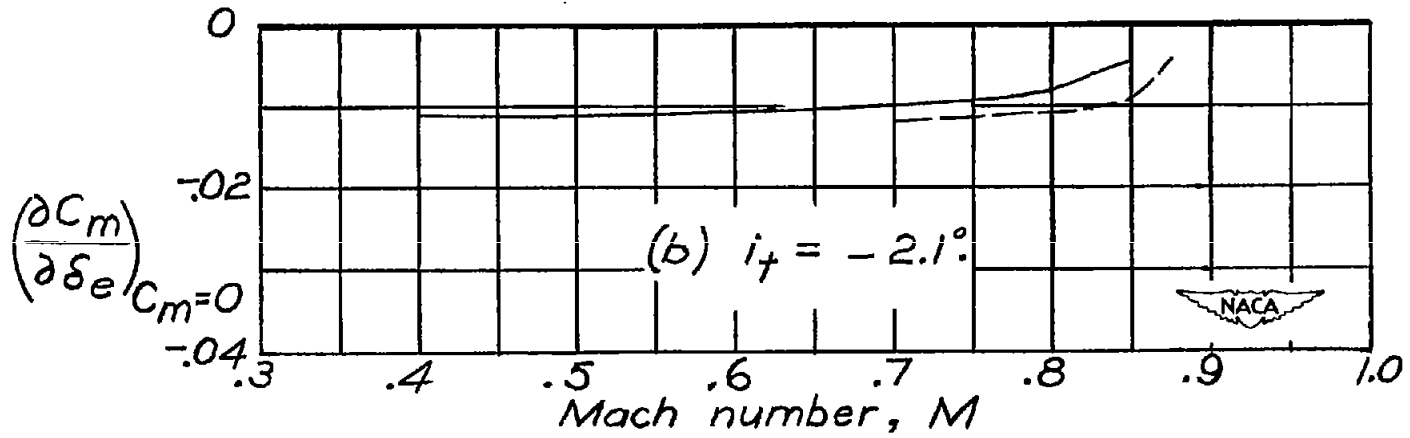
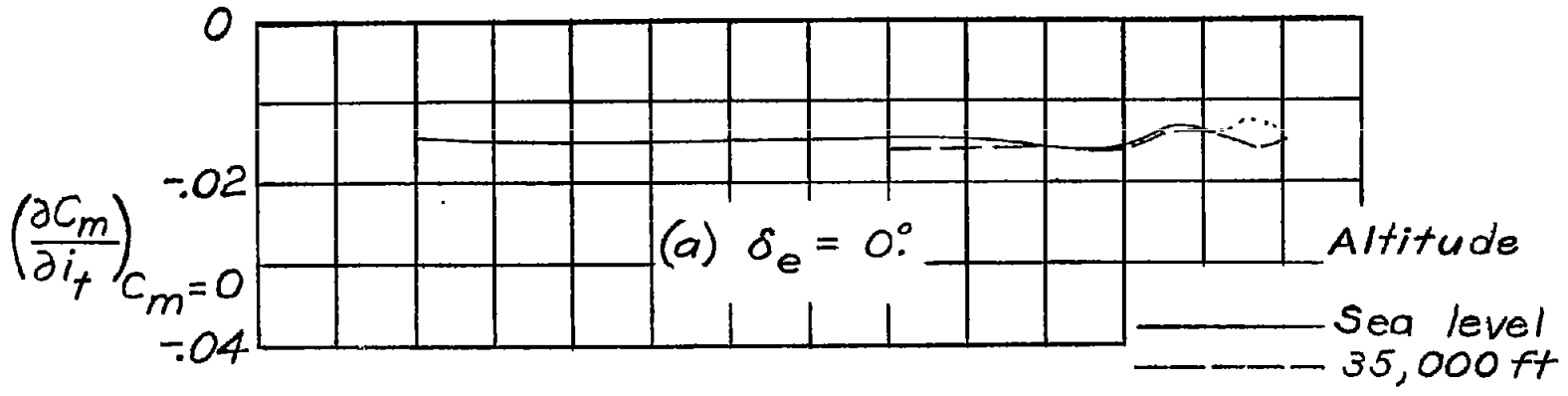


Figure 53.- Variation of horizontal-tail effectiveness $\partial C_m / \partial i_t$ and elevator effectiveness $\partial C_m / \partial \delta_e$ with Mach number for trim conditions at airplane lift coefficients corresponding to level flight at two altitudes. Complete model; $A = 2$; $\frac{W}{S} = 66.7$ pounds per square foot.

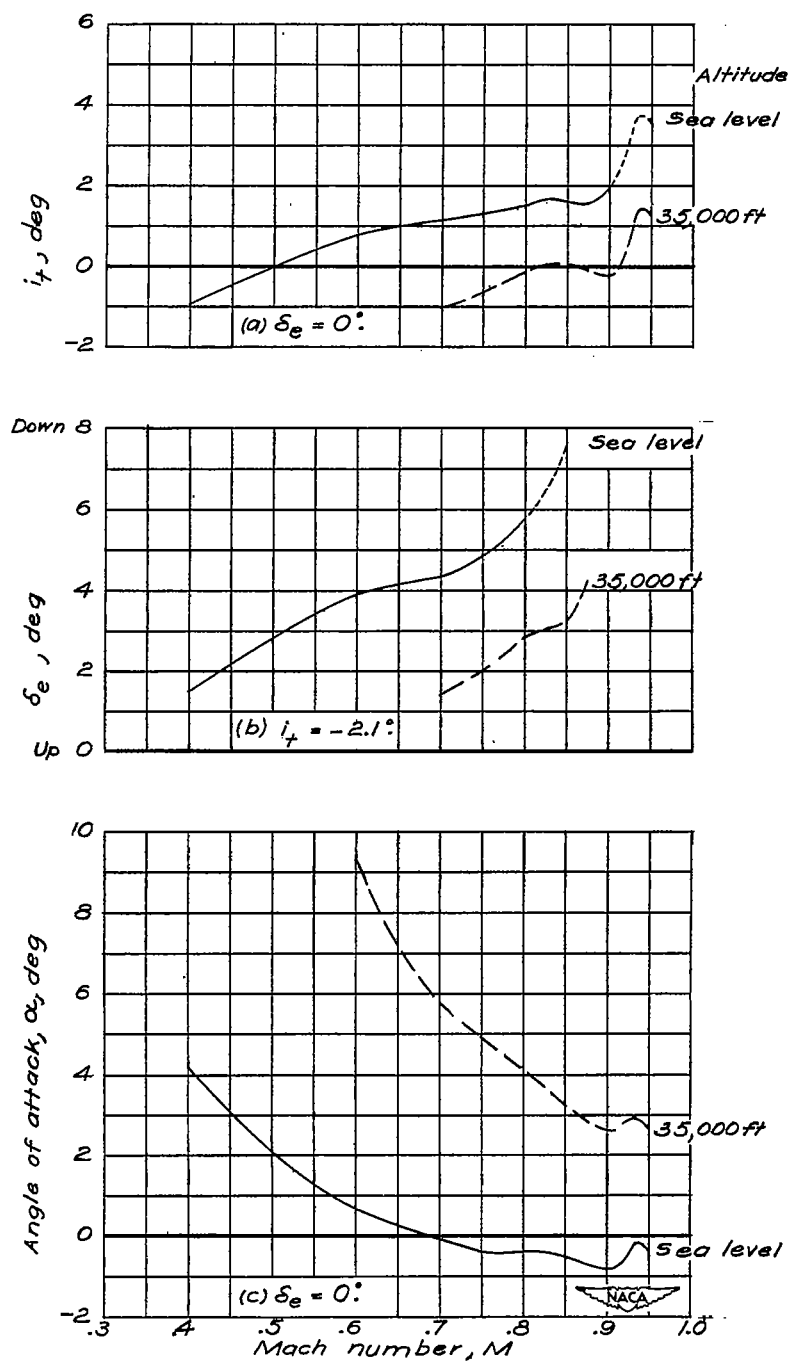


Figure 54.- Variation with Mach number of the horizontal-tail incidence required for obtaining trim, the elevator deflection required for obtaining trim, and the model angle of attack for trim conditions (horizontal tail used for obtaining trim) at airplane lift coefficients corresponding to level flight at two altitudes. Complete model; $A = 2$; $\frac{W}{S} = 66.7$ pounds per square foot.

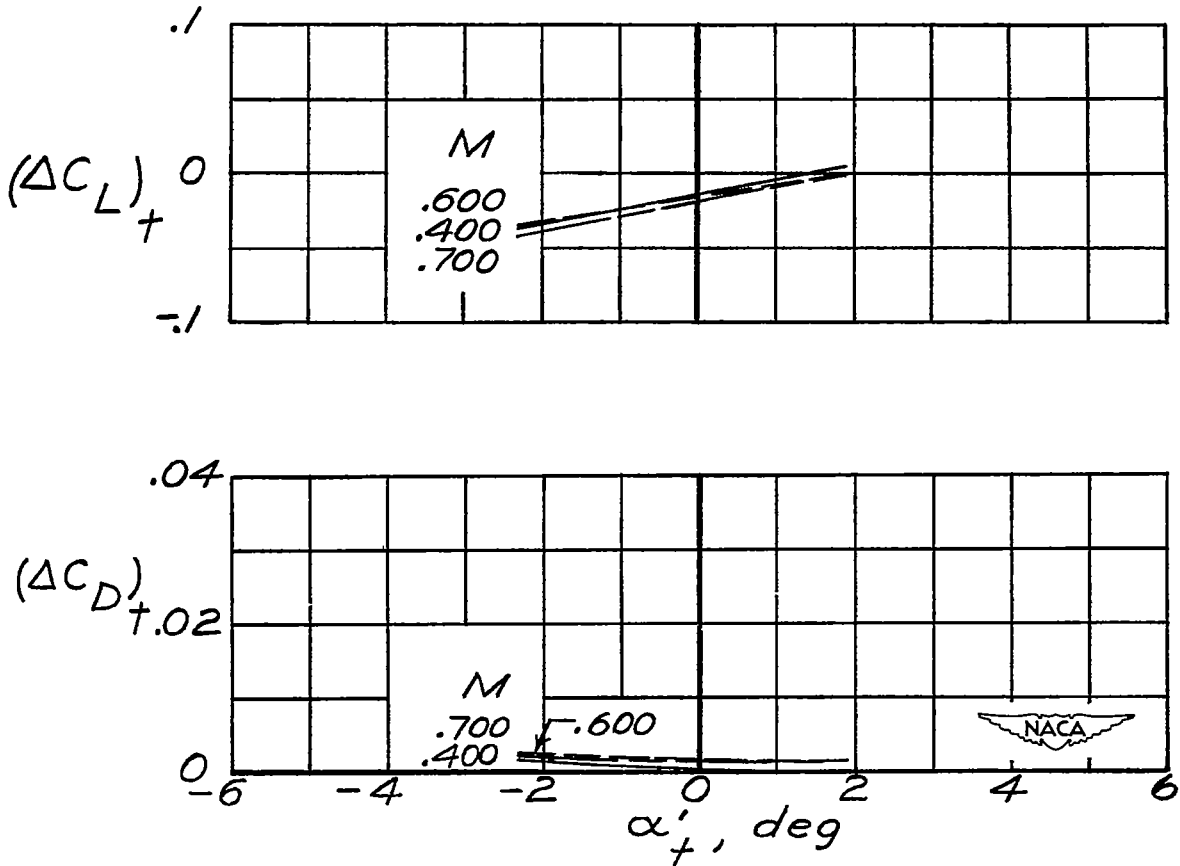


Figure 55.- Variation of incremental lift coefficient and incremental drag coefficient of horizontal tail with free-stream angle of attack of horizontal tail. Complete model less wing; $A = 2$; $\alpha = -0.2^\circ$; $\delta_e = 0^\circ$.

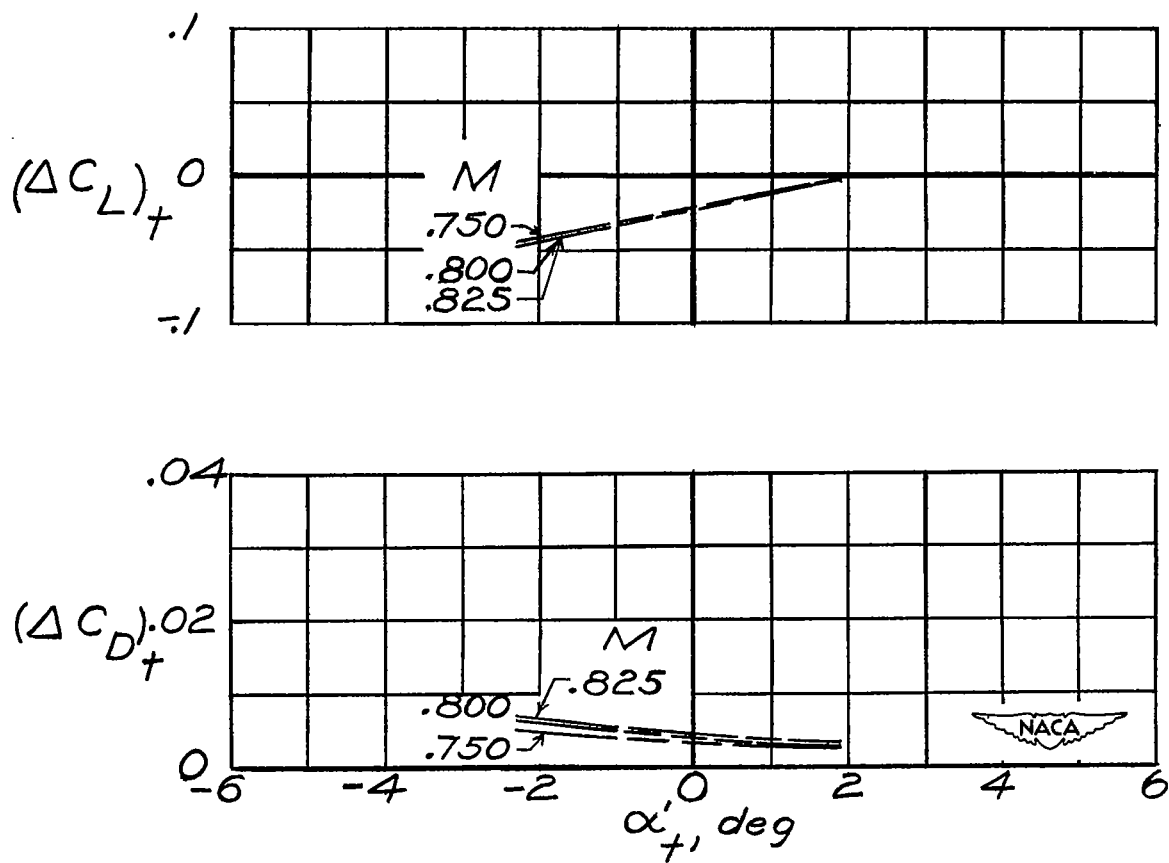


Figure 55.- Continued.

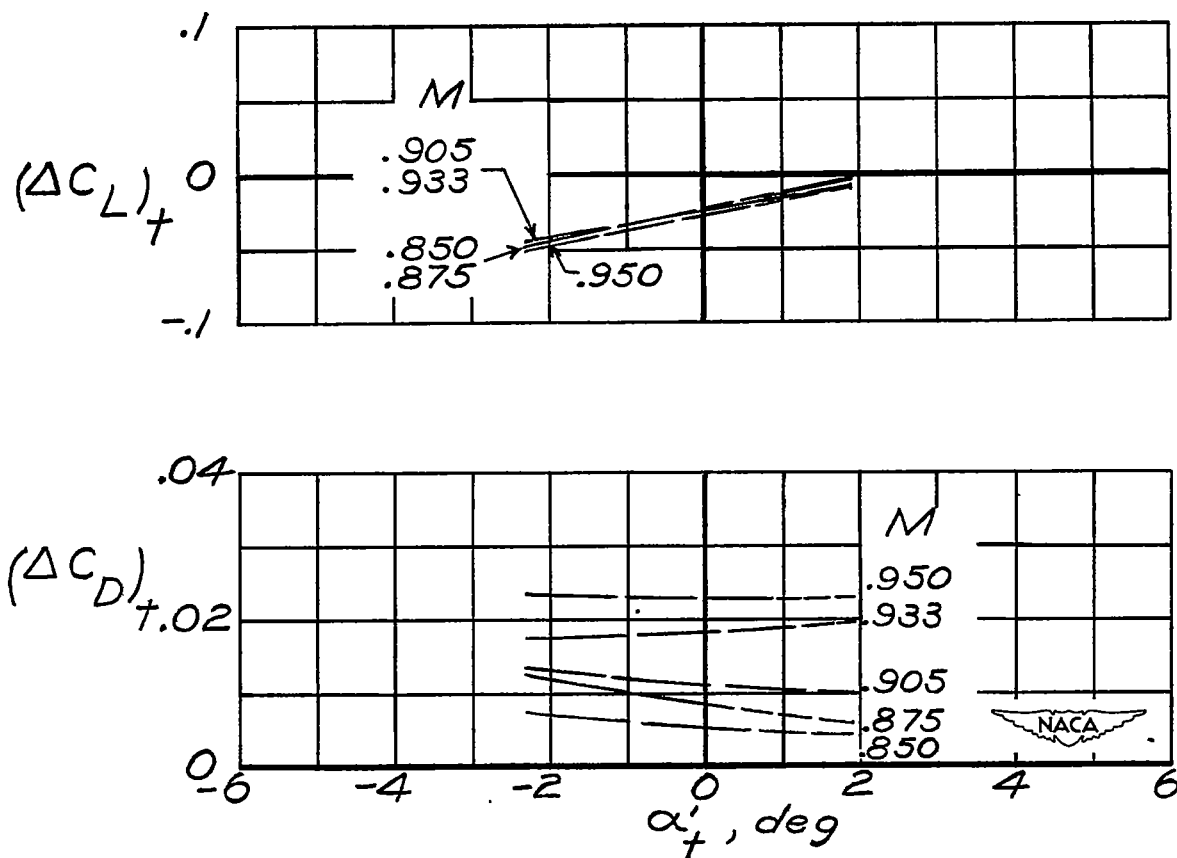


Figure 55.- Concluded.

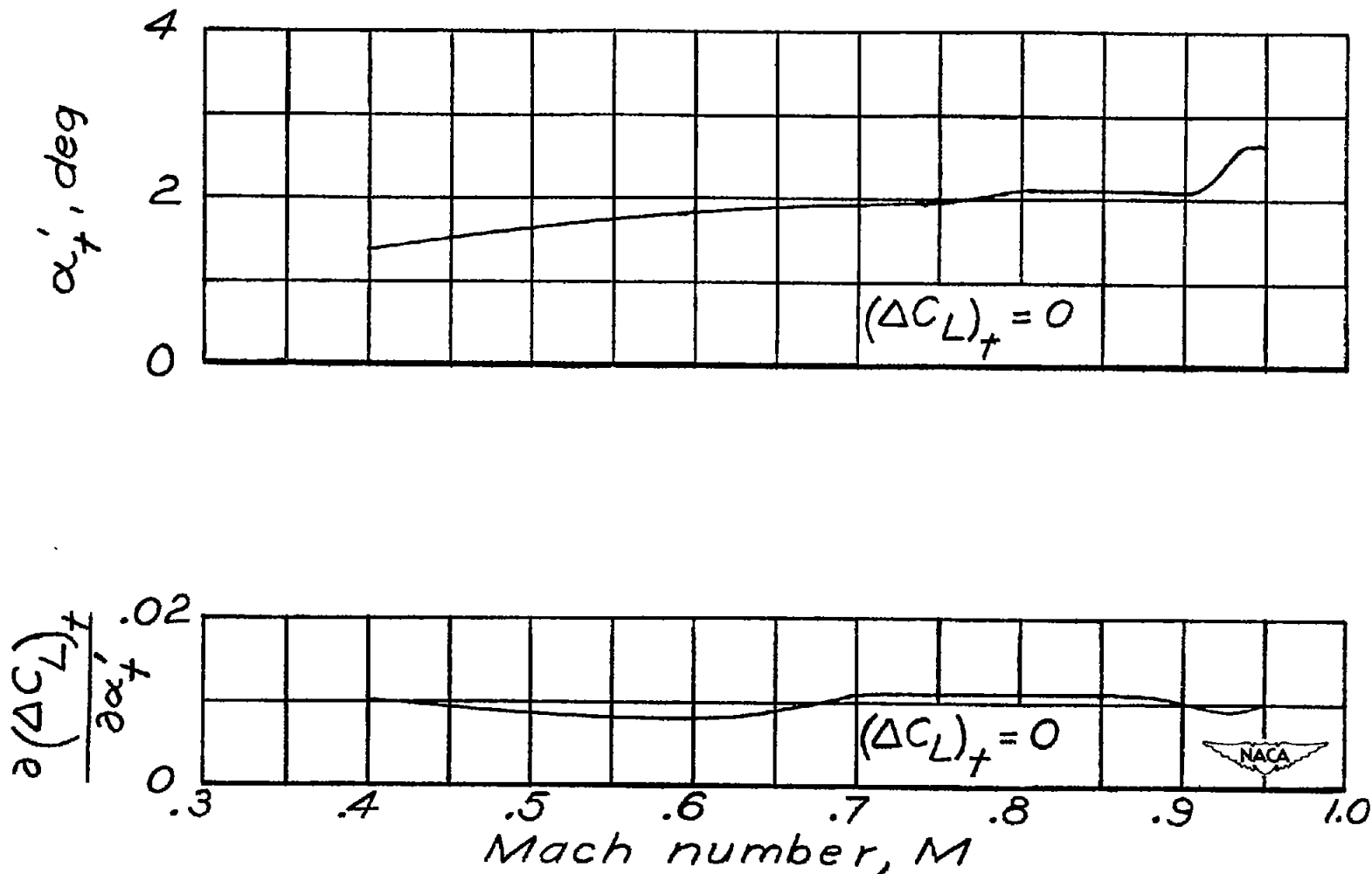


Figure 56.- Variation with Mach number of free-stream angle of attack of horizontal tail at incremental lift coefficient of horizontal tail of zero, and variation with Mach number of incremental lift-curve slope $\frac{\partial(\Delta C_L)_t}{\partial \alpha'_t}$. Complete model less wing; $A = 2$; $\alpha = -0.2^\circ$; $\delta_e = 0^\circ$.

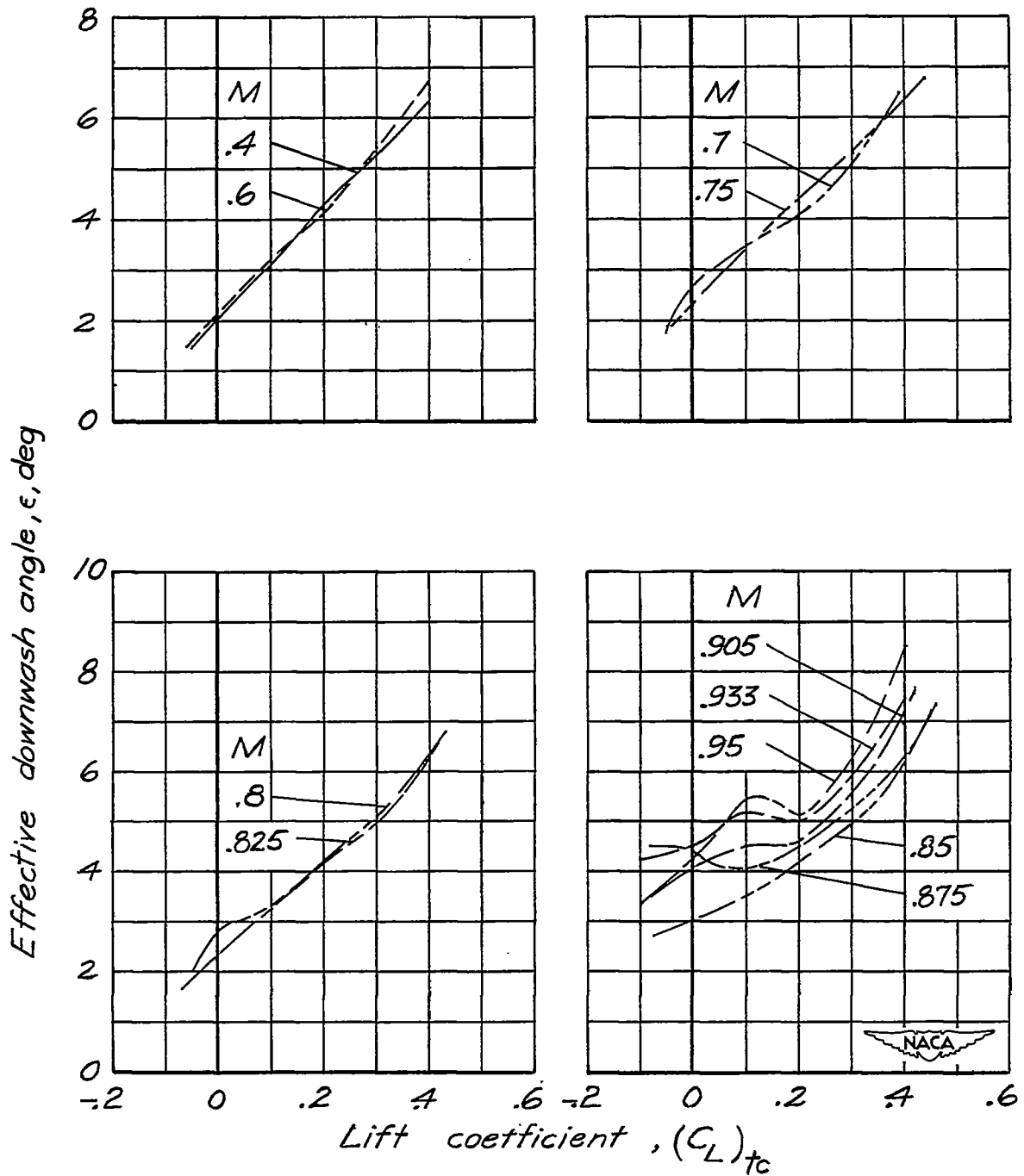


Figure 57.- Variation of effective downwash angle with lift coefficient at various Mach numbers. $A = 2$.

Effective downwash angle, ϵ , deg

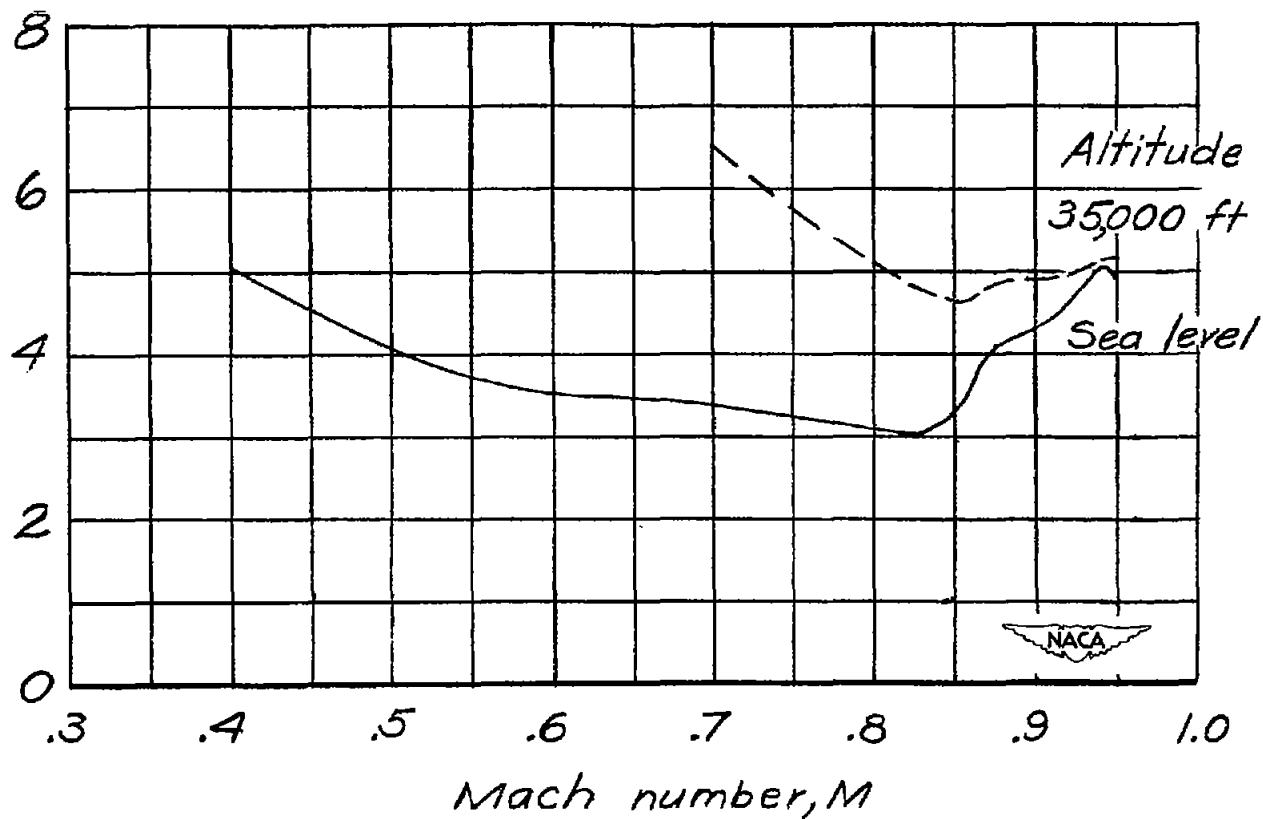


Figure 58.- Variation of effective downwash angle with Mach number at airplane lift coefficients corresponding to level flight at two altitudes for trim conditions with elevators undeflected and horizontal tail used for obtaining trim. $A = 2$; $\frac{W}{S} = 66.7$ pounds per square foot.

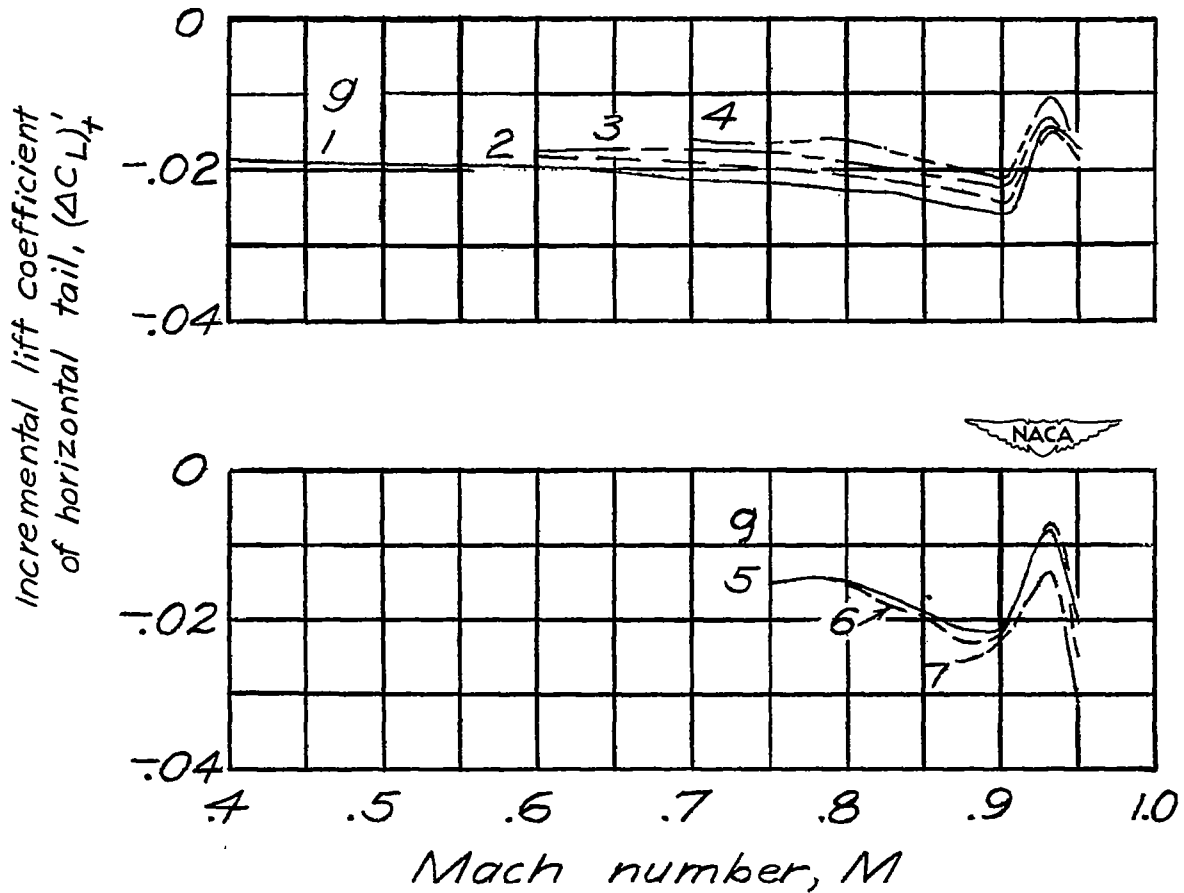


Figure 59.- Variation with Mach number of the incremental lift coefficient of the horizontal tail for trim conditions at various values of g for flight at sea level. Complete model; $A = 2$; $\frac{W}{S} = 66.7$ pounds per square foot.

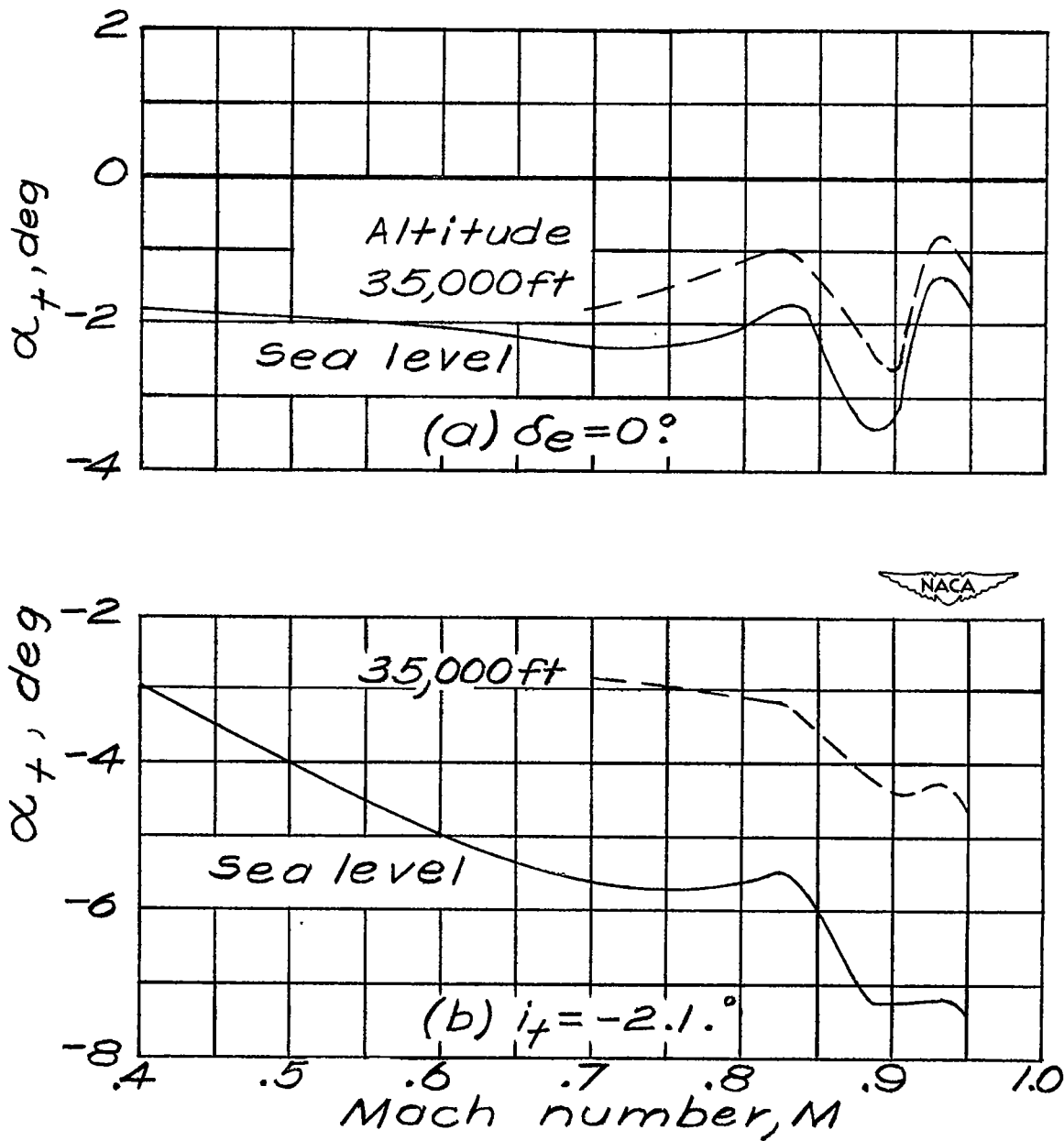


Figure 60.- Variation with Mach number of the angle of attack of the horizontal tail for trim conditions at airplane lift coefficients corresponding to level flight at two altitudes. Complete model;

$$A = 2; \frac{W}{S} = 66.7 \text{ pounds per square foot.}$$

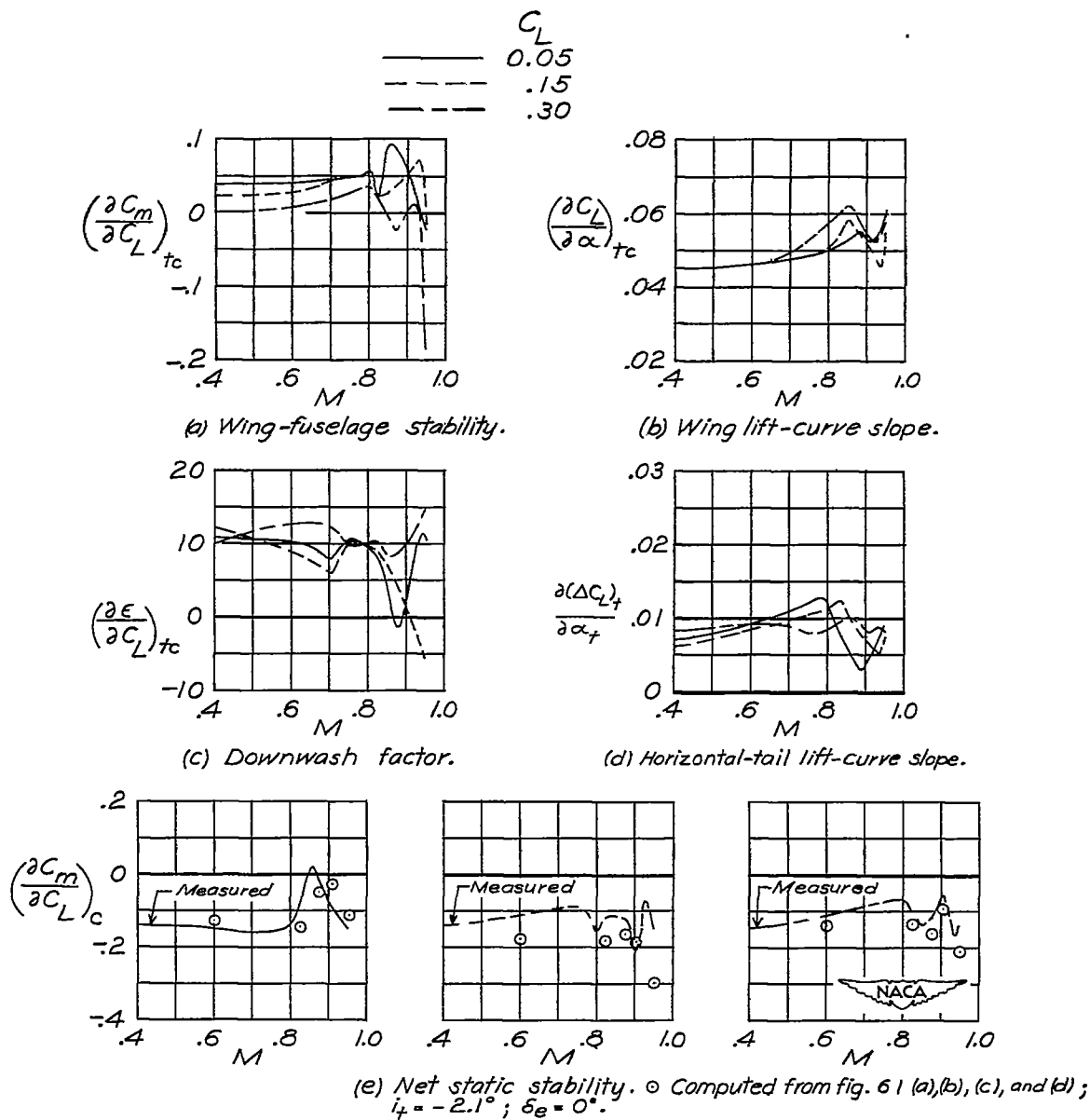


Figure 61.- Variation with Mach number of the static-longitudinal-stability parameter $(\partial C_m / \partial C_L)_c$ and of the various factors affecting longitudinal stability at three values of lift coefficient. $A = 2$.

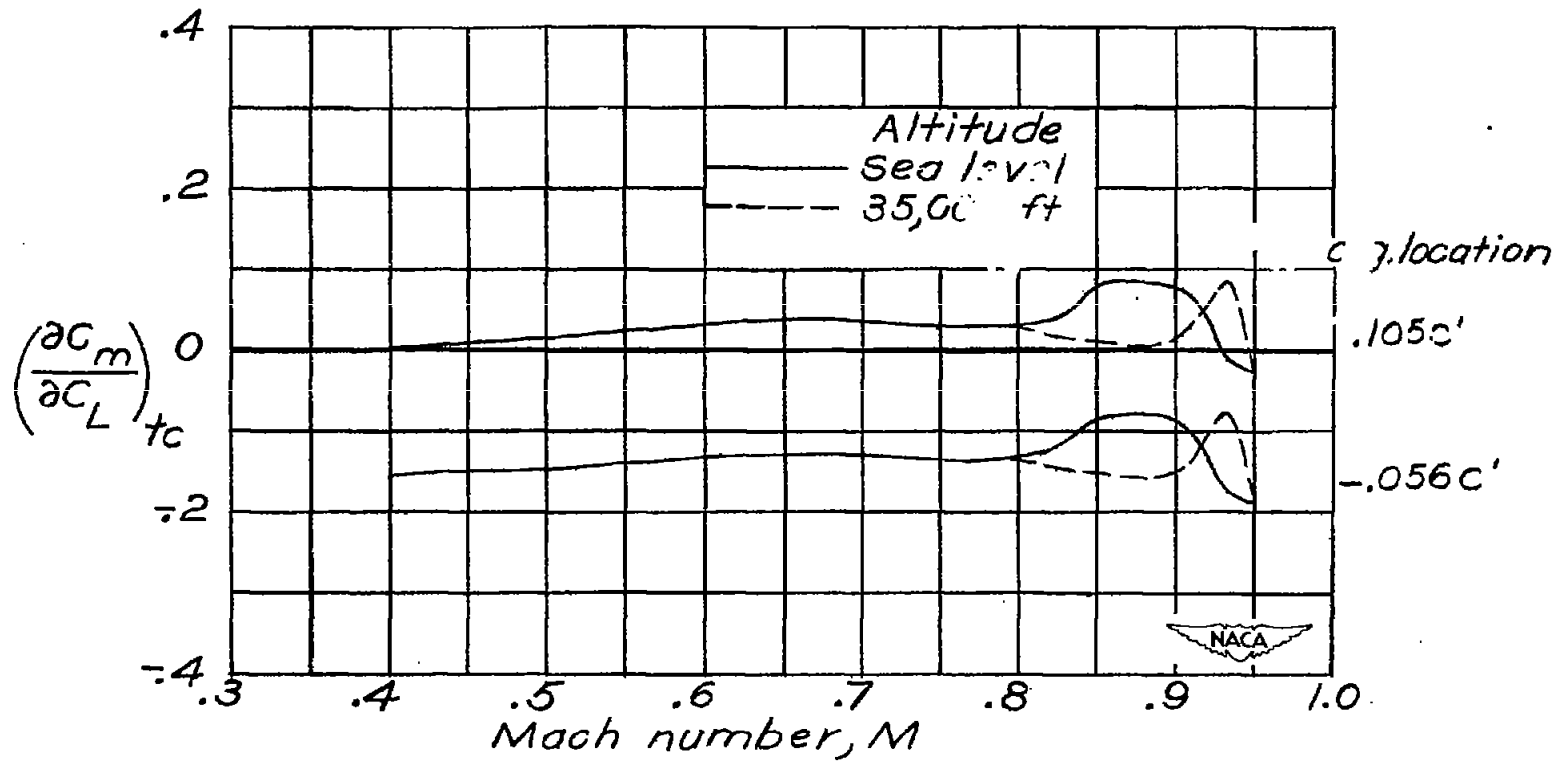


Figure 62.- Variation with Mach number of the static-longitudinal-stability parameter $(\partial C_m / \partial C_L)_{t_c}$ for two center-of-gravity positions at airplane lift coefficients corresponding to level flight at two altitudes.

Complete model less horizontal tail; $A = 2$; $\frac{W}{S} = 66.7$ pounds per square foot.

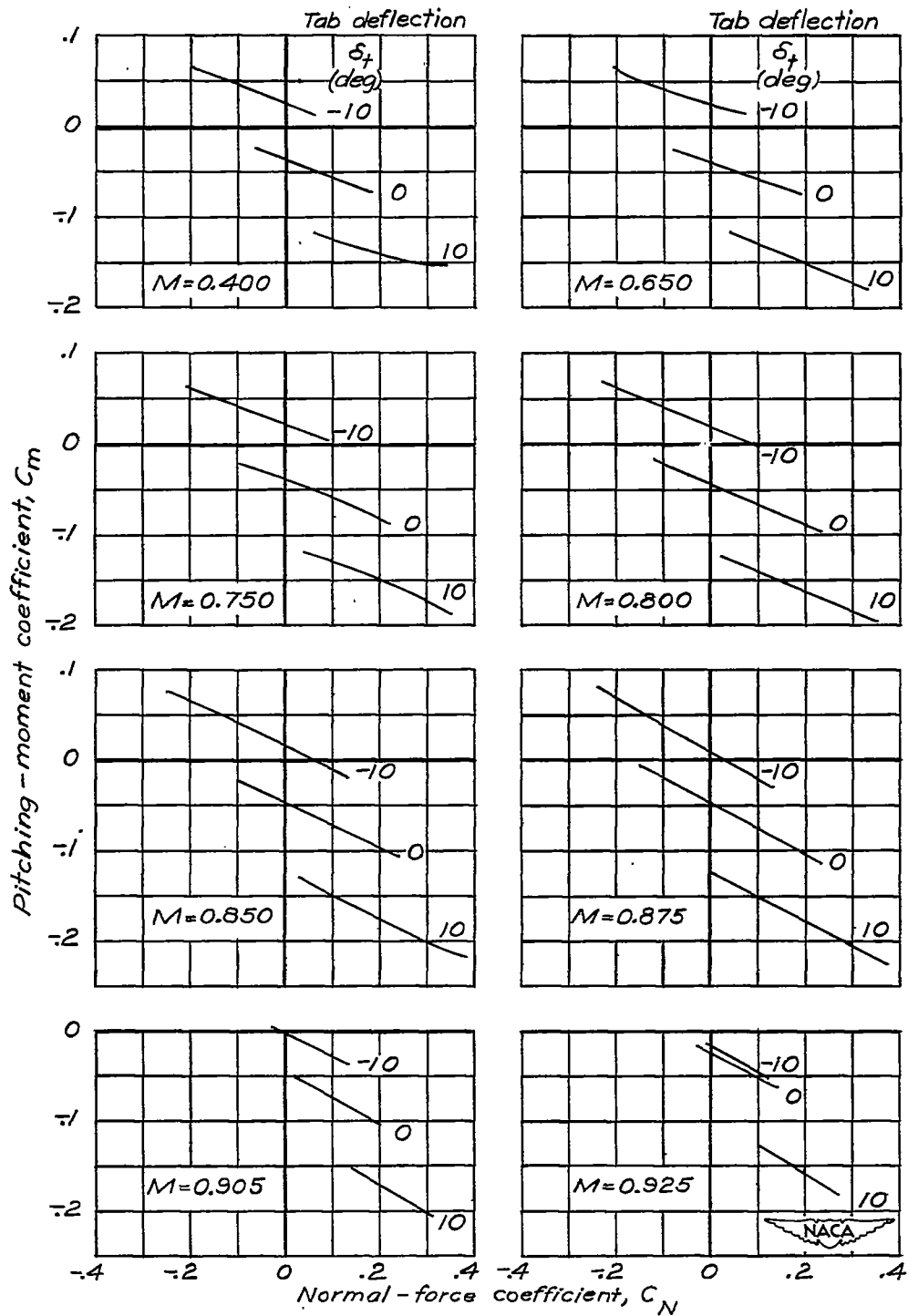


Figure 63.- Variation of pitching-moment coefficient with normal-force coefficient at various trim tab deflections for a tailless model with a wing of aspect ratio 4.01.

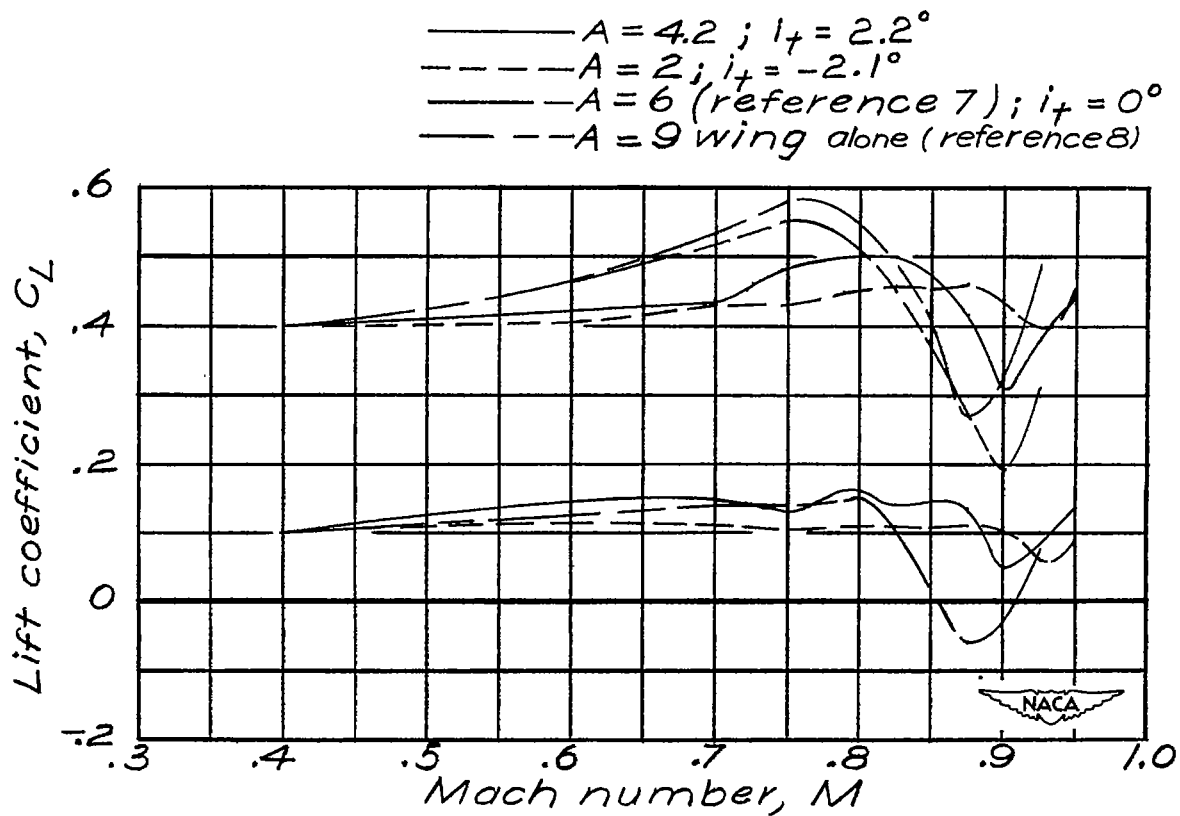


Figure 64.- Variation of lift coefficient with Mach number for various configurations at angles of attack set to give lift coefficients of 0.1 and 0.4 at a Mach number of 0.4. $\delta_e = 0^\circ$.

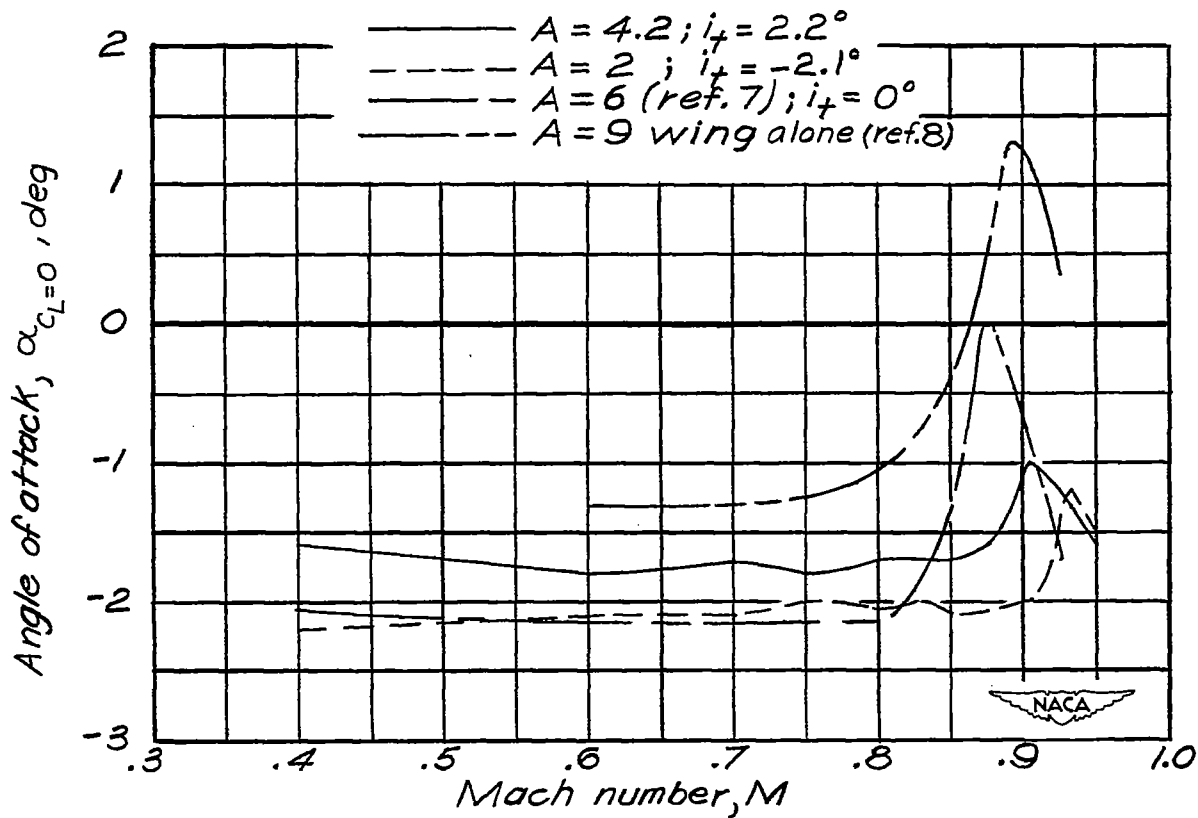


Figure 65.- Variation of angle of attack for zero lift with Mach number for various configurations. $\delta_e = 0^\circ$.

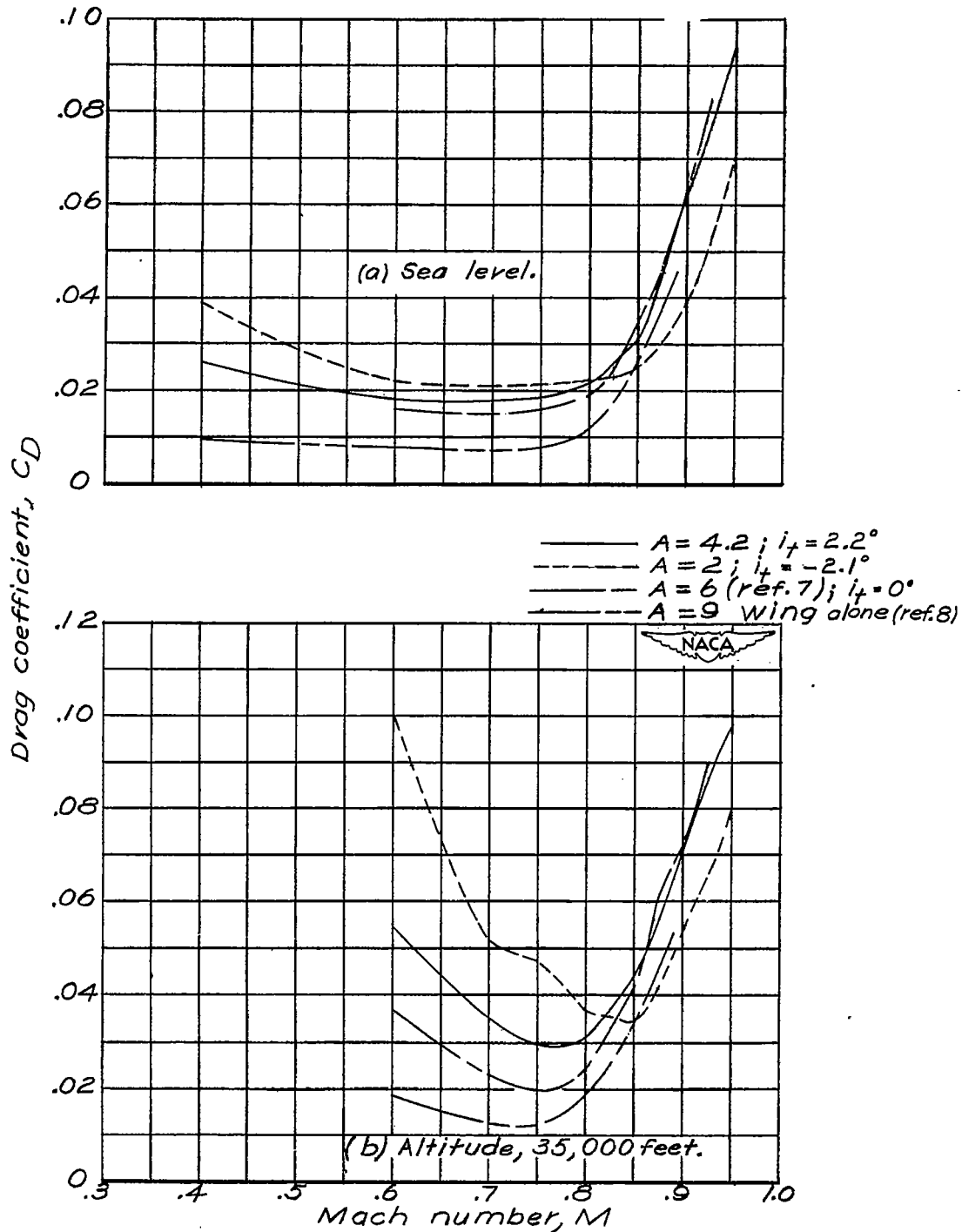


Figure 66.- Variation of drag coefficient with Mach number for various configurations at airplane lift coefficients corresponding to level flight at two altitudes. $\delta_e = 0^\circ$; $\frac{W}{S} = 66.7$ pounds per square foot.

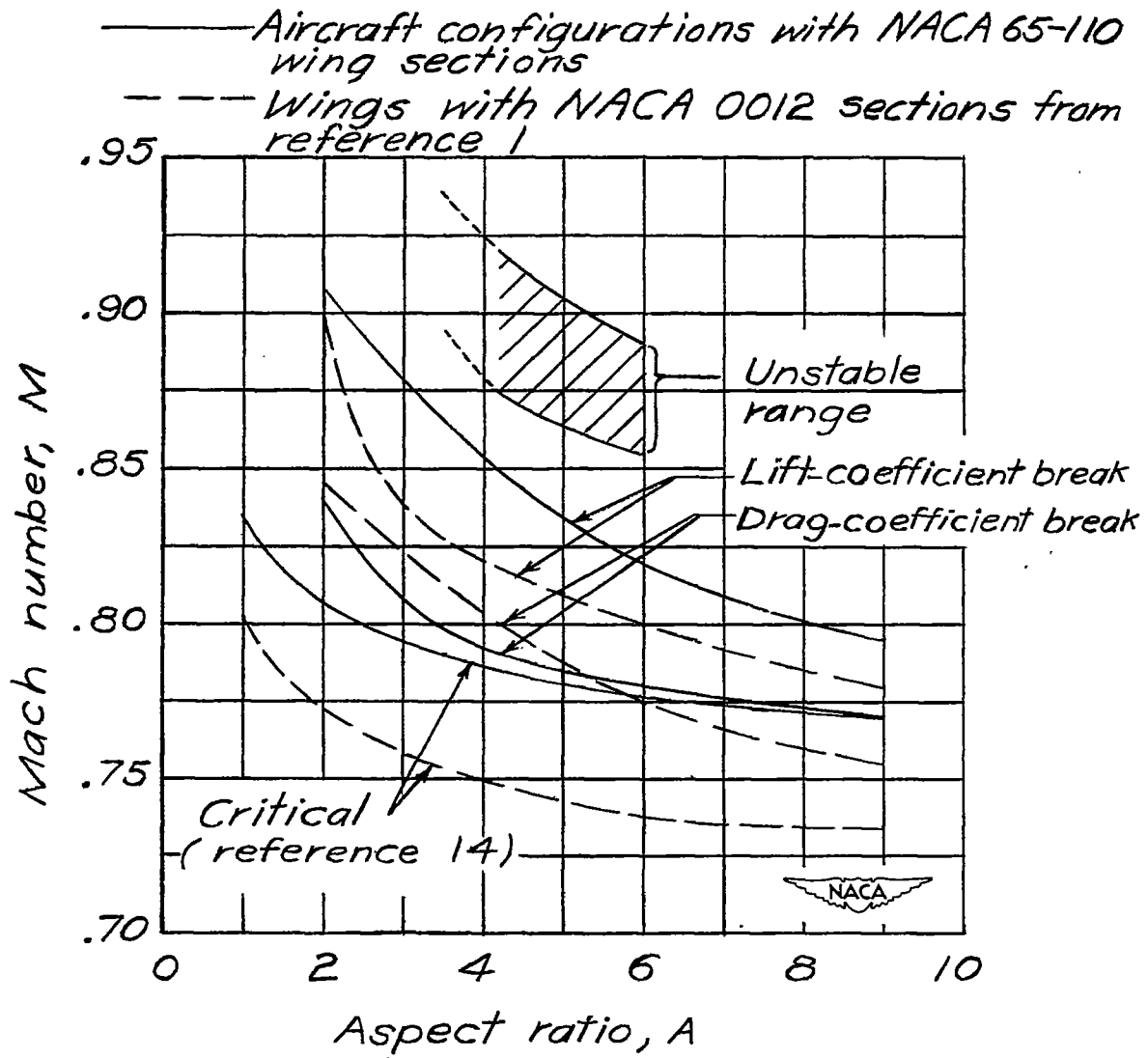


Figure 67.- Variation of critical Mach number and force-break Mach number with aspect ratio for various configurations.

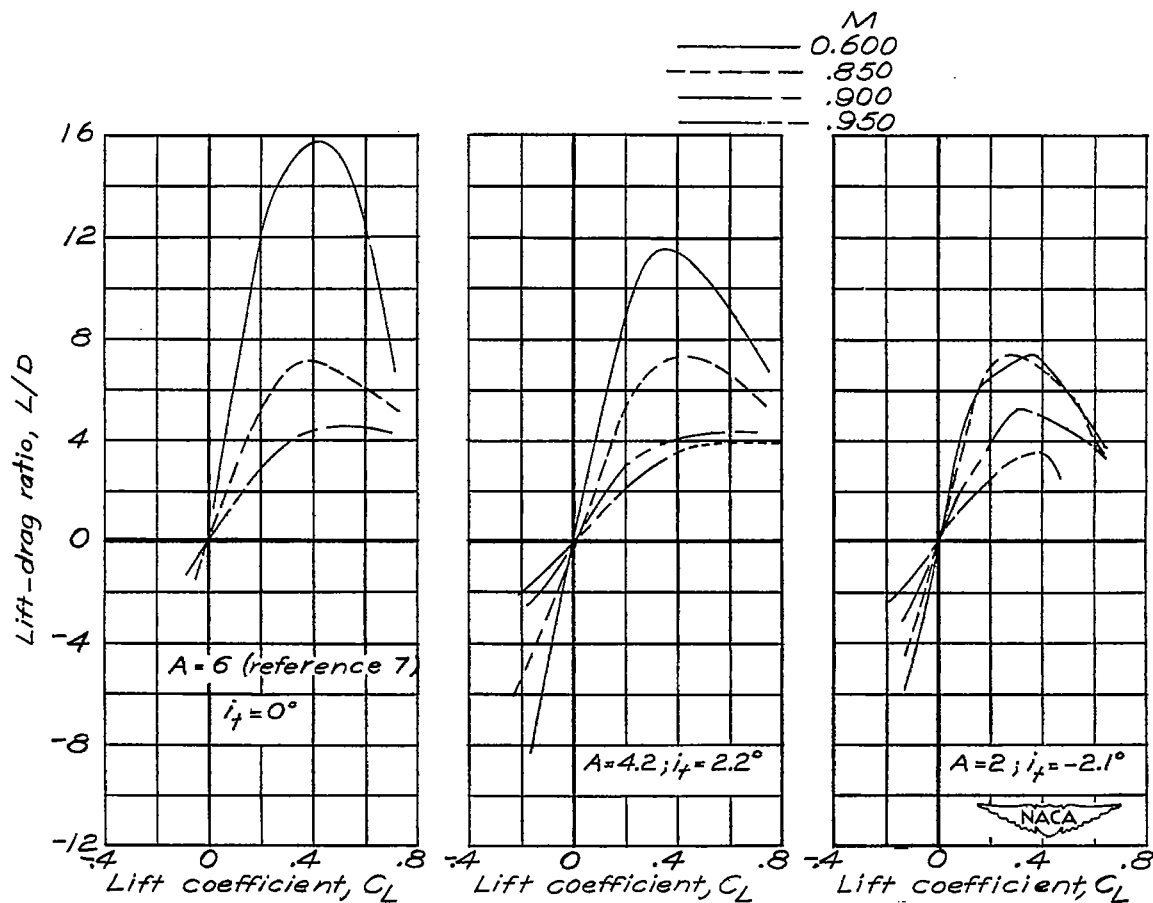


Figure 68.- Variation of lift-drag ratio with lift coefficient for various configurations. $\delta_e = 0^\circ$.

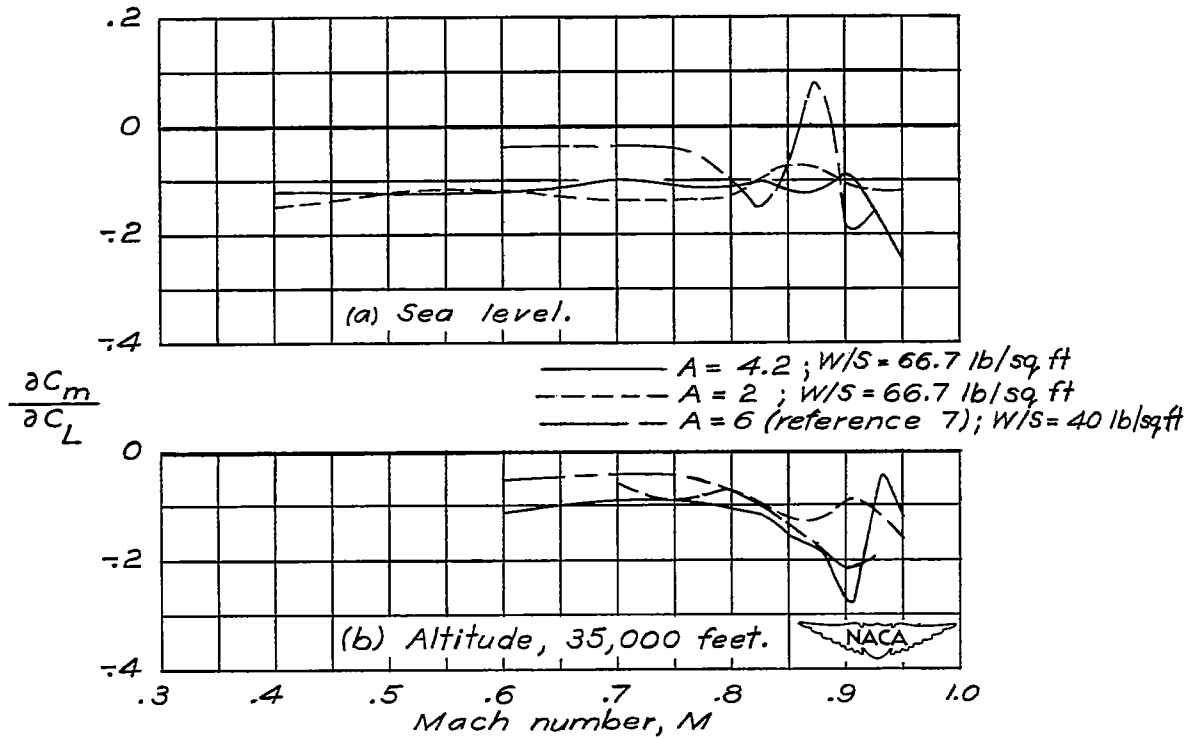
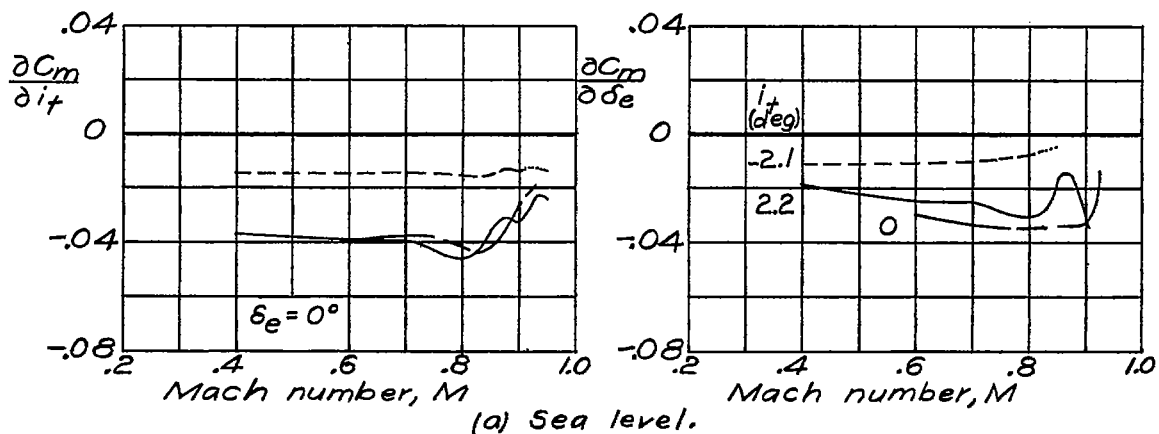


Figure 69.- Variation of the static-longitudinal-stability parameter $\frac{\partial C_m}{\partial C_L}$ with Mach number for various configurations for trim conditions (horizontal tail used for obtaining trim) at airplane lift coefficients corresponding to level flight at two altitudes. $\delta_e = 0^\circ$.



——— $A=4.2; W/S=66.7 \text{ lb/sq ft}$
 - - - $A=2; W/S=66.7 \text{ lb/sq ft}$
 - · - $A=6$ (reference 7); $W/S=40 \text{ lb/sq ft}$

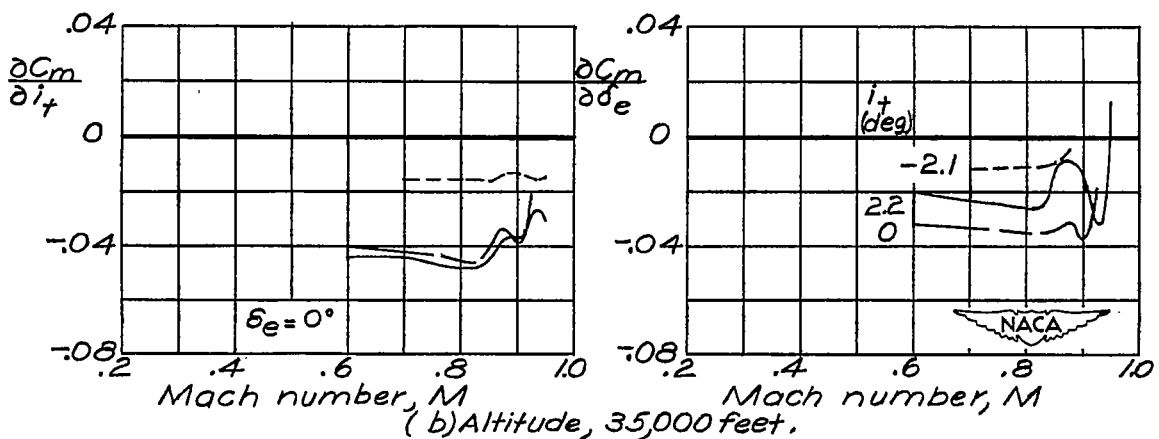
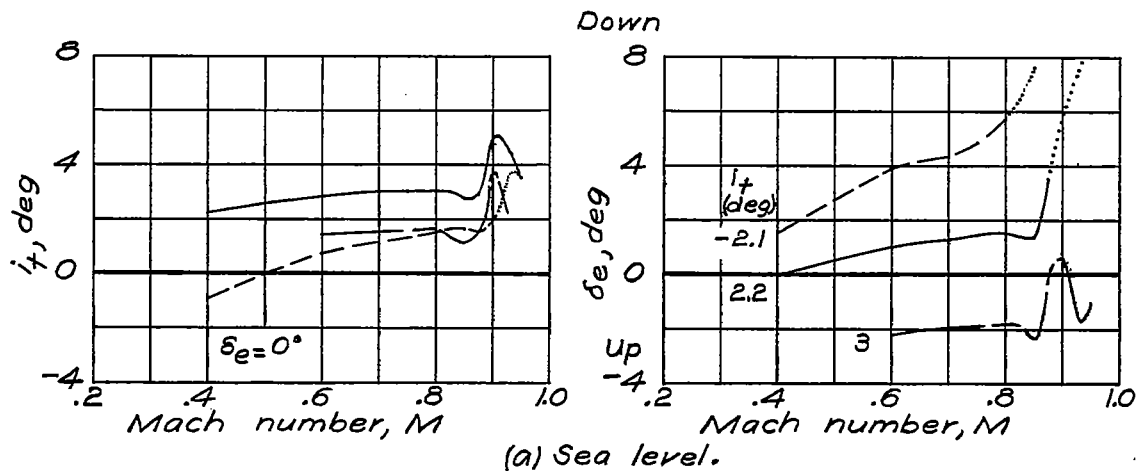


Figure 70.- Variation of horizontal-tail effectiveness $\frac{\partial C_m}{\partial i_t}$ and elevator effectiveness $\frac{\partial C_m}{\partial \delta_e}$ with Mach number for various configurations for trim conditions at airplane lift coefficients corresponding to level flight at two altitudes.



——— A = 4.2 ; $w/s = 66.7 \text{ lb/sq ft}$
 - - - A = 2 ; $w/s = 66.7 \text{ lb/sq ft}$
 - · - A = 6 (reference 7) ; $w/s = 40 \text{ lb/sq ft}$

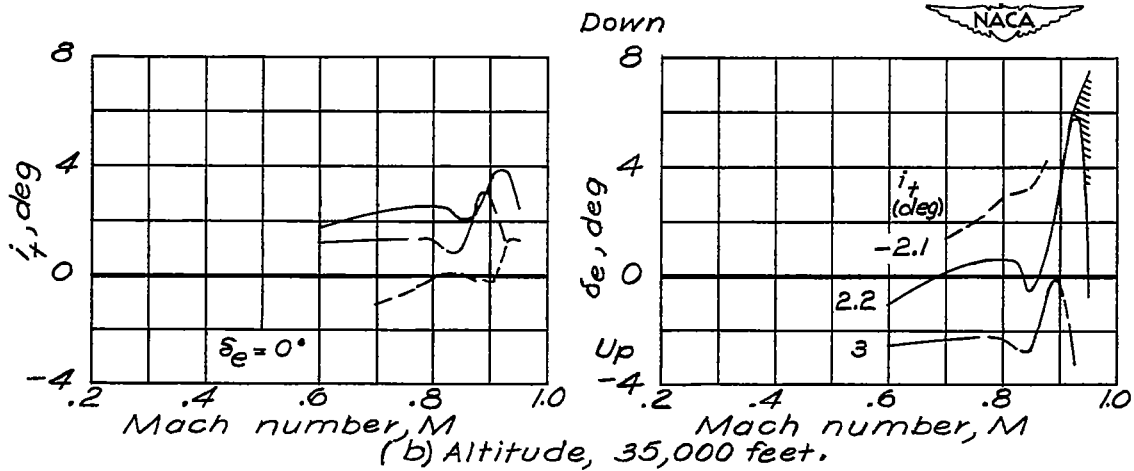


Figure 71.- Variation with Mach number of the horizontal-tail incidence required for obtaining trim and the elevator deflection required for obtaining trim for various configurations at airplane lift coefficients corresponding to level flight at two altitudes.

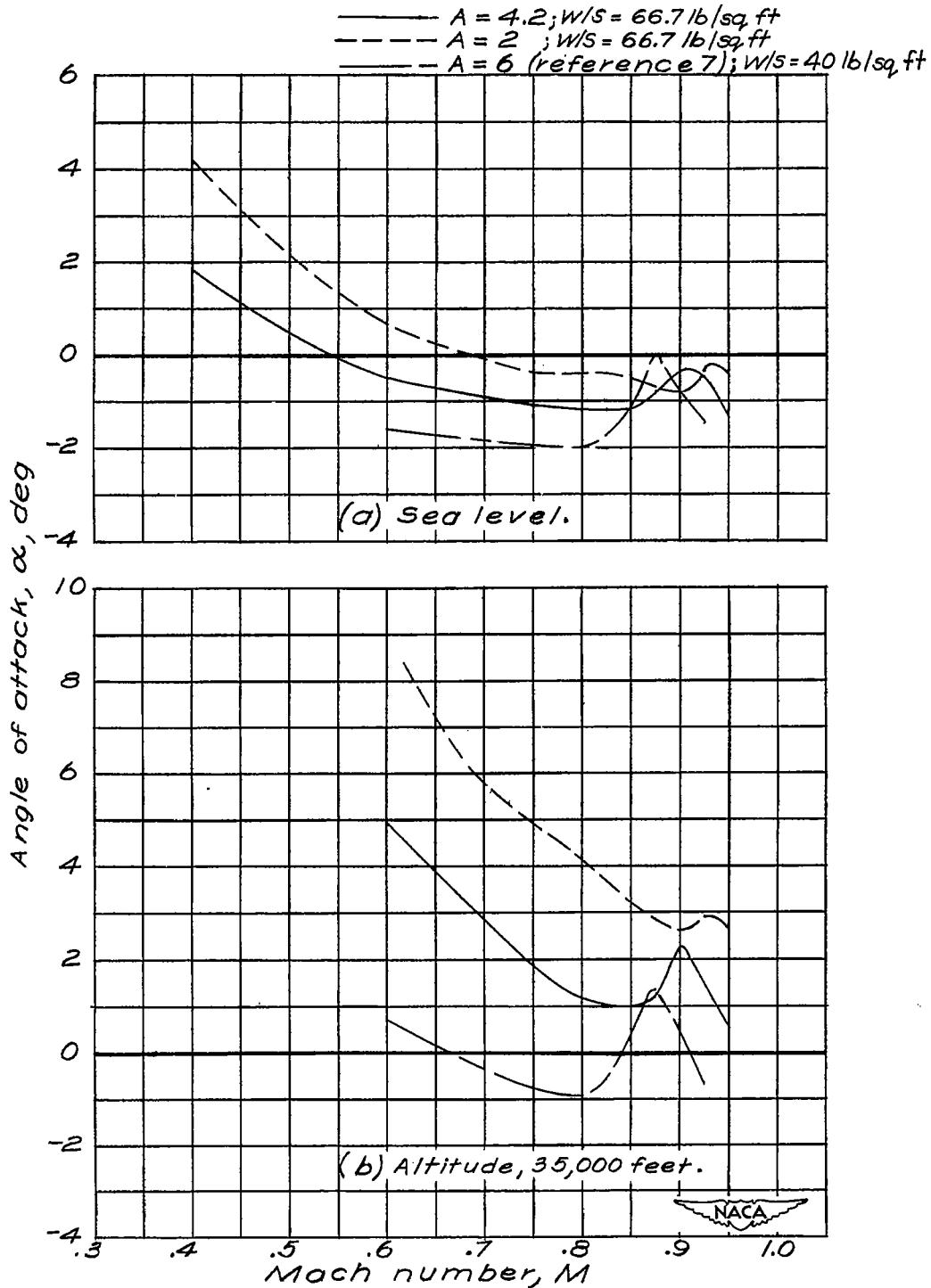


Figure 72.- Variation with Mach number of model angle of attack for trim conditions (horizontal tail used for obtaining trim) for various configurations at airplane lift coefficients corresponding to level flight at two altitudes. $\delta_e = 0^\circ$.